Part II

About the nuclear origin

Charged Particle Emissions and Surface Morphology of Pd/PdO:D$_x$ and TiD$_x$ Targets Under Electron Beam Excitation

A. Lipson[1], I. Chernov[2], ,V. Sokhoreva[2], V. Mironchik[2], A. Roussetski[3], A. Tsivadze[1], Y. Cherdantsev[2], B. Lyakhov[1], E. Saunin[1] and M. Melich[4]

1 A.N. Frumkin Institute of Physical Chemistry and Electrochemistry, Russian Academy of Sciences, Moscow 199915, Russia
2 Tomsk Polytechnic University, Tomsk, 634050 Russia
3 P.N. Lebedev Physics Institute, Russian Academy of Sciences, Moscow, 119991 Russia
4 Naval Postgraduate School, Monterey CA 93943 -5000 USA

E-mail: rusets@x4u.lebedev.ru

Abstract. We report charged particle emission from metal deuterides upon e-beam excitation of their surface. Detection and identification was made using CR-39 plastic track detectors with Cu and Al absorbers. Protons with primary energy 3 MeV and α-particles with energies E$_\alpha$> 10 MeV are observed.

1. Introduction

First principles calculations of hydrogen desorption from metal hydrides with a high hydrogen solubility [1], show that excitation of the hydrogen subsystem in those deuterides produces plasmons that create strong electric fields (F ~ 10^8 V/cm) on a lattice parameter scale (a ~ 0.3-0.4 nm). As a result, the mean energy of desorbed protons/deuterons (E$_d$), escaping from the hydride surface, is increased from kT(1/40 eV) to several eV (E$_d$ = F×a ~ 3-4 eV) or two orders of magnitude larger, effectively producing "hot" deuterons. Such a deuteron acceleration mechanism, along with a large electron screening, could strongly enhance DD-reaction product yield, even at these extremely low excitation energies.

The purpose of this present study is:

- To verify the hypothesis that excitation of the hydrogen subsystem in metal deuterides enhances DD reaction yield.

- To check feasibility of energetic alpha-particle emission under e-beam irradiation.

- To test a new triple CR-39 detector design in vacuum experiments, allowing charged particle identification

2. Experimental

Three plastic track (noiseless) CR-39 detectors are exposed to deuterated samples being excited by an electron beam. The CR-39 detectors were covered by Al and Cu foils with known stopping ranges (this arrangement can be considered as the simplest dE-E detector without time converter), see Fig.1. The Foreground counts are read out from the CR-39 surface of the detectors facing the sample. The Background counts are read from the rear sides of these same detectors that face either the vacuum chamber or the stainless steel support. The sample-detector holder assembly is mounted in the SEM vacuum chamber (p = 10^{-6} torr) and irradiated by a collimated electron beam (J = 100-300 nA, E = 30 keV). The desorbed deuterium and generated charged particles reach the detectors from the spot produced by e-beam, area S = 8x6 mm^2. The effective distance between the center of the spot and the detectors 1 and 2 is about <R$_{eff}$> = 12 mm.
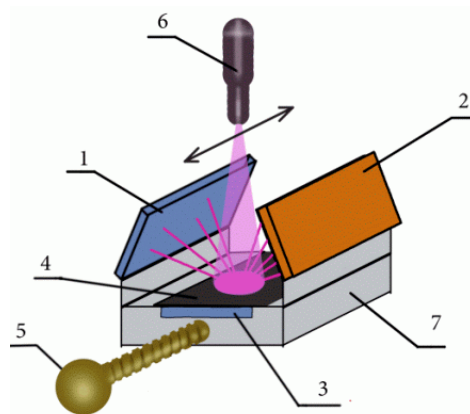
Fig.1. - 1,2 and 3 – are the CR-39 detectors covered with the 11 μm Al (1), 25 μm Cu (2) and 33 μm Al (3) foils, respectively, 4 –deuterated sample, 5-manipulator, 6-electron gun, 7- stainless support

The Landauer CR-39 detectors (2x1 cm^2) with initial total track density (N ≤ 20 cm^{-2}) were calibrated using a Van De Graaf accelerator (normal incidence protons beams with the energy ranging from 0.6 – 3.0 MeV), a cyclotron α-beam (11 – 30 MeV) and with alpha sources. Calibration functions, track diameter vs. particle energy, were obtained for various CR-39 etching times (Fig.2) or equivalently, depths. Special calibration of CR-39 detectors in a four detector experimental series has also been carried out using extended Pu-238 alpha source placed at the sample position. The calibration showed that overall efficiency of the detectors 1 and 2 is ε = 2.6 %, while the efficiency of the detector #3 is of ~ 8.0 %. Note in these experiments more than 80 % of alpha tracks detected by detectors 1 and 2 have normal incidence.

In reference experiments without e-beam stimulation two CR-39 detectors (no metal cover and one covered with 25 μm Cu) were used to obtain background levels in the SEM.
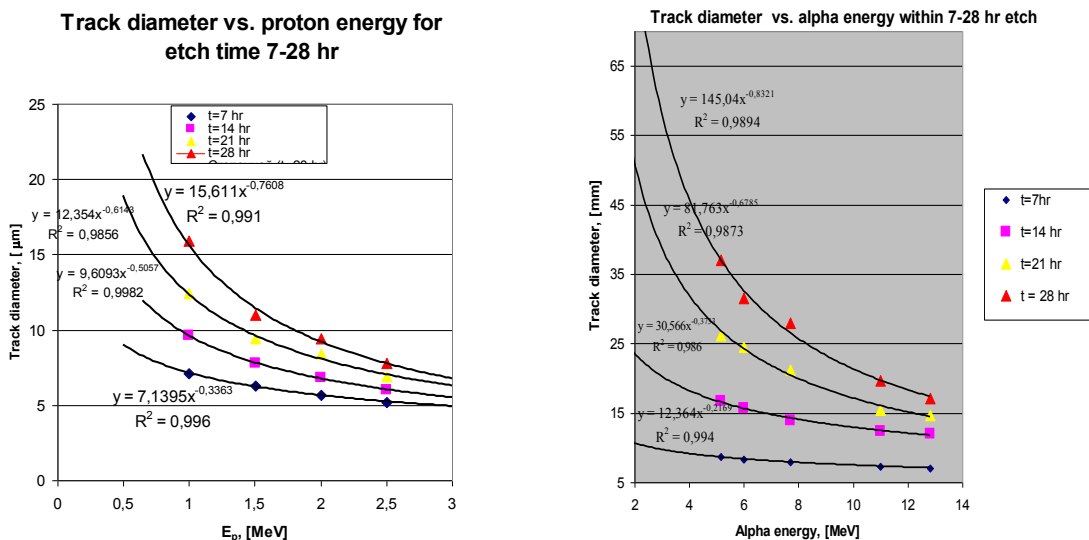

Fig.2. - Landauer CR-39 track diameter vs. charged particle energy (accelerator calibration data) for protons (left) and alphas (right) of normal incidence at various etching time (etching conditions: 6 N NaOH at t = 70°C)

The PdO/Pd/PdO samples are prepared by thermal oxidation of Nilaco (Japan) Pd foil (99.95 % purity), 50 µm thick with area S = 30 x 10 mm². Electrochemical loading uses 0.3M-LiOD solution in D_2O with Pt anode; j = 10 mA/cm² T ~ 280 K (below room temperature) in a special electrolytic cell with separated cathode and anodic spaces. (x =D/Pd ~ 0.73, about 40 min is required). The samples are rinsed in pure D_2O and then placed in liquid nitrogen in a Dewar flask to cool to T =77 K. The cooled samples are rapidly mounted (during 1 min) in the sample holder, Fig. 1, with a set of CR-39's and irradiated by the e-beam (E = 30 kV, J=0.2-0.6 µA/cm²).
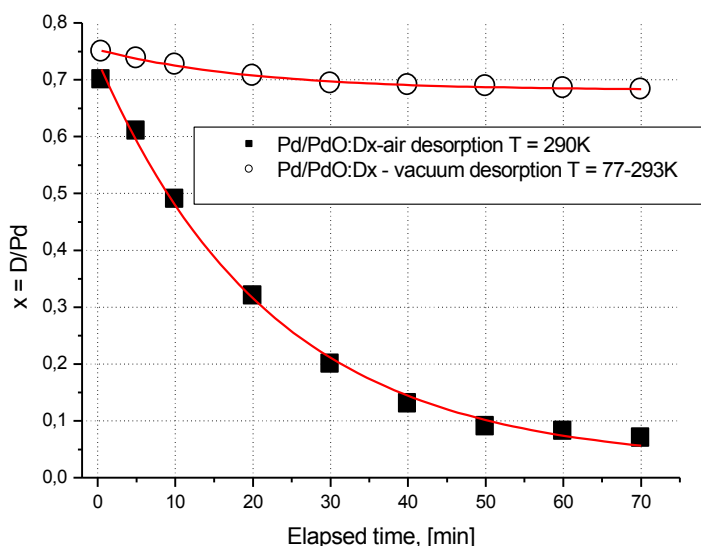
Fig.3. - D-desorption rate from the Pd/PdO:Dx samples in vacuum (electrolysis at T=280 K with cooling down to T = 77K after electrolysis termination)) and in air at ambient conditions (electrolysis at T=290K). Notice very low D-desorption rate in vacuum

D-desorption from the Pd/PdO:D_x sample in vacuum without e-beam excitation and in air are shown in Fig. 3. Under e-beam excitation the desorption rate is J_D ~ 3.3 x 10^{15} D/s-cm². This desorption rate is consistent with the rate of D-desorption in air at ambient conditions (~ 2-3x 10^{15} D/s-cm²). Results of Rutherford Back Scattering/Elastic Recoil Detection (alphas E_α = 2.2 MeV, depth 2 µm) (RBS/ERD profiles) of samples are presented in Fig.4.
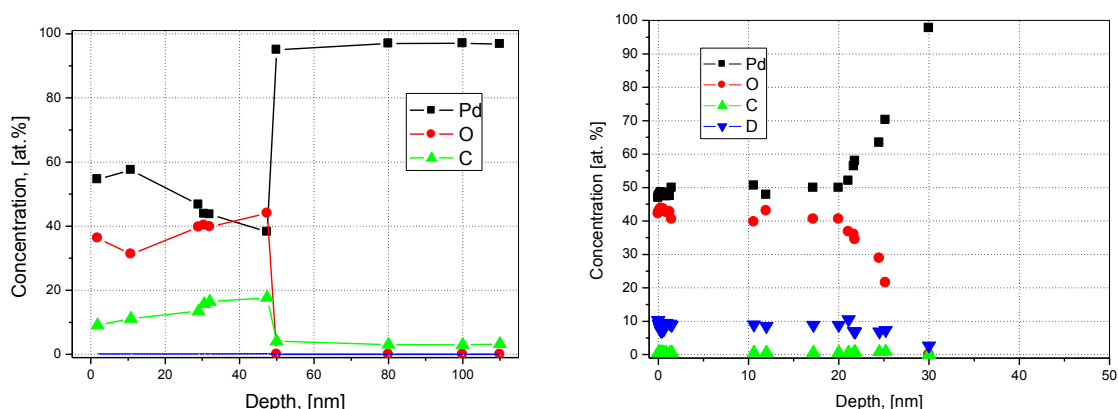
Fig.4. - RBS/ERD profiles of the Pd/PdO samples prior to D-loading –left; after electrochemical loading and D-desorption in vacuum during 50 min of e –beam (J=0.6 µA/cm2 U = 30 kV) treatment – right

After 50 min of e-beam bombardment some moderate reduction of PdO and carbon layers is observed (from 40 to 25 nm). The residual D is located within the PdO layer. SEM measurements show that e-beam bombardment

is accompanied by formation of numerous pores (from Pd through the PdO) with diameters in the range of 100 – 2000 nm (see Fig. 5). These larger diameter pores ($\varnothing > 350$ nm) have not been found in the "blank" $Pd/PdO:H_x$ samples after e-beam. Large craters with the $\varnothing \sim 10{,}000\text{-}12{,}000$ nm are also present at the $Pd/PdO:D_x$ surface after e-beam treatment.
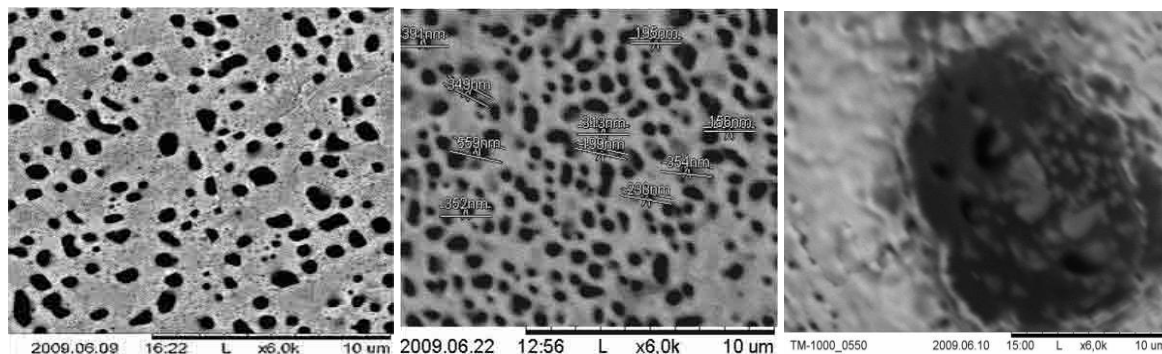
Fig.5. - SEM $Pd/PdO:D_x$-left and $Pd/PdO:H_x$-center images after electrolysis + e-beam. Notice larger diameter pore generation in $Pd/PdO:D_x$. Example of the $\sim 12{,}000$ nm diameter "crater" at the $Pd/PdO:D_x$ surface after e-beam bombardment (right).

TiD_x samples were prepared as follows. The Ti foils, 30 and 300 μm thick, have been loaded in 1M solution of D_2SO_4 in D_2O during t = 35 hr at J = 30 mA/cm^2, in order to dissolve the TiO_2 oxide layer at the Ti-surface and to provide D-penetration. The average loading (x = D/Ti = 0.1 at depth of 2-3 μm) has been determined by weight balance. The D-desorption rate for $TiD_{0.1}$, from weighing before and after e-beam irradiation, is consistent with the $J_D \sim 2.0 \times 10^{14}$ D/s-cm^2. All desorbed deuterons in TiD are released by e-beam irradiation energy, since the chemical compound is absolutely stable at T = 300 K. RBS/ERD profiles of the TiD_x samples prior to e-beam bombardment –left; after D-desorption in vacuum during 60 min of e –beam are presented in Fig.6.

RBS data taken before e-beam treatment show the presence of a TiO_2 oxide layer at the surface down to 150 nm. After e-beam excitation the stoichiometry of the Ti oxide changes toward reduction of oxygen ($TiO_{0.1}$). The O-depth does not change. The X-ray spectrum shows almost complete oxide reduction. Estimates of D-desorption rate from TiD_x using RBS data before and after e-beam gives v(D) = 1.5×10^{14} D/s-cm^2, which is 20 times lower than v(D) in $Pd/PdO:D_x$. The pore size is very small. Some large diameter craters ($\varnothing > 10$ μm) appear at the TiD_x surface after both e-beam and X-ray irradiation.

2. Charged Particle Detection and Identification

Background measurements show that there are no proton and alpha emission effects without e-beam stimulation (see Fig's. 7 and 8).

Cumulative results with Background subtracted for 4 series of runs (total time of e-beam exposure = 3300 min) are presented in Fig. 9. Peak positions are shifted with increasing of shielding thickness. Left peak is accompanied with 3-MeV protons, other peaks – with alpha-particles with energies 10 – 20 MeV.

Reproducibility of results is illustrated by Fig.10: The number of counts in the 3 MeV peak is roughly proportional to the cumulative exposure time of detectors 1 and 2 to $Pd/PdO:D_x$ samples under e-beam.
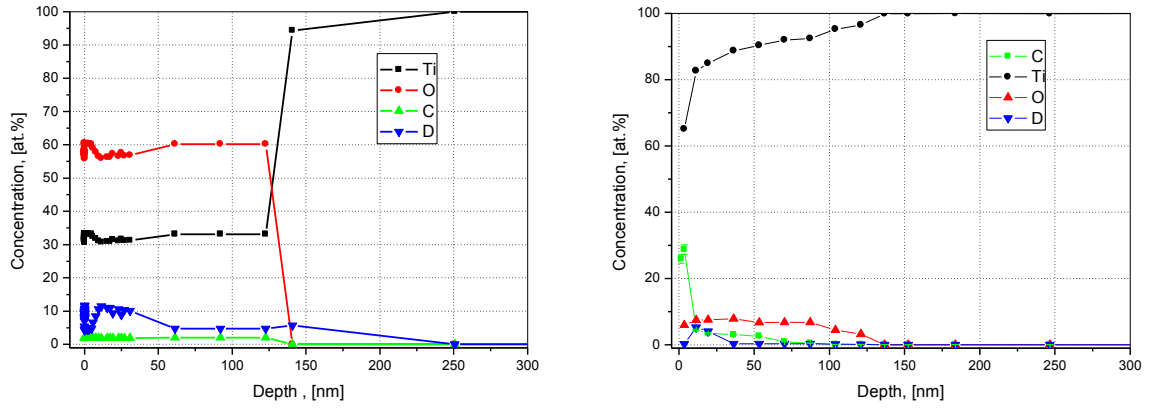
Fig.6. - RBS/ERD profiles of the TiD$_x$ samples prior to e-beam bombardment –left; after D-desorption in vacuum during 60 min of e –beam (J=0.6 µA/cm^2 U = 30 kV) treatment - right
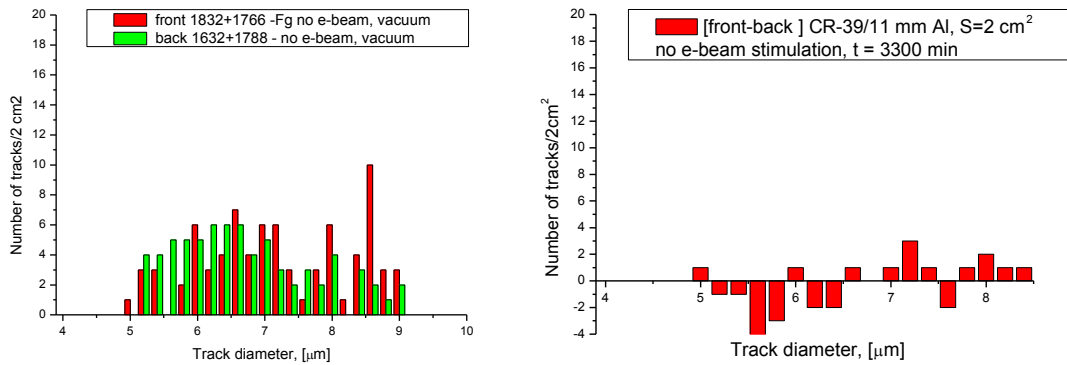
Fig.7. - Track diameter distributions for Pd/PdO:D$_x$ without e-beam stimulation: no proton and alpha effects: CR-39/11µm Al filter (4 samples, t = 3300 min). Front and back sides of detector (left). Difference of front and back sides of detector (right).
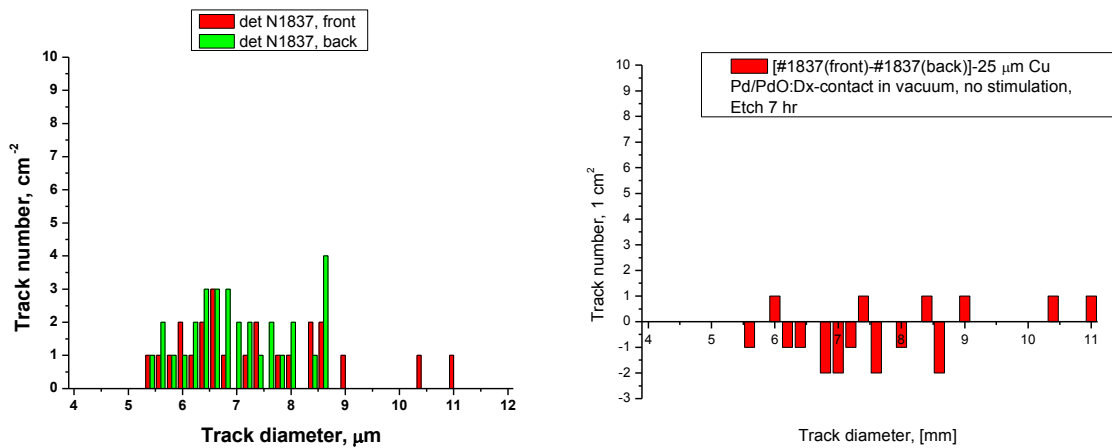
Fig.8. - Track diameter distributions for Pd/PdO:Dx without e-beam stimulation: no proton and alpha effects: 25 µm Cu covered CR-39 (4 samples, t = 3300 min). Front and back sides of detector (left). Difference of front and back sides of detector (right).
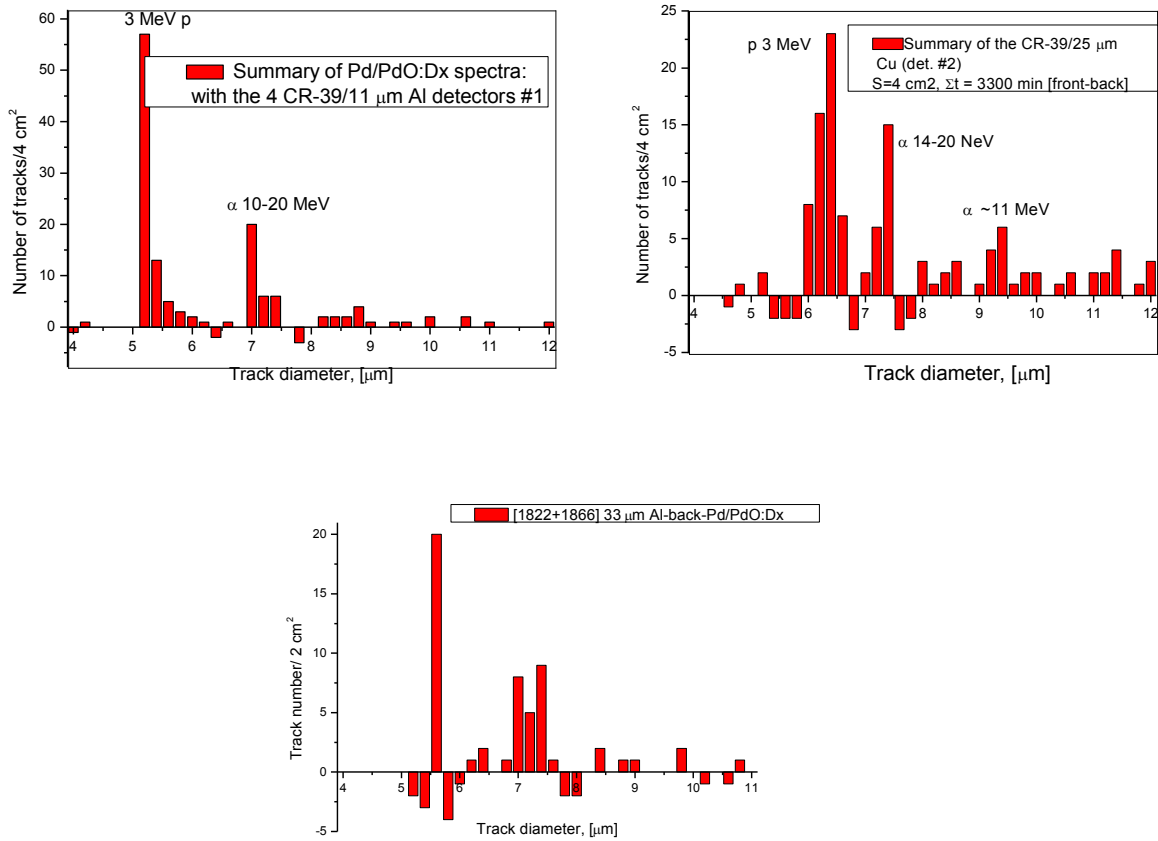
Fig. 9. - Total result with Background subtracted: Sums for 4 series of runs ($\Sigma t = 66\times50$ min, S=4 cm^2 for #1 and #2): (11µm Al)- left; (25µm Cu)- right; the det. #3-below: S=2 cm^2, t = 1800 min(33 µm Al). Notice shift of 3 MeV proton peak in these 3 detectors
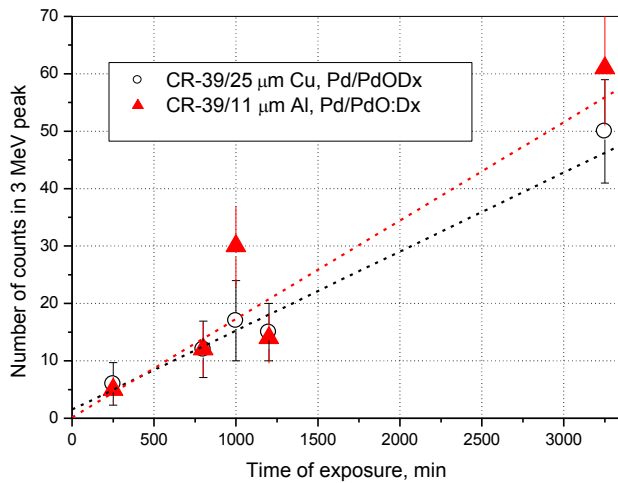
Fig. 10. - Reproducibility: The number of counts in 3 MeV peak is roughly proportional to the time of detectors 1 and 2 exposure with the Pd/PdO:D$_x$ samples under e-beam

Additional proof of the correctness of the identification and energy of observed charged particles is obtained by successive etching of the CR-39 detectors (Fig.11) and comparing the diameters at various depths with the calibration curves (Fig.2).
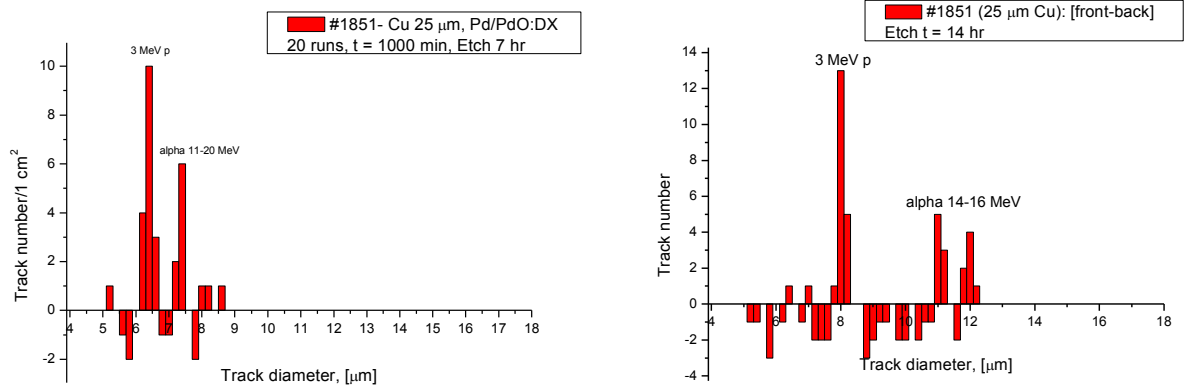
a)

b)
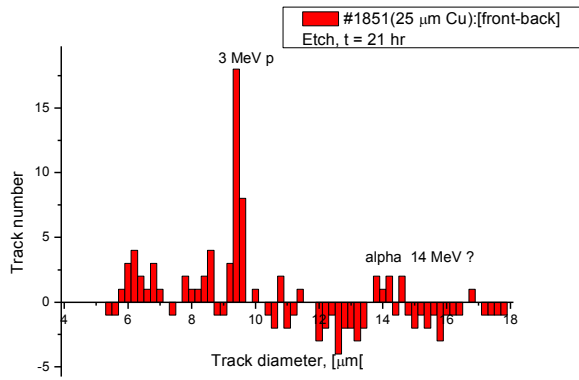
c)
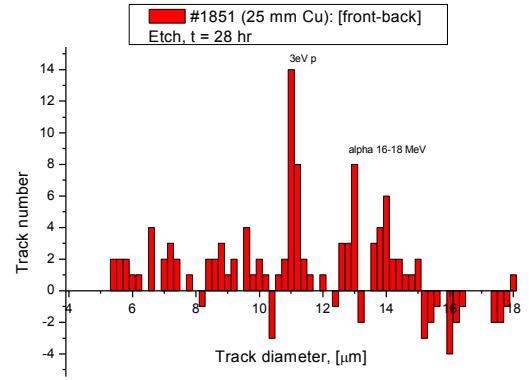
d)

Fig. 11. - Differential spectra (with the subtracting of the rear face results) of #1851 CR-39/25 μm Cu filtered detector #2 after its etching during 7 (a), 14(b), 21(c) and 28(d) hr.
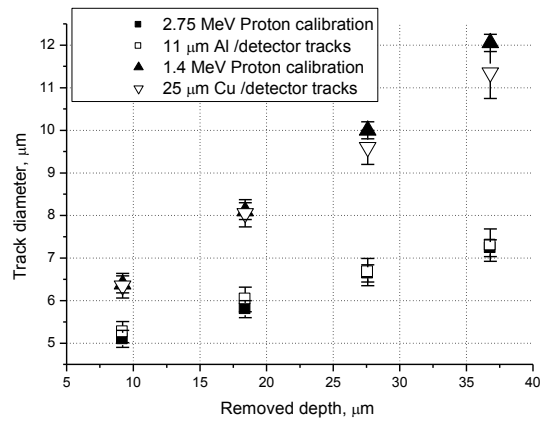
Fig. 12. - Track diameter vs. removed depth (d(h)) for "proton" tracks detected during sequential etching of the detectors 1 and 2, respectively.

Differential spectra (Foreground minus Background) of CR-39/25 μm Cu filtered detector #2 after etching during 7,14,21 and 28 h are presented in Fig.11. The same measurements were carried out for the 11 μm Al filtered detector (data not shown).

Fig. 12 presents the dependence of track diameters for proton-like tracks on removed depth. Note that in our etching conditions the bulk etch rate is $V_B = 1.3$ μm/h, and every 7 h we removed ~9.1 μm. The black squares and triangles represent the fit of experimental tracks from detectors 1 and 2 (empty squares and triangles, respectively) with d(h) functions obtained using normal incidence accelerator CR-39 bombardment at proton energies 2.75 (consistent with 3 MeV proton after its passage through 11 μm thick Al foil) and 1.4 (consistent with to 3 MeV proton after its passage through the 25 μm thick Cu foil) MeV, respectively. This provides additional evidence of stimulated emission of 3-MeV proton and energetic alpha particle emissions in $Pd/PdO:D_x$ samples.

Particle emission rates are estimated by averaging results from absorber covered CR-39 detectors (11 μm All and 25 μm Cu) with results:

- For 3 MeV protons: N_p= (1.12 ± 0.12) x 10^{-3} p/s-cm^2 of the $Pd/PdO:D_x$ sample (significance level, L ~ 10.0 σ). The yield of DD-reaction in the $Pd/PdO:D_x$ target under e-beam bombardment, taken only for movable deuterons) is found to be λ_{DD} ~ 6x10^{-19} p/DD-pair (4 orders of magnitude above the "Jones level").

- For 10-20 MeV alphas N_α = (0.46 ± 0.075) x 10^{-3} α/s-cm^2 of the $Pd/PdO:D_x$ sample, (significance level L ~ 6.0 σ).

- For the detector placed under the rare (non-irradiated by e-beam), position 3, side of the $Pd/PdO:D_x$ sample: N_p = (7.2 ± 1.6)x10^{-4} p/s-cm^2 and N_α = (4.3 ± 0.8) x 10^{-4} α/s-cm^2 of the $Pd/PdO:D_x$ sample.

Fig.13 presents the TiD_x e-beam stimulation results. Both statistically significant 3 MeV proton (5.2-5.4 μm track diameter) and 11-20 MeV alphas (7.0-7.6 μm track diameter) bands are found in the 11 μm Al covered detector (left); bands of 1.5 MeV protons (track diameter 6.0-6.6 μm, consistent with the 3 MeV proton losses in 25 μm Cu foil) and 14 MeV alphas (track diameter near 7.4 μm, consistent with ~ 17 MeV alpha losses in 25 μm Cu foil are detected (right). No statistically significant results have been found over all differential spectrum from the rare side of the TiD_x sample, position 3.
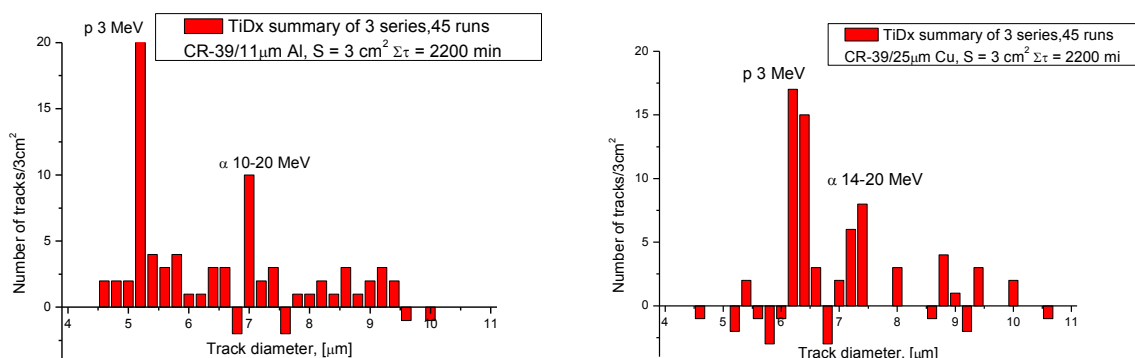
Fig.13. - TiDx e-beam stimulation results: total 42 runs of 60 min each: two CR-39 detectors [11 μm All (left) and 25 μm Cu (right)] with the Background (rear side) subtracting.

Average emission rates from foil covered CR-39 detectors (11 μm All and 25 μm Cu) for 3 MeV protons and energetic alphas in TiDx during 42 runs in 3 series (t = 2200 min) are:

• For 3 MeV protons: $<N_p> = (8.4 \pm 1.5) \times 10^{-4}$ p/s-cm^2 of TiD$_x$ sample (the significance level L = 5.6 σ). The yield of DD-reaction in the TiD$_x$ target under e-beam bombardment, taken only for movable deuterons) is found to be $\lambda_{DD} \sim 5\times10^{-18}$ p/DD-pair (6 orders of magnitude above the "Jones level").

• For 10-20 MeV alphas $<N_\alpha> = (4.7 \pm 1.0) \times 10^{-4}$ α/s-cm^2 of the TiD$_x$ sample, (the significance level L ∼ 4.5σ). The soft component of α (E ∼ 11 MeV) is not statistically significant from the non-irradiated by e-beam face of the TiD$_x$ sample.

4. Discussions

DD-reaction rate in the Pd/PdO:D$_x$

A simple model of the experiment will be used to estimate the DD-reaction rate in the Pd/PdO:D$_x$ target under electron bombardment. The e-beam stimulated D-desorption flux moving toward the Pd/PdO:D$_x$ surface will be treated as a low energy projectile or "deuteron beam". The deuterated surface of the Pd/PdO sample is treated as deuteratium "target". The deuteron (D$^+$) "current", is estimated from D-desorption rate, $J_d = 0.5$ mA/cm^2. The mean concentration of target is estimated from the mean D/Pd ratio during e-beam bombardment ($<x> \sim 0.15$ or $N_d = 1.1\times10^{22}$ cm^{-3}). The thick target yield I_{DD} is computed from:

$$I_{DD} = J_d N_{eff}(T) \times \int_0^{E_d} f(E)\sigma_{DD}(E)(dx/dE)dE$$

Here J_d – deuteron current density; $N_{eff}(T)$ – effective concentration of non-free D in metal at temperature T, captured at depth x: ($N_{eff}(T) = N_0 \exp(-\varepsilon_d \Delta T/k_B T T_0)$, where N_0 is the D concentration at $T_0 = 290$ K; f(E) – enhancement factor [f(E) = $Y_{exp}(E)/Y_b(E)$ = exp[ηπ(E)U$_e$/E]]; σ_{DD} – is the bare DD- cross-section; dE/dx – is the stopping power in target calculated with Monte-Carlo code SRIM [4].

The deuteron screening potential U$_e$ can be determine using the formula: U$_e$ = $(T/T_0)^{-1/2}$ [a ln(y) +b] [2] - an empirical equation obtained from the analysis of accelerator data for 70 elements of periodic Table (the data by Raiola et al [3]): where a = 145.3 and b=71.2 – are numerical constants; y = ky$_0$(J$_d$/J$_0$), with k = exp(-$\varepsilon_d \Delta T/k_B T T_0$), y$_0$ = Pd/D ratio at $T_0 = 290$ K, and $J_0 = 0.03$ mA/cm$^{2)}$. Substitution of $J_d = 0.5$ mA/cm^2, T=290 K and <Pd/D> = 6.7 in eq. for U$_e$ gives U$_e$ = 730±50 eV. This screening value falls roughly into the interval limited by Kasagi's (600 eV for Pd/PdO [5]) and Raiola's (800 eV for Pd [3])

The DD-reaction rate of ∼ 0.001 p/s-cm^2 in 4π ster. could be reached in the Pd/PdO:D$_x$ target (taking into account U$_e$ ∼ 730 eV) only if the mean kinetic energy of the desorbing deuterons is of the order of <E$_d$> ∼ 3-4 eV. In contrast, if the mean deuteron energy <E$_d$> ∼ kT, with the same U$_e$, the DD-reaction rate would be only ∼ 10^{-7} p/s-cm^2, or well below our detection limit. This result strongly supports the theoretical prediction [1] with regards to electron excitation of hydrogen subsystem in Pd deuteride (hot deuteron generation). The 3-4 eV deuteron flux claim serves as an evidence for the generation of a strong electric field (∼ 10^8 V/cm) on a scale of the lattice parameter (a$_0$ = 0.39 nm) due to plasmon formation in this experiment.

TiD$_x$ DD-reaction rate

Taking $J_d = 0.03$ mA/cm^2 and y$_0$ ∼ 2.0 (the surface D-concentration is x = D/Ti ∼ 0.3 during e-bombardment) one can obtain U$_e$ ∼ 130 eV. At this small screening potential, in order to produce DD-reaction rate of the order of ∼ 0.001 p/s-cm^2 , the kinetic energy of deuteron flux (in laboratory system) has to be rather higher (E$_d$ ∼ 500 eV). This high kinetic energy can be gained by D+ acceleration in a strong electric field created by electrostatic charging of the TiO$_2$ surface with e-beam. (E$_d$)$_{eff}$ = ε_0 + e E(TiO$_2$)x h(TiO$_2$). At ε_0 ∼ 3 eV (the initial kinetic energy of D+ in Ti caused by plasmon generation), E(TiO$_2$) ∼ 3.5×10^7 V/cm (electrical strength of TiO$_2$) and h(TiO$_2$) = 1.5×10^{-5} cm, the (E$_d$)$_{max}$ ∼ 500 eV(!!!) suggesting D+ acceleration by a strong electric field during deuteron drift and diffusion through the Ti oxide.

5. Conclusions

- The vacuum experiments with and without e-beam irradiation, lead to the conclusion that an electron beam ($J \sim 100\text{-}300$ nA, $E = 30$ keV) stimulus of the Pd and Ti deuterided targets (cathodes) surface can enhance the intensity of the emissions of nuclear charged particles.

- Both products of DD-reaction (3 MeV) protons and high energy alphas (11-20 MeV) are clearly identifiable in e-beam stimulation experiment with the $Pd/PdO:D_x$ and TiD_x targets.

- Signatures of 3 MeV protons and energetic alphas appear on the surface of all (2 or 3) independent detectors in the same experiment covered by metallic foil filters with different stopping ranges/powers.

- The data analysis on the $Pd/PdO:D_x$ target supports reasonable estimates of DD-reaction cross sections and the enhancement factors to a very low deuteron energy ($Ed \sim 3.0$ eV). Extrapolation of DD-reaction cross section and the enhancement factor with a reasonable screening potential $U_e = 730$ eV, satisfactorily accounts for the detected DD-reaction rate in these experiments. This calculation and the underlying data strongly support the theoretical prediction [1] with regard to electron excitation of hydrogen subsystem in Pd deuteride.

- In order to enhance charged particle yield, we plan to vary target deuterides, as well as the current and energy of electron beam. These optimization studies will bring understanding of the possible technological value of e-beam and other excitation.

- More work also should be done with respect to the energy spectra characterization and the origin of the energetic alpha emission.

6. References

[1]. V.M., Silkin, I.P Chernov et al, Phys. Rev., B **76**, 245105 (2007)

[2]. A. Lipson et al, High Energy Chem. **42**(4), 319 (2008)

[3]. F. Raiola et al, Europhys. J., A**19**, 283 (2004)

[4]. J.F. Ziegler and J.P. Biersack, code SRIM 2003

[5]. Yuki H., Kasagi J., Lipson A. G. et al // JETP Lett. 1998. v. **68**(11). p. 785-790.

Enhanced Electron Screening and Nuclear Mechanism of Cold Fusion

K. Czerski

Institute of Physics, University of Szczecin, ul. Wielkopolska 15, 70-451 Szczecin, Poland

Abstract: The enhanced electron screening effect observed in accelerator experiments for the ^{2}H(d,p)^{3}H and ^{2}H(d,n)^{3}He reaction in deuterized metallic targets may be a breakthrough in understanding the phenomenon of cold fusion. The dielectric function theory enables an extrapolation of experimental cross sections determined at higher energies down to room temperature, leading to an enhancement of the fusion reaction rates by a factor of 10^{40} compared to the value predicted for the deuterium molecule. An additional enhancement can be obtained due to a 0^+ resonance which should exist in the compound nucleus ^{4}He very close to the D-D reaction threshold. Combination of both processes offers a simple explanation of high penetration probability through the Coulomb barrier and the reaction branching ratio preferring the ^{4}He channel in heavy-water electrolysis experiments.

1. Introduction

Observation of a heat excess [1] and neutron emission [2] in the first heavy-water electrolysis experiments in 1989 seemed to be in contradiction to laws of nuclear physics. A simple calculation of the penetration factor through the Coulomb barrier at room temperature [3] gave reaction rates for the d+d fusion reactions being a factor of 10^{50} smaller than the rates needed for explanation the experimental results. On the other hand, the observed neutron emission should be about a factor of 10^7 weaker than a reaction channel responsible for the heat production and clearly correlated to the fusion of the ^{4}He nucleus [4]. Thus, the reaction branching ratios at room temperature completely contradict the experimental results obtained by means of the accelerator technique at deuteron energies of a few keV for which the mirror stripping reactions ^{2}H(d,p)^{3}H and ^{2}H(d,n)^{3}He, being equally probable, dominate by a factor $>10^6$ the electromagnetic transition ^{2}H(d,γ)^{4}He. Reproducibility of the cold fusion experiments has been highly increased in the last decade [5,6] and some important experimental conditions, under which the heat production takes place, has been found [7,8]. Nevertheless, a lack of reliable nuclear theory explaining at least some of the room temperature effects leads to an ongoing scepticism in the scientific community. Therefore, finding of the enhanced electron screening effect in metallic targets for the d+d stripping reactions [9], and similar observations of other groups [10-13] can play a key role in understanding of the cold fusion phenomenon. Screening of charges of the reacting nuclei by surrounding electrons in metallic environments increases the Coulomb barrier penetrability and results in an exponential-like enhancement of the cross sections compared to those measured for a gas target. That effect cannot explain, however, the change of branching ratios for the d+d reaction at room temperature and domination of the ^{4}He reaction channel. A simple mechanism of a single particle resonance located very close to the D+D reaction threshold in the compound nucleus ^{4}He will be presented here. Combination of the electron screening effect and the resonant process can explain most of the observed phenomena usually connected to the cold fusion and the heat excess production in heavy-water electrolysis experiments.

2. Enhanced electron screening effect

Electron screening effect can be described by a screening length *a* that corresponds to a distance from which the nuclear charges (ions) embedded in an electron gas can be treated as neutral. For strongly coupled plasmas where the average Coulomb potential energy between ions is larger than their kinetic energy, the screening length does not depend on the temperature and is of order of the Wigner-Seitz radius

$$a_{WS} = \left(\frac{3Z}{4\pi\, n_e} \right)^{1/3} \tag{1}$$

where Z and n_e are the ion charge and the density of free electrons, respectively. Dense astrophysical plasmas of White and Brown Dwarfs or of Giant Planets [14] are very good examples for strongly coupled plasmas.

Similarly, deuterons moving in metallic environments can also be considered using plasma physics methods. For the simple Bohr screening, the screened Coulomb potential energy between two reacting deuterons can be presented as follows

$$V(r) \;=\; \frac{e^2}{r}\,\exp\!\left(-\frac{r}{a}\right) \;\approx\; \frac{e^2}{r} \;-\; \frac{e^2}{a} \tag{2}$$

Now the screening length a is of order of the Bohr radius. For projectile energies used in accelerator experiments where $r \ll a$, the deuteron-deuteron potential can be simply described as the Coulomb potential reduced by a constant, the screening energy $U_e = e^2/a$. Thus, the "screened" cross section dependent on the penetration factor through the Coulomb barrier P corrected for the electron screening, can be expressed by the only weakly on energy dependent astrophysical S-factor

$$\sigma_{scr}(E_{cm}) \;=\; \frac{1}{\sqrt{E_{cm}(E_{cm}+U_e)}}\; S(E_{cm})\;\exp\!\left(-\sqrt{\frac{E_G}{E_{cm}+U_e}}\right) \tag{3}$$
$$=\; \frac{1}{\sqrt{E_{cm}E_G}}\; S(E_{cm})\;P(E_{cm}+U_e)$$

Here E_{cm} denotes the energy in the center of mass system and E_G is the Gamow energy defined as follows:

$$E_G \;=\; 2\mu\pi^2\,\frac{(Z_1 Z_2)^2 e^2}{\hbar^2}$$

where Z_1 and Z_2 are the charges of reacting nuclei and μ stays for the reduced mass. The screening energy U_e corresponds to a reduction of the Coulomb barrier height in the expression for the penetration factor. In comparison to the bare nuclei, the cross section for reactions in metallic environments exponentially increases for decreasing projectile energies, whereby U_e can be taken from fits to the experimental data. The U_e values determined in our experiments for C, Al, Zr, Pd and Ta targets are depicted in Fig. 1. For heavier metals the screening energy amounts to about 300 eV that is one order of magnitude larger than the value 25±5 eV obtained in the gas target experiment [15].
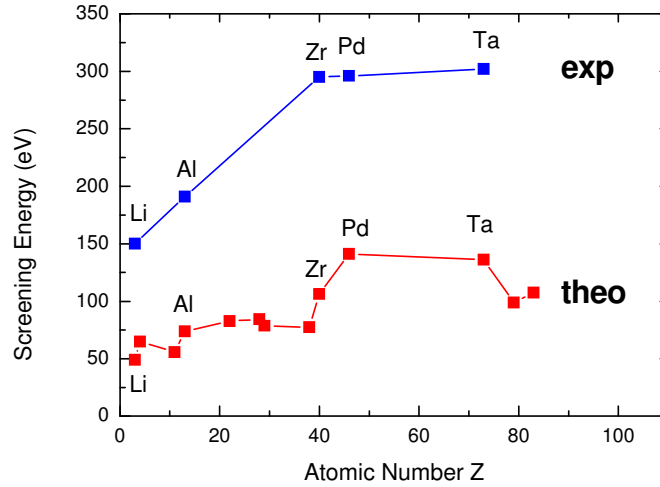
Fig. 1. - Experimental and theoretical electron screening energies obtained for C, Al, Zr, Pd and Ta targets.

The screening effect in metals can be described within the self-consistent dielectric function theory [9]. It enables to treat the electron screening as a static polarization of the metallic medium induced by the positively charged deuterons. The screened Coulomb potential $V(r)$ is a solution of the Poisson equation and can be expressed as a Fourier transform

$$V(r) = \frac{e^2}{r} \ \Phi(r) \ = \frac{1}{(2\pi)^3} \int \frac{4\pi \ e\varphi_1(q) \ e\varphi_2(q)}{\varepsilon_v(q) \ \varepsilon_c(q) \ q^2} \ \exp(i\vec{q}\vec{r}) \ d^3q \tag{4}$$

The wave-number dependent dielectric functions ε_v and ε_c describe polarization of valence and core electrons of host atoms induced by a charged impurity. $\Phi(r)$ and $\varphi_i(q)$ functions are the screening function and electronic charge-form factors of reacting nuclei, respectively (for details see [9,18]). Additionally, the cohesion screening contribution arising from the difference in binding energies between two reacting deuterons and the compound nucleus ^{4}He in the crystal lattice has to be included [9]. The theoretical calculations describe the observed material dependence of the screening energy qualitatively correctly (see Fig. 1). The main contribution to the theoretical values is provided by polarization of the free valence electrons, although the contribution of bound electrons (core polarization) and the cohesion screening cannot be neglected. However, the absolute values of the theoretically calculated U_e fail by a factor of about two. No reason for such a large discrepancy between theoretical and experimental values has been found so far. Recent experiments carried out under ultra high vacuum conditions [16,17] show that this discrepancy can be even larger. On the other hand, since the experimental screening energies obtained for insulating materials are rather small (<50eV) [12,13] we can conclude that the large screening energies should result from conduction electrons.

An independent test of the enhanced screening effect can be obtained by study alpha radioactive decays in different insulating and metallic environments. Higher screening energies for metallic environments result in a slight decrease of life times of alpha decays [17,20].

3. Nuclear reactions at room temperature

Since the astrophysical S-factors for fusion reactions are usually known down to lowest projectile energies the only uncertainty of nuclear reaction rates at room temperature results from the screening energy U_e. However, the screening energy as defined in Eq.(2) loses its physical sense for the closest approach distances comparable with the screening length a. That corresponds to projectile energies comparable or smaller than the value e^2/a. Thus, in order to apply Eq.(3) for calculation of the reaction cross section at room temperature, we have to replace U_e by an energy-dependent effective screening energy U_{eff}. Similar to U_e, the effective screening energy can be still interpreted as an appropriate reduction of the bare Coulomb barrier which should match to the penetration through the screened Coulomb potential. Therefore, U_{eff} has to be calculated from a condition setting equal the penetration factors as applied in Eq.(2) and that obtained within the WKB approximation with the screened potential $V(r)$:

$$\sqrt{\frac{E_G}{E_{cm}+U_{eff}}} \ \exp\left(-\sqrt{\frac{E_G}{E_{cm}+U_{eff}}}\right) \ = \ \exp\left(-\frac{2\sqrt{M}}{\hbar} \int_{R_1}^{R_2} \sqrt{V(r)-E_{cm}} \, dr\right) \tag{5}$$

Here R_1 and R_2 are the classical turning points in the WKB expression, and M is the deuteron mass. The results of calculations for Pd are presented in Fig.2. There are two well defined limits: at the high energy (E_{cm}>1 keV) and at the low energy (E_{cm}<10 eV). The ratio between the low-energy and the high-energy U_{eff} value amounts to about 0.58, being nearly independent of the actual deuteron-deuteron potential. Additionally, the cohesion screening energy has to be added leading to the total screening energy at the zero projectile energy U_0 that is equal to about 0.78 of the high-energy limit U_e [9].

At deuteron energies below 10 eV, the effective screening energy remains almost constant, hence the expression for the cross section takes a very simple form. Starting from Eq.(3) we obtain

$$\sigma_{scr}(E_{cm}) \cong \frac{1}{\sqrt{U_0 E_{cm}}} S_0 \exp\left(-\sqrt{\frac{E_G}{U_0}}\right) \ \propto \frac{1}{\sqrt{E_{cm}}} \qquad \text{for} \qquad E_{cm} \to 0 \tag{6}$$

where U_0 and S_0 are the screening energy and the S-factor taken at the projectile energy zero, respectively. Surprisingly, the cross section increases at low energies as the barrier-penetration factor stays constant and the wave-length dependence dominates [9]. The same expression is also valid for other nuclear reactions at room

temperature. Taking into account that the U_e for the deuteron stripping reaction ^{2}H(d,p)^{3}H amounts to about 500 eV [17] (U_0=360eV), the reaction cross section at room temperature reaches value σ_{scr}=10^{-15} b which is comparable with the cross sections for nuclear transitions induced by the weak interactions. It means that the fusion reaction at room temperature should be measurable by use a suitable experimental set-up.

For the electrolysis experiments, a very useful quantity that can experimentally be determined is the nuclear reaction rate defined here without number densities of involved nuclei as follows

$$R_{scr}(E_{cm}) = \sigma_{scr}(E_{cm})v_{rel} = \sigma_{scr}(E_{cm})\sqrt{\frac{2E_{cm}}{\mu}} \cong \frac{\sqrt{2}S_0}{\sqrt{\mu U_0}}\exp\left(-\sqrt{\frac{E_G}{U_0}}\right) \qquad (7)$$

Here v_{rel} is the relative velocity between the reacting nuclei and μ denotes the reduced mass. Due to the energy dependence of the cross section at very low energies (see Eq.(6)), the reaction rate depends only on U_0 and not on E_{cm}. Therefore, no assumption about the distribution of the deuteron velocity at room temperature is necessary.

Nuclear reaction rates at room temperature very strongly depend on both the Gamow and screening energies. In order to illustrate it we compare the nuclear reaction rates of three fusion reactions between hydrogen isotopes for which the screening energy should be the same: ^{2}H(d,p)^{3}H, ^{2}H(p,γ)^{3}He and ^{3}H(p,γ)^{4}He. Without any electron screening contribution, the first reaction induced by nuclear forces ought to be much more probable than the others mediated by electromagnetic interaction, which is confirmed by large differences between the values of the astrophysical S-factors (see Table 1). However, as it was argued in the work of Koonin and Nauerberg [3], the small reduced masses in the channels p+d and p+t result in small Gamow energies, which consequently leads to an increase of reaction rates at very small projectile energies (see Fig. 2). Correspondingly, for small screening energies below 200 eV, the ^{2}H(p,γ)^{3}He reaction is the most probable reaction at room temperature. However, if the screening energies would be higher the ^{2}H(d,p)^{3}H reaction dominates. Its reaction rate will be for U_0=360 eV by a factor of about 10^3 larger than the values for the other reactions. On the other hand, this relatively large screening energy can provide the neutron production rate in the ^{2}H(d,n)^{3}He reaction of about 10^{-15} neutrons per deuteron pair and second. This is above the neutron production rate estimated in the experiment of Jones et al. [2] but significantly below the nuclear reaction rates necessary for explanation of the heat excess observed in the experiment of Fleischmann and Pones [1].

4. D-D threshold resonance

The observation of the excess heat production is probably connected to the fusion of ^{4}He [4] with the rate by about a factor of 10^7 larger than the neutron emission. Thus, beside the screening effect an additional phenomenon changing the branching ratios and increasing the reaction rates at room temperature should obviously exist. Alteration of the branching ratio by a factor of 10^7 might be achieved within the classical nuclear physics without any exceptional mechanisms. An example for such an approach could be a narrow resonance in the ^{4}He nucleus lying close to the d+d reaction threshold. Supposing a nearly single-particle width of this resonance for the deuteron channel and simultaneous quenching of the nucleon decay channels, one can explain major experimental results concerning the cold fusion. The deuteron width of the resonance can be expressed by the R-Matrix formula

Table 1. Astrophysical S-factors, Gamow energies and reduced masses for three different fusion reactions between hydrogen isotopes.

Reaction	d + d → t + p	p + d → ^{3}He + γ	p + t → ^{4}He + γ
S_0 (keV barn)	55.5	2.5·10^{-4}	2.6·10^{-3}
E_G (keV)	986.3	657.7	739.7
μ (amu)	1.00728	0.67141	0.75506
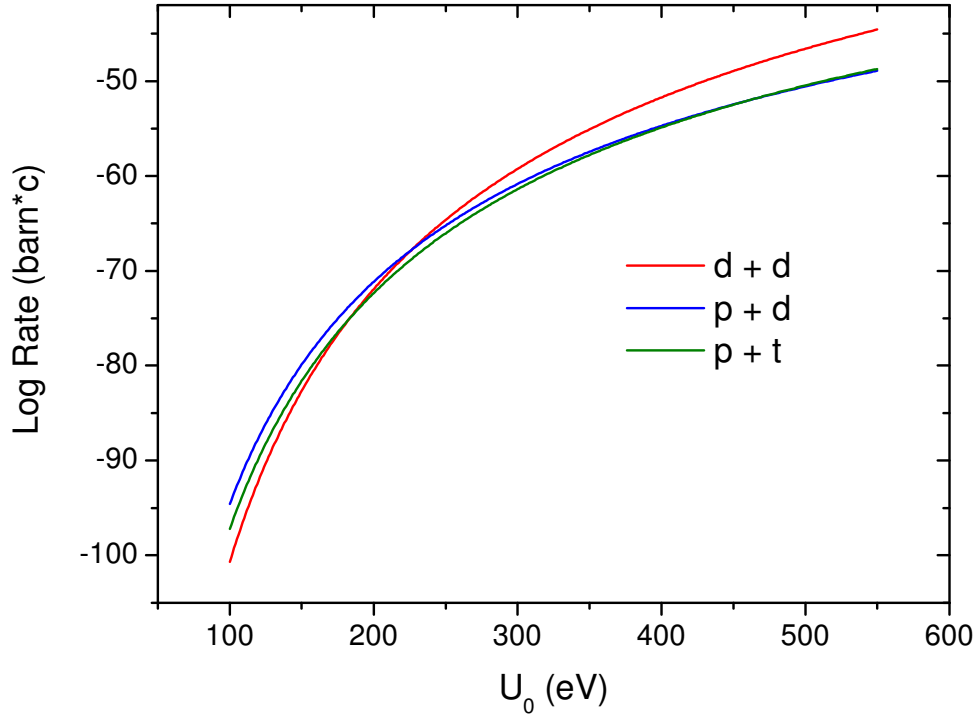
Fig. 2. - Nuclear reaction rates for three different fusion reactions in dependence of the electron screening energy U_0 (presented in log scale).

$$\Gamma_d = 2P_d \frac{3\hbar^2}{2\mu\ a_d} |\theta_d|^2 \tag{8}$$

where P_d, μ and a_d are the penetration factor, the reduced mass and the channel radius for the d+d channel, respectively, and $|\theta_d|^2$ denotes the dimensionless reduced resonance width. Since the total resonance width Γ is assumed to be dominated by the deuteron width ($\Gamma \approx \Gamma_d$), its value will drop for low sub-Coulomb deuteron energies very rapidly with decreasing penetration factor. On the other hand, the resonance strength, observed for instance for the proton decay channel, is given by the ratio $\Gamma_d\Gamma_p/\Gamma$ and should be independent of the resonance energy if we take into account that the proton width Γ_p remains nearly constant. Thus, the height of the single particle resonance ($\sim \Gamma_d\Gamma_p/\Gamma^2 \approx 1/\Gamma_d$) strongly increases as the resonance energy decreases – we speak about so-called narrowing of the single particle resonance. For the resonance energy of about 10 eV, the resonance width would be of a few eV and its height would raise by a factor larger than 10^6. Furthermore, the hypothetical resonance could change the reaction branching ratios within the resonance width in favour of those supposed for the cold fusion. The 0^+ assessment of spin and parity of this resonance makes forbidden its gamma decay to the ground state being also 0^+ in agreement with heavy-water electrolysis experiments where no gamma emission has been observed. Due to the single particle nature of this resonance, the neutron and proton decay channels should be negligible compared to the d+d partial width. Therefore, the decay of the resonance can only take place by non-radiative electromagnetic channels as the internal pair creation, the electron conversion or in the process we call the deuteron conversion where the energy excess of the compound nucleus ^{4}He of about 24 MeV will be transferred to a neighbouring deuteron. Decay probabilities of non-radiative channels leading to a direct fusion of ^{4}He in metallic environments will be discuss in a separated paper [19].

The small width of the supposed resonance would also explain the problems connected to the reproducibility of cold fusion experiments. Small local changes of the lattice structure can vary the resonance energy by e few eV due to alteration of the screening energy as already determined for alpha decays [17]. Thus, dependently on local crystal defects, the deuteron density and other target material parameters that are not usually controlled in the experiments, the ^{4}He fusion cross section can be resonant or not and consequently we could observe an enhanced production of helium by many orders of magnitude only at special material conditions.

5. Conclusions

We have shown that the electron screening effect plays a crucial role for room temperature nuclear reactions. The enhancement factor of the nuclear reactions due to electron screening is material dependent and reaches at room temperature for heavy metals a factor of about 10^{40} compared to the cross sections calculated for the gaseous deuterium [3]. The electron screening effect makes possible to observe experimentally also other reactions between hydrogen isotopes using an appreciate set-up (see Table 1). Contradictory to previous calculations, the ^{2}H(d,n)^{3}He and ^{2}H(d,p)^{3}H reactions should still have the largest cross sections at room temperature. The corresponding reaction rates are in agreement with small amounts of ^{3}H and ^{3}He found in the heavy-water electrolysis experiments.

Domination of the ^{4}He channel by a factor of about 10^7 over other open channels in experiments where a heat excess has been measured can be explained by a 0^+ single particle resonance placed in the compound nucleus very close to the reaction threshold. De-excitation of this resonance state should only take place by non-radiative electromagnetic channels that are very difficult to detect experimentally. Furthermore, an interplay between the electron screening effect that strength depends on local crystal structure of the target material and the resonance reaction mechanisms is able to clarify difficulties with regard to a bad reproducibility of the cold fusion experiments. Crystal defects or changes of local deuteron density can shift the resonance energy even by a few eV resulting in the non-resonant reaction mechanism and suppression of the ^{4}He fusion channel. Thus, controlling of the microscopic structure of target materials in future cold fusion experiments ought to be very important.

On the other hand, a material enabling large fusion rates at room temperature should also ensure a high deuteron density and a relatively low deuteron binding energy in the lattice. The latter condition is necessary in order to reach large deuteron mobility, which further increases the reaction probability by many orders of magnitude. Therefore, Pd still seems to be an ideal material for study nuclear reactions at room temperature.

References

[1]. M. Fleischmann, S. Pons and M. Hawkins, J. Electroanal. Chem. 261 (1989) 301
[2]. S.E. Jones et al., Nature 338 (1989) 737
[3]. S.E. Koonin and M. Nauenberg, Nature 339 (1989) 690
[4]. A. De Ninno et al., Proceedings of the ICCF-10, Massachusetts 2003, Cambridge
[5]. S. Szpak and P.A. Mosier-Boss (ed.), Technical Report 1862, Office of Naval Research, San Diego, California, 2002
[6]. M.C.H. McKubre, Proceedings of the ICCF-10, Massachusetts 2003, Cambridge
[7]. M.C.H. McKubre and F.L. Tanzella, Proceedings of the ICCF-7, Vancouver, Canada, 1998
[8]. K. Czerski, A. Huke, A. Biller, P. Heide, M. Hoeft and G. Ruprecht, Europhys. Lett. 54 (2001) 449; Proceedings of the International Conference on Nuclear Asrophysics "Nuclei in the Cosmos", July 6-11, 1998 Volos, Greece, edited by N. Prantzos and S. Harissopulos (Editions Frontières), p. 152
[9]. K. Czerski, A. Huke, P. Heide, G. Ruprecht, Europhys. Lett. (2004)
[10]. H. Yuki et al. JETP Lett. 68 (1988) 823
[11]. J. Kasagi et al., J. Phys. Soc. Jpn. 71 (2002) 2281
[12]. F. Raiola et al., Eur. Phys. J. A 13 (2002) 377
[13]. F. Raiola et al., Eur. Phys. J. A 547 (2004) 193
[14]. S. Ichimaru, Rev. Mod. Phys. 65 (1993) 252
[15]. U. Greife et al., Z. Phys. A 351 (1995) 107
[16]. K. Czerski, A. Huke, L Martin, N. Targosz, D. Blauth, A. Górska, P. Heide, H. Winter, J. Phys. G, **35** (2008) 014012
[17]. K. Czerski, P. Heide, A. Huke, A.I. Kilic, I. Kulesza, N. Targosz-Ślęczka, Acta Physica Pol. B **40** (2009) 903
[18]. A. Huke et al., Phys. Rev. C 78 (2008) 015803
[19]. K. Czerski K. et al., to be published
[20]. H.B. Jeppesen et al., Eur. Phys. J. A32 (2007) 31

Investigation of Anomalous Densities of High-energy Alpha-Particles Tracks in CR-39 Detectors during Electrolysis of Heavy Water on Palladium Cathodes.

U. Mastromatteo, R. Aina
STMicroelectronics Srl, Cornaredo, MI

E-mail: ubaldo.mastromatteo@st.com

Abstract. Recently, several researchers claim the finding of anomalous alpha-particles generation during very simple electrolysis experiments with heavy water and palladium cathodes. The phenomenon seems to improve if deuterium formation on the cathode is associated with deposition of palladium nanostructures coming from chlorides of the same metal present in the electrolytic solution. Due to the relevance of the claims and considered the simplicity of the experimental apparatus, several tests have been performed in order to confirm the claimed results. The results of these tests will be the object of this scientific report.

1. Introduction

Palladium is an element of Group X which has the peculiar characteristic to be extremely permeable to hydrogen; indeed, it is able to adsorb this gas up to 900 times its volume at room temperature. When adsorbed, the gas redistributes itself in the metal lattice, but it is not clear if this behavior is due to the formation of hydride or is only a temporary binding. The very high permeability to hydrogen (and its isotopes) is used in the industry to purify this gas with systems forcing it to flow through palladium membranes, which stop the impurities.

In 1989 M. Fleishmann and S. Pons reported the "strange" result of anomalous temperature rising measurements on an electrolytic cell with a palladium cathode. The electrolyte was LiOH in heavy water D_2O. The sensational impact of their claim was due to the fact that the entity of extra heat generated was not compatible with a chemical origin and consequently its source should be a nuclear reaction.

The concentration of H-D in palladium depends from the thermodynamic parameters; in the cathode, by effect of applied potential, concentration rises up prominently. This mechanism, named "loading", is used to achieve the wanted thermodynamic non equilibrium in order to increase the deuterium concentration in the cathode, the necessary condition to have excess heat production. According to Fleishmann and Pons claim, the temperature raise, which were observed at high "loading" maintaining constant the applied power, would be explained invoking a nuclear mechanism in the metal lattice: D atoms reduce their relative distance, overcoming the electrostatic repulsion of the Coulomb barrier getting to nuclear fusion events. Palladium matrix should act as a sort of catalyst for the reaction. From 1989 many researchers, working both in civil and military field, began an experimental activity on these phenomena, indicated with the acronym LENR (low energy nuclear reactions). In particular, researchers tried to set up excess heat experiments, also varying the experimental embodiment; moreover, theoretical studies were developed to explain the mechanism of low temperature nuclear fusion. The attention was especially dedicated to the production of energetic particles and gamma radiation. In fact, their detection should be a clear clue that nuclear reactions were involved. Concerning particle emission, according the classical theory, during fusion a flux of them (alpha, neutron, gamma ….) has to be generated to carry almost a part of the energy produced. Unfortunately, many trials to detect them were unsuccessful. The prevalent opinion is that LENR does not produce the neutrons flux as for the standard model of this kind of reactions, even if it is hard to explain why. By the way, several scientists continued to look for neutron emission, but the results are not representative. Another research line was the detection of other corpuscular emission, based on the use of well known plastic detectors. Precise protocols are implemented for alpha particles in order to distinguish between the particles generated during the electrolysis and those normally present in the environment as by-product of Radon decay. Radon is a radioactive gas present in particular rocks. Many experiments were performed in the past and are going on to check for alpha emission during palladium loading using a plastic detector, called CR39 (Fig.. 2). When a particle hits the detector, it breaks the polymer chains and the damage becomes visible by a chemical etch in NaOH solution. The etch rate depends on the

temperature of the bath. After etch, a small conical hole appears in correspondence of the incidence path of the particle having the geometrical axis direction depending from the incidence angle.

Fig. 1 - Experimental embodiment.

Fig. 2 – CR39 detector
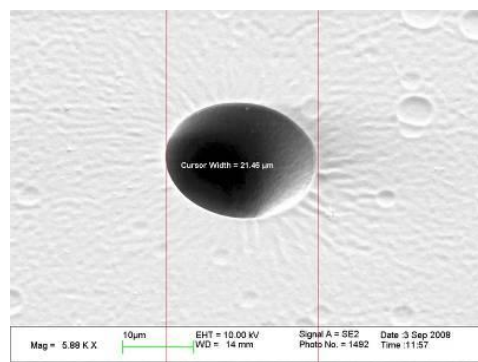
Fig. 3 - SEM photo of an alpha particle track after etch

2. Experimental Details

Two kinds of experiments were performed:

- Electrolysis of LiCl electrolyte in D2O;
- Codeposition of Pd on the cathode adding PdCL2 in the solution. Effects of high and low electrolysis current densities were also tested;
- Comparison of all the test results with CR39 detectors placed in the same embodiment, but without electrolysis.

In the very simple embodiment (Fig. X) the electrolytic cell was a glass tube with an internal diameter of 9 mm having a flange to accommodate an O ring for sealing. Another identical glass tube, empty, was connected to the one with the electrolyte with interposed the CR39 plastic detector having a size 23mm x 35mm x 1.39 mm, produced by INTERCAST EUROPE. CR39 for nuclear measurement is very pure and without defects. The cathode was formed by a palladium wire (diameter 50 μm) fixed on sensible side of detector and between the cathode and CR39 a 11 μm Mylar foil was interposed to prevent the contact of the electrolyte with the detector; all the embodiment parts were fixed together by a metallic clamp. The cell was filled with 8 ml of 0.5 M LiCl/D2O solution. D2O used was undertaken at double distillation to assure its purity. Power supply was a current generator able to generate up to 3 A; voltage and current were continuously monitored by a digital multimeter. The current was incremented in step of 1 mA till 10 mA every 8 hours; at 10 mA the electrolysis went on from 3 to 10 days. To evaluate the counts two reference samples were prepared like experiment 1, 10 mA constant for three days, using only light water for electrolysis.

3. Etch

After any experiment, the detector development process to count the high energy tracks was performed in a NaOH 6.25 M solution, at a temperature of 70°C; the solution was contained in a beaker heated by an hot plate electronically controlled at +- 0.2 °C. The etching time was 6 hours. After the etch the detectors were rinsed in D.I. water, then neutralized in HCl diluted for 10 minutes and finally rinsed again in D. I. water and dried in a flux of filtered nitrogen gas.

Fig. 4 - Heated etch bath (NaOH)

4. Track Analysis

The count track was performed using a system formed by a Leica binocular microscope in transmission configuration with a webcam and a PC running dedicated software for image acquisition. CR39 detectors were put on a plate with a hole 12 mm wide just to analyze detector area faced to the inner part of the cell during the electrolysis. To analyze the exposed area of 1.186 cm^2 125 photos with 10x objective were taken.

The experiments using CR39 have the aim to demonstrate the existence of nuclear reaction inside the palladium cathode; because the "mark" of these reactions are particles emission, it is necessary that the number/density of them detected on CR39 after deuterium electrolysis are SIGNIFICANTLY higher than the same figures related, for instance, in absence of current flow or using light water. Moreover, because of the direct contact between the cathode and the detector, it is expected to detect a higher density over all in the detector area close to palladium cathode.

The results do not show a significant difference with respect to the detectors used as reference (light water). The Mylar film interposed between cathode and detector acts like a shield for particles with energy less than a specified value which depends on the film thickness. To evaluate the penetration thickness of the particle in Mylar the freeware software SRIM was used. This code calculates stopping power, projected range and other parameters for proton and alpha particles with energy up to 10 MeV. For Mylar 11 μm thick used in the experiments the minimum energy for alpha particle to go across the film is 2.5 MeV. All particles less than 2.5 MeV are stopped. The absence of a significant increase of trace number on detector excludes particles emission with more than 2.5 MeV.

Table 1. Track Density (cm^{-2})

	Blank		Electrolysis
# 1	189	# 1	222
2	154	# 2	296
		# 3	136
		# 4	112
		# 5	74

Fig. 5 - System for tracks count

5. Experiment without MYLAR

In the specific literature, the first experiments based on the electrochemical loading and CR39 detectors were performed without any protection film between the detector and the electrolyte. The solution used was D2O with a small addition of palladium chloride salt (LiCl or LiSO4); the possibility that during electrolysis a surface damage of the detector happened was not evidently taken into account.
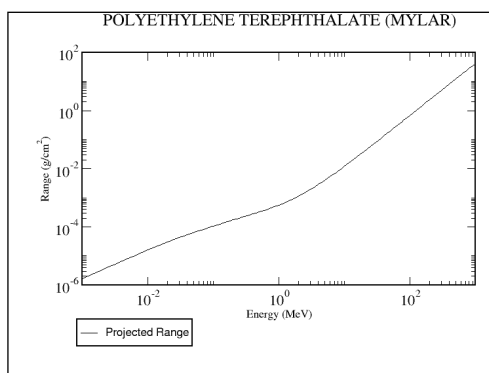
Fig. 6 - Stopping power curve for Mylar

Some researchers reported positive results in terms of high count of traces identified as particle emission from cathode just with experimental arrangements which did not use any interposed film. Comparing images of the reported traces with similar relative at radioactive emission from americium or uranium the difference is very evident. To investigate this point some experiments without Mylar were performed. After electrolysis, just to a naked eye detectors showed some milky and rough appearance; moreover, the area just in contact with palladium wire showed a marked white line. Optical microscope analysis highlighted the presence of many "balls" in coalescence each other; similar structures did not resemble at all with traces from nuclear particle. SEM analysis on some detectors confirmed this strong difference. The surface damage can be so caused from chemical etch of liquid on plastic surface.
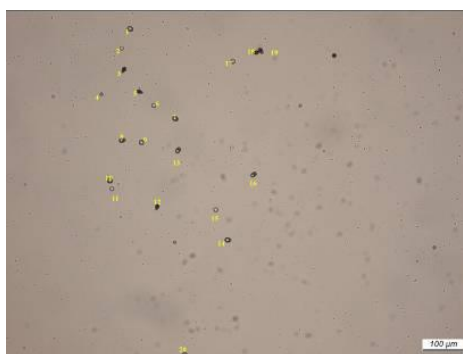
Fig. 7 - Example of CR39 area count
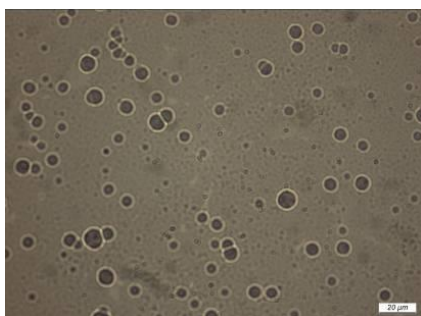
Fig. 8 - Artifact on CR39 surface, without Mylar

Fig. 9 - Artifacts in CR39 area faced cathode, without Mylar protection

6. Codeposition Pd/D

Szpac and Mosier-Boss performed some experiments in which palladium, coming from palladium salt present in the solution, was codeposited on cathode together with deuterium gas generation with the purpose to have nanostructure of palladium on the cathode were the "loading" could reach an atomic D/Pd ratio close to 1. The same authors reported positive result concerning particle emission during electrolysis. To verify this claim, two trials of codeposition were performed, using as palladium source palladium chloride PdCl2, added in the solution at 0.05 M, concentration. During these experiments two different procedures in increasing the electrolysis current were used. In trial A the starting current was 10 mA up to complete Pd deposition, then raised to 20 mA and maintained at this level for three days; in trial B the electrolysis started at low current – 0.6 mA – then maintained at this level until the palladium deposit on cathode was complete. In both cases it was possible to determine the end of palladium deposition by the solution color change from orange to transparent. So, for the experiment B the current was gradually raised up to 50 mA and the reaction went on for 7 – 10 days. The maximum current density was 0.5 A/cm^2 for experiment 1 and 5 A/cm^2 for experiment 2. At the end cell was disassembled and the detector etched in the chemical bath. In both experiments the Mylar foil was interposed.

Table 2. Codeposition Parameters

| Exp. -A-		Exp. -B-	
10 mA	Pd dep.	0.6 mA	Pd dep.
20 mA	3 days	2 mA	1 day
		5 mA	1 day
		20 mA	3 days
		50 mA	2 days

7. Results

In the case of trial A after few hours a non uniform sponge-like palladium deposit was formed on the cathode; in trial B the deposit instead was very uniform and compact. Cathode of trial B, analyzed in a SEM, showed a globular structure (cauliflower type) plus palladium dendrites present over the entire active surface. Same results are reported from Szpak and Mosier Boss with a cell put in a strong electric field. Concerning trace count, no difference was found with respect to reference sample using light water.

For both the experiments an 11 microns thick Mylar foil was interposed between the cathode and the CR39 detector. At the end of the experiments the detectors have been treated as previously described and the cathode submitted to SEM analysis.

In Fig 10 it is shown a SEM image of the cathode surface where it is possible to observe the dendritic and globular structure of the deposited Pd. Similar structures are reported in [2]; moreover it is useful to notice that the dendritic structure, as reported in [2], should be present only in experiment where the cell is placed inside a strong electric field: no electric field was present in our experiments. The track count reported in Tab. 3, does not show significant differences compared with "blank" samples, neither with electrolysis experiments without Pd codeposition.

Table 3. Track Density (Codepos.)

Exp. -A-	113 tr./cm^2
Exp. -B-	146 tr./cm^2
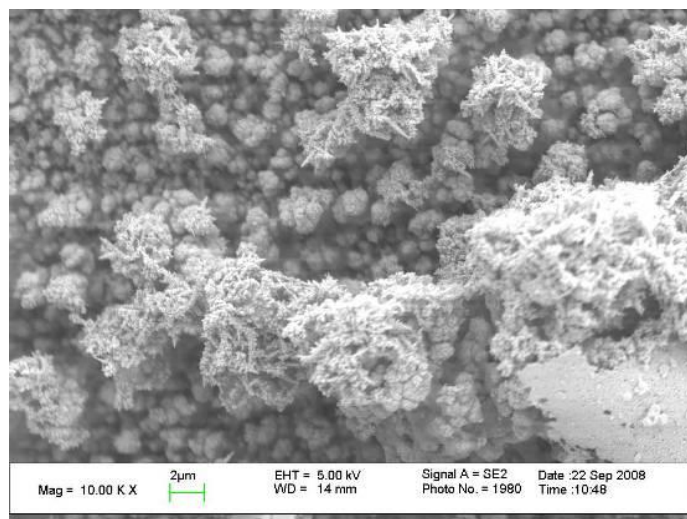
Fig. 10 - SEM photo of dendritic structures on the Pd cathode

8. Conclusions and acknowledgments

The experiments described above did not highlight a meaningful increase of Alfa particles nuclear tracks with energy greater than 2.5 MeV respect to the background of blank experiments, during electrolysis in heavy water with palladium cathodes. Same results came out also in experiments where palladium chloride salts were added to the electrolyte, in order to have nanostructures of Pd deposited on the cathode and increase deuterium loading in the Pd lattice. So, the outcomes of the experiments seem to confirm what is also reported in references [3] and [4].
A new series of test with simple electrolysis and codeposition is planned in the first part of the year 2010 using a different supplier for the CR39 detectors in order to reduce the background tracks level.

We are particularly grateful to Dr. P. Neri of INTERCAST EUROPE for the supply of CR39 detectors and Dr. F. Celani for the supply of heavy water and Pd cell cathode wires.

9. References

[1] R.A. Oriani, J.C. Fisher: *Proceedings of* 11th ICCS, 2004
[2] S. Szpak, P.A. Mosier-Boss, F.E. Gordon: *Proceedings of* 11th ICCS, 2004
[3] http://earthtech.org/experiments/PACA/report.htm
[4] http://earthtech.org/CR39/index.html

Neutron Detection: Principles, Methods, Issues (and Tips)

M. Angelone

Associazione EURATOM-ENEA sulla Fusione,ENEA C.R. Frascati, Via E. Fermi, 45 - 00044 Frascati (Rome) Italy

e-mail: maurizio.angelone@enea.it

Abstract. The production and detection of neutrons in the so called "cold fusion" phenomena is claimed since the first announcement by Fleischmann and Pons in 1989. In the last twenty years the same claim has been made by other authors despite they were operating under different experimental conditions. However, most of the scientific community is yet sceptic about the actual emission of neutrons from events that in a more general statement are known as "low energy nuclear reactions in condensed matter" (CMNS) and the methods adopted by the various authors are often subjected to several criticisms. Indeed CMNS phenomena are rather complex and relate with several different subjects so synergy among various experts is necessary. Among these subjects, neutron detections requires a particular care and expertise because the measurements are carried out with a very low signal to noise ratio. In this paper a very brief review of the main physical laws and basic detection principles for neutrons are addressed. It is not in the author's intention to investigate whether or not neutrons are actually emitted in CMNS phenomena, however, some tips that could allow to unambiguous measurement of neutrons from a CMNS type experiment will be addressed too.

1   Introduction

Since the first announcement by Fleischmann and Pons [1] and just after by Jones [2] and Scaramuzzi [3] who claimed the production and detection of 2.5 MeV neutrons from DD nuclear reactions produced by *"Electrochemically Induced Nuclear Fusion of Deuterium"*, the actual emission of neutrons from the so called *"cold fusion"* phenomena is a matter of discussion among the scientists.

In the last twenty years a great debate has arisen to establish whether or not neutrons are actually emitted and at which energy. Many authors attempted the neutron detection under experimental conditions often far different [4,5] from these discussed in [1-3]. The results were often contradictory and in some cases claim for detecting neutrons of higher energy were made [6,7]. On the other hands, some authors considering the "strange" and not reproducible results, suggested that from the so called *"low energy nuclear reactions in condensed matter"* (CMNS) phenomena, neutrons are not produced. Following these authors, the observed "anomalous" heat production is to be ascribed to nuclear reactions which led to the production of charged particles. However, recently in a attempt to measure such charged products some authors claimed they found 14 MeV neutrons [8].

The above short story of "cold fusion" phenomena is far to be complete, but clearly points out that the question of whether neutrons are actually produced and at which energy is still open. More debating is the question "how" neutrons are produced. Even within the community working on CMNS there are different ideas. Indeed CMNS phenomena are rather complex and relate with several different subjects so synergy among them is necessary. Among these subjects, neutron detections requires a particular care and expertise because the measurements are carried out with a very low signal to noise ratio. It is not in the scope of this paper to review the various experiments nor to put specific questions or criticism to any of the papers available in the literature and reporting about neutron measurements from CMNS experiments. The present paper represents an attempt to clarify some basic aspects about the neutron physics and detection.

Last, but not least, in the author's opinion time has came to try to measure neutrons in a CMNS experiment (if any) in unambiguous manner. This can be attained in a series of experiments where the detection of neutrons is detailed designed, carefully performed and repeated.

2   Neutron Sources

The neutron was discovered in 1932 by Chadwick and since the early days of its discovery the "strange and intriguing" properties of the neutron were studied with great interest by the physicists.

Neutrons can be produced by nuclear reactions. There are a number of reactions routinely used for producing neutrons, among them typical sources of neutrons are :

$$D+D \rightarrow n + {}^3He + (Q=\ MeV); \quad D+T \rightarrow n + {}^4He + (Q=14.1\ MeV); \quad {}^4He + {}^9Be \rightarrow n + {}^{12}C\ (Q = 5.7\ MeV)$$

$$\gamma\ (2.76MeV) + {}^9Be \rightarrow n + {}^8Be$$
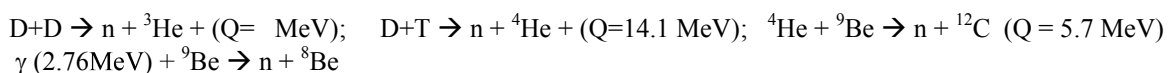
Since neutrons are neutral they are not sensitive to the coulomb barrier of the nucleus and thus can easily interact with them. The type and probability of interaction can be foreseen if the initial state of the nucleus and the energy of the neutron is known. Neutrons cannot be accelerate since they are neutral, but always they loose energy as soon as they interact with matter. This means that if *monoenergetic* neutrons of energy E_0 are produced, after moving in the surrounding material the neutrons will have a continuous spectrum ranging from the initial energy E_0 down to the thermal one (E_{th}).

3   Neutron Interactions

The neutron-matter interaction is depending upon the so-called cross-sections. The latter, for a given nucleus in a known initial state, depends upon the energy of the incoming neutron. The concept of "cross section" is familiar in the nuclear and atomic physics and relates with the "probability of occurrence of a certain process when a particle is interacting with another particle or nucleus. Strictly speaking the cross-section is not a probability but an area since it is measured in barn (1 barn = 10^{-24} cm^2). Physically the cross-section can be regarded as the area seen by the projectile when approaching the nucleus and to which "actually" it interact. The larger the area the larger the "probability" (cross section, σ) of a certain interaction. This concept can easily be explained by quantum physics if the incoming particle (the neutron in our case) is assumed to be a wave of probability [9,10]. As a consequence of the neutron-nucleus interaction there are many different "final" states, each one characterized by some "typical" reaction products. The j-th final state will have cross section σ_j, so we can define the total cross-section as the sum of the above different "final" states : $\sigma_{Tot} = \Sigma_j \sigma_j$. In this sense, if we consider the ratio $f_j = \sigma_j / \sigma_{Tot}$, f_j is the probability of having the reaction of type j.

σ_{Tot} is the so-called *microscopic* total cross-section which must not be confused with the *macroscopic* cross-section for a given material defined as $\Sigma = \sigma_{Tot} * N$ where N is the number of nuclei per unit volume. Σ is measured in cm^{-1} and $L = 1/\Sigma$ (cm) is the *mean free path* and gives the mean distance travelled in a medium by a neutron of a energy E before to produce an interaction.

The total cross-section can be divided into two broad families, the *elastic scattering* and the *NON-elastic* scattering cross sections, respectively. The latter comprises several different types of cross sections (Inelastic scattering, compound nucleus reactions or radiative capture, fission, charged product reactions, spallation, stripping etc.), each representing a specific type of n-nucleus interaction. The basic difference between these two broad families is in the neutron energy. Roughly speaking for energy lower than a 0.1 MeV the n-nucleus interaction is an elastic scattering. As soon as the neutron energy increases and reaches at least that of the first exited level of the target nucleus, inelastic scattering (that is one of the above mentioned reactions) can occur, each one with a probability defined by f_j.

The cross sections of the various nuclides as function of the neutron energy are available in a number of nuclear data libraries (e.g.[11]). From the analysis of some typical neutron cross-sections versus the neutron energy (Fig. 1), it can be seen that they behave in a rather standard mode but for a fixed neutron energy E_n the cross section value can be very different, depending upon the nucleus. Three different energy regions can be observed:

1) *the 1/ $\sqrt{E_n}$ or 1/v region* (v being the neutron velocity), in the very low energy part and up to 1-2 eV);

2) *the resonance region* from the eV region and up to ~10 keV;

3) *the high energy region* (>0.1 MeV).

The cross sections values at the thermal energy E_{th} (σ_{th}, where E_{th} = 0.025 eV at T=300°K) depends upon the isotopes and can change of many order of magnitude. The σ_{th} values varies from 10^{-3} b for D and O up to 10^6 b for ^{135}Xe. At low (thermal) energy, the neutrons move slowly so, compared to "fast" neutrons they need a longer time to cross a nucleus so the probability to be captured is higher for thermal neutrons than for the fast ones. On the other hands, the scattering cross-section at the thermal energy results of the same order of magnitude for all the nuclides. The latter fact can be intuitively explained considering the scattering between the neutron and the nucleus similar to that occurring between two rigid spheres. In this case the scattering cross section σ_s is proportional to the nucleus cross section area πR^2, R being the nucleus radius which in turn is given by R= *A$^{1/3}$ where A is the atomic mass and $r_0 \approx 1.5*10^{-13}$ cm. Indeed, the elastic scattering cross section is slightly varying with the neutron energy for most of the nuclei.

The neutron cross section behaviour can be explained in a rigorous mode by quantum mechanics (e.g. [9]).

3.1   Prompt and delayed Gamma-Rays

A peculiar aspect of the neutron-matter interaction is the production of the so called "*mixed n-γ field*" in which the neutrons and gammas are simultaneously present. The measurement of this mixed field represents a possible approach to demonstrate the neutron production in physical phenomena. Since gammas are *always* produced by

neutrons, if neutrons are measured but no gammas are observed (both during and after the neutron emission), caution is mandatory before to claim that a neutron emission was actually observed.

It is fundamental to distinguish between two classes of gammas emitted from a medium interacting with neutrons: *a)* prompt gamma-rays; *b)* delayed (or activation) gamma rays.

The prompt gamma-rays are those emitted in "real-time" whilst the neutrons are moving and producing n-nucleus interaction (e.g. inelastic scattering). The n-interactions excite the nuclei which decay by emitting gammas in a very short time (10^{-14} sec, so the name *prompt*). The prompt gamma-rays energy spectrum range from a few hundred of keV up to 15 MeV and even more, depending upon the nucleus.

Comparison among Thermal Cross Sections
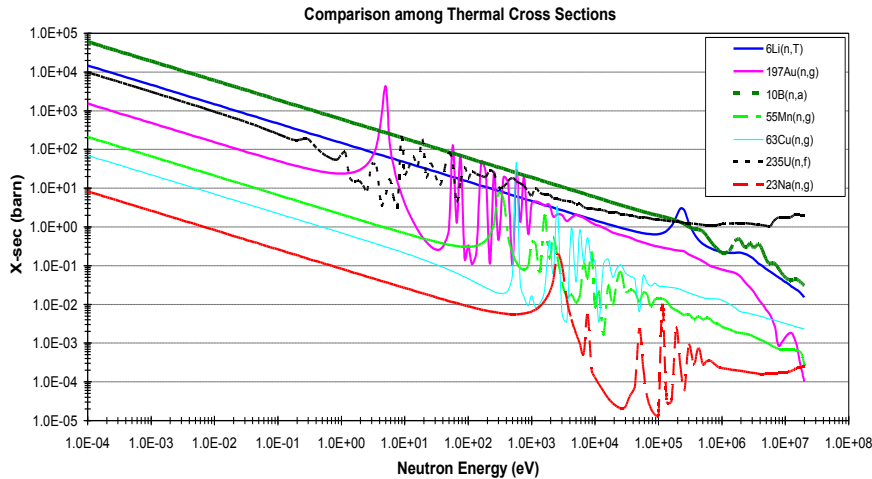
Fig. 1. - Cross-section versus neutron energy for some materials.

It is important to stress that the prompt gamma-ray emission is observed at any neutron energy and the energy of the emitted gammas can be neutron energy dependent. The latter property is used for performing elemental analysis by prompt gamma ray neutron activation analysis (PGNAA). PGNAA can also be used to measure the intensity and the energy (by analyzing the gamma–ray lines) of the neutron source.

The *delayed gamma-rays* are emitted by the excited states of the neutron activated materials which in turn are produced by the (n,x) nuclear reactions (here x means, n', p, d, α etc.). These excited states decay by alphas and/or betas (some time directly by gammas, this is the *isomeric transition*) but the daughter nuclei are still exited and usually decay by emitting one or more gammas of energy ranging from a few tens of keV up to 3 (or more) MeV. The delay time also known as decay time, can be very variable. Again from the produced gamma-ray lines it is possible to know the energy of the neutron source and also its intensity. The detection of the "activation" products is the most direct and safe method to demonstrate that neutrons have been actually produced.

The prompt as well as the delayed gamma-ray emission can be foreseen for each nuclide provided that the energy of the neutron is known. Libraries of nuclear data are available for this purpose (e.g.[11]).

4   Neutron Detection

The detection of neutrons can be attained by considering their interactions with matter. As already explained the n-matter interaction depends upon the neutron energy so we must expect that there are different type of detectors at different neutron energies. Always a neutron is detected using an in-direct method, that is thanks to the conversion of a neutron into something else, so we will detect gammas or charged particles. The conversion process is produced inside the "detecting" medium which not necessarily is the detector.

Among the many detectors developed so far to measure the neutrons (see e.g. [12]), we can distinguish two broad families: *a)* active detectors, *b)* passive detector.

Are considered active the detectors that need an external bias for operating (e.g. fission chambers, scintillators, ionization chambers, Geiger-Muller etc.). It is also important to distinguish between detectors operating in pulse or in current mode. The first type is recommended for sources emitting burst of neutrons. The current mode is suggested for long lasting neutron emissions but also for high (and some time low) intensity sources. When close to the neutron source and or to the detector are present sources of EM radiation caution is necessary and shielding is strongly suggested. Proper shielding is also requested for the cables that can act as antenna. Screened or super-screened cable are recommended.

The passive detectors instead, do not need any external biasing (e.g. thermoluminescent detectors, activation foils, CR-39 etc.) even if internal junctions are possible. The use of passive detectors require other type of cautions specific for each detector. For example, thermoluminescent dosimeters usually do not withstand high temperature

and require an accurate background dose measurement with long lasting exposure. CR-39 must not be exposed to sun or heated as well and must be handled with care since any surface damaging can result in a wrong track. Their response can also be enhanced by using a thin layer of plastic to produce recoil protons or other charged particles. The most simple detectors to be used are the activation foils for which a few recommendation are mandatory the main being to avoid contamination (to be cleaned before the experiment) or exposition to neutron sources before the experiment.

Basing upon the claimed results, the detection of neutrons in a CMNS experiments consists basically in a short-lasting neutron emission that typically starts suddenly, as a burst. The claimed level of the neutron emission is very variable from a few counts up to many hundreds so pulse detectors seem appropriate although the count rate can be very low. Assuming, as working hypothesis, the neutrons to be emitted from a DD reactions, neutrons will have an energy of about 2.5 MeV so almost all the detectors above mentioned can be used to detect them.

A problem is represented by the need to separate the background from the "true" signal especially if the counts are just a few. Under these circumstances it seems also difficult to perform the spectrometry since the statistics is an important aspect of the latter measurements. The measurement of the background prior the experiment is mandatory, but the background must be also measured after the end of the experiment to verify that no changes in the environments have happened in the meantime. Whether possible the spectrometry of the background radiation must be performed. Both n and γ background must be measured.

Due the many problems envisaged in the past in the CMNS experiments and also accounting for the many criticisms it is suggest to use a redundant array of different type of detectors rather than to use a single detector. The simultaneous signature of the various detectors will guarantee about the neutron (and gamma) emission.

Active detectors such as fission chambers or scintillators of large sensitive volume, seem more appropriate since allow also for the measurement of the time dependent neutron emission that can help in the analysis of the physical problem. To enhance the response of the detectors (e.g. fission chambers, H3-tube, Li-6 covered or coated detectors) the neutrons can be slowed down by using a few centimetres of moderators (e.g. polyethylene) located in front of the detector or all around the neutron source.

Another important point is the simultaneous detection of neutrons and prompt gammas by coupling the neutron detectors with some gamma detectors (in this case γ-spectrometry is also feasible). Some materials such as H, emits typical prompt gamma-rays (2.2 MeV for H) so their detection can be a further and independent proof of the neutron emission.

It ought to be stressed that instrumentation borrowed from the health physicist usually is not recommended for this type of measurements since most of this instrumentation have low sensitivity (and high sensitivity for both type of radiation is needed), are not very fast since usually measure the "level" of radiation and also cover a very large energy and sensitivity range but their response can be too slow.

Another measurement that is always possible is that of the "activation" products due to neutrons emission. In this case some activation foils (e.g. Au, In) can be used. To increase the sensitivity large surfaces and several grams of materials must be used and the foils must wrapped inside a moderator (polyethylene) or can also be introduced in the aqueous solution. To increase the signal to noise ratio the measurements should be carried out in a "low background" laboratory.

If Pd or Ti plates are used as electrodes in a CMNS experiment, it is expected that some (low) activation is also present in these materials. Ti reacts both with fast and thermal neutrons while Pd only with thermal neutrons. Both natural Ti and Pd are a mixture of several isotopes and almost all of them react with neutrons. The characteristic gamma-ray lines can be detected by a spectroscopic apparatus (e.g. using a Germanium detector). A calibration before the experiment is suggested using plates made with the same material and irradiated in a reference neutron flux, in order to study both the γ-ray spectra for a comparison and in case to get a quantitative analysis of the neutron production in the CMNS experiment.

5   Monte Carlo simulation of a CMNS experiment

To better understand the issues to be faced in a CMNS experiment when attempting to measure the neutron emission a simulation of a "typical" experiment was performed by using the Monte Carlo code MCNP.

The model is reported in Fig.2. A glass cylinder (2 mm thick) is filled with water and it is containing a neutron source. The detector is at a fixed distance from the source and the system is housed in a concrete box with walls and roof having the same thickness (15 cm) while the floor is more thick (30 cm). The neutron source is at 1m from the floor while the dimensions of the concrete box are 4x4x6 m^3.

By changing the dimensions (radius) of the glass cylinder (and thus the quantity of water contained in it) as well as the energy of the neutron source (DD and DT neutrons), the neutron and gamma spectra in a region simulating the detector and located next to the cylinder (see picture) are calculated. The detector is a cylinder of air and its distance from the centre of the neutron source is kept constant as the cylinder radius changes.

5.1 Results of the simulation

The calculation was performed using two neutron source energies: E_{DD}= 2.5 MeV and E_{DT}=14 MeV. A second calculation was run enveloping the water cylinder in a second cylinder made of stainless steel (SS) 1 cm thick. The SS cylinder in some papers was used as "electromagnetic" shield but the use of shields made of Al or μ-metal, is suggested when using (variable) magnetic fields. This shield will have an impact also on the neutron and gamma emission and must be accounted for.

In Fig. 3 the neutron spectra calculated at the detector position are shown. The calculations were performed for three different radii of the glass cylinder: R= 1.0; 2.5 and 5.0 cm respectively. Fig. 3 shows the effect of the increasing radius on the calculated neutron spectrum at the detector location. As the water thickness increases the neutron spectrum enlarges. For R= 5 cm, the typical tail at the low energy part of the spectrum is visible as well as the thermal peak. It is interesting to note that the neutron background spectrum and intensity do not change very much. For comparison the neutron spectrum due to DT neutrons is also reported.
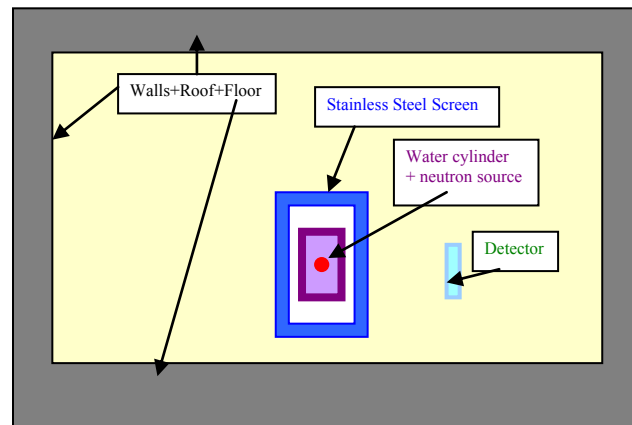
Fig. 2. - MCNP Model of a CMNS experiment
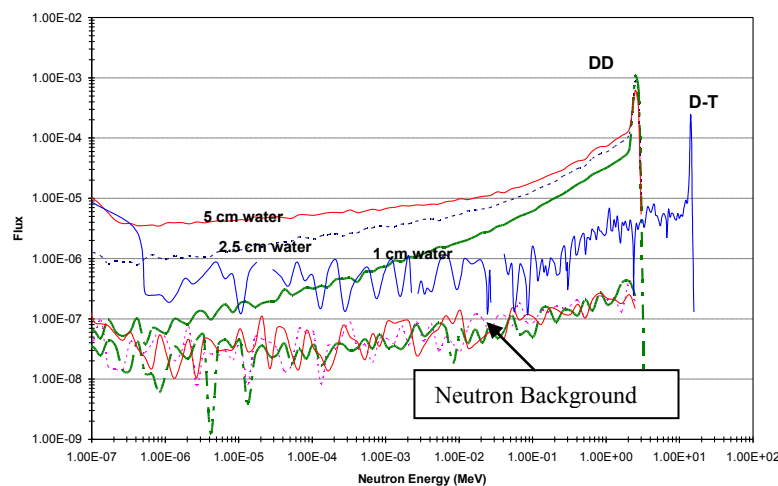
Fig. 3. - Calculated neutron spectra as a function of the Radius R at the detector's position

In Fig. 4 the prompt gamma-ray spectra calculated for the DD source are reported together with the spectrum calculated for the case of the SS cylinder enveloping the neutron source. The effect of higher neutron energy (DT source) on the "prompt" gamma-ray spectrum is shown too. The above results point out several important facts:

a) The neutron spectrum depends upon the neutron source energy and the amount and type of material surrounding it. The background, due to wall return effects, depends mainly on the geometry of the system (source-walls distance).

b) Any material interposed between the neutron source and the detector can affect the "shape" of the neutron spectra as well as will modify the spectrum of the prompt gammas.

c) The "prompt" gamma-ray spectrum depends upon the neutron energy.

d) Walls, roof and floor always contribute to the total response via scattered neutrons (and gammas). A more general statement is that any material and structure surrounding the source affects the detector's response.

6   Tips for unambiguous neutron detection in a CMNS experiment

The above discussion, together with the short notes reported on the neutron detection, allows us to summarize the discussion and to give a few suggestions and tips for unambiguous detection of neutrons that indeed, is what is still requested to a CMNS experiment.

To be unambiguous neutron detection must provide a clear and not questionable signature of the event. For this reason a simple but affordable system is suggested. The detectors should have a large volume to increase the detection efficiency (but also the background is increased), operate in pulse mode and over all be based upon different principia. So fission chambers can be coupled with scintillators as well as with activation foils. Scintillator can simultaneously measure and discriminate neutrons and gammas provided that a proper discriminating electronics is set-up . Calibration is also needed for all the detectors both with respect the energy and whether possible efficiency. The "neutron source" can be enveloped by a moderator in order to slow-dawn neutrons and enhance the response of the used detectors (some scintillators, e.g. NE-422, are sensible to slow neutrons, while NE-213 is sensible to high energy neutrons (> 1 MeV)). Since the neutron emission is expected in the range of some MeV a few centimetres (3-5) of polyethylene can be sufficient. Activation of ^{197}Au, ^{109}Ag or ^{113}In which are sensible to thermal neutrons and have a relative short activation time is possible. The use of short life nuclides is suggested for activation since the expected neutron fluences are not too high.
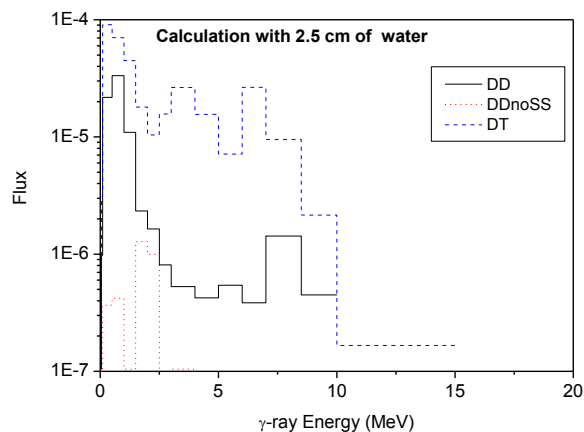
Fig. 4. - Prompt gamma-ray spectra calculated for a DD neutron source also enveloped in a SS shield. The prompt gamma-ray spectrum obtained with DT neutrons is also reported for comparison.

A detector based on ^{109}Ag can be particularly suited for a CMNS experiment since it allows for neutron activation to be detected, its short half-live (about 24 sec) β-decay can be efficiently measured by a beta counter (e.g. a simple Geiger-Muller tube) so following the decay curve. This instrument will give a double, independent and unambiguous signature of a neutron activation. The advantage is that the activation is not influenced by any possible external EM noise or field while the measured activation will follow a well known decay curve.
Last, but not least, the measurements must be repeated and the results reproducible.

References

[1] M. Fleischmann and S. Pons, "Electrochemically Induced Nuclear Fusion of Deuterium",
    J. Electroanal. Chem. **261** (1989) 301
[2] A. De Ninno, A. Frattolillo, G. Lollobattista, L. Martinis, M. Martone, L. Mori, S. Podda, F. Scaramuzzi,
    Europhysics Lett. **9** (1989) 221
[3] S.E. Jones al."Observation of Cold Nuclear Fusion in Condensed Matter", *Nature* **338** (1989) 737
[4] T. Mizuno, T. Akimoto, A. Takahashi and F. Celani, "Neutron Emission from a D$_2$ Gas in Magnetic Fields
    Under Low Temperature", J.P. Biberian, Editor, *Proc. of the 11-th Int. Conf. on Cold Fusion, Marseille,
    Oct. 31-Nov. 5, 2004,World Scientific, pp. 312*
[5] A. Takahashi, T. Iida, F. Maekawa, H. Sugimoto, S. Yoshida, Windows of Cold Nuclear Fusion and Pulsed
    Electrolysis Experiments, *Fus. Technol.* **19** (1991) 380
[6] A. Takahashi, T. Takeuchi, M. Wanatabe, "Emission of 2.45 MeV and Higher Energy Neutrons from D$_2$O-Pd
    Cell Under Biased-Pulse Electrolysis", *J. Nucl. Sci. Technol.* **27**(7) (1990) 663

[7] P.A. Mosier-Boss, S. Szpak, F. E. Gordon, L. P.G. Forsley, "Use of CR-39 in Pd/D co-deposition experiments", *Eur. Phys. J. Appl. Phys.* **40** (2007) 293

[8] P.A. Mosier-Boss, S. Szpak, F. E. Gordon, L. P.G. Forsley, Triple tracks in CR-39 as the results of Pd-D Co-deposition: Evidence of Energetic neutrons", *Naturwissenchaften* (2008)

[9] A. Foderaro, *Neutron Interaction theory,* The MIT Press, Cambridge (Massachusetts) 1971

[10] K.S. Krane, *Introductory nuclear physics,* John Wiley & Sons, New York,

[11] A. Koning et.al. (Ed.), The JEFF-3.1 Nuclear Data Library, JEFF Report 21, OECD/NEA, Paris (2006)

[12] G. F. Knoll, Radiation Detection and Measurement, John Wiley & Sons, New York , Second Ed. (1989)

Search for Nuclear Reaction Products in Gas Phase Experiments – Deuterium Permeation and Absorption –

A. Kitamura[1], Y. Sasaki[1], Y. Miyoshi[1], Y. Yamaguchi[1], A. Taniike[1], Y, Furuyama[1], A. Takahashi[2], R. Seto[2] and Y. Fujita[2]
[1]*Division of Marine Engineering, Graduate School of Maritime Sciences, Kobe University, Higashinada-ku, Kobe 6580022, Japan*
[2]*Technova Inc., Chiyoda-ku, Tokyo 1000011, Japan*

E-mail: kitamura@maritime.kobe-u.ac.jp

Abstract. Employing both *in situ* and *ex situ* accelerator analyses, we have attempted to replicate the Iwamura-type nuclear transmutation of Sr to Mo under deuterium permeation through a variety of multilayered CaO/Sr/Pd samples. Apparently positive results have been obtained in 8 of 14 runs, although the identification of Mo peaks in the PIXE analysis is not definite. It is implied that sputtering loss of the atoms could be responsible for the observed tendency that the areal density of Sr decreases in most cases, while there are modest increases in Mo. In addition to the accelerator analyses, γ-ray detection has been tried for samples implanted with W atoms in expectation of transmutation from ^{183}W to radioactive ^{191}Pt.
In another series of experiments, we examined heat and ^{4}He generation by deuterium absorption in nano-sized Pd powders, as reported by Arata and Zhang. In order to determine the cause of the large isotope effects observed, nuclear ash including charged particles, neutrons and gamma rays was examined.

1. Introduction

Iwamura *et al*. claimed [1] that nuclear transmutation occurs during forced permeation of deuterium (D) through multi-layered films of X/CaO/Pd, with X being the element to be transmuted, *e.g.*, ^{133}Cs transmuted to ^{141}Pr, ^{88}Sr to ^{96}Mo, etc. We have attempted to replicate the transmutation using a modified exposure system to enable *in situ* characterization of the sample, which was installed at the end of a beam line of a tandem electrostatic accelerator 5SDH2. In addition to this system with a reversed flow direction, a stand-alone D permeation system was used to examine the phenomenon by *ex situ* PIXE analysis. The results have been presented in ref. [2], and are briefly summarized in the present paper.

Arata and Zhang recently reported [3] that highly pure D_2 gas charging of Pd nano-powders in the form of Pd·ZrO_2 nano-composite induced significantly higher temperatures inside the reactor vessel than on the outside wall for more than 50 hours, while runs with H_2 gas showed almost no temperature difference. To verify that the excess heat originated in a nuclear process, a QMS was employed to show the existence of ^{4}He as nuclear ash in the vessel and in the powder after the charging. The charging system is a sophisticated, yet simplified, version of the previous-generation DS reactor [4]. Replication experiments using systems similar to the DS reactor with Pd-black seem to be successful [5,6].

However, few reports on replication experiments producing heat and ^{4}He with the new configuration have been published in spite of the extreme importance of the phenomenon. It is crucial to confirm the phenomenon of heat and ^{4}He generation with fully quantitative reliability.

We have initiated our own replication experiments to confirm the phenomenon and to investigate the underlying physics. We have reported the first results of deuterium/hydrogen absorption and accompanying heat generation in ref. [7-11], where an anomalously large absorption energy and isotope effects were found. In the latter half of the present paper, a description of our efforts to detect possible nuclear reaction products is given.

2. Deuterium permeation experiments

2.1 Summary of PIXE analysis

We have tried to replicate the nuclear transmutation of Sr ($2 - 50\times10^{15}$ cm^{-2}) to Mo under deuterium permeation through a variety of multilayered samples; (v)/M$_n$/CaO/Sr/Pd/(D$_2$), (v)/Pd/M$_n$/CaO/Sr/Pd/(D$_2$), (v)/Sr/Pd/CaO/Pd/(D$_2$), and (v)/Pd/CaO/Sr/Pd/(D$_2$), where (v) stands for vacuum and "M" for a layer of CaO(18nm)/Sr/Pd(22nm). The D flow rate was $0.03 - 0.6$ sccm, and the fluence was $0.1 - 2\times10^{23}$ cm^{-2}. The deuterium loading reached 0.86 for the sample (v)/Pd/M$_9$/CaO/Sr/Pd/(D$_2$), and the areal densities of Mo were $0 - 4.7\times10^{15}$ cm^{-2}. Apparently positive results were obtained in 8 of 14 runs, although the identification of Mo peaks in the PIXE analysis was not definite.

A tendency has been observed, however, for the areal density of Sr to decrease in most cases, while there are modest increases in that of Mo. Figure 1 shows the areal densities of Sr and Mo atoms as a function of time, or equivalently the deuterium fluence. In the former the density values are normalized to the initial values to show that almost all samples have decreasing density of Sr, while the absolute values are plotted in the latter. Although some samples have contaminant Mo atoms inherently, most samples show increasing density of Mo.
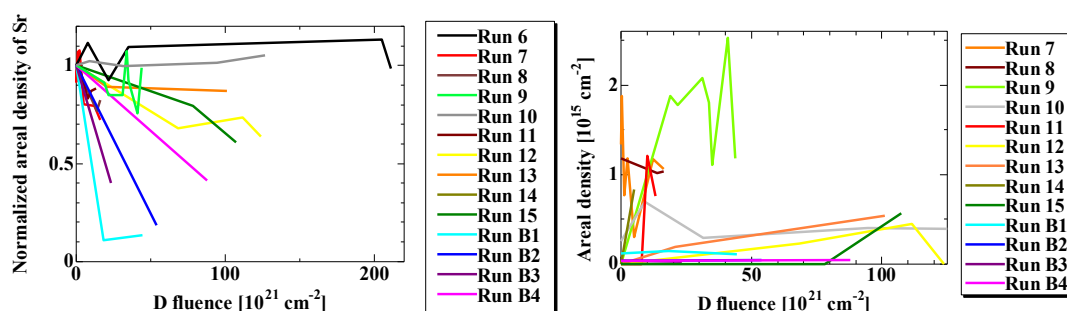
Fig. 1. - Temporal variation of areal densities of Sr (left) and Mo (right).

These results imply that sputtering loss of the atoms by 3-MeV protons and/or 4-MeV ^{4}He used for PIXE and ERDA analyses could be responsible for these changes. Although a simulation program ACAT has shown that the contribution of sputtering to the decrease would be 2 orders of magnitude smaller than the decrease observed, the sputtering yield for deposited atoms weakly bonded to the bulk atoms should be much larger than the bulk atoms. This could account for the decrease in areal densities of Sr and Mo, which could result in the apparently smaller transmutation yield.

2.2 Radioactivity measurement

If the transmutation product is a radioisotope, detection will be much easier. If we assume the regularity of transformation that the atomic number and the mass number increase by 4 and 8, respectively, we can expect, for example, a production of ^{191}Pt (emitting 0.538-MeV γ rays with a half life of 2.86 d) from ^{183}W. We prepared samples with a structure (V)/Pd/CaO/W/Pd/(D$_2$). The thickness of the first Pd layer and the second CaO layer were 38 nm and 2 nm, respectively. The tungsten atoms were introduced into the samples by implantation with 380-keV W^{++} ions accelerated by the tandem Pelletron 5SDH2, and were expected to be distributed at a depth of 40 nm with a range straggling of 16 nm.

Gamma ray measurements were performed with an NaI(Tl) scintillation probe during permeation, and an HPGe detector after finishing the permeation. Unfortunately, we were statistically unable to find the 0.538-MeV γ ray peak in the spectra. This means that the areal density of ^{191}Pt was below 10^7 cm^{-2}.

3. Absorption experiments

3.1 Experimental apparatus

Among possible nuclear reaction products, neutrons and γ rays are detectable outside the gas absorption chamber. During the absorption runs using the A$_1$-A$_2$ system, these were simultaneously monitored with a BF$_3$ neutron dose rate meter and a scintillation probe, respectively [7-9]. The radioactivity of some samples after the absorption runs was also measured using an imaging plate. However, we have not succeeded in finding meaningful signals in these measurements.

X rays and charged particles have a mean free path or a range too small to allow measurements outside the chamber wall. An experimental system shown schematically in Fig. 2 was prepared for charged particle measurements independently of the A_1-A_2 heat measurement system. A solid state detector, a Si surface barrier detector (SSBD) or an ion implanted Si detector (IISD), is located inside the reaction chamber containing a sample holder on which several tens of milligrams of the Pd·Zr oxide complex samples are mounted. A sheath heater is wound around the holder for sample baking, and the holder temperature is measured with an alumel-chromel thermocouple attached on the side of the holder. During the sample baking a retractable shield plate is inserted between the sample and the SSBD/IISD to avoid its deterioration by heating. Energy calibration of the SSBD/IISD is done with use of an ^{241}Am checking source placed on the retractable shield. During the calibration and before deuterium absorption runs, the chamber is evacuated with a TMP-diaphragm pumping kit. The deuterium gas is introduced into the reaction chamber through a liquid nitrogen cold trap and a "SuperNEEDLE" valve which enables precise control of the gas flow rate mechanically.

3.2 Examples of the measurement

In the initial stage of this study, we used an SSBD with a depletion layer thickness of 200 μm and the used sample PZ1. The energy spectra recorded during a 5-day run D-PZ1#3B through D-PZ1#4B and evolution of the counting are shown in Fig. 3(a) and (b), respectively. Here, the run number following "#" is advanced for every run after each gasfill-evacuation cycle, while the number preceding "#" is advanced for every new piece of the sample PZ (Pd·ZrO$_2$).

We see several counts in the energy range from 2 to 4 MeV and a few counts at 7 - 9 MeV. Although these could be caused by charged particles, we cannot rule out the possibility that these are due to electronic noise induced by mechanical shock or oscillation. It is shown in Fig.3(b) that these counting increased during phases of pressure change. Although it is fascinating to imagine that some nuclear events are occurring when

Fig. 2. - Schematic of the system B for particle measurement.

(a)

(b)
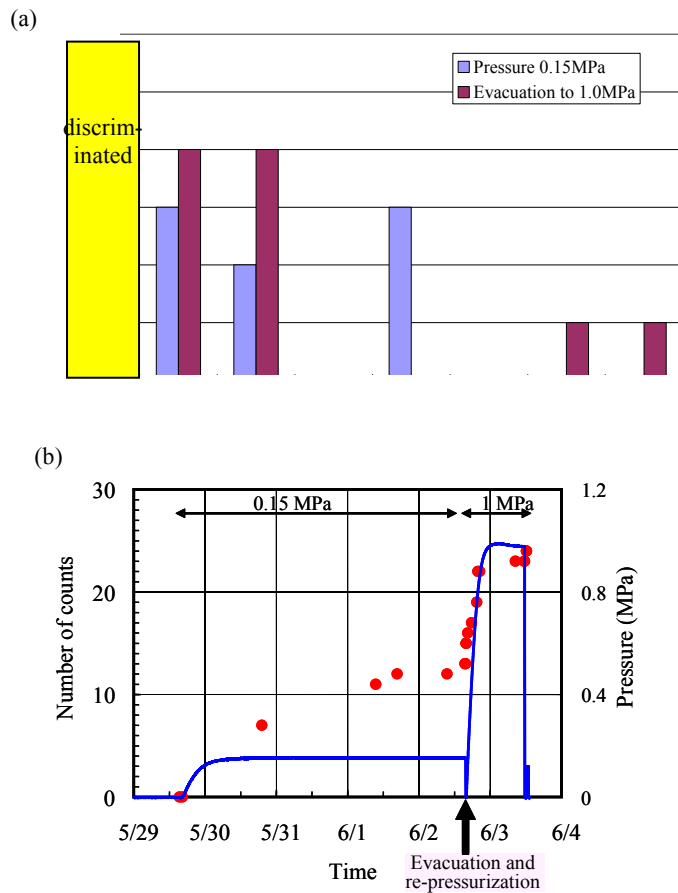
Fig. 3. - (a) Spectra recorded by SSBD with a 200-μm-thick depletion layer, and (b) Evolution of counting in the "1-12 MeV" range of the spectra measured by the SSBD during the run D-PZ1#3B through D-PZ1#4B.

218

deuterium atoms flow into/out of the Pd lattice, we cannot draw such a conclusion at present.

It is known that any SSBD suffers from deterioration or breakdown when it is used in a hydrogen atmosphere. The output pulse height from the SSBD used in the run D-PZ1#3B through D-PZ1#4B was reduced by a factor of about 30% and the FWHM increased by a factor of about 5. Although the deteriorated characteristics was stabilized after the initial use for several hundred hours, it was better to abandon it in the succeeding runs using virgin samples. We used an IISD with a depletion layer thickness of 500 μm which is known to endure use in a hydrogen atmosphere.

Figure 4(a) and (b) show the energy spectra and evolution of pressure and counting of the IISD and other radiations monitored outside the reaction chamber during the runs D-PZ14#1B (blue), D-PZ15#1B through D-PZ15#2B (red). The broken line in (a) shows the spectrum of ^{241}Am-α particles used for energy calibration of the detectors. We observe several tens of counts in the energy range 2 - 5 MeV in these runs. In (b) the IISD countings are integrated over the runs D-PZ14#1B, D-PZ15#1B-2B, and the baking period. They are reset between the operations.

The integrated IISD counting increased during the baking period between D-PZ14#1B and D-PZ15#1B, which is due largely (85%) to signals lying in the energy range 4.7 - 5.6 MeV. This indicates that the upper surface of the retractable shield plate has a contamination of ^{241}Am. It was found that the active surface of the IISD could see the contamination spot in case of insufficient retraction of the shield plate during the runs. This can account for the increase in the counting also during the runs D-PZ14#1B and D-PZ15#1B-2B.

As shown in Fig. 4(a), the spectra during these runs are a little different from that of the ^{241}Am-α particles,

Fig. 4. - (a) Spectra recorded by the IISD with a 500-μm-thick depletion layer, (b) Evolution of pressure and IISD counting and other radiations during the runs D-PZ14#1B through D-PZ15#2B.

which is also implied by the difference between the counting in the energy range 1 - 8 MeV and that in the range 4.7 - 5.6 MeV. The energy shift of the ^{241}Am-α particles by about 0.8 MeV is consistent with the energy loss of 5.486-MeV α-particles in a 5 mm·MPa hydrogen gas. We see again, however, a tendency that the counting increases during the phase of pressure change. It could be possible that the signals lying in the energy range 2.0 - 4.5 MeV originate in charged particles emitted through some nuclear phenomenon in the sample.

Finally, it is noted that we observed no increases in the signals of neutrons and gamma rays.

3.3 Summary of charged particle measurements in gas charging system
We have observed several to several tens of counts in the 1 - 10 MeV range, which appeared to be emitted coincidentally with pressure change. However, we cannot rule out the possibility that they are due to electronic noise or contamination of ^{241}Am. Up to now, we have obtained no firm evidence of charged particle emission. We are planning detection of X-rays as another candidate for the reaction products.
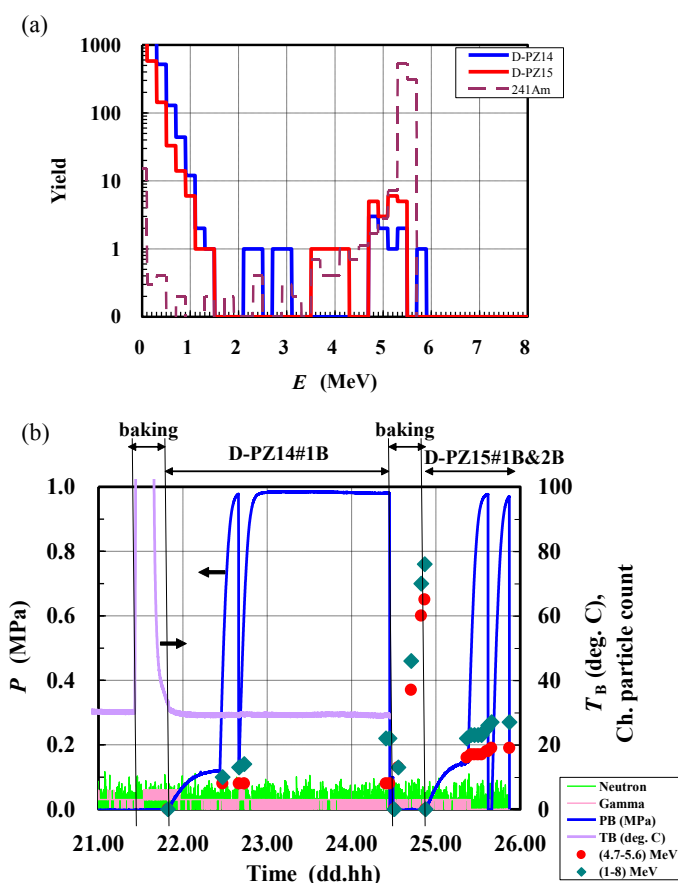
4. Concluding Remarks

Employing both *in situ* and *ex situ* accelerator analyses, we have attempted to replicate the Iwamura-type nuclear transmutation of Sr to Mo under deuterium permeation through a variety of multilayered CaO/Sr/Pd samples. Apparently positive results have been obtained in 8 of 14 runs, although the identification of Mo peaks in the PIXE analysis is not definite. It is implied that sputtering loss of the atoms could be responsible for the observed tendency that the areal density of Sr decreases in most cases, while there are modest increases in Mo. Gamma ray measurement for samples implanted with W atoms has also been performed in expectation of transmutation from ^{183}W to radioactive ^{191}Pt, but we have not yet obtained positive results.

In deuterium absorption experiments of Pd·Zr oxide nanopowders, detection of possible nuclear ash including charged particles in addition to neutrons and gamma rays has been examined. We have observed several to several tens of counts in the 1 - 10 MeV range, which appeared to be emitted coincidentally with pressure change. However, we cannot rule out the possibility that they are due to electronic noise or contamination of ^{241}Am. Up to now, we have obtained no firm evidence of charged particle emission.

In both of the above measurements, one of the problems is that the signal-to-noise ratio is rather small. If any nuclear reaction is occurring in the former experiments, it is necessary to find a way to increase the reaction rate not only from a detection point of view but also from a practical application point of view. In the latter, if any nuclear reaction emitting charged particles is responsible for the anomalous heat evolution, it should be possible to detect millions of charged particles. We need further study to look for the conditions suitable for such a reaction and its detection techniques.

5. References

[1] Y. Iwamura, M. Sakano and T. Itoh: *Jpn. J. Appl. Phys.* **41** (2002) 4642-4650; Y. Iwamura *et al.*: *Proc. ICCF12, 2005, Yokohama, Japan* (World Scientific Publishing Co. Pte. Ltd, 2006) 178-187.

[2] A. Kitamura, T. Yamaguchi, T. Nohmi, Y. Sasaki, Y. Miyoshi, A. Taniike, Y. Furuyama, and A.Takahashi: *Proc. 9th Meeting of Japan CF-Research Society* (2009) 23-28; *http://www.lenr-canr.org/acrobat/KitamuraAcmnsresear.pdf*.

[3] Y. Arata and Y. Zhang: *J. High Temperature Society*, 2008, No. 1; Y. Arata, and Y. Zhang: *Proc. 12th Int. Conf. on Cold Fusion* (ed. A. Takahashi, Y. Iwamura, and K. Ota, World Scientific, 2006) pp. 44-54.

[4] Y. Arata, and Y. Zhang: *Condensed Matter Nuclear Science, Proc. 12th Int. Conf. on Cold Fusion* (ed. A. Takahashi, Y. Iwamura, and K. Ota, World Scientific, 2006) pp. 44-54.

[5] V. A. Kirkinskii, A. I. Kumelnikov: *Proc. ICCF13, Sochi, 2007* (Publisher Center MATI, Moscow, ISBN 978-5-93271-428-7) pp. 43-46.

[6] J. P. Biberian and N. Armanet: ibid. pp.170-180.

[7] Y. Sasaki, A. Kitamura, T. Nohmi, Y. Miyoshi, A. Taniike, A. Takahashi, R. Seto, and Y. Fujita: *Proc. 9th Meeting of Japan CF-Research Society* (2009) 29-34; *http://www.lenr-canr.org/acrobat/SasakiYdeuteriumg.pdf*.

[8] A. Takahashi, A. Kitamura, T. Nohmi, Y. Sasaki, Y. Miyoshi, A. Taniike, R. Seto, and Y. Fujita: *Proc. 9th Meeting of Japan CF-Research Society* (2009) 35-41; *http://www.lenr-canr.org/acrobat/TakahashiAdeuteriumg.pdf*.

[9] A. Kitamura, T. Nohmi, Y. Sasaki, A. Taniike, A. Takahashi, R. Seto, and Y. Fujita: *Physics Letters A*, **373** (2009) 3109–3112.

[10] Y. Sasaki, A. Kitamura, Y. Miyoshi, T. Nohmi, A. Taniike, A. Takahashi, R. Seto, and Y. Fujita: paper S7_O5, this conference.

[11] A.Takahashi, A. Kitamura, T. Nohmi, Y. Sasaki, Y. Miyoshi, A. Taniike, R. Seto, and Y. Fujita: paper S2_O4, this conference.

Impurity Measurements by Instrumental Neutron Activation Analysis on Palladium, Nickel and Copper Thin Films

A. Rosada[1], E. Santoro[2], F. Sarto[3], V. Violante[3], P. Avino[4]
[1]*FIM, R.C. Casaccia, ENEA, Rome, Italy*
[2]*FPM, R.C. Casaccia, ENEA, Rome, Italy*
[3]*FPM, R.C. Frascati, ENEA, Rome, Italy*
[4]*DIPIA, ISPESL, Rome, Italy*

E-mail: emilio.santoro@enea.it

Abstract. Nowadays, the main cold fusion experiments are performed during electrolysis processes onto palladium, nickel and copper thin films. In studies devoted to verify the nuclei formation during these tests, a specific research activity has been developed at ENEA Research Centers: different experiments were set up for verifying and testing the data present in literature.
Each step of the procedure has been analyzed and deeply investigated: the materials such as electrolysis equipments, electrolytic solutions, electrodes, etc. were preliminarily analyzed by Instrumental Neutron Activation Analysis (INAA) for identifying and reducing all the pollution sources.
Successively, different experiments were performed using films of palladium, nickel and copper as electrodes. At the end of each test, all the materials and the electrolytic solutions used and the blank as well, were analyzed by INAA for checking and measuring the presence of nuclei originating from nuclear transmutations.

1. Introduction

Some abnormal electrochemical facts have long been known to the scientific community, not related to the chemical phenomena occurring during the electrolysis: unexpected excess of heat and X-ray emission The possibility of obtaining more heat than that generated by electrochemical reactions, was shown by Fleischmann and Pons in 1989 [1]. After, Jones [2] considered the possibility of cold fusion reaction p/D taking place in the lattice of a metal at temperature slightly above ambient temperature, cold compared to peak thermonuclear fusion temperatures (10^8 K) [3].

While there are clear evidences [4-7] on excess heat not justified through electrochemical reactions, there is less clearness, but still high uncertainty about the other related phenomena such as neutron production [3,8], ^{4}He production [5,7,9], tritium production [10-12], nuclear ash formation [13-16].

Because these possibilities are just random, sporadic, of low intensity and not related to each other, it should be considered the X-ray emission and the production of new species from nuclear transmutation reactions occurring during the experiments. Our attention is addressed to this second task for understanding what may actually happen in condensed matter.

Some authors [13,14] stated that after electrolysis experiments on mono- or multi-layered thin films of Pd and Ni, performed using both light and heavy water and various electrolytes (e.g., Na_2CO_3 or LiOH), new atomic species may be observed in condensed matter. According to these authors, some of the observed species are present at low levels and cannot be regarded as impurities, but real nuclear transmutation products. Some other authors reported the observations of new atomic species hypothesizing their production by nuclear transmutations in condensed matter during electrolysis experiments on mono-and multi-layered thin-films [16].

The main critical point of this approach is the contamination levels of the single components used during the electrolysis process. For these reason we set up some experiments analyzing the electrodes with relative blanks and the electrolytic solutions with relative standards by the Instrumental Neutron Activation Analysis (INAA). Preliminarily, some candidate materials have been undergone to INAA, discarding those without minimum impurities content; after, the blanks (i.e., electrodes and electrolytes) and the electrodes and operated electrolytes exhausted, were analyzed.

From the analytical point of view, the INAA was chosen because it is a non destructive analytical method (i.e., all samples can be stored and analyzed again) and highly sensitive (very low limit of detection, LOD, high sensitivity and high precision) (table 1), is a bulk method (INAA is an analytical technique that allows to analyze the entire mass of the sample) [17], permits the determination in the same sample up to 50-60 elements with no chemical sample manipulations (no errors due to excess contamination, positive artifacts, or down due to loss of material, negative artifacts).

Table 1. Nuclear data (radioisotope, cross section, half-life, peak energy and limit of detection) of the elements investigated in this study (a: calculated according to ref. 18; h: hour; m: minute, d: day; y. year).

Element	Product nuclide	Cross Section [19] (barn)	Half life		γ-Ray used (keV)	LOD[a] (ng)
Ag	^{108}Ag	35	2.41	m	632.9	0.1
Ag	^{110m}Ag	37.2	250.4	d	657.7	
Al	^{28}Al	0.232	2.246	m	1778.8	30
As	^{76}As	4.3	26.3	h	559.2	0.001
Au	^{198}Au	98.8	2.70	d	411.8	6×10^{-5}
Br	^{80}Br	8.5	17.4	m	617.0	0.002
Br	^{82}Br	2.69	1.47	d	776.5	
Cl	^{38}Cl	0.428	37.2	m	1642.4	2
Co	^{60}Co	37.2	5.272	y	1332.5	0.06
Cr	^{51}Cr	15.9	27.7	d	320.0	0.1
Cu	^{64}Cu	4.5	12.74	h	1345.8	
Cu	^{66}Cu	2.17	5.1	m	1039.0	0.4
Eu	^{152}Eu	5900	12.7	y	1408.0	2
Fe	^{59}Fe	1.15	45.1	d	1099.2	20
Ga	^{72}Ga	4.71	14.1	h	834.0	0.002
Hf	^{181}Hf	12.6	42.4	d	482.2	0.02
Mg	^{27}Mg	0.038	9.45	m	1014.4	20
Mn	^{56}Mn	13.3	2.58	h	846.6	8×10^{-5}
Mo	^{99}Mo	0.45	2.75	d	141.0	0.03
Na	^{24}Na	0.53	15.02	h	1368.6	0.004
Ni	^{58}Co	0.113	70.78	d	810.7	6
Pd	^{109}Pd	12	13.46	h	88.1	
Pd	^{109m}Pd	0.2	4.69	m	188.9	
Sb	^{122}Sb	6.25	2.70	d	564.0	0.001
Se	^{75}Se	51.8	120.4	d	264.6	0.1
Sm	^{153}Sm	206	1.948	d	103.1	5
Ta	^{182}Ta	21	115	d	1221.3	0.01
V	^{52}V	4.88	3.75	m	1434.2	0.9
W	^{187}W	37.8	24.0	h	685.7	0.001
Zn	^{65}Zn	0.78	243.8	d	1115.5	0.1

In this study we analyzed the following elements: Ag, Al, As, Au, Br, Cl, Co, Cr, Cu, Eu, Fe, Ga, Hf, Mg, Mn, Mo, Na, Ni, Pd, Sb, Se, Sm, Ta, V, W, Zn.

2. Experimental Part

2.1 Electrolysis process

2.1.1 Apparatus and Conditions. The experimental cell (Fig. 1), 15 mL polyethylene vessels, have been constructed using pure polyethylene (PET) (Kartell S.p.A., Milan, Italy) containers at very low impurity levels. The anode is a Pt wire (99.98% pure Pt) wrapped in the shape of a planar spiral. The cathode is a metallic thin film containing Cu, or Ni, or Pd, deposited onto a polyethylene disk (12 mm diameter and 1 mm thickness) made of the same ultrapure material of the cell; after the etching treatment of the supports the films were prepared by sputtering contemporaneously over two adjacent polyethylene targets to obtain a blank film electrode whit the same deposition of the working one. The cathode contact is made with a "C" shape platinum wire inserted into a polyethylene support to prevent the electrolysis between anode and cathode connections. The electrolysis conditions were: time 1-5 hours, solution $LiSO_4$ 10^{-4}, 10^{-3} and 1M, current 5-190 mA and voltage: 3-7 V.

Before the process, all the equipments were cleaned. The cleaning procedure is the following: washing

with 18 MΩ×cm^{-1} ultrapure distilled deionized water; washing with HNO$_3$ 65% (Merck Specpure, Darmstadt, Germany) for 1 minute; rinsing with 18 MΩ×cm^{-1} ultrapure distilled deionized water; rinsing with KOH 20% in ethanol (ultrapure reagent) (Carlo Erba, Milan, Italy); rinsing with ethanol (ultrapure reagent) (Carlo Erba); rinsing several times with 18 MΩ×cm^{-1} ultrapure distilled deionized water; drying at room temperature. The Pt wire is cleaned by acetone and ethylene in a previous supplementary step. The handling occurs with acrylic gloves. The film preparation, cleaning procedure, cell assembly and all the experiments were performed in a class 100 clean room using dust-free gloves. The tools used to assemble the cell components has been selected to avoid the presence of contaminants.
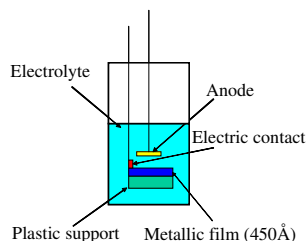

Fig. 1 - Electrolytic cell

2.1.2 Electrolysis Experiments. Two series of experiments were performed [20]: 1) mono layer, double layer (Cu/Ni) and multi layer thin-films (Cu/Ni/Pd/Ni/Pd) electrodes (450, 250/450, and 250/450/450/450/450 Å thicknesses, respectively) either electrolyzing Li$_2$SO$_4$ 10^{-4} and 1M solutions (ultrapure compounds dissolved in 18 MΩ×cm^{-1} ultrapure distilled deionized water); 2) mono and double layer electrodes (Cu; Ni; Cu/Ni and Cu/Pd) and Li$_2$SO$_4$ 10^{-3} and 1 M.

2.2 INAA analysis

2.2.1 Sample and Standard Preparation. After electrolysis the thin-film cathodes were removed in a clean room: the spent cathodes and relative blanks, put directly into the irradiation vessels, were irradiated and analyzed; 1 or 2 mL of spent solutions and relative blanks were put into the irradiation vessel, gently dried in stove at 40°C, and then irradiated. All the other samples (PET supports, Pt wire, lab gloves and lab papers) were undergone to the same treatment. The standards were prepared starting from calibrated solutions 1000 µg mL^{-1} of each pure element (Carlo Erba). Known quantities of each solution were exactly dosed by mean of a micropipette (Eppendorf) into the irradiation vessel, gently dried in stove at 40°C, and irradiated.

2.2.2 Irradiation. The samples are undergone to two different neutron irradiations: 1) in the pneumatic channel position (Rabbit) of the TRIGA MARK II reactor at the R.C. ENEA-Casaccia for 1 minute at neutron flux of $1.25×10^{13}$ n×cm^{-2}×s^{-1} (fluence $7.5×10^{14}$ n×cm^{-2}); 2) in the rotating rack (Lazy Susan) of the TRIGA MARK II reactor for 30 hours at neutron flux of $2.6×10^{12}$ n×cm^{-2}×sec^{-1} (fluence $2.8×10^{17}$ n×cm^{-2}). The rack is maintained in constant rotation to make consistent and uniform flow and energy spectrum of neutrons incident.

2.2.3 Measurements. The γ measurements were carried out by mean of a counting system constituted by a HPGe detector (EG&G Ortec, Oak Ridge, TN, USA) (resolution 1.70 keV at 1332.50 keV, relative efficiency 23%, peak to Compton ratio 58:3), an ORTEC 672 amplifier and a multichannel buffer ORTEC 918A connected to 8k channel analyzer through data acquiring system ADCAM MAESTRO II. The energy and efficiency calibrations were performed by ^{137}Cs-^{60}Co (furnished by Laboratorio Metrologia delle Radiazioni Ionizzanti, ENEA-Casaccia) and ^{152}Eu (furnished by Centre Energie Atomique, France) sources, respectively.

3. Results and Discussion

3.1 Preliminary tests on electrodes, solutions and equipment
Preliminary some tests are performed on materials used in the experiments: in particular, we analyzed blank electrodes, electrolytic solutions, PET support, Pt wire, lab gloves and lab paper.

Table 2 shows the element levels, expressed as Bq, in blanks (mono-, double- and multi-layer electrodes and Li_2SO_4 1 M electrolyte).

Table 2. Activities of some elements determined in blank electrodes (Bq) and electrolytic solution (Bq mL^{-1}) after Rabbit irradiation.

Element	Mono Cu	Mono Ni	Mono Pd	Double Cu/Ni	Multi Cu/Ni/Pd/Ni/Pd	Li_2SO_4 1 M
Ag	<5840	<1500	<2200	<2790	<1660	<114
Al	<62	209±1	468±8	2223±12	558±14	3954±50
As	<41	<2	<5	<13	<12	<123
Au	<13	2±1	<3	<5	<3	
Br	<391	<29	145±30	404±111	<133	8920±662
Cl	<32	<30	111±16	168±18	78±15	<81
Cu	298000±2490	2330±105	<166	259140±1308	163560±1742	
Mg	<89	<21	<26	<51	<39	<252
Mn	56±17	66±4	109±5	118±8	143±10	<94
Na	<8	<3	<4	<3	<7	1217±80
Ni	46±16	322±8	<13	318±26	698±36	
Pd	1093±348	7±1	27869±178	337±6	43933±421	
V	<19	<13	205±7	609±10	130±13	<520

It can be noted that typical environmental contaminants such as Al, Br, Cl and Na, are at levels around or below the Minimum Detectable Activity (MDA). The electrodes are clean: the only interesting issue regards a significant activity of Cu and Pd and of Ni and Pd in mono-layer Ni and Cu electrodes, respectively. This is most likely due to a memory effect despite an accurate cleaning of the sputtering system. For the electrolyte, the only relevant fact concerns the activities of Al, Br and Na: the levels depend on the impurities composition of the lithium sulfate.

Table 3 shows the levels of the elements investigated in materials used in the experiments such as PET support, Pt wire, laboratory gloves, laboratory paper and the two solutions (Li_2SO_4, 10^{-3}M and 1M).

Table 3. Activities of some elements determined in PET support after etching, lab gloves, lab paper (Bq), Pt wire (Bq g^{-1}) and electrolytic solution (Bq mL^{-1}) after Lazy Susan irradiation.

Element	PET support	Lab gloves	Lab paper	Pt wire	Li_2SO_4 10^{-3} M	Li_2SO_4 1M
Ag	6.19±0.12	<238	<0.75	1986±46	<0.05	<0.2
Co	0.27±0.07	52±21	18.1±0.6	<33	0.26±0.03	<0.2
Cr	9.43±0.35	<4430	115±6	<15000	4.8±0.2	<10
Eu	<0.08	<224	<1.6	<503	<0.05	<1.6
Fe	<0.35	<500	7.8±1.6	<229	0.79±0.07	<0.7
Hf	4.42±0.05	<407	37±1	<239	<0.11	<0.7
Ir	0.16±0.03	<239	<1.1	3020100±18138	<0.05	<0.4
Ni	<0.13	<410	<2	<44	<0.07	<0.4
Sb	<0.06	<185	46±1	<553	0.16±0.03	1.7±0.2
Se	<0.1	<213	<2	<249	<0.07	1.1±0.4
Ta	0.59±0.11	<374	629±8	1510±61	0.64±0.10	0.98±0.29
Zn	1.14±0.11	3919700±47784	820±12	148±52	0.59±0.10	1.76±0.29

The main considerations regard the levels of Zn in lab gloves, Ta and Zn in lab paper and Ag, Ir, Ta and Zn in Pt wire. The highest level of Zn in laboratory gloves is due to the ZnO or $ZnSO_4$ present inside the gloves as lubricant. This level should be not significant for our experience because, being inside the gloves, Zn can not be transported in the experiment. Maybe, other contamination source of Cr, Hf and Zn is the mould during the etching process. Finally, the values of such elements can justify a possible contamination from Pt wire.

Table 4 shows the results of the elements investigated after the first series of experiments using Li_2SO_4 as electrolytic solution on mono- (Cu, Pd and Ni), double- (Cu/Ni) and multi-layers, obtained subtracting the blank level. Among elements the Au levels are due to a contamination from the platinum anode because of the erosion occurring during the electrolysis process. Other considerations can be applied to Zn, and Mo, W, Cr which belong to the same chemical group and have the same chemical behavior. Further, they participate both to the preparation of the thin-film during the etching process and during the deposition of the thin-film. For these reasons, they can derive from a contamination occurring before the experiments. The most interesting result is the V level: in the various electrodes V amount is reproducible and ranges between 204 and 228 ng except for the mono Pd-layer (25 ng). Finally, levels of other elements are around or below MDA (e.g. As) and index of minimum contamination (e.g. Na)

Table 4. Activities (Bq) of some elements determined in spent electrodes and V amount (ng) after the first series of experiments. The second column reports the irradiation position (IP): R as Rabbit and LS as Lazy Susan. n.d.: not determined.

Element	IP	Mono Cu	Mono Ni	Mono Pd	Double Cu/Ni	Multi Cu/Ni/Pd/Ni/Pd
Activities						
Ag	R	<4150	n.d.	n.d.	<3750	<3430
Ag	LS	n.d.	42±1	<0.5	<0.6	<0.6
Al	R	446±8	<137	<39	<167	<145
As	R	<27	<5.2	<2.4	<16	<8.8
Au	R	<9	38±4	<3.4	15±7	16±7
Au	LS	n.d.	8490±33	1423±8	592±3	1481±11
Br	R	<200	<98	<70	390±138	<156
Br	LS	n.d.	66±1	<8	27.3±0.6	<8
Cl	R	<7	<28	<34	<29	<35
Co	LS	n.d.	2.5±0.5	<0.4	<0.6	2.3±0.4
Cr	LS	n.d.	129±4	<7.4	64±3	<11
Fe	LS	n.d.	<1.3	<1.2	4.5±0.4	<1.6
Mg	R	<57	<37	<16	<55	<49
Mn	R	94±13	99±7	<13	113±11	29±10
Mo	LS	n.d.	9.3±0.5	<0.8	1.4±0.2	32.4±0.4
Na	R	<9	18±7	<6	<12	<10
Sb	LS	n.d.	34±1	5.7±0.4	8.4±0.6	21.2±0.9
V	R	12766±81	12733±81	1507±29	13795±102	17424±425
W	LS	n.d.	578±2	<42	<50	112±3
Zn	LS	n.d.	82±2	71±1	11.8±1.4	92±4
Amount						
V		212	210	25	228	204

Table 5 shows the levels of the elements investigated in this study during the second series of experiments. For Cu/Ni double layers we are set up two different tests. Although it is already considered the subtraction of the blank, there are measurable levels of Ag, Cr, Fe, Se, Ta and Zn. This may be due to minimal presence of contaminants (detectable only by INAA). These contaminants are deposited on the cathode during the electrolysis process: even if they are measurable, this is really an apparent enrichment and, according to us, this is not due to transmutation phenomena in condensed matter. Furthermore, the levels of some elements, expressed as ng, show that ultra-trace levels of contamination should always be considered.

Table 5. Activities (Bq) and amount (ng) of some elements determined in spent electrodes after the second series of experiments (Lazy Susan irradiation position).

Element	Mono Cu	Mono Ni	Double Cu/Ni	Double Cu/Ni	Double Cu/Pd
Activities					
Ag	3.6±0.3	144±2	8.89±0.24	39.1±0.63	6.03±0.30
Co	<0.37	<0.39	<0.50	1.33±0.39	8.9±0.3
Cr	598±3	341±2	69±2	733±3	475±3
Eu	1.85±0.83	<1.07	<0.81	<1.46	<1.24
Hf	<0.94	<1.2	<1.1	<1.3	<1.2
Ir	76±6	451±3	156±1	407±3	154±1
Ni	<1.2	<1.34	<1.67	<1.70	2.08±0.20
Sb	<0.82	<0.82	<0.73	<1.04	<1.34
Se	5.88±0.32	4.15±0.32	<0.59	2.36±0.33	<0.88
Ta	9.75±0.44	6.46±0.48	<2.1	6.75±0.61	21.3±1.3
Amount					
Ag	27±2	1083±28	67±2	294±8	45±3
Co	<0.66	<0.70	<0.89	2.4±0.7	15.9±0.6
Cr	1020±9	582±3	117±3	1250±9	810±7
Fe	3410±160	2500±180	3060±270	3990±270	4790±25
Zn	1509±78	825±3	354±24	567±33	920±50

4. Conclusion

INAA was useful to investigate the possible formation of new species attributable to the transmutation phenomena. For this purpose we studied each system component and, after the experiments, the electrodes and electrolytes. Resuming the results it can be evidenced: a) the Ag, Au, Ir, Ta and Zn levels are due to contamination problem from platinum anode (mainly because of the erosion occurring during the electrolysis process); b) the presence of Cr, Hf, Mo, W and Zn can be attributed to mould during the etching process and to their participation to the thin-film preparation; c) the contamination of Ag, Co, Cr, Fe and Zn at very low levels (detectable only by INAA) can be attributed to cathode deposition during electrolysis. Actually, this is an "apparent" enrichment and not due to transmutation phenomena in the condensed matter

The only anomaly which is difficult to give some explanations regards the V levels (ranging between 25-280 ng) found in the first experiment. The proportionality with the applied current and the evidence on all kind substrates is pointing in the direction of an eventual contamination.

Finally, our consideration regards the future researches: a good strategy is to use suitable markers (e.g. radiotracers).

5. Reference

[1]   M. Fleischmann and S. Pons: *J. Electroanal. Chem.* **261** 201 (1989).
[2]   S.E. Jones, E.P. Palmer, J.B. Czirr, C.L. Decker, G.L. Jensen, J.M. Thorne, S.F. Taylor, J. Rafelsky. *Nature* **338** 737 (1989).
[3]   F. Scaramuzzi: *Account. Res.* **8** 77 (2000).
[4]   L. Bertalot, L. Bettinali, F. De Marco, V. Violante, P. De Logu, T. Dikonimos Makris, A. La Barbera: *Procedings of the II Annual Conference on Cold Fusion*, edited by T. Bressani, E. Del Giudice, G. Preparata, **33** 3 (SIF, Como, 1991).
[5]   M.H. Miles, B.F. Bush, G.S. Ostrom, J.J. Lagowsky: *Procedings of the II Annual Conference on Cold Fusion*, edited by T. Bressani, E. Del Giudice, G. Preparata, **33** 363 (SIF, Como, 1991).
[6]   M.C.H. McKubre, R. Rocha-Filho, S.I. Smedley, F.L. Tanzella, S. Crouch-Baker, T.O. Passell, J. Santucci: *Procedings of the II Annual Conference on Cold Fusion*, edited by T. Bressani, E. Del Giudice, G. Preparata, **33** 419 (SIF, Como, 1991).
[7]   D. Gozzi, F. Cellucci, P.L. Cignini, G. Gigli, M. Tomellini, E. Cisbani, S. Frullani, G.M. Urciuoli: *J. Electroanal. Chem.* **452** 253 (1998).
[8]   S.E. Jones, F. Scaramuzzi, M. Fabrizio, C. Manduchi, G. Mengoli, E. Milli, G. Zannoni: *Proceedings of the Rome Workshop on the Status of Cold Fusion in Italy*, edited by B. Stella, 74 (Rome, 1993).
[9]   E. Yamaguchi and T. Nishioka: *Proceedings of the 3rd International Conference on Cold Fusion*, edited by H. Ikegami, 179 (Nagoya, Japan, 1992).
[10] S.F. Taylor, T.N. Claytor, D.G. Tuggle, S.E. Jones: *Fusion Technol.* **26T** 180 (1994).
[11] T. Aoki, Y. Kurata, H. Ebihara, N. Yoshikawa: *Fusion Technol.* **26T** 214 (1994).
[12] V. Violante, E. Santoro, F. Sarto, L. Capobianco, A. Rosada: *Energia Ambiente Innovazione* **2** 38 (2003).
[13] G.H. Miley and A. Patterson: *J. New Energy* 1 5 (1996).
[14] J. Bockris, G.H. Lin: *J. New Energy* **1** 111 (1996).
[15] G.H. Miley, G. Narne, M.J. Williams, A. Patterson, J. Nix, D. Cravens and H. Hora: *Proceedings of the 6th International Conference on Cold Fusion*, edited by M. Okamoto, 629 (Lake Toya, Japan, 1996).
[16] Y. Iwamura, T. Itoh and M. Sakano: *Proceedings of the 8th International Conference on Cold Fusion*, edited by F. Scaramuzzi, 141 (Lerici, 2000).
[17] P. Avino, G. Capannesi, A. Rosada: *Toxicol. Environ. Chem..* **88** 633 (2006).
[18] L.A. Currie: *Anal. Chem.* **40** 586 (1968).
[19] J.C. Leclerc, A. Cornu: *Neutron Activation Analysis Table* (Heyden, London, 1989).
[20] V. Violante, P. Tripodi, D. Di Gioacchino, R. Borelli, L. Bettinali, E. Santoro, A. Rosada, F. Sarto, A. Pizzuto, M. McKrube and F. Tanzella: *Proceedings of the 9th International Conference on Cold Fusion* 376 (Beijng, China, 2002).

Mass Spectrometry: Critical Aspects of Particles Detection related to Condensed Matter Nuclear Science

M.L.Apicella, E.Castagna, S.Lecci, M.Sansovini, F.Sarto, V.Violante RdA

ENEA, Frascati Research Centre,Technical Unit for Nuclear Fusion
Via Enrico Fermi, 45 - 00044 Frascati (Rome) ITALY

E-mail: francesca.sarto@enea.it

Abstract. The detection of transmutations in Fleischmann and Pons experiments is a critical issue in order to assess the nuclear origin of the excess heat production. A very accurate study in this field has been carried out in ENEA, aimed to investigate the possible occurrence of nuclear transmutation in nickel hydride thin films. The research work, which took several years and involved an international collaboration between many research laboratories, came to the conclusion that the experiments didn't produce any evidence of transmutation experiments, pointing out the importance of using state of the art instrumentation in performing such a kind of study.

1. Introduction

In the last decades some scientific papers have been published on the study of nuclear transmutation reactions in condensed matter, in which the formation of new nuclear products as a consequence of eventual nuclear reactions was investigated. In this contest, a specific research activity based on electrolysis experiments has been developed at ENEA, by using Instrumental Nuclear Activation Analysis (INAA) [1] and Secondary Ions Mass Spectrometry (SIMS) [2, 3]. SIMS is a very powerful technique to approach this problem, since it is able to measure the atomic composition of a material with very high sensitivity, but also the isotopic abundance of each atomic specie, that, if different from the natural distribution, is a solid evidence of the occurrence of a nuclear reaction. Actually, the "appearing" of new elements which were not detected before, in Fleischmann and Pons (F&P) experiments, can be likely caused by contaminations, which are very critical to be ruled out due to the extremely low signals involved in the transmutation investigation.

In this communication, we review some previous results [2,3] concerning the study of nuclear ashes in nickel hydride thin films undergone to electrochemical experiments and report new experimental data which allow to get a definite and coherent interpretation of the complete research work.

2. Experimental methods

The electrochemical cells used in the F&P experiments were made of pure polyethylene. The anode was made of 99.98% Pt wire wound in the form of a flat spiral and the cathode was a thin film of Ni deposited by ion beam sputtering on a polymeric substrate made of the same pure polyethylene material of the cell. During the sputtering process, two identical films were deposited, one to serve as a control while the other was used for electrochemical loading with hydrogen to form nickel hydride. The electrolyte was 1M Li_2SO_4 in pure H_2O (distillated at 18 MΩ). Electrolysis was performed for time periods varying from 4 min to 20 hours. Additional details of the all the experimental setup can be found in previous publications [2, 3].
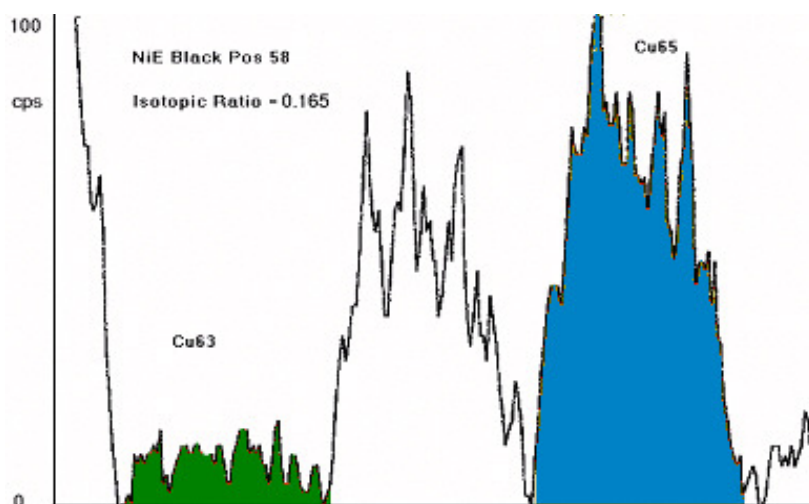
Fig. 1 - SIMS spectrum of the active film in the range of 63-65 nominal masses.

3. Results and discussion

Copper was selected as a marker for the experiment, because it is the most likely product of the reaction between protons and Ni and, in addition, Cu has only two stables isotopes having nominal masses of 63 a.u. and 65 a.u., respectively.

SIMS analysis was performed on the surface of the thin-film cathodes, both on the electrolyzed sample and its relative control one. The used facility was a Quadruple Analyzer SIMS, which had 0.5 a.u. mass resolution and allowed to analyze both the samples in the same measurements run. Preliminary results showed, "apparently", a quite big shift of the Cu isotopic ratio (see Fig. 1), being the $^{63}Cu/^{65}Cu$ mass ratio equal to 0.165 instead of the natural value of 2.2; in addition, by repeating the analysis in different zones of the sample, the observed discrepancy with the natural value was more significant into the center of the electrode than on the border [2].

In order to confirm the results, the measurements were repeated by a Super SIMS facility, the access to which was granted thanks to the scientific collaboration with the National Research Laboratory (NRL, Washington D.C., USA) [4]. Super-SIMS (also called Accelerator-SIMS) is the combination of Secondary Ion Mass Spectrometry with Accelerator Mass Spectrometry (AMS). The main advantage of this technique compared to conventional SIMS is the virtually complete suppression of molecular background and dark-counts. Detection limits for trace elements can therefore be improved by orders of magnitude and are only limited by contamination and count rates, achieving levels as low as ppb to ppt. The new measurements did not confirm the old ones, reporting a value of the Cu isotopic ratio equal to the natural one, within the measurement accuracy, in both the electrolyzed and the reference samples [3]. Speculations on the possible explanation of the discrepancy between the previous and the new results and on the presence of possible artifacts in both measurements were presented in ref. [3].

The possibility to repeat the measurement with a high resolution Time Of Flight (TOF) SIMS allowed the story to come to a conclusion. The employed instrument was the TOF MiniSIMS manufactured by SAI (Scientific Analysis Instruments), whose used was granted thanks to the collaboration with Assing S.p.A. (Italy). The TOF MiniSIMS has superior mass resolution (m/Δm higher than 600 in the mass range of interest), that makes it able to distinguish between single elements and organic compounds. The new analysis revealed that the peak at the nominal mass 65 was constituted by two contributions, the more intense of which was assigned to an organic compound ($C_5H_5^+$), while the other at 64.93 a.u. well fit $^{65}Cu^+$ (see Fig. 2, bottom graph). The peak at 63 a.u. was also made by two sub-bands, one at higher mass assigned to $C_5H_3^+$ and the other at 62.93 a. u. to $^{63}Cu^+$ (see Fig. 2, top graph). Based on the above identification of the peaks, the mass ratio of the copper isotopes resulted to be 2.0, which well match to the natural value (2.2).
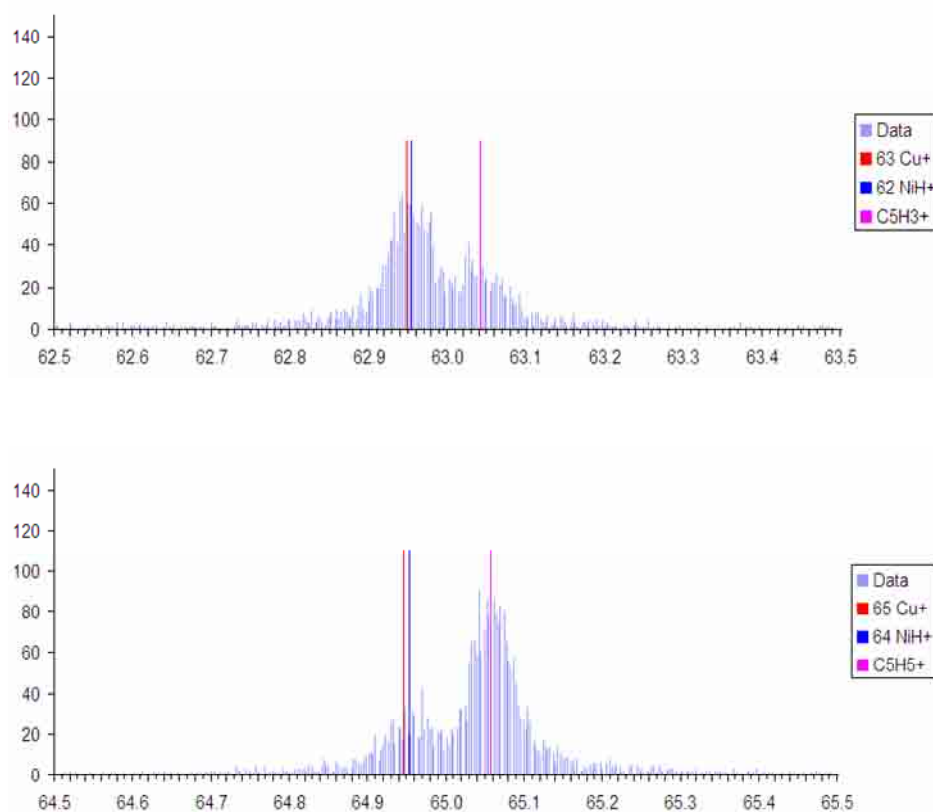
Fig. 2 - TOF-SIMS high resolution spectrum of the active film, in the range of 63 nominal mass (top) and 65 nominal mass (bottom).

The organic compounds detected by the TOF MiniSIMS were probably produced during the SIMS beam bombardment of the sample, emerging from the zones of the polyethylene substrate where the nickel film was more damaged. The higher the exposed area of the polymeric substrate (in the middle of the sample, because of the film micro-cracks) the larger the "apparent" shift.

The reason why the measurement performed by using SUPER-SIMS did not revealed the organic compound, although the instrument had a very high mass resolution, is that the high energy of the impinging ions destroys any organic compounds which may be produced. This did not happen in the case of TOF MiniSIMS and Quadruple SIMS used in the first analysis, which both have the energy of the primary ions in the range of a few keV.

4. Conclusions

In conclusion, after the first experimental campaign we repeated two times the isotopic composition measurements, on the same samples, by using two high performance SIMS. The new analysis revealed that the Cu isotopic ratio was the natural one and that the apparent shift was due to the organic compound C5H5. Then, the apparent isotopic shift was an artifact produced by the not enough resolution of the SIMS used in the first measurement performed in 2003. Then the experiments didn't produce any evidence of transmutations.

The work highlighted the importance of using status of the art instrumentation in performing transmutations studies.

5. References

[1] P. Avino, E. Santoro, F. Sarto, V. Violante, A. Rosada, "Neutron activation analysis for investigating purità grade of copper, nickel and palladium thin films used in cold fusion experiments", J. Radioanal. Nucl. Chem. (2011) DOI 10.1007/s10967-011-1296-3.

[2] V. Violante, M.L. Apicella, L. Capobianco, F. Sarto, A. Rosada, E. Santoro, M. McKubre, F. Tanzella, C. Sibilia, "Serch for Nuclear Ashes in Electrochemical Experiments", Proc. of *10th Int. Conf. on Cold Fusion (ICCF-10)*, Cambridge, Massachusetts, USA, World Scientific Inc. (2003), pp. 405-420.

[3] M. Apicella, E. Castagna, G. Hubler, M. McKubre, F. Sarto, C. Sibilia, A. Rosada, E. Santoro, F. Tanzella, V. Violante, "Progress on the Study of Isotopic Composition in Metallic Thin Films Undergone to Electrochemical Loading of Hydrogen, Proc. *12th Int. Conf. on Cold Fusion (ICCF12)*, Yokohama, Japan, (2005), pp. 264-271.

[4] Accelerator Super-SIMS facility at the Swiss Federal Institute of Technology Zurich (ETH, Zurich, Switzerland), by Dr. M. Doebely.

[5] Millbrook ToF MiniSIMS Analysis Report No 334, Analyst: Dr John Eccles; www.assing.it

Evidence for Fast Neutron Emission During SRI's SPARWAR/GALILEO Type Electrolysis Experiments #7 and #5, Based on CR39 Track Detector Record

A.S. Roussetski[1*]A.G. Lipson[2], F. Tanzella[3], E.I. Saunin[2], and M. McKubre[3]

[1] *P.N. Lebedev Physics Institute of Russian Academy of Sciences, Moscow 119991, Russia*
[2] *A.N. Frumkin Institute of Physical Chemistry and Electrochemistry, Russian Academy of Sciences, Moscow 119991, Russia*
[3] *SRI International, Menlo Park, CA, 94025, USA*

E-mail: rusets@x4u.lebedev.ru

Abstract. We have reported [1] the detailed analysis of the CR-39 detector (Landauer) from SRI's #BE013-7 (#7) Pd deposition experiment where the detector was separated from the cathode wire by a 6 μm Mylar® film. The Mylar® protected the CR-39 surface from chemical, mechanical, and electrostatic (spark discharge) damage during electrolysis. Inthis report we compared those results with that of the CR-39 detector, installed as in #7, in an identically operated cell using light water and with the background detector placed 2 m from the electrolytic cell.

1. Introduction

For the last 3 years claims have been made that during Pd electroplating onto Ag-wire cathodes (or other metal wires) from Pd/D_2O solution, high intensity emissions of charged particles were observed [2]. The emissions have been detected using CR-39 track detectors. The typical pit densities observed in these experiments is 10^7-10^8 pit/cm^2 and the pits are primarily located on surface of the CR-39 nearest where the cathode wire was pressing directly onto the CR-39.
The purpose of this present study is:

- To search for reality of nuclear emissions reported using Pd electrodeposition technique and CR-39 detectors. To separate pits caused by mechanical defects (electric discharge) from that of nuclear origin.
- To test applicability of our track identification technique (see A. Roussetski et al, ICCF-12, Yokohama, 2005 [1], Fig.1) based on in depth destructive etching of the CR-39 detectors, allowing us to obtain track diameter evolution vs. removed depth, to the Pd electrodeposition experiment.
- To apply the CR-39 technique to in-situ neutron detection near an electrolytic cell. To compare the results with that obtained in Blank (H_20 electrolysis) and Background (no cell) experiments as well as with a BF_3 proportional detector count rate.

A series of experiments have been performed where Pd was electrodeposited onto Ag-wire cathodes with CR-39 plastic track detectors separated from the electrolyte and electrodes, with the cell placed in an external magnetic field [3]. The Blank (H2O electrolysis) and Background (CR-39 2 m from the cell) experiments were performed using same series Landauer CR-39 sheet as used in the original D2O experiment. Contrary to earlier studies, the CR-39 detectors in this study were not in contact with the cathode or electrolyte, protecting the CR-39 surface from mechanical stress and electrostatic (discharge) damage during electrolysis. In addition to the CR-39 detector, a low self-efficiency proportional BF3 spherical neutron dosimeter was employed in each experiment.

2. Experimental

The same lot of CR-39 chips (2cm x 1cm, Landauer Inc.) were used in all experiments and calibrations. After exposure the chips were immediately exposed to 6N NaOH at 70°C for 7 hours yielding an etch rate of 1.3µm/hr.   Pd was electrodeposited onto Ag-wire cathodes with CR-39 plastic track detectors separated from the electrolyte and electrodes, with the cell placed in an external magnetic field [3]. The detectors from the #7 and #5 experiments were separated from the cathode and electrolyte by sheets of 6 µm Mylar® and 60 µm polyethylene, respectively. The blanks were performed using the same electrochemical parameters, salts, and CR-39 placement as in the #7 and #5 experiments substituting H_2O for D_2O.   The background CR-39 detectors were held 2m from the operating cell. A Ludlum proportional BF3 spherical neutron dosimeter with self-efficiency of 2.5x10-3 (with respect to Cf-252 fast neutrons) was employed in each experiment.

Calibration chips were exposed to proton beams of 1.0 - 2.5 MeV from a Van DeGraaf accelerator–and etched at 1.3µm/hr. Fig. 1 shows the raw data and the calibration curve obtained from proton bombardment on CR-39 chips identical to those used in the electrolysis experiments. During analysis the CR-39 detectors were etched three more times, at a bulk etch of rate 1.3 µm/hr. Track detection was performed manually using the "PAVICOM" track processing facility in Lebedev Physics Institute, Russian Academy of Sciences, Moscow.. Proton recoil track distributions from a weak Cf-252 neutron source (120 n/s) are presented in Fig.2.
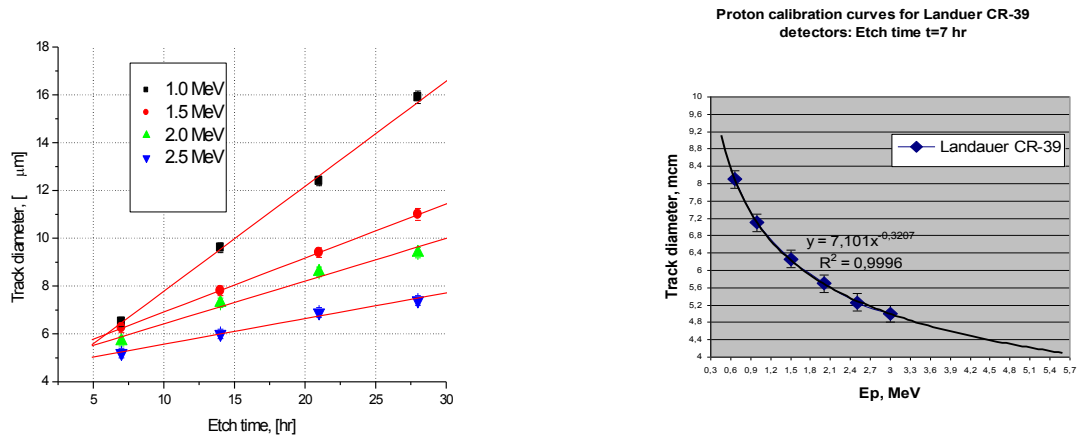

Fig.1 - Track diameter vs. etching time for four different proton energies (left). Proton calibration curve (right).
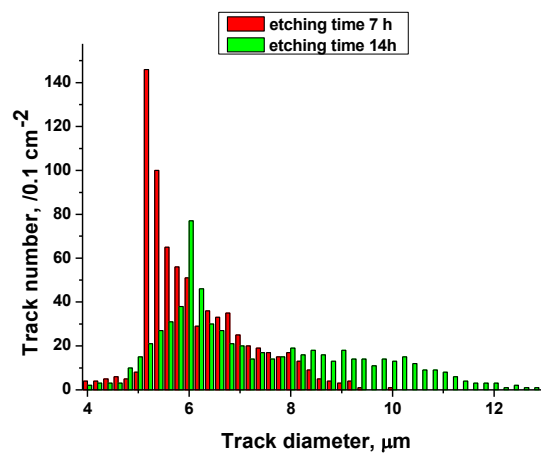

Fig.2 - Proton recoil track distributions (track number vs. track diameter) obtained with Cf-252 neutron source.
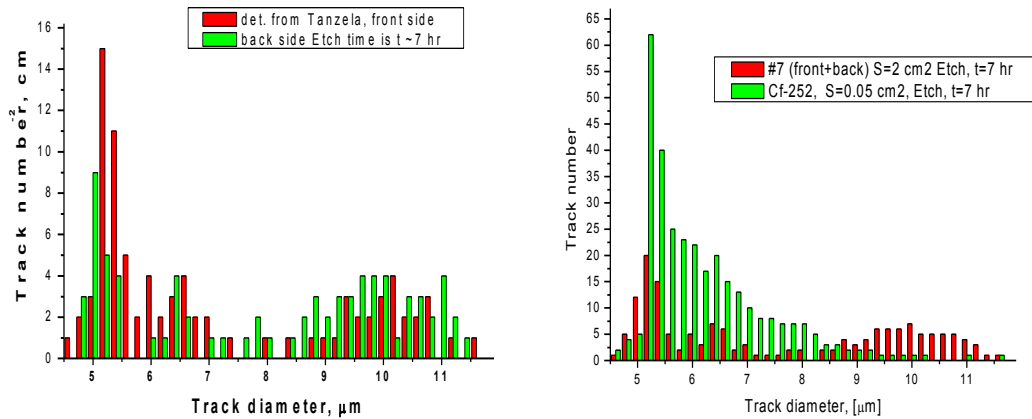
Fig.3 - Tracks from #7 detector, after 1st etch (left picture); Comparison to neutron calibration (right picture).

3. Results

After the 7-hr etch the proton recoil spectrum from experiment #7 is located between 4.5 and 9.0 µm track diameter with a maximum near 5.2 µm. This maximum is consistent with the mean recoil proton energy in the range of 2.2-2.5 MeV. The broader recoil spectrum after the 14-hr etch is between the between 5.0 and 12.0 µm proton recoil track diameters with the maximum near 6.0 µm. This shift in maximum track diameter from 5.2 to 6.0 µm is consistent with 2.2-2.5 MeV protons. The neutron detection self-efficiency of CR-39 after the second etch (1.2×10^{-4}) is about factor of 1.3 higher than that after the first etch (0.9×10^{-4}) due to the increase in proton recoil critical angles at the greater depth. Fig. 3 shows the track diameter results measured from both sides of the #7 detector after the first etch compared to that for Cf-252 recoil. For the front side: the total number of circular and elliptic tracks (normal and oblique incidence) is N=77 cm^{-2}, with about 30 % of all tracks having elliptical shape. For the backside: N=40 cm^{-2}. In the range of 4.5-8.0 µm the track diameter plot for #7 looks similar to that for Cf-252.

Fig. 4 shows a comparison of #7 data with that from the H$_2$O experiment and the Background after the 1st etch. The Blank and the Background data show no sign of proton recoil from fast neutrons proving that there was no accidental neutron irradiation of CR-39 sheet during transit.

Fig.5 compares all above background tracks from the #7 (D$_2$O) track detector after the 2nd etch with that from the Cf-252 calibration. The above background track distribution in the range of 4.5-11.0 µm is nearly identical to that from the Cf-252 recoil measurements. The D$_2$O detector showed 101 tracks/cm^2. Fig.6 compares all above background tracks from the #7 (D$_2$O) track detector after the 2nd etch with that from the H$_2$O experiment and the background detector. Fig.7 shows a rough reconstruction of the protons recoil spectra for CR-39 detectors obtained during the D$_2$O electrolysis run #7 and during exposure to a Cf-252 neutron source after the 2nd etch. The reconstruction was
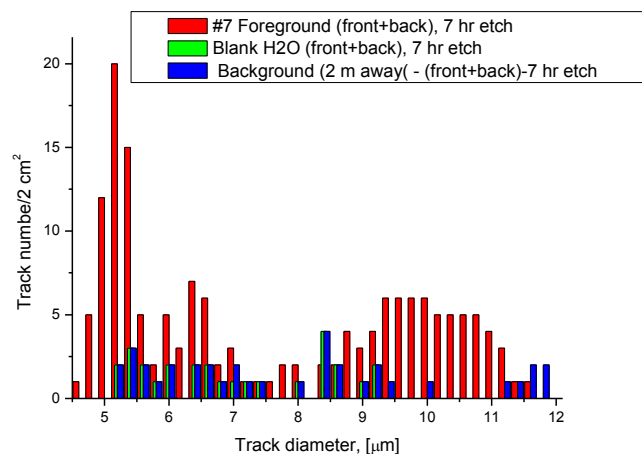

Fig.4 - Comparison of #7 data after 1st etch with that from Blank experiment and Background.
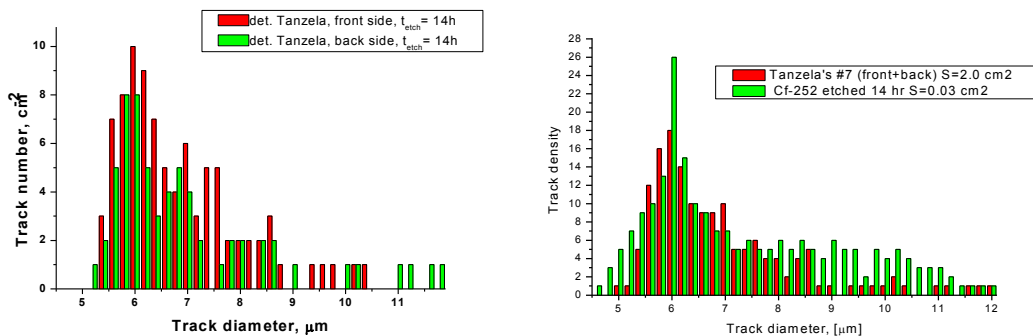
Fig.5 - Comparison of the #7 track detector distribution after the 2nd etch with that of the Cf-252 recoil .

deduced from the track density vs. track diameter histograms, taking into account the track diameter vs. proton energies after the 2nd etch and the critical incidence angle θ_c vs. proton energy.

We also noted that statistically significant counts were recorded by the BF$_3$ dosimeter during the D$_2$O runs #5 and #7.

3. Discussion

After the 1st etch the average track density on both sides of the detector <N(fg)> is 58.5 tracks/cm^2. The total background track density on both sides of blank detector <N(bg)> is 6.0 tracks/cm^2. After subtraction <ΔN> is 52.5 ± 8.0 track/cm^2. Assuming a "neutron source" was a cathode wire in a 2π-geometry with respect to the CR-39 surface, the neutron count rate/intensity (I$_n$) would be 2<ΔN>/(t × ε_s), where the CR-39 self-efficiency after the 1st etch (ε_s) is 9.2 x 10^{-5} and t is the electrolysis time. Assuming that the neutrons were emitted when the current was greater than 0.5 mA (t = 15 days), I$_n$ = 0.90 ± 0.14 n/s. If we assume that the neutron emission was observed only when neutron dosimeter read above its background (t = 4 days), I$_n$ = 3.38± 0.53 n/s. So, the neutron emission rate in the D$_2$O run #7 is in the range of 1.0-3.0 n/s. After the 2nd etch, <N(fg)> = 88 cm^{-2}, while <N(bg)> = 26 cm^{-2}, and ε_s = 1.17 x10^{-4}. I$_n$ is again is in the range of 1.0-3.0 n/s as shown after the 1st etch.

The #5 CR-39 detector used in SRI BE010-5 PdD$_x$ deposition electrolysis experiment had a 60 µm polyethylene film adhered to both faces while immersed in the electrolyte and in contact with the cathode. Although the front face was found to be covered with high density pits (defects) making it almost impossible to distinguish real nuclear tracks from defects, the rear face of #5 detector shows proton recoil tracks similar to those found on both faces of the # 7 CR-39 (with a track density 50 -70% of that of #7).   These pit densities are shown in Fig. 8 and actual pits are shown in Fig. 9.
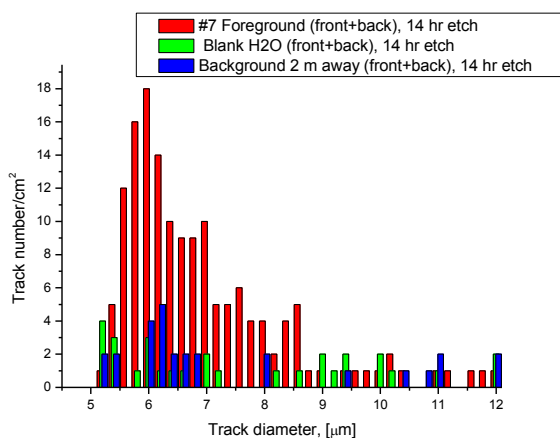

Fig.6 - Comparison of Foreground #7 data (taken from both sides) with that from Blank experiment (H$_2$O electrolysis) and the Background (detector is placed 2m away of the electrolytic cell) - 14 hr etch
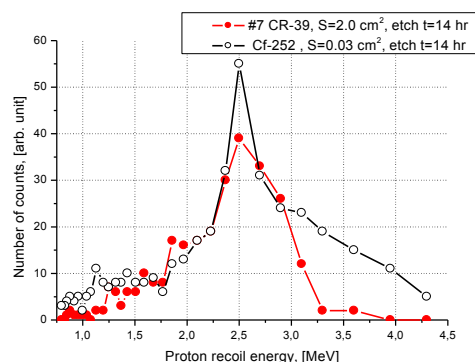
Fig.7 - Rough reconstruction of the protons recoil spectra from both the D$_2$O run and the Cf-252 exposure.
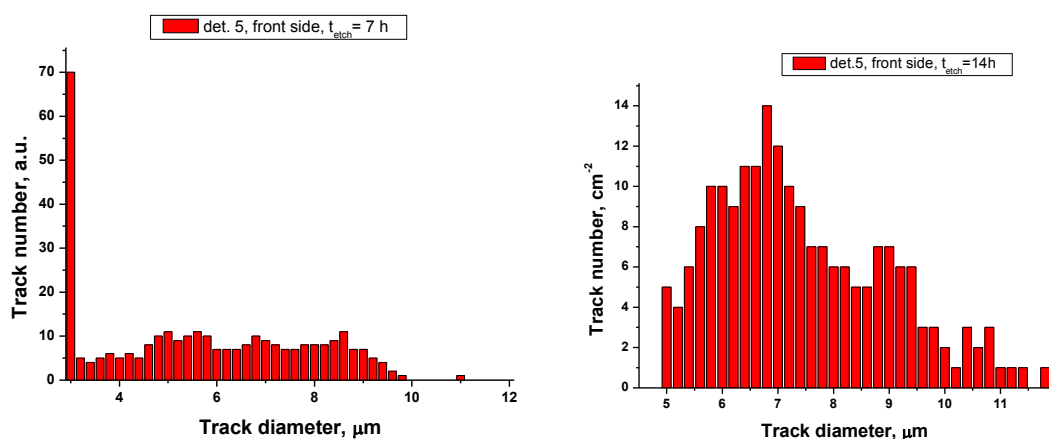
Fig.8 - Individual pit density at the front side of #5 detector: 7 hr (left) and 14 hr (right) etch

The analysis of the back side of detector #5 after the 1st etch showed $N(Fg) = (30.0\pm5.5)$ recoil protons/cm^2, $N(Bg) = 6 \pm4$ cm^{-2}, $\Delta N = 24.0 \pm 6.8$ p/cm^2, and $<In> = 2<\Delta N>/(t\epsilon_s) = 0.30\pm0.08$ n/s. After the 2nd etch (back side only): $N(Fg) = 45$ cm^{-2}, front $N(Fg) = 63$ cm^{-2}, $<N(fg)> = 54.0\pm7.3$ cm^{-2}. Background $<N(bg)> = 26\pm5$ cm^{-2}, $\Delta N = 28\pm9$ cm^{-2}, and $<In> = 2<\Delta N>/(t\epsilon_s) = 0.29\pm0.09$ n/s in 2π solid angle. If t = 1 day In = 6.0 ± 1.6 n/s in 2π solid angle. These results are shown in Fig. 10.

At a self–efficiency to fast neutrons $\epsilon_s = 7.6\times10^{-3}$ (R~ 0 cm) and detector-source distance of 10 cm, the total efficiency of BF$_3$ sphere for fast neutrons (ϵ_t) would be 7.6×10^{-5}. The sensitivity of the detector to fast neutrons (minimal detectable emission rate) can be expressed as: $S = 3[<N_b>/(\epsilon_t 2\tau)]^{1/2}$, where $<N_b>$ is the averaged background count rate, and τ is the duration of neutron detection. For detector #7: $<N_b> \approx 6.0$ cps, $\tau = 15$ days, resulting in $S \approx 150$ n/s, (300 n/s, when t=4 days). This results is 100 times higher than that measured by the CR-39 detector in that experiment. This is also true for the results measured in experiment #5.

4. Conclusions

- Entire results of two CR-39 detectors analysis show that a weak, but statistically significant emission of fast neutrons has been observed in the SRI's #7 and #5 runs replicating SPAWAR Pd-depostion experiment (in the presence of an external electromagnetic field).

Fig.9 - Proton recoil tracks at the front side of #5 detector and the defects ("ground beef") after 2nd etch.

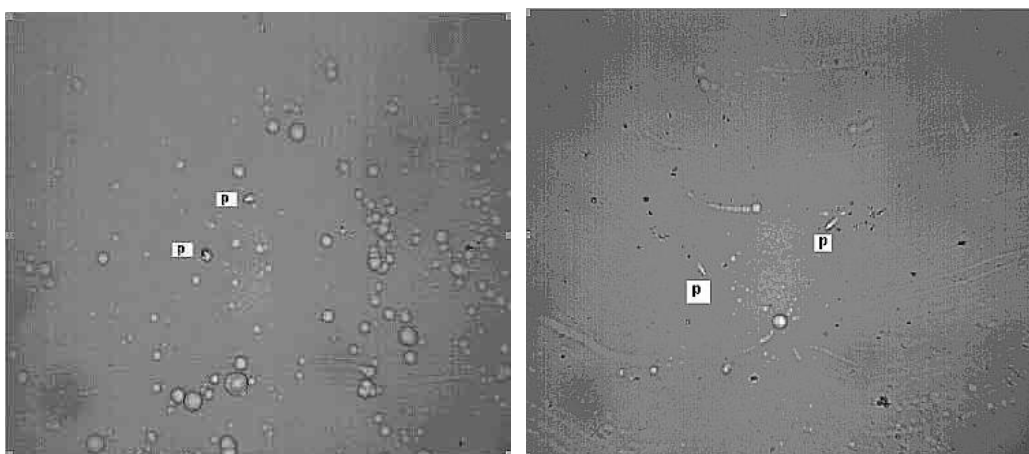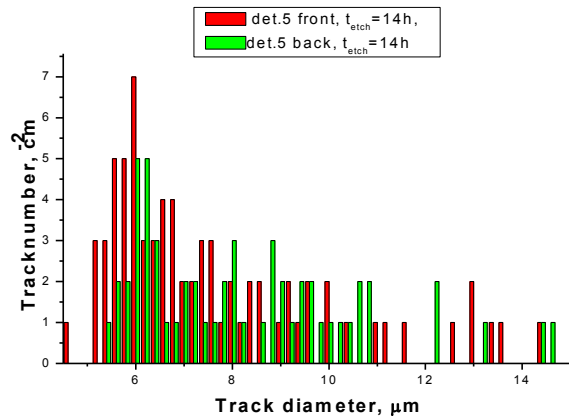Fig.10 - Comparison of the back and the front side proton recoil spectra at t = 14 hr etch

- The #7 detector separated from the elctrolyte by a 6 μm Mylar® film shows "clean" front and back faces, containing only nuclear tracks (proton recoil). While the #5 detector, submerged in the electrolyte but covered with a 60 μm PE film, had vast areas covered by defects ("ground beef") on the front face lower (than #7) proton recoil density at the back side
- The small diameter defect pits were eliminated by in-depth etching (>18 μm) allowing us to distinguish real proton recoil tracks caused by neutrons as well as by energetic charged particles (protons and alphas) emitted from the PdD_x powder being deposited on top of the detector during electrolysis.
- Comparison of proton recoil spectra (track number vs. their diameter) of the analyzed detectors with that of their respective Blank and Background runs and with the tracks from Cf-252 source gives solid evidence for a fast neutron emission taking place during the runs #7 and #5.
- Comparison of the neutron emission rates obtained from CR-39 analysis with that deduced from SRI (proportional BF3 detector) measurements shows a of the results, suggesting orders of magnitude higher neutron emission recorded by SRI detector than that calculated from the noiseless CR-39 measurement data .
- Because of the huge discrepancy between the CR-39 and BF_3 dosimeter results and since the dosimeter has very low neutron sensitivity we assume that the excess dosimeter counts contain significant electromagnetic noise, induced by the electrolysis power supply.
- In order to provide additional confirmation for our CR-39 results on neutron emission in SRI experiments, a high-efficiency neutron spectrometer would be desirable.

Acknowledgements

5. References

[1] A.S. Roussetski et al, *Proceedings of ICCF12, Yokohama, 2005*; Condensed Matter Nuclear Science, edited by A. Takahashi, p. 304-313.
[2] P.A. Boss et al, *Eur. Phys. J. Appl. Phys*. **40**, 293 (2007)
[3] F.L. Tanzella et al, *Presented at the 8th International Workshop on Anomalies in Hydrogen/Deuterium Loaded Metals, Catania, 2007*.

On the products of nucleus reactions formed during deuterium diffusion through palladium membrane

Dmitriy D. Afonichev[1], Evgeniy G. Galkin[2]
1 Institute for Metals Superplasticity Problems, RAS, , Ufa, Russia
2 Institute of Organic Chemistry, UCC RAS, Ufa, Russia

E-mail: afondd@mail.ru

Abstract. We report on the results of experimental observation of interaction of deuterons in a palladium membrane in deuterium gas under the pressure of $P=0,07$ Mpa. The temperature fluctuation with an amplitude of $\Delta T=4\div5^0$ C was observed. After a 42 hour experiment, a significant increase in the number of of tritium (^3T) atoms, $N>10^9$, has been revealed, while no traces of ^4He have been found.

Introduction. The results of the investigation of cold nuclear fusion by M. Fleischmann and S. Pons published in 1989 [1] are not accepted by scientific community until now because of rather small amount of products of nucleus reactions and difficulties with reproduction of their experimental results in other laboratories. The aim of our work is to develop experimental equipment capable of synthesizing essential amount of such products. Our idea is based on the assumption that the composition and the structure of the material saturated by deuterium may have an essential influence on the processes occurring in the solid body at low energy reactions. On our opinion, the intrinsic properties of the metallic matrix determine not only the ability of the material to accumulate deuterium but also the possibility for deuterium nucleus to move and interact.

In our work [2] we have reported on the results of deformation of titanium saturated with deuterium and on the process of saturation. It was concluded that the results depend on the initial structure of the sample. On the basis of the analysis of our results and the results available in the literature, we have proposed a mechanism of nuclear fusion via tritium channel [3].

To confirm the proposed mechanism one should carry out an experiment on generation of a large number of products of low energy reactions. Our experimental setup is based on the following prerequisites:

1. the synthesis of cold fusion products should be continuous,
2. the experiments should be performed at high temperature in order to increase the rate of deuterium diffusion,
3. it is necessary to provide a directed motion of deuterium through metal.

The simplest possibility to satisfy all three conditions is to conduct the experiment in the gaseous atmosphere of deuterium. Since the process takes place at the metal surface [4], the reaction should be facilitated during deuterium diffusion through a membrane. The directed motion can be achieved by a glow discharge at one side of the membrane.

Experimental procedure. In Fig. 1, the experimental equipment is schematically shown.

Fig. 1. Schematic of the experimental equipment: 1 reaction chamber, 2 ceramic tube, 3 nichrome curl of the furnace, 4 stainless steel cylinder, 5 Pd membrane, 6 high voltage vacuum feedthrough, 7 anode, 8 low voltage vacuum feedthrough, 9 control thermocouple, 10 measuring thermocouple, 11 adjustable power supply of the furnace, 12 adapter, 13 computer.
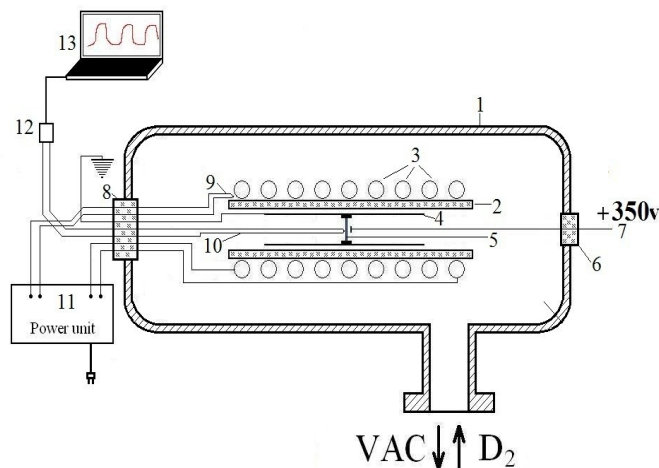
Fig. 1 Schema of experimental chamber

The structure of a palladium foil (Pd -99,8) having thickness of s = 0.1 mm was processed in accordance with the principles developed in [2]. The disk type membrane was sealed in the tube made of stainless steel. The induction furnace provides heating of the tube up to $T=700^0 C$. After vacuumization of the reactionary volume, it was filled with deuterium under P<0,07 MPa. Glowing discharge was applied (DC), (I=40 ma, U=350 v).

Mass-spectrometric analysis of gas content before and after the process was made on the mass-spectrometer "Thermo Finnigan MAT 95 XP" (the resolution R=10000, the scanning range of mass numbers 1 – 18, the ionization energy 70 eV).

The concentration of tritium was measured by a scintillation method according to the procedure described earlier [2].

For the level of neutrons and gamma-quanta measurement a spectroscopic radiometer SRPS-2 was used. The threshold level of neutrons Nпн = 30±2 1/50 sec and gamma-quanta Nпг = 700±15 1/5 sec was not exceeded during the experiment.

Experimental results. Temperature in the vicinity of the membrane was recorded constantly and it is shown in Fig. 2. It can be seen that after two hours the temperature starts to fluctuate, while the discharge current remains constant.
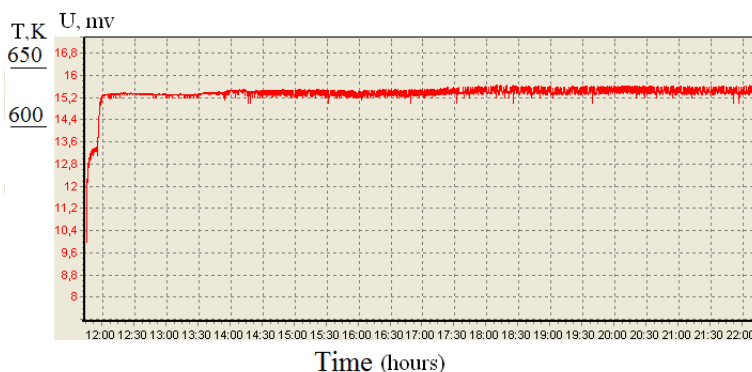
Fig.2 Change in temperature near the membrane

Fig. 3 shows temperature fluctuations in an increased scale. The fluctuations are not stable since the duration of intervals with relatively small and relatively large temperature change. The presence of temperature fluctuations can be explained in terms of the model of low temperature fusion due to resonant transfer of neutron from deuteron proposed in [3]. Deuterons are accumulated in the vicinity of the membrane surface. Afterwards they move to the structure defects and form pairs of quasi-ions D_2^+. During this process the internal stresses grow in the membrane. When these stresses attain certain value, the

quasi-ions leave the metal interior and move in the field of a crystal lattice. There occurs a resonant transfer of neutron from one deuteron to another, resulting in formation of proton and triton nuclei accompanied by heat emission. Since a large number of deuteron pairs participate in this reaction, the temperature fluctuations can be detected even by a thermocouple. When internal stresses are decreased the motion of deuterium pairs ceases, high thermal conductivity of hydrogen isotope gas results in sharp cooling and the temperature of the membrane decreases. Then the process repeats.
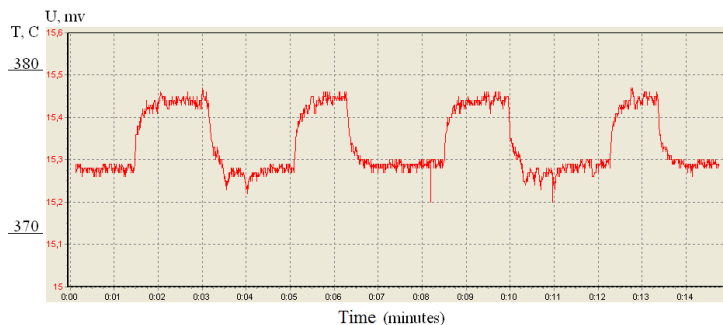
Fig. 3 Fluctuation of temperature after t=36 hours of discharge applied

The process was stopped after t = 42 hour. A part of gas (**v**=100 ml) was collected in metallic vessel and then analyzed by a mass-spectrometer. The remaining gas was absorbed by Ti powder (m=3 g) to analyze for tritium.

The quadrivalent helium was not detected. The amount of ^{4}He was on the background level.

During the experiment, the neutron and gamma quanta did not exceeding the background level. Tritium was measured by scintillation method, and the total amount was N>10^9 atoms.
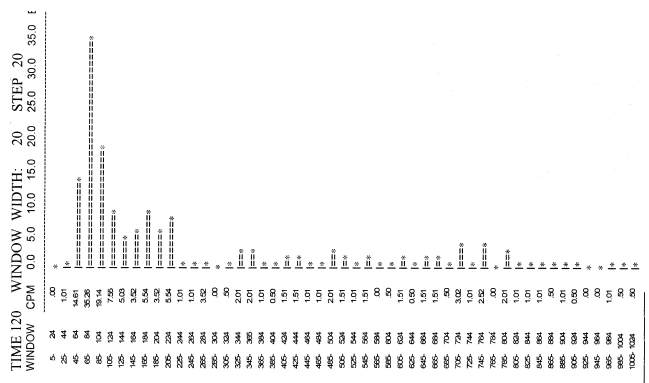
Fig.4 Energy spectrum of tritium solution

Conclusions. A device producing heat and tritium was proposed.

Temperature fluctuations with the amplitude of $\Delta T=4-5^0$ C were recorded.

The essential increase in the amount of tritium, N>10^9 atoms, was registered.

It was shown that the low temperature reaction in deuterium medium occurs via the tritium channel.

References

[1] Fleischmann M, Pons S., *J Electroanal* 1989; 261-301.

[2] Afonichev D.D., Murzinova M.A., *Int J Hydrogen Energy* 2003; 28(9): 1005–1010.

[3] Afonichev D.D., *Int. J. Hydrogen Energy* 2006, 31, 551-553.

[4]. Tsarev V.A., *Sov Phys Usp* 1992; 835:842.

Hot Spots, Chain Events and Micro-nuclear Explosions

M.Srinivasan
Formerly of the Bhabha Atomic Research Centre (BARC), Mumbai, India

E-mail: chino37@gmail.com

Abstract. In 1990 the BARC group presented results at several fora, based on our neutron multiplicity studies as well as tritium measurements, that suggested micro-nuclear explosions seem to occur at localized hot spots in which both Tritium and neutrons are generated, subject to the n/T branching ratio anomaly. It was estimated that about 10^8 to 10^{10} tritium generating lenr reactions take place in these hot spots accompanied by a very small fraction of neutrons. During the last few years several researchers have reported detecting a variety of transmutation reaction products in localized sites, often associated with some type of crater formation. Other experimenters have reported online detection of flashes of "thermal hot spots" in their cathodes. It is therefore tempting to speculate that perhaps the concept of micro-nuclear explosions can be extended to heat generating helium producing reactions too, as well as nuclear reactions responsible for transmutation products. Many theoretical models such as those that depend on the catalyzing role of some exotic intermediate agent (such as Bose-Einstein condensates, deuteron clusters, Erzions, poly neutrons, trapped neutrons etc) seem to point to the possibility of occurrence of chain events. Two decades into the CMNS era, it is therefore worthwhile re-examining the merits of the micro-nuclear explosion hypothesis and seek independent experimental evidence to either corroborate or refute such a hypothesis.

1.   Summary of the early BARC findings

Two decades of wide ranging research has shown that low energy nuclear reactions take place primarily on the surface rather than in the bulk metal, the growing preference for thin films, small diameter wires and nano powders being an indication of this. Further there is convergence of perception that even on the surface, these reactions occur only at certain special locations referred to as "Nuclear Active Environment" (NAE) [1] which are thought to be created during the dynamic transport of deuterons (or protons) in and out of the metal, often initiated by some type of triggering mechanism. However the exact nature of the NAE continues to be elusive.

In the present paper we wish to bring into the conversation the aspect of "localised time" in addition to localised space, governing the occurrence of these reactions. In other words we raise questions regarding the temporal characteristics of the NAE. It is reasonable to expect that NAEs will not all be created simultaneously and uniformly over the entire host metal surface and also, once created, would not be able to continue catalyzing nuclear reactions for "ever". Thus it may be postulated that NAEs are continuously generated and destroyed and during their "lifetime" they trigger a certain number of nuclear reactions. A pertinent question that then arises is : what could be the duration of the lifetime of the NAEs ? Could it be possible that their lifetimes is as small as nanoseconds or microseconds?

This line of thinking leads us to postulate that the lenr phenomenon could comprise of a series of "bursts" of nuclear reactions, each burst composed of "x" numbers of nuclear reactions generated by an NAE site during its lifetime. What could be the temporal characteristics of the reactions within a single nuclear "burst"? Could these individual reactions be "chain correlated", with each new reaction being triggered by the previous or an "exotic" agent or particle responsible for catalyzing these reactions? Alternately the entire "x" numbers of reactions could all take place simultaneously in a coherent fashion, in a "flash"; In either case we are presented with a micro-nuclear explosion!

These speculative considerations are not entirely imaginative but arise out of the multiplicity distibution of neutron counts measurements that our group had carried out during the first few years following the Fleischmann-Pons announcement, with both electrolytically loaded Pd cathodes as well as gas loaded Ti targets. These early measurements led us to conclude, even as far back as 1989 [2], that micro-nuclear explosions are possibly responsible for the generation of tritium in highly localised hot spots. In this paper we first review the sequence of experimental findings that led us to such a conclusion and then go on to examine whether there is any case for extending the concept of micro-nuclear explosions to other nuclear reactions that have been observed in the lenr field.

2. Summary of the early BARC findings

Within days of the Fleischman-Pons announcement in march 1989 a dozen independent groups from various divisions of BARC set up electrolytic cells using whatever materials were readily available. Clear evidence was obtained for the production of neutrons and tritium, signatures of the occurrence fusion reactions, but with the difference that tritium production was higher by several orders of magnitude as compared to neutrons. A comprehensive review of these early BARC results in which over 50 researchers were involved [3] has just been re-published [4]. The main findings are summarised below :

2.1 BARC finding # 1 - Neutron to tritium branching ratio: Majority of the BARC cells produced both neutrons and tritium [5] with the neutron to tritium yield ratio being in the range of $\sim 10^{-7}$ rather than the expected value of unity. BARC groups were among the first to publish [2] this unexpected feature of neutron and tritium production in electrolytic cells. This so called "branching ratio anomaly" has since been observed by several other groups also, inclusive of with devices where in the deuterium loading into titanium samples was effected by gas loading methods. The branching ratio anomaly essentially signifies that on an average one neutron is generated for every 10 million tritons. Surprisingly neutron and tritium production was also noticed in a couple of instances even after the cell current had been switched off in the case of electrolytic cells or with unpurturbed TiD_2 targets just sitting on the table, a behaviour which has since come to be alluded as "life after death" in CMNS literature.

2.2 BARC finding # 2 - Simultaneity of production of neutrons and tritium: In electrolysis experiments neutron yield is measured online using standard neutron pulse detector set ups (BF_3 counters, proton recoil type scintillators etc), while tritium production is measured off line employing liquid scintillation techniques, with the electrolyte being sampled typically once or twice a day or at times once in a few days. In the BARC experiments it was noted that invariably the tritium levels indicated a jump only after one or more neutron emission "spikes" had been detected. Figs 1 & 2 reproduced from Reference [5] bring out this behavior.
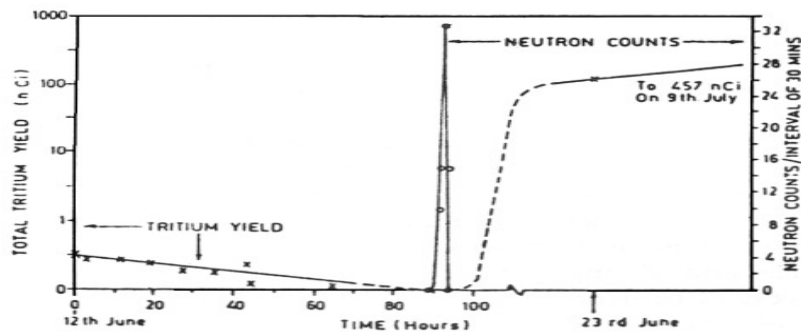
Fig. 1 - Concomitant generation of neutrons and tritium during run 2 of the first Milton Roy cell.

It was inferred from these that neutrons and tritium are probably produced simultaneously. Simultaneity in time would also imply co-generation at the same spatial location as a product of the same event, since it is difficult to conceive of a mechanism responsible for concomitant generation from spatially separated sites since otherwise we are faced with an action-at-a-distance problem.

2.3 BARC finding # 3 - Multiplicity distribution of neutron emission: BARC groups were the first [2,6] and perhaps the only group so far, to have carried out a detailed experimental analysis of the

statistical characteristics of the neutrons emitted by lenr devices. The question we asked ourselves was : Are the neutrons put out by these devices being emitted one at a time following Poisson statistics or are they emitted in bunches of 2, 10 or 100s ? We were inspired to ask such a question primarily because one of us had, decades earlier, carried out a Masters thesis study on the neutron density (or flux) fluctuations in a zero energy experimental fission reactor using the so called Feynmann alpha method [7]. He had the experimental background and familiarity with the statistical analysis methodology readily available to quickly set up the hardware to measure the multiplicity distribution of neutron emission. The details of this are elaborated on further in Section 3 below in view of its central importance to the main theme of the present paper.
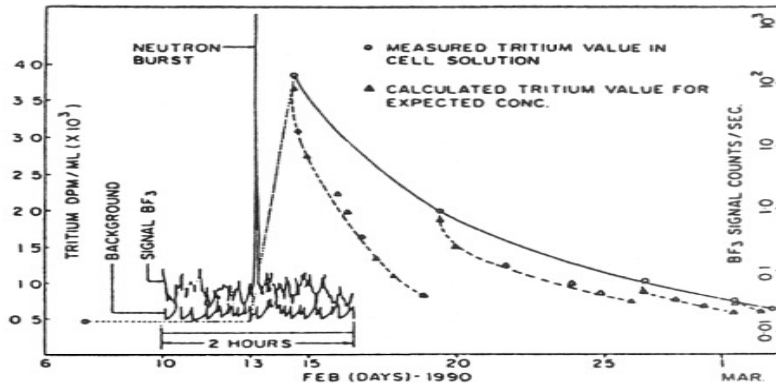
Fig. 2 - Increase of tritium concentration in electrolyte following neutron burst in ROMG cell.

The results of neutron multiplicity studies, repeated on many different lenr devices, clearly indicated that a non negligible fraction (6 to 15%) of the neutrons produced were in bunches of 20 to 400, the exact fraction and magnitude of the bunches being dependent on the efficiency of the neutron detection set up, the characteristics of the lenr device and the type of the deuterium loaded target metal. The intriguing question raised by this finding which has puzzled this author for the last two decades is : what could be the mechanism by which such bunched neutron generation takes place?

2.4 Implication of BARC findings 1, 2 and 3 taken together: If for every neutron produced 10 million tritons are generated "simultaneously" and if say a 100 neutrons are emitted in a bunch then it could be surmised that 10^9 tritons are produced in the form of a micro-nuclear explosion. In this context we have already considered arguments which suggest that all this must be taking place at a highly localized site, because otherwise we would be obliged to invoke an appropriate action-at-a-distance mechanism. In the following it is shown that this is precisely what the autoradiographic images seem to indicate.

2.5 BARC finding # 4 – Tritium found mainly in hot spots in gas loaded Ti targets: BARC groups deployed autoradiography as a very powerful tool to identify the location of tritium embedded in deuterated titanium targets [8]. The samples were placed close to but not touching medical x-ray films giving exposure times in the region of 20 to 60 hours. Both deuterium and hydrogen loaded palladium and titanium samples were investigated. We also carried out a number of basic studies to understand the mechanism of production of images in photographic films deploying various thin absorbers between the target and the photographic film. Such experiments clearly ruled out the possibility that these images could be artifacts caused by chemical reaction of the metallic sample being in direct contact with the emulsion of the photographic film. Besides, in the case of titanium targets, the presence of tritium in the surface layers of the target could be cross checked by measuring the 4.5 kev Ti K-α x-ray, as well as the direct measurement of the 18 Kev tritium βs [9]. In the case of Pd samples however the threshold for production of Pd K-α x-ray is too high for the 18 Kev tritium βs and only direct counting of the tritium β particles needs to be adopted.

It was conclusively established in a variety of gas/plasma loaded titanium target experiments that in the case of machined (cold worked) samples, the tritium generated by low energy nuclear reaction processes is invariably lodged in lattice defect spots and crevices where the metal was subject to severe cold working (edges for example) [10]. For example the plasma focus anodes which were subject to several

charge discharge shots in particular gave spectacular images of the top surface [11]. The auto-radiographic images of rod TA 1, repeatedly measured again and again over a period of five years were remarkably reproducible showing that tritium remains entrenched for years in the same spot in titanium . This observation is indicative of the fact that the tritium must have been produced at these spots and could not have migrated and accumulated there after being generated elsewhere.

Thus as concluded in sec 2.4 the first three BARC findings alone are adequate to support the micro-nuclear explosion hypothesis. But the spotty autoradiographs in titanium further strengthens this speculative hypothesis.

3. Brief review of the neutron multiplicity measurements

3.1 Basis of time resolved detection of individual neutrons of a simultaneously emitted bunch:
When a bunch of simultaneously produced fast neutrons impinges on a large hydrogenous moderator assembly in which one or more thermal neutron detectors such as BF_3 or He^3 gas proportional counters are embedded, because of the statatistical time spread (typically about 25 μs) that occurs during the neutron slowing down process, a certain fraction of the total number of neutrons emitted would get separately and individually detected in a time resolved manner, the exact fraction depending on the geometrical efficiency and other factors. The resultant time series of electronic pulses issuing from the neutron detector set up can then be analysed for its statistical properties, especially the degree of departure from Poissonian nature, in order to yield information on the neutron multiplicity spectrum.

3.2 Experimental techniques for statistical analysis:
Two different techniques were used to determine the statistical characteristics of the pulse train issuing from the BF_3 or He^3 neutron counter banks. In the first method the frequency distribution of counts in 20 ms time bins was recorded [6]. In each sweep of the pulse train there were 1000 such bins, with a 280 ms separation between the 20 ms bins (as required by the data acquisition system), consuming in all a real time duration of 5 minutes per 1000 bin sweep. (The duration of the counting interval selected, namely ~20 ms, was a compromise between the total volume of data required to be stored and the resolution time of the study.)

The second approach to measuring the statistical characteristics of the pulse train was an adaptation of the "artificial dead time" method [6,12] developed originally for investigating neutron density fluctuations in experimental fission reactors [7,13] as well as for the passive neutron assay of plutonium in the safeguards field [14,15]. When more than one neutron from a neutron burst is registered by the BF_3 or He^3 detectors, the corresponding electronic pulses will all be time correlated and closely spaced within about 100 μs of each other. In such events the second, third and subsequent pulses of the "family of pulses" are diverted by a 100 μs wide "artificial dead time gate" into a separate "burst counts analyzer", while the leading pulses are totalized separately. The computerized burst counts analyzer then carries out a frequency of counts analysis to give the multiplicty spectrum of the neutron counts.

3.3 Theoretical considerations[16] :
For a purely random (Poisson) pulse series wherein N_0 is the average count rate and τ is the counting bin time interval (in this case 20 ms) and for the case when $N_0\tau$ is <<1, the probability of registering one count in a single 20 ms interval is $N_0\tau$, while $[(N_0\tau)^2/2!]$ gives the probability of getting doubles, $[(N_0\tau)^3]/3!)$ that of getting a multiplicity of three counts and so on. Note that the probability of getting higher order multiplicity counts decreases steadily, since $N_0\tau$ is much less than unity.

If now there are ζ burst events per second generating ν neutrons per burst, superimposed on the random background and the neutron detection efficiency is ε, then the contribution of the burst events to the overall count rate would be ζνε. The probability of getting r counts in time τ from burst events is governed by a binomial distribution. Table I of ref. [16] summarizes the expressions for the contribution to the various orders of multiplicity counts from random and burst events. Table II of the same paper gives numerical examples with typical parameters for the expected frequency distribution of counts for random and bunched neutronic events. The main point brought out is that whereas for random events and low count rates, the probability of getting doubles, triples etc. is extremely small, in the case of burst

events these probabilities are non-negligible. It is noteworthy that for burst events the peak of the multiplicity distribution actually shifts to higher multiplicity values as the product $v\varepsilon$ increases. Thus when the product $v\varepsilon$ exceeds unity (as for example when a bunch of 100 neutrons are emitted in a single event and detection efficiency ε is 10% in which case the magnitude of $v\varepsilon$ is 10) the probability of registering three or four counts per interval could be even higher than that of singles or doubles counts!

4. Summary of neutron multiplicity measurement results

Neutron Multiplicity measurements were carried out both with a large cathode area Milton Roy type Pd-D_2O electrolytic cell [3,5] as well as some gas/plasma loaded TiD_2 targets. In these "first attempt" experiments conducted in 1989 only the frequency spectrum type analysis was performed. Unfortunately the overall neutron detection efficiency was only around 1 to 1.5%, primarily due to the poor geometrical arrangement of the detector assembly with respect to the source of neutrons. In general we were happy to note that the equipment functioned very satifactorily, with the no source background counts both of the foreground detector as well as the background detector strictly obeying Poisson statistics. Never were multiplicities beyond doubles ever recorded in background runs. One of the unexpected surprises, as already commented upon, was that both a shut off but previously operated electrolytic cell, as well as stand alone TiD_2 targets, produced neutrons even in an unpurturbed state. In all these runs the neutron yield was in the form of distinct spikes superimposed on a steady background.

The 1994 campaign was conducted with a newly procured Milton Roy cell. This time the electrlolyte used was LIOD instead of NaOD which was used in the 1989 runs. (The manufacturer recommended only NaOD. This is being emphasized since use of LiOD could have had a bearing on the neutron production characteristics of the new Milton Roy cell.) We used a large annular neutron detector set up inside the central location of which the electrolytic cell was mounted giving a neutron detector efficiency as high as $\sim$ 10%. For statistical analysis of the pulse train the improved artificial dead time technique discussed earlier was employed. The experiment was conducted over a a two month period : The first 15 days were used to collect background data. The second one month was with the fully operating Milton Roy cell in place ; For the last 15 day run LiOD electrolyte was replaced by LiOH. We thought we were doing a control run; but it turned out that the Pd cathodes probably still had deuterium loaded from the previous one month run. It was evident from the neutron counts data that the deuterium was slowly getting replaced with hydrogen over the 15 day period.

Detailed descriptions of all these measurements and results are available in refs. [2 to 6, 12,16]. In all the runs the foreground counter gave clear evidence of several higher order neutron multiplicity events. In some cases in the 1989 campaign the peak of the multipilicity spectrum was in the 4 or 5 neutron pulses region. Since the overall neutron detection efficiency in those runs was only $\sim$ 1 % this would imply that in these runs approximately 400 to 500 neutrons were produced in each of the "explosive bursts". In the 16th June 1989 run with the first Milton Roy cell for example wherein a two hour long neutron spike episode occurred multiplicities as high as 15 were recorded during the last 5 minute interval, implying that a burst of 1500 neutrons was produced in a flash incident.

ln the 1994 campaign during the D_2O run with the new Milton Roy cell in spite of the higher neutron detection efficiency, the maximum multiplicity recorded was only around 8 counts, pointing to a burst strength of not more than 80 neutrons. It must however be noted that in this experiment the average magnitude of the neutron output was only $\sim$ 10 % above the background values and there were no clearly distinguishable spikes superimposed on the background values. In response to a possible criticism that a mere 10 % above background levels could be "suspect", it may be pointed out that when the LiOD was replaced with LiOH the neutron count rate steadily decreased to background values over a 15 day period confirming that the neutrons are indeed produced by lenr processes [12].

5. Discussion and Conclusions

On the whole there is unmistakable evidence that whenever lenr sources produce neutrons, a significant fraction (6.5% to 25%) [6,12] of these are emitted in the form of bunches of magnitude varying from 20 to several hundreds, the exact magnitude depending on the type of lenr source. In this context it is however worth emphasizing that, for example, if the neutron detection efficiency ϵ is say 1 % and one neutron count is registered it could still have resulted from a single burst of 100 neutrons on account of

the 1% detection efficiency! Thus the balance 75% to 93.5 % which although detected as singles counts could still have resulted from bunched neutron emission. The key to successful observation of neutron multiplicity is high neutron detection efficiency and perhaps use of the dead time method.

We are suggesting that each of the hot spots where tritium was found to be concentrated in our measurements could perhaps be associated with an NAE site discussed in lenr literature [1]. Based on the BARC findings we therefore postulate that once an NAE is formed a rapid cascade of 10^8 to 10^{10} tritium producing nuclear reactions takes place in rapid succession in this local site, in a sort of chain or cascade event, during which process on an average for every ten million tritium nuclei generated one neutron is also emitted as a very low probability offshoot side reaction event!

We then go on to further speculate that if neutrons and tritium could be produced in micro-nuclear explosions then possibly other nuclear reactions such as those responsible for heat and helium as well as transmutation products could also possibly take place in similar micro-nuclear explosions. As noted earlier the observed craters in post run cathodes could be an indication of such events.

However we emphasize that the main experimentall measured parameter fuelling all these speculations is neutron multiplicity and hence statistical analysis experiments of the type described in this paper warrant attempts at replication.

Acknowledgements

6. References

 [1]   E. Storms : *The Science of Low Energy Nuclear Reaction* (World Scientific, Singapore, 2007)

[2]   P.K. Iyengar: *Proc. 5th Int. Conf. on Emerging Nuc. Ener. Systems, July 1989, Karlsruhe, Germany,* 291, (World Scientific, Singapore 1989)

[3]   P.K.Iyengar et al **:** *Fusion Technology, **18***, 32 (1990)

[4]   M. Srinivasan : *Low Energy Nuclear Reactions and New Energy Technology Sourcebook* Vol **2,** edited by Jan Marwan and Steven B Krivit, (American Chemical Society, Oxford University Press 2009)

[5]   P.K. Iyengar and M. Srinivasan : *Proc. Ist Int. Conf. on Cold Fusion, Salt Lake City, UT, USA* (1990)

[6]   M. Srinivasan, A.Shyam, S.B.Degwekar and L.V.Kulkarni : *Proc.1st Int. Conf. on Cold Fusion, Salt Lake City, UT, USA,* 175 (1990)

[7]   R.E.Uhrig: *Random Noise Techniques in Nuclear Reactor Systems*: (Ronald Press, New York, 1970)

[8]   R.K.Rout, A.Shyam, M.Srinivasan, A.B.Garg and V.Shrikande : *Fusion Technol, **30***, 273 (1996)

[9]   T.C.Kaushik, A.Shyam, M.Srinivasan, R.K.Rout and L.V.Kulkarni : *Indian J. Technol, **28**,* 667 (1990)

[10] M. Srinivasan et al: *Proc. Int. Workshop on Anomalous Nuclear Effects Deuterium/Solid Systems. Brigham Young University, Provo UT, USA, 1990* (American Institute of Physics, 1991)

[11] R.K.Rout, M.Srinivasan, A.Shyam and V.Chitra : *Fusion Technol, **19***, 391 (1991)

[12] A. Shyam, M. Srinivasan, T.C.Kaushik, L.V.Kulkarni : *Proc. 5th Int. Conf. on Cold Fusion, Monte Carlo, Monaco* 191 (1995)

[13] M.Srinivasan and D.C.Sahni : *Nukleoni,k **9***, 155 (1967)

[14] S.B.Degwekar**:** *Ann. Nucl. Energy, **16***, 409 (1989)

[15] S.B.Degwekar and M.Srinivasan : *Ann. Nucl. Energy **, 20,*** 463, (1993)

[16] P.K. Iyengar and M. Srinivasan : *Paper A4 in Report BARC 1500, Dec. 1989* (Bhabha Atomic Research Centre, Trombay, Bombay 1989)

Comparison Between Piezonuclear Reactions and CMNS Phenomenology

A. Petrucci[1], R. Mignani[2], F. Cardone[3]

[1] *LNF-INFN via Enrico Fermi* 40 - 00044 Frascati (Rome)

[2] *Dipartimento di Fisica E.Amaldi, Università degli Studi Roma Tre Via della Vasca Navale, 84 - 00146 Roma, Italy*

[3] *Istituto per lo Studio dei Materiali Nanostrutturati (ISMN CNR) Via dei Taurini - 00185 Roma, Italy*

E-mail: petruccia@fis.uniroma3.it

Abstract. The purpose of this paper is to place side by side the experimental results of Piezonuclear reactions, which have been recently unveiled, and those collected during the last twenty years of experiments on low energy nuclear reactions (LENR). We will briefly report the results of our campaign of experiments on piezonuclear reactions where ultrasounds and cavitation were applied to solutions of stable elements. These outcomes will be shown to be compatible with the results and evidences obtained from low energy nuclear reaction experiments. Some theoretical concepts and ideas, on which our experiments are grounded, will be sketched and it will be shown that, in order to trigger our measured effects, it exists an energy threshold, that has to be overcome, and a maximum interval of time for this energy to be released to the nuclear system. Eventually, a research hypothesis will be put forward about the chance to raise the level of analogy from the mere comparison of results up to the phenomenological level. Here, among the various evidences collected in LENR experiments, we will search for hints about the overcome of the energy threshold and about the mechanism that releases the loaded energy in a suitable interval of time.

First of all we would like to warn the reader that due to the limited length allowed for the manuscript we will only mention the results and the main experimental features both for piezonuclear reactions and CMNS experiments and leave the comprehensive descriptions to the references. The subject will be dealt with on a qualitative level since the goal of this paper is only to show a new possible perspective and promote discussion on it.

1. Evidences of Piezonuclear reactions

All of the experiments that we have carried out, involved the application of ultrasounds with a frequency of 20 kHz and suitable power (between 100 and 130 Watts) to liquids either bidistilled deionised water [1, 2, 3] or solutions of bidistilled-deionised water and some standard stable chemical elememts [4, 5]. In [1, 2] we report two evidences: an increase of the proportion of a few high mass number stable isotopes (including uranium) and an increase of the proportion of a few nuclear species within the particular atomic mass range 238<M<264 (including transuranic elements). In the third experiment [3], aimed at detecting elements in the so called rare-earth mass range, ICP mass gave evidence of a significant peak corresponding to a nuclide with atomic mass (137.93±0.01) amu and half-life 12±1 sec, identified as $Eu_{63}{}^{138}$. The candidate identified, $Eu_{63}{}^{138}$, does not exist in nature; it is an artificial (discovered in 1995-97 [6]) that can be produced at the present time in nuclear reactors and by synchrotrons. The ionising radiation measurements, by LR115 detectors, that were carried out during the application of ultrasounds in all of these experiments, did not provide any evidence of ionising radiation above the background level. Further experiments were designed in order to try and detect possible neutron emission [4,5]. We subjected to cavitation, bidistilled deionised water, solutions of Lithium, Aluminium, and Iron. Being equal all the experimental conditions, but the element, we obtained reproducible evidences of neutrons bursts only with Iron. A further unusual circumstance was the lack of any gamma radiation (above the background level) that usually comes along with the emission of neutrons. Neutrons were measured by

three techniques: bubble detectors, Boron screened CR39 and Boron Trifluoride. A further experiment was performed in order to verify the effects of these new mechanisms induced by ultrasounds and cavitation on radioactive nuclei [7,23,24]. The evidences indicated that the initial quantity of Thorium became half in a interval of time 10000 times faster than Thorium half life. However it turned out that this process was not a mere acceleration of the usual Thorium decay by emission of alpha particles, since the number of tracks on the CR39 detectors that monitored the radioactive process was not compatible with this possibility [23,24].

2. Evidences of Low Energy Nuclear reactions

We will try and group the apparently anomalous results obtained by different teams and techniques in LENR in order to point out the possible analogies among these outcomes and those collected in the experiments of piezonuclear reactions. We will summarise the results by referring to the book "The Science of Low Energy Nuclear Reactions" by Edmund Storms [8]. Independently from the method used to induce LENR there were clear signs of transmutations and most of the times the resulting products were Fe, Zi, Cu, Ni, Cr and other nuclides with comparable mass and binding energy per nucleon. Besides, the nuclides belonging to the substrates, used in all of the experiments, had considerable atomic mass ranging from 48 up to 197 amu (Ti, Ni, Pd, W, Au). The environment, in which the substrate was immersed, contained different substances and chemical compounds which contained much lighter nuclides like H, D, Li, Na, K, C, N, O, Cl, and sometimes other heavier ones compatible with the atomic mass of the nuclides of the substrate. Both in piezonuclear reactions experiments and in LENR experiments there are transmutations that involve medium weight or heavy mass number nuclides and produce other intermediate and heavy mass number nuclei[1] (neither fusion nor fission can be invoked [8]). In LENR neutron emission was very low and infrequent while in piezonuclear reactions it was not infrequent but nevertheless it was low and apparently not compatible with known nuclear reactions because of the lack of gamma rays (above the background level). Gamma rays are expected either to follow emissions of neutrons or, at least, to come from the interaction of neutrons and matter (mostly Hydrogen in this case). However, further and more discriminating measurements will certainly be necessary. As to other kinds of radiation emitted during LENR, many different types were detected, which, however have not helped in identifying clear common features among the different experiments and techniques. Among all of them it is worth noting that some teams detected a strange radiation showing unknown features and behaviour [8, 9] which, from our point of view, could be put beside the strange lack of gamma rays which, at least from hydrogen neutron capture, should be emitted. As it will become clear from the next section, it was not our goal to perform extra power or heat measurements during piezonuclear reaction experiments, and hence no comparison can be made on this ground.

3. Local Lorentz Invariance Breakdown

The theoretical background, on which our experiments have been designed and carried out, is based on the concept of breakdown of Local Lorentz Invariance (LLI) [10, 11, 12]. Our phenomenological theory concentrates on the structure of local (microscopical) space-time (flat and rigid according to LLI) when LLI is broken. The coefficients of the local Minkowski metric tensor are hypothesised to be function of the energy of the process. This means that space-time is locally deformed and plays an active part in the dynamics of the physical process whose features and flow deeply depart from their usual appearance. The theory predicts that the space-time of strong interactions begins to be deformed when the energy of the process overcomes a threshold equal to 367.5 GeV [10, 11]. Besides it clearly states that there is no isochrony between the time of the experimenter and that of the hadronic process. To put it in a more practical way, this means that in order to deform space-time around a nucleus (or nuclei) and hence trigger "anomalous" processes, in the fashion of those presented above from piezonuclear reactions, one has to use a microscopical mechanism that loads an amount of energy higher than the energy threshold and then it is capable to release it in an suitable interval of time or in other words it is capable of a

---

[1] In piezonuclear reactions the heavy nuclides which can be placed side by side to the LENR substrate are those contained in the alloy of the sonotrode.

suitable power (energy divided by time). This theoretical background shows that our experiments were not in wake of the LENR ones, but their target was to obtain some evidences that would corroborate the two predictions mentioned above about the threshold energy and the release mechanism[2].

4. LLI and anomalous nuclear processes

It has been shown that the results of LENR experiments and those of piezonuclear reactions are compatible. Thus, despite the apparent diversity of the experimental set-ups and conditions, it is possible to hypothesise that similar outcomes are brought about by similar microscopical mechanisms that trigger alike anomalous nuclear processes. Now, let us evidence the phenomenological aspects that, within piezonuclear experimental set-ups, fulfil the two conditions mentioned above. Once that these aspects are clear we will try and analyse some LENR set-ups and evidences in order to make out similar features. The collapse of a generic bubble under the huge pressure of ultrasounds, that induces shock-waves on its surface, is regarded as the microscopical mechanism to fulfil the two requirements. As mentioned before, we obtained neutrons only with the solutions of Iron and their emission took place after 40 – 50 minutes the ultrasounds had been turned on, which can be interpreted as the time to reach and overcome the energy threshold. However, the overcoming the energy threshold needs to be referred to the context and the environment where the process takes place and in particular to the types of nuclides involved. The collapse of the bubble concentrates energy in a smaller and smaller region of space (which is actually space-time whose volume is still an open question of the theory), making the energy density higher and higher. In this region of space-time nuclear species are forced. The overcoming of the threshold is achieved by the complementary contributions of the external energy (ultrasounds) and internal energy, i.e. that of the nuclides taking part in the collapse. In this sense, the first preliminary clue is that the higher the atomic mass the less external energy and the shorter time interval it takes to deform locally the space-time. Thus, a first preliminary phenomenological sketch of piezonuclear reactions can be depicted as follows: pressure combined with a mechanism that allows an abrupt release of energy within a suitable interval of time bring about piezonuclear effects. The pressure is produced by ultrasounds, the mechanism is the collapse of the bubble[3]. Their synergy along with nuclides with high atomic mass form the Nuclear Active Environment (NAE) in our experiments. Now let us try and see if it is possible to spot within LENR experimental set-ups, where ultrasounds are not used, the counterparts of pressure and bubble collapse. Due to the preliminary character of these ideas we will focus our attention on one of the many different techniques and in particular on the evidences collected by an electrochemical cell with Pd/D co-deposition which, first of all, is the LENR technique more similar to that used by Fleischmann and Pons and more over it seems the farthest from the piezonuclear reactions set-up. In particular, we refer to the experimental set-up and procedure used by Mosier-Boss et al. which is described in [15]. In their experiments the metals used for the cathode were Ni, Ag, Pt, Au and the solution contained $PdCl_2$ and $LiCl$ or KCl in heavy water. In control experiments $PdCl_2$ was substituted for $CuCl_2$. We will not go through the description of the experimental process, but we will only say that the procedure comprises different phases when the Pd/D co-deposition is formed and when current is periodically increased and an intense electric or magnetic fields is applied. All the details can be found in [15, 16, 17, 18] and the references cited in them. Our target is to look through these details and make out those features that may fulfil the two requirements mentioned above: energy threshold (pressure or energy density) and releasing time (releasing mechanism). Bubble collapse is a far from equilibrium process where energy is locally concentrated around the surface of the bubble and suddenly released with great intensity. Thus, we will have to search in the electrolytic technique for leads pointing toward these three characteristics (far from equilibrium, local loaded energy, local abrupt release of it). From the description in [16] the researchers state that "the experimental protocol covers three time periods" and that the third period of time is used "to put the system in a far from equilibrium condition" which is obtained by applying an intense static electric or magnetic field and by letting the electrolysis proceed by keeping increasing the current from time to time. It is fairly reasonable to consider that a co-deposition of Pd/D is in itself an unstable structure in which atomic bonding between Palladium atoms are deformed, stretched, and weakened by

---

[2] This explains why we have never used deuterated substance, never look for Helium or Tritium and never attempted to measure the presence of extra heat.

[3] Critical parameters are the dimension of the bubble and the number of ions of the specific nuclide present on the its surface.

the presence of Deuterium. To confirm this, one can put forward the fact that LENR experiments have begun to be carried out in the last few years not by loading Deuterium in bulky Palladium, but rather by co-depositions Pd/D or by nanostructured Pd. These methods produce greater quantities of anomalous evidences than those with solid Pd [8, 15, 19]. That the loading of mechanical energy in Pd is brought about by Deuterium, is confirmed by experiments in which the solution contained $CuCl_2$ instead $PdCl_2$. Copper does not absorb Deuterium, no lattice deformation is brought about, no mechanical energy gets loaded and hence no reactions take place [15]. The statements by Storms [8] in his book seem to move in the same direction. He reports that "...the basic material used as cathode is not active initially even when it is made of Palladium - activation is required. Nevertheless, the base material does affect the morphology and subsequent activity of the deposited layer...". All of these conjectures can be considered a sound and promising lead[4] from the experimental conditions about the possible fulfilment of the first requirement of LLI breakdown hypothesis: existence of an energy threshold. We concentrate now on the second requirement: the mechanism to release this loaded energy. In the experimental accounts [16, 20] the researchers mention a shape change in some areas of the cathode at the end of the electrolysis. Indeed, the structure at the cathode is a complicated and microscopically feeble equilibrium of three layers: the substrate (Ni, Ag, Pt, Au), the co-deposition Pd/D and the solution. We reckon that the application of an electric or magnetic field and the increasing current during electrolysis may generate microscopical conditions compatible with those found in piezonuclear reaction experiments where cavitation took place. As a bubble is a local frail inhomogeneity within a liquid which can be squeezed and deflated[5] by squeezing it using ultrasounds, the locally frail structure of Pd/D co-deposition presents local inhomogeneities or hollows (e.g. gradients of the density of Pd and/or D atoms) whose sudden and violent collapse can be induced by bringing the systems to a far from equilibrium condition (electric or magnetic field, periodical increase of current, continuous flow of Deuterium through the co-deposited layer). As Iron atoms (not light elements) are entrapped in the interface gas/liquid of bubbles and are launched against each other during the collapse and forced in a smaller and smaller volume of space-time until the energy threshold is reached and overcome in a precise interval of time, Palladium atoms might endure similar processes as hollows in Pd/D co-deposition are made collapse. In [8] cracks are indicated as "...the only environments obviously common to all successful experiments...". Always in [8] it is said that Palladium expands as it is loaded with Deuterium and cracks of different dimensions form during this process. Besides cracks are said to be present in Pd/D co-depositions or Palladium black. Some questions are raised as to how cracks are involved in the cold fusion process, or as to how cracks operate to allow Coulomb barrier penetration, or as to how dimensions of cracks influences the formation of a NAE. Eventually, cracks are said to be good candidates to be a NAE. From our point of view and from these statements, cracks can be considered in this experimental system the counterparts of bubbles in cavitation [21,22]. However we reckon that it is not correct look at the NAEs that form in our experiments and in all of the LENR/CMNS experiments from the point of view of the well known nuclear processes and all the concepts involved in them like Coulomb barrier and other quantum mechanical concepts. We believe that this statement is more than corroborated by loads of compatible anomalous evidences collected in these 20 years by different institutions and researchers, different techniques spread all over the world. Before concluding, we would like to point out one more thing. We said that, high atomic mass nuclides contribute to facilitate the overcoming of the energy threshold when they are forced in a smaller and smaller region of space-time. This qualitative picture may induce to think that starting from Palladium, one should obtain heavier nuclei like in a sort of new type nuclear fusion. However in [16] it is reported of transmutations whose products were Aluminium, Magnesium, Chlorine, Silicon which are all lighter nuclides than Palladium. Since these transmutations are thought to be brought about by space-time deformation, it is possible that a heavy nuclide be ripped apart into lighter nuclides by tidal forces i.e., in more picturesque way, as an astronaut would be as he were falling into a black-hole.

---

[4] A lead in the sense that deeper investigation, experimental, theoretical and phenomenological will have to be carried on from this point.
[5] We remind that in our phenomenological model the generic bubble deflates while being squeezed by a shock-wave. In other words it is not treated as mean to compress the gas contained in it in order to reach hot fusion conditions.

References

[1] Cardone, F. & Mignani, R. Possible evidence for transformation of chemical elements in cavitated water. Int. J. Mod. Phys. B 17, 307 (2003).

[2] Cardone, F., Mignani, R., Perconti, W., Pessa, E. & Spera, G. Possibile evidence for production of an artificial radionuclide in cavitated water. Jour. Radioanalytical Nucl. Chem. 265, 151 (2005).

[3] Cardone, F., Mignani, R., Perconti, W., Pessa, E. & Spera, G. Nucleosynthesis of an artificial radionuclide by cavitation. Gravitation and Cosmology 11, 1-2 (41-42) (2005).

[4] Cardone F., Cherubini G., Mignani R., Perconti W., Petrucci A., Rosetto F., Spera G. Neutrons from Piezonuclear Reactions. Annales de la Fondation Louis de Broglie (in press)

[5] Cardone F., Cherubini G. & Petrucci A. Piezonuclear Neutrons. Physics Letters A 373 (2009) 862866.

[6] Horigouchi T., Koura H. & Katakura J.(eds.), Chart of Nuclides 2000 (Jap. Nucl. Data Com., JNDC); Nucl. Data Evaluation Lab. Korea Atomic Energy Res. Inst. 2000-2002 BNL, U.S.A. version.

[7] Cardone F., Mignani R. & Petrucci A. Piezonuclear decay of Thorium. Physics Letters A 373 (2009) 1956–1958

[8] Storms, E. The Science of Low Energy Nuclear Reaction - A Comprehensive Compilation of Evidence and Explanations about Cold Fusion. World Scientific, Singapore (2007).

[9] Urutskoev, L.I.,Liksonov, V.I. & Tsinoev, V.G. Observation of transformation of chemical elements during electric discharge. Ann. Fond. L.de Broglie 27, 701 (2002).

[10] Cardone, F. & Mignani, R. Energy and Geometry World Scientific Singapore (2004).

[11] Cardone, F. & Mignani, R. Deformed Spacetime Springer, Heidelberg (2007).

[12] Will. C.M. Theory and experiment in gravitational physics Cambridge University Press, Cambridge (1993).

[13] Cardone, F. & Mignani, R. Piezonuclear reactions and Lorentz invariance breakdown. Int. Jour. Modern Phys. E 15, 911 (2006).

[14] http://www.newnuclear.splinder.com/tag/towards+clean+nuclear+energy

[15] Mosier-Boss, P.A., Szpak, S., Gordon, F.E. & Forsley, L.P.G. Use of CR-39 in Pd/D co-deposition experiments. Eur. Phys. J. Appl. Phys. 40, 293-303 (2007)

[16] Szpak, S.,Mosier-Boss, P.A.,Young, C. & Gordon, F.E. Evidence of nuclear reactions in Pd lattice. Naturwissenschaften (2005) 92:394-397

[17] Mosier-Boss, P.A., Szpak, S., Gordon, F.E. & Forsley, L.P.G. Triple tracks in CR-39 as results of Pd/D Co-deposition: evidence of energetic neutrons. Naturwissenschaften (2009) 96:135-142

[18] Szpak, S.,Mosier-Boss, P.A. & Gordon, F.E. Further evidence of nuclear reactions in the Pd/D lattice: emission of charged particles Naturwissenschaften (2007) 94:511-514

[19] Celani, F., et al Deuteron electromigration in thin Pd wires nano-particles: evidence for ultrafast deuterium loading and anomalous large thermal effects. Proceedings of the ICCF14 Washington DC, USA, 9-15 August 2008

[20] Szpak, S.,Mosier-Boss, P.A.,Young, C. & Gordon, F.E. The e®ect of an external electric field on surface morphology of co-deposited Pd/D ‾lms. J. Electroanal Chem. (2005)

[21] Carpinteri, A., Cardone, F. & Lacidogna, G. Piezonuclear Neutrons From Brittle Fracture: Early Results of Mechanical Compression Tests. Strain 45, 4, 332 (2009)

[22] Cardone, F., Carpinteri, A., & Lacidogna, G. Piezonuclear neutrons from fracturing of inert solids. Phys. Lett. A 373, 4158 (2009)

[23] Cardone F., Mignani R. & Petrucci A. Reply to " Comment on ' Piezonuclear decay of thorium'

[Phys. Lett. A 373 (2009) 1956]" [Phys. Lett. A 373 (2009) 3795]

[24] Cardone F., Mignani R. & Petrucci A. Reply to " Comment on ' Piezonuclear decay of thorium'

[Phys. Lett. A 373 (2009) 1956]" [Phys. Lett. A (2009), in press] (in press)

Piezonuclear reactions in inert solids revealed by neutron emissions from brittle fracture

A. Carpinteri[1], F. Cardone[2], G. Lacidogna[1], A. Manuello[1], O. Borla[1,3]
[1]*Department of Structural Engineering and Geotechnics, Politecnico di Torino, Italy*
[2]*Istituto per lo Studio dei Materiali Nanostrutturati (ISMN-CNR), Roma, Italy*
[3]*Istituto Nazionale di Fisica Nucleare, INFN sez. Torino, Italy*

E-mail: giuseppe.lacidogna@polito.it

Abstract. Neutron emission measurements by means of ^{3}He neutron detectors were performed on solid test specimens during crushing failure. The tests were carried out at the Laboratory of Fracture Mechanics of the Politecnico di Torino. The materials used were marble and granite, selected in that they present a different behaviour in compression failure (i.e., a different brittleness index) and a different iron content. All the test specimens were of the same size and shape. Neutron emissions from the granite test specimens were found to be of about one order of magnitude higher than the natural background level at the time of failure. These neutron emissions should be caused by nucleolysis or piezonuclear "fissions" that occurred in the granite, but did not occur in the marble: $Fe_{26}^{30} \rightarrow 2\,Al_{13}^{14} + 2$ neutrons. The present natural abundance of aluminum (7-8% in the Earth crust), which is less favoured than iron from a nuclear point of view, is possibly due to the above piezonuclear fission reaction.

1. Introduction

We consider samples of marble and granite rocks, containing different amounts of iron, loaded in compression until failure [1,2]. As ultrasounds induce cavitation in the liquids and then bubble implosion accompanied by the formation of a high-density fluid or plasma [3], so shock waves due to compression rupture induce a particularly sharp strain localization in the solids and then material interpenetration accompanied by an analogous formation of a high-density fluid or plasma [2]. Our experiment follows a different path with respect to those of other research teams, where only fissionable or light elements (deuterium) were used, in pressurized gaseous media [4,5], in liquids with ultrasounds and cavitation [6], as well as in solids with shock waves and fracture [7-12]. We are treating with inert, stable and non-radioactive elements at the beginning of the experiments (iron) [1,2,13], as well as after the experiments (aluminum). During the experiments neutron emissions in thermal and fast energy range were detected.

The materials selected for the compression tests –performed at the Laboratory of Fracture Mechanics of the Politecnico di Torino (Director Prof. Alberto Carpinteri)– were Carrara marble (calcite) and green Luserna granite (gneiss). This choice was prompted by the consideration that, test specimen dimensions being the same, different brittleness numbers [14] would cause catastrophic failure in granite, not in marble. The test specimens were subjected to uniaxial compression to assess scale effects on brittleness [15]. Four test specimens were used, two made of Carrara marble, consisting mostly of calcite, and two made of Luserna granite, all of them measuring 6x6x10 cm^3. The same testing machine was used on all the test specimens: a standard servo-hydraulic press with a maximum capacity of 500 kN, equipped with control electronics. This machine makes it possible to carry out tests in either load control or displacement control. The tests were performed in piston travel displacement control by setting, for all the test specimens, a velocity of 10^{-6} m/s during compression.

Neutron emission measurements were made by means of a ^{3}He detector placed at a distance of 10 cm from the test specimen and enclosed in a polystyrene case so as to prevent the results from being altered by acoustical-mechanical stresses. During the preliminary tests, thermodynamic neutron detectors of the bubble type BD (bubble detector/dosimeter) manufactured by Bubble Technology Industries (BTI) were used, and the indications obtained persuaded us to carry on the tests with ^{3}He detectors [2].

2. Testing and neutron measurements

The neutron detector used in the tests is a ^{3}He type with electronic of preamplification, amplification and discrimination directly connected to the detector tube, which is of the type referred to as "long counter". This detector was calibrated for the measurement of thermal neutrons; its sensitivity is 65 cps/n$_{thermal}$ ($\pm$ 10% declared by the factory) i.e., the flux of thermal neutrons was 1 thermal neutron/s cm^2, corresponding to a count rate of 65 cps. The laboratory neutron background was measured at 600 s time intervals to obtain sufficient statistical data. Before starting the tests the average background count rate was:

$$3.8 \times 10^{-2} \pm 0.6 \times 10^{-2} \text{ cps}$$

corresponding to an equivalent flux of thermal neutrons of

$$5.8 \times 10^{-4} \pm 0.9 \times 10^{-4} \text{ n}_{thermal}/\text{s cm}^2.$$

During the compression tests neutron emissions were measured on four specimens, two made of marble, denoted with P1, P2, and two of granite, denoted with P3, P4. The test specimens were arranged with the two smaller surfaces in contact with the press platens, with no coupling materials in-between, according to the testing modalities known as "test by means of rigid platens with friction".

The electronics of the ^{3}He detector was powered at least one hour before the background estimation, in order to avoid intrinsic thermal effects. The neutron background was measured during 600 s time intervals repeatedly, so to obtain sufficient statistical data for a preliminary period of more than three hours. Then the background measures were performed fixing at 60 s the acquisition time to make sure there were no variations. The acquisition time was fixed at 60 s and the results of count rate measurements are given in Fig. 1a and b together with the diagrams of the force applied to the test specimens as a function of the time elapsed since the beginning of its application. The measurements of neutron emissions obtained on the marble test specimens yielded values comparable with the background, even at the time of test specimen failure. The neutron measurements obtained on the two granite test specimens, instead, exceeded the background value by about one order of magnitude at the test specimen failure.
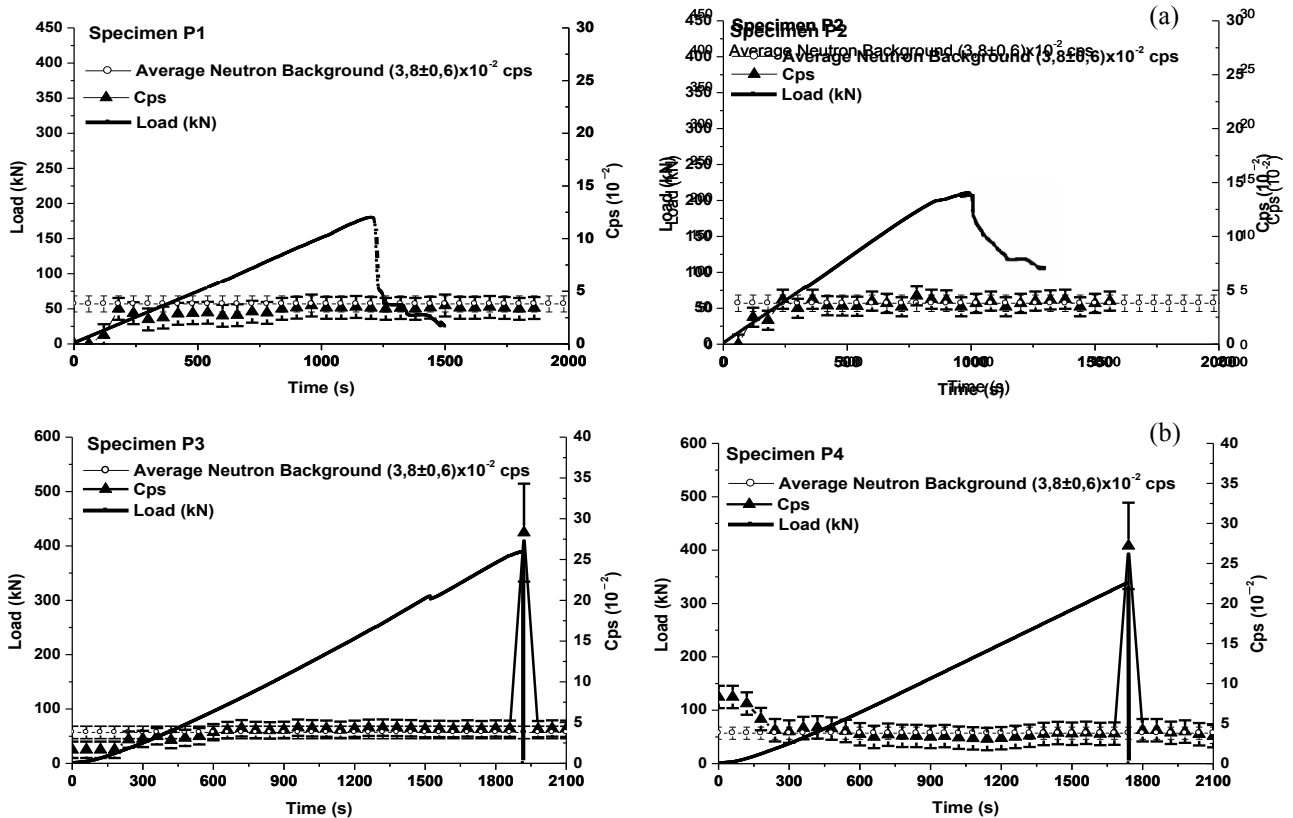

Fig. 1 – (a) Load vs. time and cps curves for test specimens P1 and P2 in Carrara marble, and (b) for test specimens P3 and P4 in Luserna granite.

After 20 min, test specimen P1 reached a peak load of ca 180 kN, corresponding to an average pressure on the bases of 50 MPa; after 15 min, test specimen P2 reached a peak load of ca 200 kN, corresponding to an average pressure on the bases of 55.6 MPa.

Test specimen P3 reached at time T(P3) = 32 min a peak load of ca 400 kN, corresponding to an average pressure on the bases of 111.1 MPa. When failure occurred, the count rate was found to be

$$28.3 \times 10^{-2} \pm 5.7 \times 10^{-2} \text{ cps}$$

corresponding to an equivalent flux of thermal neutrons of

$$43.6 \times 10^{-4} \pm 8.8 \times 10^{-4} \text{ n}_{thermal}/\text{s cm}^2.$$

Test specimen P4 reached at time T(P4) = 29 min a peak load of ca 340 kN, corresponding to an average pressure on the bases of 94.4 MPa. When failure occurred, the count rate was found to be

$$27.2 \times 10^{-2} \pm 5.5 \times 10^{-2} \text{ cps}$$

corresponding to an equivalent flux of thermal neutrons of

$$41.9 \times 10^{-4} \pm 8.5 \times 10^{-4} \text{ n}_{thermal}/\text{s cm}^2.$$

Notice how the above neutron measurements occurring in P3 and in P4 at failure are well beyond the background interval and how the value obtained on P3 is greater than the value measured on P4. We believe that this result, albeit with the due caution, may be ascribed to the unstable failure of these test specimens and the greater quantity of energy released by P3 compared to P4 at the time of failure. Figure 1a and b summarise the evolution of the neutron count rates together with the load vs. time curves for the four test specimens.

3. Discussion and remarks

Experimental data from rocks tested in compression generally indicate that this is a brittle material, since it exhibits a rapid decrease in load carrying capacity when deformed beyond a peak load. When the softening diagram is very steep, or even shows simultaneously decreasing strain and stress values, the material is said to present a snap-back or catastrophic behaviour. This is in contrast with ductile materials which retain considerable strength beyond the peak as shown in Fig. 2 [14-19].
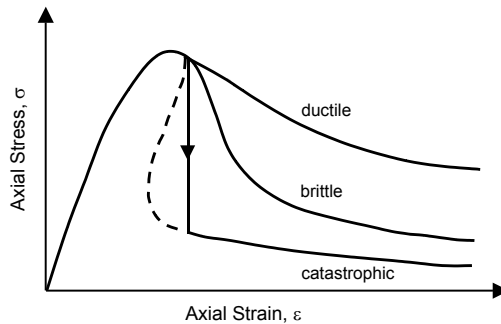
Fig. 2 – Ductile, brittle, and catastrophic behaviour.

In this study, all compression tests were conducted through feedback control of the axial displacement of piston travel on test specimens having the same dimensions. The complete failure process was observed only for P1 and P2 marble specimens, whose behaviour was seen to be ductile compared to the brittle catastrophic failure behaviour displayed by granite specimens P3 and P4. For the latter two, in fact, failure occurred instantaneously, without showing the descending branch of the load-time curve (Fig. 1a and b).

The elastic strain energy accumulated in the test specimens up to failure, ΔE, is given in Table 1. Moreover, for each test specimen, it is possible to draw some conclusions on the release rate of the elastic energy accumulated.

Table 1. Elastic strain energy at the peak load, ΔE.

Test specimen	Material	ΔE [J]	ΔE [eV$\times 10^{20}$]
P1	Carrara marble	124	7.75
P2	Carrara marble	128	8.00
P3	Luserna granite	384	24.00
P4	Luserna granite	296	18.50

One of the conditions to be met for piezonuclear reactions to take place is that the ratio, r, between the power of released energy, W=ΔE/Δt, and the power threshold [13,21]:

$$W_{strong} = 7.69 \times 10^{11} \text{ W} = 4.8 \times 10^{30} \text{ eV/s} \tag{1}$$

be greater than or equal to 1 [13,20]:

$$r = W / W_{strong} \geq 1. \tag{2}$$

Accordingly, based on the data obtained from the tests, the time interval of released energy, Δt, in granite test specimens in which piezonuclear reactions have occurred, should satisfy the following relationship:

$$\Delta E/\Delta t \geq W_{strong}, \tag{3}$$

and hence:

$$\Delta t \leq \frac{\Delta E}{W_{strong}} = \frac{384}{7.69 \times 10^{11}} = \frac{24 \times 10^{20}}{4.8 \times 10^{30}} = 0.5 \times 10^{-9} \text{s} = 0.5 \text{ ns} \tag{4}$$

Equation (4) was written by considering the energy accumulated in P3 which was greater than the energy accumulated in P4. For the marble test specimens, in which peak load is clearly followed by a softening branch, energy release surely occurred over a period of time too long to permit the production of piezonuclear reactions.

Considering that the elastic strain energy accumulated in specimen P3 is released at the pressure wave velocity v (for granite v ~ 4000 m/s), the extension of the energy release zone results to be equal to:

$$\Delta x = v \, \Delta t \sim 4000 \, \text{m/s} \times 0.5 \, \text{ns} \sim 2 \mu\text{m} \, .$$

Such energy release band width Δx could correspond to the critical value of the interpenetration length w_{cr}^{c} assumed by Carpinteri and Corrado [19] to explain the critical conditions for the catastrophic behaviour of solids in compression (Fig. 3). Accordingly, neutron emissions in granite may be accounted for by the fact that the power threshold for piezonuclear reactions is exceeded, as well as by the type of catastrophic failure that occurs, which entails a very fast energy release, over a time period of the order of a nanosecond.

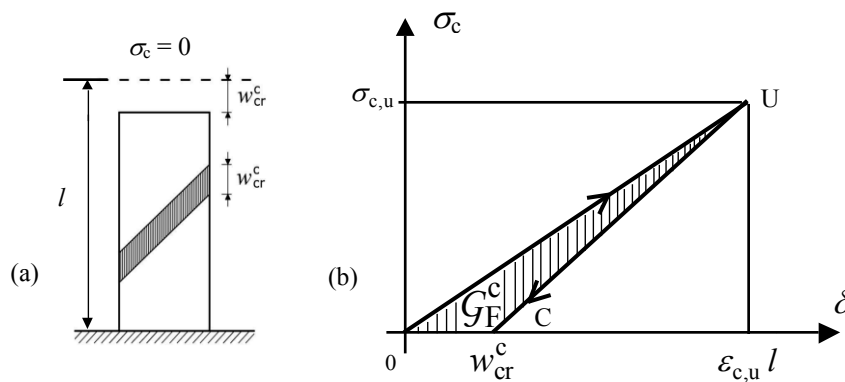Fig. 3 – Catastrophic behaviour in a solid specimen during compression. (a) Conditions of complete interpenetration and critical value of the interpenetration length w_{cr}^{c}. (b) Stress vs. displacement response; $\sigma_{c,u}$ = ultimate compression strength; $\varepsilon_{c,u}$ = ultimate compression strain; $\delta = \varepsilon_{c,u} \, l$ = ultimate displacement, G_{F}^{c} = crushing energy.

If we consider the elastic energy stored in the sample and the temperature equivalent to this energy together with the final pressure before fracture, the material of the sample is in a region of the phase-space corresponding to a transition from solid to liquid phase. Our conjecture is that in the interpenetration layer of thickness w_{cr}^{c} the conditions are realized for a high density fluid, over-saturated but in metastable conditions. On the other hand, these locally extreme conditions could catalyse in the interpenetration band the formation of a plasma from the gases which are present in the solid materials (even at room conditions).

From this experiment it can be clearly seen that piezonuclear reactions giving rise to neutron emissions are possible in inert non-radioactive solids, in addition to liquids [1-3,13]. Anyhow, it is also evident that the availability of an amount of stored energy for the reactions exceeding the microscopic nuclear deformed space-time threshold

$$E_{0, strong} = 5.888 \times 10^{-8} \text{ J} = 3.675 \times 10^{11} \text{ eV}$$

is not sufficient *per se* [21]. The energy must be contained in a space-time (and energy) hypervolume such that r ≥ 1, i.e., such that the phenomenon will actually develop in deformed space-time conditions [13,20]. From Table 1, in fact, it can be seen that it was $\Delta E > E_{0, strong}$ in all the test specimens loaded in compression, but r was greater than 1 only in granite test specimens. Hence, even for piezonuclear reactions in solids, the notion of stored energy must be combined with the notion of speed of energy release as is the case for liquids [1-3].

Another factor to be taken into account is the composition of the materials in which piezonuclear reactions may be produced. As we have already specified in the Introduction [1,2], the fact that the marble used in the tests contains only iron impurities (not more than 0.07% of Fe_2O_3), and granite instead contains a considerable amount of iron (around 3% of Fe_2O_3), could be another factor contributing to the phenomenon in question, by analogy with the case of piezonuclear reactions in liquids. In fact, piezonuclear reactions with neutron emissions were obtained in liquids containing iron chloride or iron nitrate subjected to ultrasounds and cavitation [3,13]. In the experiments on liquid solutions [3,13], aluminum atoms appeared at the end in a final quantity as large as about seven times the small initial quantity [22]. More precisely, they increased from 3.99 ppb to 27.70 ppb, without evident reasons, if we exclude possible transmutations.
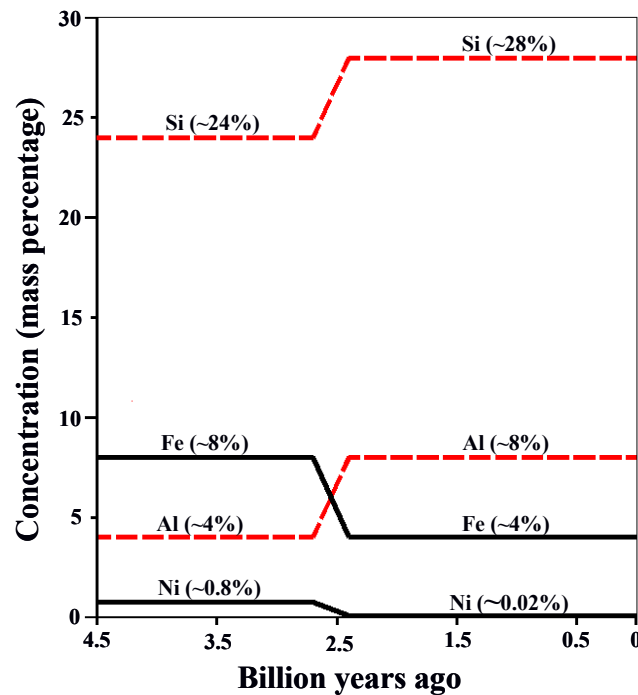

Fig. 4 – Evolution in mass percentage concentration of Si, Al, Fe and Ni in the Earth crust during the last 4.5 billion of years (age of the planet Earth).

Therefore, our conjecture is that the following piezonuclear fission reaction should have occurred also in the compression tests on granite specimens [1,2]:

$$Fe_{26}^{56} \rightarrow 2\,Al_{13}^{27} + 2 \text{ neutrons} \qquad (5)$$

In addition to the previously reported and still unpublished observations in liquid experiments, other strong reasons of a very general nature push us to emphasize this type of explanation.

The present natural abundance of aluminum (7-8% in the Earth crust), which is less favoured than iron from a nuclear point of view (it has a lower bond energy per nucleon), is possibly due to the above piezonuclear fission reaction. This reaction –less infrequent than we could think– would be activated where the environment conditions (pressure and temperature) are particularly severe, and mechanical phenomena of fracture, crushing, fragmentation, comminution, erosion, friction, etc., may occur. If we consider the evolution of the percentages of the most abundant elements in the Earth crust during the last 3 billion years (Fig. 4), we realize that iron and nickel have drastically diminished, whereas aluminum, silicon and magnesium have as much increased [23-25]. It is also interesting to realize that such increases have developed mainly in the tectonic regions, where frictional phenomena between the continental plates occurred.

Acknowledgments

4. References

[1]   A. Carpinteri, F. Cardone and G. Lacidogna: *Strain* **45** 313 (2009). Presented at the Turin Academy of Sciences on December 10, 2008. Proc. of the Turin Academy of Sciences, in print
[2]   F. Cardone, A. Carpinteri and G. Lacidogna: *Phys. Lett. A* **373** 4158 (2009)
[3]   F. Cardone, G. Cherubini and A. Petrucci: *Phys. Lett. A* **373** 862 (2009)
      See also: F. Cardone et al.: http://www.arxiv.org/abs/0710.5115
[4]   Y. Arata, and Y. Zhang,: *Proc. Jpn. Acad.* **71**, Ser. B 304 (1995)
[5]   Y. Arata, H. Fujita and Y. Zhang: *Proc. Jpn. Acad.* **78**, Ser. B 201 (2002)
[6]   R. P. Taleyarkhan et al.: *Science* **295** 1868 (2002)
[7]   K. Diebner: *Kerntechnik* **3** 89 (1962)
[8]   S. Kaliski: *J. Tech. Phys.* **17** 99 (1976)
[9]   S. Kaliski: *J Tech. Phys.* **19** 283 (1978)
[10] F. Winterberg: *Atomenergie-Kerntechnik* **44** 146 (1984)
[11] B. V. Derjaguin et al.: *Nature* **341** 492 (1989)
[12] M. F. Fujii et al.: *Jpn. J. Appl. Phys.* Pt.1 **41** 2115 (2002)
[13] F. Cardone and R. Mignani, *Deformed Spacetime* (Springer, Dordrecht, 2007, chaps 16-17)
[14] A. Carpinteri: *J. Mech. Phys. Solids* **37** 567 (1989)
[15] A. Carpinteri: *Int. J. Fract.* **44** 57 (1990)
[16] A. Carpinteri and N. Pugno: *Nature Mat.* **4** 421 (2005)
[17] J.A. Hudson, S.L. Crouch and C. Fairhurst: *Eng. Geol.* **6** 155 (1972)
[18] RILEM TC 148-SSC (2000): *Mater. Struct.* **33** 347 (2000)
[19] A. Carpinteri and M. Corrado: *Eng. Fail. Anal.* **16** 2530 (2009)
[20] F. Cardone and R. Mignani: *Int. J. Mod. Phys. E Nucl. Phys.* **15** 911 (2006)
[21] F. Cardone and R. Mignani, *Energy and Geometry* (World Scientific, Singapore, 2004, chap. 10)
[22] F. Cardone, R. Mignani and A. Petrucci, private communication
[23] A. D. Anbar: *Science* **322** 1481 (2008)
[24] G. Favero and P. Jobstraibizer: *Coord. Chem. Rev.* **149** 367 (1996)
[25] K. O. Konhauser, E. Pecoits, S. V. Lalonde, D. Papineau, E. G. Nisbet, M. E. Barley, N. T. Arndt, K. Zahnle and B. S. Kamber: *Nature* **458** 750 (2009)

Li+D and D+D Fusion Assisted with Acoustic Cavitation

Y. Toriyabe, E. Yoshida and J. Kasagi

Laboratory of Nuclear Science, Tohoku University, 1-2-1, Mikamine, Taihaku, Sendai, Miyagi, 982-0826, Japan

E-mail: toriyabe@lns.tohoku.ac.jp

Abstract. We have studied the Li+D and D+D fusion reactions in liquid Li by bombarding deuteron beams with energies below 70 keV. In the present work, an ultra sonic target system was developed to form acoustic cavitation bubbles in the liquid Li, in order to investigate the effect of the enhanced dynamic motion of the target. It was found that the ultra sonic effect strongly depends on a target condition and the D+D reaction could be enhanced very much due to the liquid Li cavitation. In addition, the D+D reaction rate is not constant but time dependent. Preliminary analyses indicate that decrease of the Coulomb energy barrier is about 2000 eV for a relatively stable condition. On the contrary, the Li+D reaction shows no meaningful effect for incident energies down to 30 keV. The present results indicate that not only density increase but also another mechanism enhancing reaction rates should be exist in liquid Li acoustic cavitation process.

1. Introduction

It has been shown that the nuclear reaction could be strongly affected by target condition and environment, and has been suggested that a dynamic mobility of deuteron in condensed matter is an essential factor to enhance the D+D reaction rate as well as a high deuterium density. In this paper, we try to establish unusual target conditions and to show enhanced nuclear reactions in such conditions. We employed a liquid metal (Li) as a host material where the D+D and Li+D reactions occur; the advantage of the liquid metal to the solid is possible existence of a screening effect of positive charges due to freely moving ions in addition to that of negative charges. Furthermore, the acoustic cavitation is applied to enhance the effects due to a dynamic motion of the target. In order to achieve these conditions, we developed an ultra sonic target system incorporated into a vacuum chamber to form Li cavitation bubbles in the target.

The reaction rates of the Li+D and D+D reactions in the Li cavitation bubbles were measured for the deuteron beam bombardment with energies below 70 keV; the density and kinematical effects were investigated. We also tried to detect bubble fusion under such a dynamic condition.[1-3]

2. Experiment

2.1 Ultrasonic System and Li Cavitation

Figure 1 (left) shows a schematic view of the ultra sonic system with the situation of vibration amplitudes depending on the position. It should be noted that the sonic wave is not transverse but longitudinal wave to form alternate dense and sparse conditions. A bolt-clamped Langevin-type transducer (BLT) generates a high amplitude sonic wave. A piezoelectric element is lead zirconate titanate (PZT). When the BLT is driven with an appropriate frequency, it outputs a high amplitude wave because of vibration resonance with four piezoelectric elements. Since the resonance condition is determined by the wavelength of the sonic wave, the total length of the system is an important factor. We designed the total length in such a way that the Li target is placed at an anti-node and that the resonance frequency is near 19 kHz. An aluminum horn connected to the BLT amplifies the vibration amplitude; the maximum amplitude is 10 μm. The horn has a flange at the node position of the sonic wave and is fixed with the vacuum chamber.

A situation of bubble growth and collapse through ultra sonic cycles is shown in Fig. 1 (right). At the sparse timing, a nucleus is born, the bubble shrinks and expands through a several cycles and it finally

collapses at the dense timing. Thus, it is considered that the state with high pressure, density and temperature can be achieved and light emission, so called sonoluminescence, occurs.
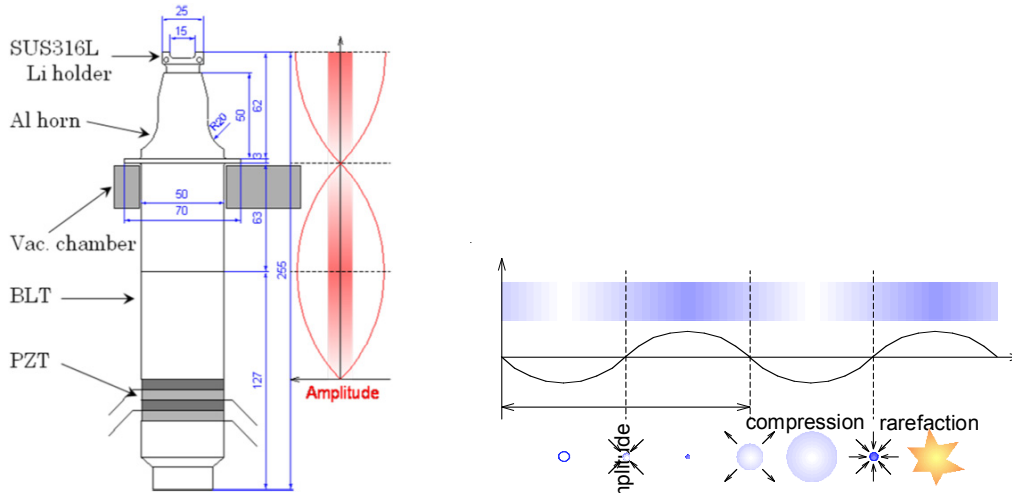

Fig. 1 – (left) A schematic view of an ultra sonic system. (right) Bubble growth and collapse through ultra sonic cycles.

However, the acoustic cavitation is a very complex process and there is no general theory to explain the mechanism and characteristic. Furthermore, almost no reports are found on the cavitation of the liquid metal. In a simple model, the threshold pressure for cavitation formation is mainly determined by surface tension of the liquid σ(T) and expressed as

$$P_{th} \sim P_0 - P_s + \sqrt{\frac{16\pi(\sigma(T))^3}{3kT \cdot const.}}, \tag{1}$$

$$P_{th}(Li) \sim 10 \times P_{th}(H_2O) \sim 1.6[GPa]. \tag{2}$$

From the empirical eq. (1), we need ten times higher pressure than water to produce cavitation bubbles.

Figure 2(a) shows a surface of clear liquid Li in the vacuum chamber; we see a distinct reflection of the light from outside of the chamber. When we apply the ultra sonic wave, the cavitation occurs and bubbles reflect the light diffusely; we see countless white dots as shown in Fig. 2(b). We note that these white dots are not sonoluminescenece but diffused light reflection since they appear just as a reflection of the light. The cavitation bubbles cover all Li surface as shown in Fig. 2(c).
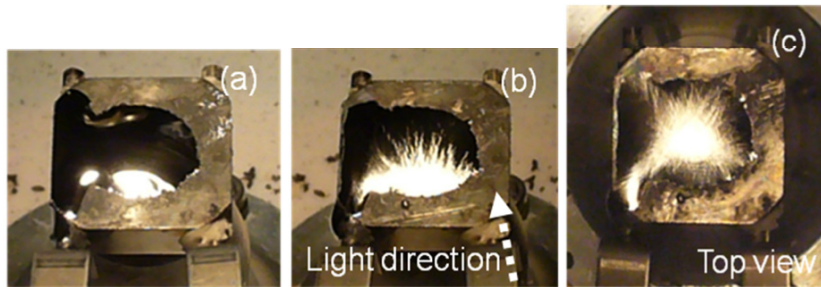

Fig. 2 – Liquid Li cavitations. (a) Clear liquid Li surface without ultra sonic wave. (b, c) Li cavitation bubbles. White dots are bubbles reflecting the light.

2.2 Li+D and D+D Measurement

We used enriched ^{6}Li metal, consisting of 95% ^{6}Li and 5% ^{7}Li. The Li metal is very active material, and the surface is easily oxidized and/or contaminated. Therefore we designed and constructed a new vacuum chamber which has a glove box. In order to keep the surface clean, we handled the Li metal in Ar atmosphere in the glove box. The contamination, however, cannot be avoidable because of the residual gas when the chamber is evacuated. Thus, we removed the contamination every 1 or 2 hours by using a scraper attached to the chamber. We kept the Li temperature considerably higher than the melting point (180 $^\circ$C). Below 300 $^\circ$C, the vapor pressure of Li (10^{-6} Pa) is much lower than the vacuum of the chamber (typically 5×10^{-5} Pa). Thus Li evaporation can be avoided even in the cavitation condition.

The liquid Li was irradiated by deuteron beams with energy ranging from 30 to 70 keV. We kept the input power constant to be about 500 mW, in order to stabilize the ultra sonic effect. The beam was injected to the chamber at an angle of 60° with respect to the vertical direction. A Si detector placed at 125° was used to detect charged particles emitted in the nuclear reactions.

In order to elucidate the ultra sonic effect, we compared the yields of the Li+D and D+D reactions for the ultra sonic ON and OFF measurement. However, it was found that the target condition was very sensitive and was easily changed within a several minutes due to high activity of Li. Therefore a data acquisition system, in which the measurements with and without the ultra sonic were performed alternatively, was developed to reduce systematic errors. As is shown in Fig. 3, the beam was turned OFF and ON every 3 or 10 seconds while the ultra sonic wave was turned OFF and ON every 13 seconds so as to accumulate the 4 data sets in one cycle.

In Fig. 3, the reading of the infrared thermometer, which is considered to show the temperature of the Li surface, is also shown. It periodically increases and decreases synchronized with the ultra sonic ON/OFF cycle. It is not plausible that the change of the reading corresponds to real change of the temperature because of its instant response. At present, we conjecture that near-infrared lights are emitted in the Li cavitation as the sonoluminescence.
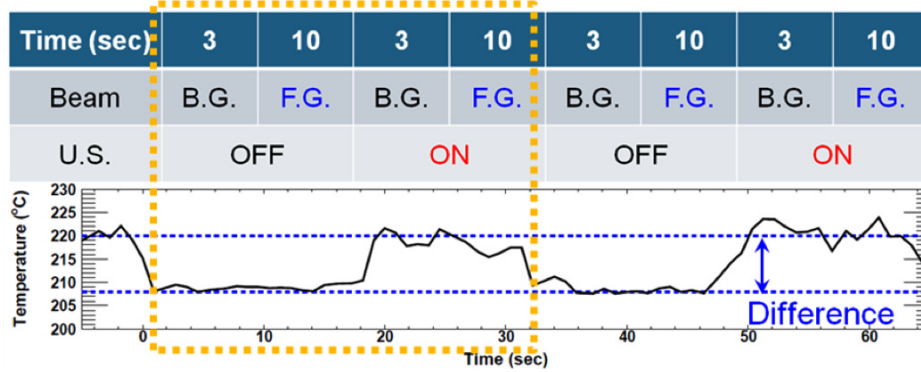
Fig. 3 – An alternate data acquisition cycle and infrared thermometer output.

3. Result

A typical energy spectrum is shown in Fig. 4. The blue peak is the 11.2-MeV α particle from the ^{6}Li+D reaction. During the deuteron bombardment, deuterons are being accumulated in the Li target and an incident deuteron collides with them to make the D+D reaction. The red peak is 3-MeV proton from the D+D reaction. We can estimate the deuteron density in the Li liquid by counting α and proton counts as

$$\frac{Y_p}{\frac{1}{2}Y_\alpha} = \frac{\int N_D(x)\cdot\sigma_{D+D}(x)\cdot dx}{N_{Li}\cdot\int\sigma_{Li+D}(x)\cdot dx} \Leftrightarrow \frac{N_D}{N_{Li}} \sim \frac{2\int\sigma_{Li+D}(E)(x)\cdot\frac{1}{dE/dx}\cdot dE}{\int\sigma_{D+D}(E)\cdot\frac{1}{dE/dx}\cdot dE}\cdot\frac{Y_p}{Y_\alpha}. \quad (3)$$

The maximum deuteron density deduced in the present measurements is 0.1% of the Li.

Fig. 4 – Energy spectrum.

We show an example of measurements in Fig. 5. We plot the yield of the Li+D and D+D reactions as a function of elapsed time with black marks for ultra sonic OFF and blue marks for ON. In the case of the Li+D reaction shown in Fig. 5(a), the yield is constant and the difference between the ultra sonic ON and OFF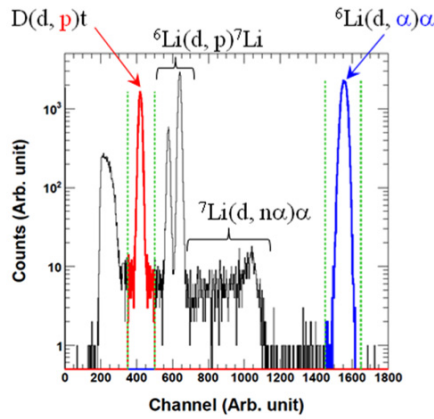 is within the error. On the other hand, the yield of the D+D reaction increases gradually probably due to increase of deuteron density in the liquid Li. Of particular significant, however, is the fact that the D+D reaction is enhanced by the ultra sonic wave. In Fig. 5(c) one already sees large difference between ON and OFF. Figure 5(b) shows the ratio of the yield for the ultra sonic ON to that for OFF. One can see that the D+D reaction with the ultra sonic is really enhanced several times, while no enhancement is observed for the Li+D reaction. In this run, we obtained the averaged ON/OFF ratio to be 3.5 for the D+D reaction. After 2 hours, the ultra sonic effect was lost and the ratio became back to unity.

Fig. 5(d) shows time spectra of events; the abscissa is the correlated time with the ultra sonic. The BLT is driven with the resonance frequency of 18.85 kHz, corresponding to a 53-μs cycle. We measured the time difference between the standard signal and the event signal. In the case of the ultra sonic OFF, the reaction occurs randomly and the time spectrum is flat as is shown with a black line. However, we cannot find clear time correlation with the ultra sonic, either, as shown with a blue line up to now.
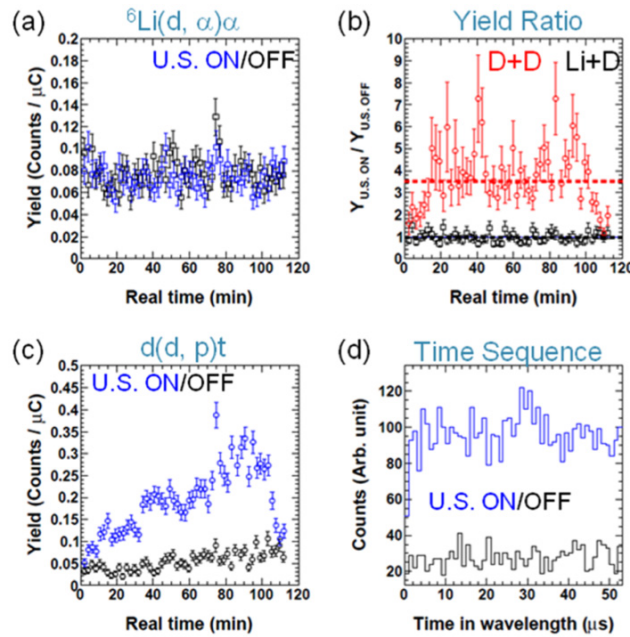

Fig. 5 – Time behaviors of Li+D and D+D reaction yields. (a) Li+D reaction yield, (b) yield ratio: ultra sonic ON/OFF, (c) D+D reaction yield, (d) micro time sequence of D+D reaction.

Fig. 6 (left) shows a histogram on the time correlation between two successive events; the abscissa corresponds to the time interval of the two successive events. It is known that reactions occur randomly and constantly, i.e., for Poisson distribution, the expected spectrum shows an exponentially decreasing function. For the generalized Poisson process in which the reaction rate is not constant but varies as time, the probability expressed

$$P = \frac{(\lambda(t))^k}{k!} e^{-\lambda(t)},$$

(4)

$$f(t) \sim e^{-\lambda(t)}, (\lambda(t) = \int_0^t r(x)dx)$$

where f(t) and r(t) are reaction interval and reaction rate, respectively.

In Fig. 6 (left), a histogram for the measurement without the ultra sonic (the black line) shows an exponential curve as expected. On the contrary, the blue line for the ultra sonic ON has three components; (1) homogeneous Poisson process (high reaction rate), (2) homogeneous Poisson process (low reaction rate) and (3) non- homogeneous Poisson process. The reaction rate r(t) for each process is estimated as shown in Fig. 6 (right). First, there is a high density phase (1) that is 13 times larger than the normal phase (2). Furthermore, we found the shoulder, not exponential component, in the time interval spectrum as shown in red curve (3). That means the reaction rate is not constant λ_0 but has time dependence $\lambda(t)$.
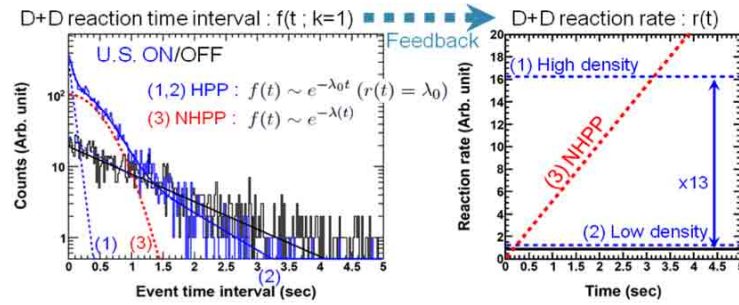

Fig. 6 – D+D reaction time interval (left) and reaction rate (right).

Vibration amplitude dependences and incident energy dependences of the Li+D and D+D reactions are shown in Fig. 7. In the figure, Y axis corresponds to the ultra sonic ON/OFF ratio. The intensity of cavitation is obviously increased with increase of the vibration amplitude. However, the yield ratio decreases for the D+D reaction because the intense cavitation stirs the liquid Li and absorbed deuterons diffuse out immediately from the spot where part of the beam is being accumulated. We carried out many measurements and found that the cavitation effect strongly depends on the target condition. Up to now, we have not found the way to keep the good condition for a long period.

We selected the data measured under a relatively stable condition and show the energy dependence of the yield ratio in Fig. 7 (right); i.e., the data under the condition of vibration amplitude of 1.9 μm, surface temperature of 220 °C, and beam input of 500 mW. The D+D reaction yield ratio has obvious energy dependence. As the incident energy becomes lower, the yield ratio increases. If the reaction is enhanced by the change of the deuteron density only, the energy dependence cannot be observed. Thus, the observed dependence on the incident energy clearly indicates that not only density effect but another mechanism to enhance the reaction should be effective in the liquid Li cavitation process. We fitted the experimental ratios to the calculations with the following equation

$$\frac{\sigma_{U.S.ON}(E)}{\sigma_{U.S.OFF}(E)} \sim \frac{\sigma(E+U)}{\sigma(E)} \sim \exp(15.64 z_1 z_2 \sqrt{\mu} \frac{U}{E^{3/2}}),$$

(5)

and obtained an effective energy difference U. If we assume that the enhancement is caused by Gamow factor only, the effective energy difference is U = 1980 eV for D+D fusion in center of mass system as shown in solid lines in Fig. 7.
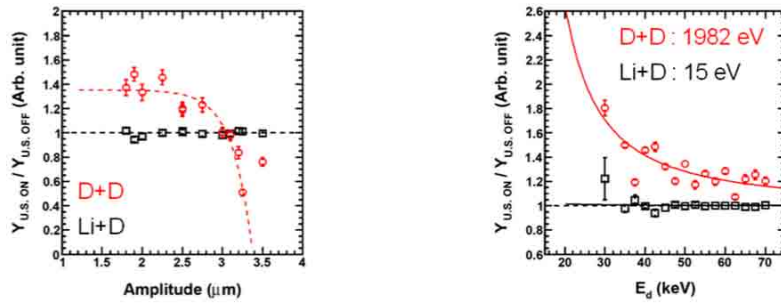
Fig. 7 – Vibration amplitude dependence and incident energy dependence of Li+D and D+D reactions.

4. Conclusion

We have developed an ultra sonic target system to form the Li acoustic cavitation bubbles in the vacuum chamber. The Li+D and D+D fusion reactions were measured during the low energy deuteron bombardment to the Li target. In this paper, we show the first experimental result with acoustic cavitation. It is found that the ultra sonic effect strongly depends on the target condition, the D+D reaction could be quite enhanced under the cavitation, and the reaction rate is not constant but time dependent. The decrease of the Coulomb energy barrier is about 2000 eV for the relatively stable condition. On the contrary, the Li+D reaction shows no meaningful effect. The present results indicate that not only density effect but also another mechanism to enhance the reaction rate should exist in liquid Li acoustic cavitation.

5. References

[1] R.P. Taleyarkhan, *et al*., *Science* **295** 1868 (2002)
[2] R.P. Taleyarkhan, *et al*., *Phys*. *Rev*. *E* **69** 36109 (2004)
[3] R.P. Taleyarkhan, *et al*., *Phys*. *Rev*. *Lett*. **96** 179903 (2006)

The effects of nuclear reactions in solids on the phonon dispersion relation

K. Tsuchiya[1], **S. Sasabe**[2] **and M. Ozaki**[3]

1) Tokyo National College of Technology, 1220-2 Kunugida, Hachioji, Tokyo 193-0997

2) Tokyo Metropolitan University, 1-1 Minami-Ohsawa, Hachioji, Tokyo 192-0397

3) Tokyo University of Agriculture, 1-1-1 Sakuragaoka, Setagaya, Tokyo, 156-8502

E-mail: tsuchiya@tokyo-ct.ac.jp

Abstract. In this study, theoretical predictions about the effects of nuclear reactions in solids on the phonon dispersion relations are shown. As an initial model, we have tried to treat one dimensional palladium deuteride and have obtained possible changes of phonon dispersion relations due to DD reactions. This method will be applied to the detection of nuclear reactions in solid by using nuclear scattering or Raman spectroscopy.

1. Introduction

In solid state physics, phonon dispersion relation is one of the most important information, because it includes not only the geometric and the electronic structures of the crystals but also the interaction between ions or electrons. For example, a lattice with only one atom in a primitive cell only has acoustic lattice vibration. However, a lattice with more than one atom in a primitive cell has acoustic and optical modes of vibration. Furthermore, interactions between impurity ions are also effective on the features of phonons. If nuclear reactions occur in solids, they will change the lattice and electronic structures and interactions between impurity ions and so on. Therefore, the changes of phonon dispersion relations will give us the evidences of nuclear reactions in solids. In this study, the possible changes of the phonon dispersion relation due to the nuclear reaction in solid were discussed. In this section, the theories of phonon dispersion relation of solids [1,2] are introduced briefly. Firstly, we define the equilibrium positions of ions in crystalline solids as $R_{nm}=r_n+k_m$, where r_n and k_m mean position of the n-th primitive cell and position of the k-th ion in the cell, respectively. Then the total kinetic energy is defined using displacement vector u_{nm} from R_{nm} as

$$K = \frac{1}{2}\sum_{nmj} M_m \left(\dot{u}_{nm}^j\right)^2,\tag{1}$$

where M_m is the mass of the m-th ion in the primitive cell and the summation for j is done over Cartesian components. And the total potential energy is written in the 2nd order approximation as

$$V = V_0 + \frac{1}{2}\sum_{nmj}\sum_{n'm'j'} C_{nmn'm'}^{jj'} u_{nm}^j u_{n'm'}^{j'},\tag{2}$$

where C is the second order partial derivative of V with respect to the displacement. They give the equation of motion for each ions which is written as

$$M_m \ddot{u}_{nm}^j = -\sum_{n'm'j'} C_{nmn'm'}^{jj'} u_{n'm'}^{j'}.\tag{3}$$

In this equation, every components of the displacement satisfy Bloch theorem

$$u_{nm}^j = e^{i\mathbf{q}\cdot\mathbf{r}_n} u_{0m}^j\tag{4}$$

and coefficient C has a symmetry

$$C_{nmn'm'}^{jj'} \rightarrow C_{mm'}^{jj'}(\mathbf{h}) \quad (\mathbf{h} = \mathbf{r}_{n'} - \mathbf{r}_n).\tag{5}$$

Defining the Fourier transformed formula as

$$\sum_{\mathbf{h}} C_{mm'}^{jj'}(\mathbf{h}) e^{i\mathbf{q}\cdot\mathbf{h}} \equiv G_{mm'}^{jj'}(\mathbf{q}) \tag{6}$$

and assuming the oscillatory solution as

$$u_{nm}^{j}(t) = e^{-i\omega t} u_{nm}^{j}(0), \tag{7}$$

we obtain phonon dispersion relation as

$$\sum_{m'=1}^{M}\sum_{j'=1}^{3} G_{mm'}^{jj'}(\mathbf{q}) u_{0m'}^{j'}(0) = M_m \omega^2 u_{0m}^{j}(0) \tag{8}$$

where M is the number of ions including in a primitive cell. For the case of a monatomic lattice which has only one ion in a primitive cell, eq.(8) is rewritten as

$$\begin{pmatrix} G^{11} & G^{12} & G^{13} \\ G^{21} & G^{22} & G^{23} \\ G^{31} & G^{32} & G^{33} \end{pmatrix} \begin{pmatrix} u^1 \\ u^2 \\ u^3 \end{pmatrix} = M\omega^2 \begin{pmatrix} u^1 \\ u^2 \\ u^3 \end{pmatrix}. \tag{9}$$

This equation has three solutions. One corresponds to the longitudinal mode, and the other two corresponds to the doubly-degenerated transverse mode. The typical solutions are sketched in Fig.1. For the case of a diatomic lattice with a heavy and a light ion in a primitive cell, eq.(8) is rewritten as

$$\begin{pmatrix} G_{11}^{11} & G_{11}^{12} & G_{11}^{13} & G_{12}^{11} & G_{12}^{12} & G_{12}^{13} \\ G_{11}^{21} & G_{11}^{22} & G_{11}^{23} & G_{12}^{21} & G_{12}^{22} & G_{12}^{23} \\ G_{11}^{31} & G_{11}^{32} & G_{11}^{33} & G_{12}^{31} & G_{12}^{32} & G_{12}^{33} \\ G_{21}^{11} & G_{21}^{12} & G_{21}^{13} & G_{22}^{11} & G_{22}^{12} & G_{22}^{13} \\ G_{21}^{21} & G_{21}^{22} & G_{21}^{23} & G_{22}^{21} & G_{22}^{22} & G_{22}^{23} \\ G_{21}^{31} & G_{21}^{32} & G_{21}^{33} & G_{22}^{31} & G_{22}^{32} & G_{22}^{33} \end{pmatrix} \begin{pmatrix} u_1^1 \\ u_1^2 \\ u_1^3 \\ u_2^1 \\ u_2^2 \\ u_2^3 \end{pmatrix} = \omega^2 \begin{pmatrix} M_1 u_1^1 \\ M_1 u_1^2 \\ M_1 u_1^3 \\ M_2 u_2^1 \\ M_2 u_2^2 \\ M_2 u_2^3 \end{pmatrix}. \tag{10}$$

The typical solutions are sketched in Fig.2. In real case, these relations should be calculated for each directions of wave propagation.
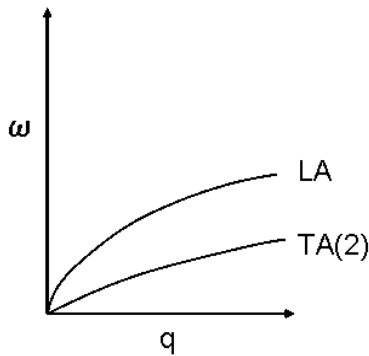

Fig. 1 - Phonon dispersion relation of monatomic lattice. Characters LA and TA(2) mean longitudinal acoustic and doubly-degenerate transverse acoustic modes, respectively.
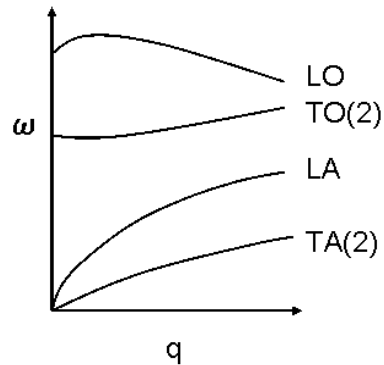
Fig. 2 - Phonon dispersion relation of diatomic lattice. Characters LA and TA(2) mean longitudinal acoustic and doubly-degenerate transverse acoustic modes, respectively. Characters LO and TO(2) mean longitudinal
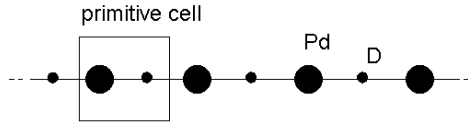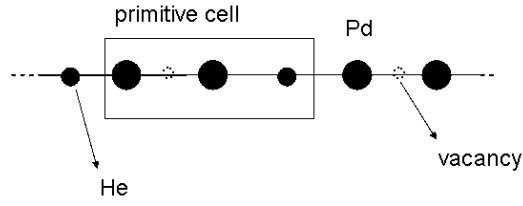
Fig. 3 - One-dimensional PdD lattice

Fig. 4 - A model of structure changed one dimensional PdD lattice due to nuclear reaction

2. Change of the phonon dispersion relation due to the nuclear reaction

We discuss the phonon dispersion relation of palladium deuteride using the one dimensional PdD lattice. It is a very simple model which is illustrated in Fig.3. In this case, the dimension of the dynamical matrix is 2×2 with 2 solutions. The solutions are easily obtained by using the method described in section 1. And the typical dispersion curves are similar to Fig.2. If we consider some nuclear reactions and they change the structure of the lattice in Fig.3, they will also change phonon dispersion relation. For example as illustrated in Fig.4, if deuterons are disappeared and He's are produced, a primitive cell contains two palladiums, one He and one vacancy. This lattice roughly corresponds to the He concentration of 10^{22} atom/cm^3 in the three-dimensional lattice. It is unrealistic situation. However, our model gives possible changes of phonon dispersion relation by assuming the lowest dimensional lattice and the highest deuteron concentration. For example, the occurrence of the nuclear reactions at a definite small domain with high deuteron concentration in the palladium deuteride may influence the phonon states of the whole lattice. At the moment, phonon dispersion relation will be changed under the influence from the domain. It will be detected by using neutron scattering or Raman spectroscopy. Of course it suggests the DD reaction. At this time, the dimension of the dynamical matrix is changed into 3×3 with 3 solutions. This means that some unknown phonon dispersion branches are created at the reaction. Therefore, if we measure the phonon dispersion relation of palladium deuteride and find unknown extra dispersion branches, they may be evidences of nuclear reactions. It is a model with oversimplification. In real case, more complicated and local reactions should be considered. For example, multi-body fusion or more complicated reaction [3] should be considered. However, the structure changes due to the nuclear reaction always tend to increase dispersion branches

Here, we would like to show the examples by doing one dimensional calculation of longitudinal mode for the lattices illustrated in Figs.3 and 4. Firstly, calculation for PdD lattice illustrated in Fig.3 has done. It is a simplified one dimensional lattice with alternate arrangement of Pd and D atoms. If we only consider the vibrations along the line, it means longitudinal mode. In this case, the total kinetic energy is written as

$$K = \frac{1}{2}M\sum_n \dot{u}_{2n}^2 + \frac{1}{2}m\sum_n \dot{u}_{2n+1}^2, \qquad (11)$$

where M and m mean mass of Pd and mass of D, respectively. And the total potential energy in harmonic approximation with neighboring interaction is written as

$$V = \frac{1}{2}k\sum_n (u_n - u_{n+1})^2, \qquad (12)$$

where k means elastic constant. Using them, the equations of motion are derived as

$$M\ddot{u}_{2n} = -k(2u_{2n} - u_{2n+1} - u_{2n-1})$$
$$m\ddot{u}_{2n+1} = -k(2u_{2n+1} - u_{2n+2} - u_{2n}), \qquad (13)$$

where displacement u_n for the n-th atom is a function of time. Using a similar procedure with the general case in section 1, we obtain secular equation

$$\begin{vmatrix} 2k - M\omega^2 & -2k\cos(qa) \\ -2k\cos(qa) & 2k - m\omega^2 \end{vmatrix} = 0. \qquad (14)$$

The well known solutions of eq.(14) are

$$\omega_\pm^2 = k\left(\frac{1}{m} + \frac{1}{M}\right) \pm k\sqrt{\left(\frac{1}{m} + \frac{1}{M}\right)^2 - \frac{4\sin^2(qa)}{mM}}. \tag{15}$$

They give phonon dispersion relation which has one acoustic mode and one optical mode. Secondly, we consider one dimensional lattice illustrated in Fig.4. In this case the total kinetic energy is written as

$$K = \frac{1}{2}M\sum_n \dot{u}_{3n}^2 + \frac{1}{2}(2m)\sum_n \dot{u}_{3n+1}^2 + \frac{1}{2}M\sum_n \dot{u}_{3n+2}^2, \tag{16}$$

where the 1st, the 2nd and the 3rd terms mean total kinetic energy of Pd sitting on the left side of He, of He and of Pd sitting on the right side of He, respectively. The total potential energy is written as

$$V = \frac{1}{2}\alpha\sum_n (u_{3n+2} - u_{3n+1})^2 + \frac{1}{2}\alpha\sum_n (u_{3n+1} - u_{3n})^2 + \frac{1}{2}\beta\sum_n (u_{3n} - u_{3n-1})^2. \tag{17}$$

In this equation, the 1st and the 2nd terms mean interactions between neighboring Pd and He with elastic constant α. The 3rd term means interaction between neighboring Pd's with elastic constant β. Equations of motion for each atom are written as

$$M\ddot{u}_{3n} = -(\alpha + \beta)u_{3n} + \alpha u_{3n+1} + \beta u_{3n-1}$$
$$2m\ddot{u}_{3n+1} = -\alpha(2u_{3n+1} - u_{3n+2} - u_{3n})$$
$$M\ddot{u}_{3n+2} = -(\alpha + \beta)u_{3n+2} + \beta u_{3n+3} + \alpha u_{3n+1}. \tag{18}$$

And the secular equation is obtained as

$$\begin{vmatrix} \alpha + \beta - M\omega^2 & -\alpha e^{iql} & -\beta e^{-iql} \\ -\alpha e^{-iql} & 2\alpha - 2m\omega^2 & -\alpha e^{iql} \\ -\beta e^{iql} & -\alpha e^{-iql} & \alpha + \beta - M\omega^2 \end{vmatrix} = 0. \tag{19}$$

Expanding the secular equation, we obtain a cubic equation for ω^2 as

$$mM^2\omega^6 - \{\alpha M + 2(\alpha + \beta)m\}M\omega^4 + \alpha(\alpha + 2\beta)(m + M)\omega^2 - \alpha^2\beta\{1 - \cos(3ql)\} = 0, \tag{20}$$

which has three positive real solutions. They correspond to one acoustic mode and two optical modes. For the case of $q=0$, this equation reduces to

$$\omega_0^2\left[mM^2\omega_0^4 - \{\alpha M + 2(\alpha + \beta)m\}M\omega_0^2 + \alpha(\alpha + 2\beta)(m + M)\right] = 0. \tag{21}$$

The solution for acoustic mode is $\omega_0=0$ and the solutions for the optical mode are

$$\omega_{0\pm}^2 = \frac{\alpha M + 2(\alpha + \beta) \pm |\alpha M - 2\beta m|}{2mM}. \tag{22}$$

For the case of $\alpha M > 2\beta m$, we obtain

$$\omega_{0+}^2 = \alpha\left(\frac{1}{m} + \frac{1}{M}\right) \qquad and \qquad \omega_{0-}^2 = (\alpha + 2\beta)\frac{1}{M}. \tag{23}$$

For the case of $\alpha M < 2\beta$, we obtain

$$\omega_{0+}^2 = (\alpha + 2\beta)\frac{1}{M} \qquad and \qquad \omega_{0-}^2 = \alpha\left(\frac{1}{m} + \frac{1}{M}\right). \tag{24}$$

They give the difference of two optical mode at $q=0$. If we find these changes of dispersion relation, we can know the change of the structure from the lattice in Fig.3 to the lattice in Fig.4. This corresponds to the detection of some nuclear reactions in solids.
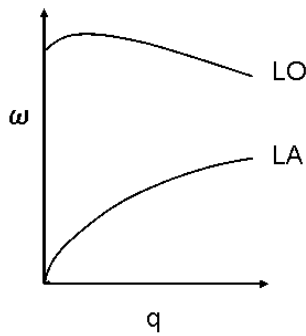
Fig. 5 - Phonon dispersion relation of the longitudinal vibration of the one dimensional lattice illustrated in Fig.3.
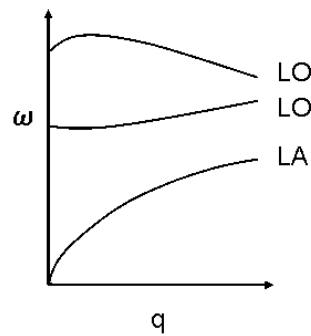
Fig. 6 - Phonon dispersion relation of the longitudinal vibration of the one dimensional lattice illustrated in Fig.4.

3. Conclusions

If some nuclear reactions have happened in solids, the lattice structure is changed and the number of the ions in a primitive cell is increased. Even if these changes are spatially inhomogeneous, this tendency is unaltered. In this case, the dimension of the dynamical matrix becomes larger and this causes an increase of dispersion branches. Therefore, if we measure the phonon dispersion relation of palladium deuteride and find unknown extra dispersion branches, they may be evidences of nuclear reactions.
These discussions can be applied to the analysis of Raman observation of the palladium deuterides [4,5] .

Acknowledgments

4.   References

[1] C.Kittel, *Introduction to Solid State Physics*, (John Wiley and Sons, Chapter 5)
[2] N.W.Ashcroft and N.D.Mermin, *Solid State Physics*, (Holt-Saunders, Chapter 22)
[3] A.Takahashi, *Proceedings of JCF8*, pp51 (2007)
[4] R.Sherman, H.K.Birnbaum, J.A.Holy and M.V.Klein, *Phys. Lett*., **62**A 353 (1977)
[5] K.Tsuchiya, A .Watanabe, M.Ozaki and S.Sasabe, *Proceedings of ICCF14* , to be published

Nuclear Transmutation in Non- equilibrium Systems by Ultra-closed Range Casimir Effect

Xing-liu Jiang*, Y. Zhang , Z. Zhang

Shenzhen Vortex Condensation Tech. Co. Ltd, Shenzhen, 518052，China
*A Professor emeritus of Beijing University of Aeronautics & Astronautics,
E-mail: jiangxl@buaa.edu.cn

Abstract. Quantum physics predicts the existence of an underlying sea of zero-point energy at every point in the universe. The breakthrough of seeing, understanding and devising a converter of the energy available in quantum oscillation might be the opening point of an energy filled 21st century for humanity.

It is well known that phenomena of electrical discharge always bring on transient energy concentration temporally and spatially. Highly localized nuclear activation in electrochemical systems and other electrical discharge processes had been observed at many laboratories in the world. Based on the theory of vortex dynamics, the strange phenomena of "cold fusion", such as the excess heat, anomalous nuclear transmutation and so forth, are considered to be interpretable by torsion coherence with the zero-point energy induced by localized intense field emission of micro-protrusion of the cathode, and the dynamic Casimir effect of transient evolution of triple region of gas, liquid solution, and electrode protrusion. In fact this process induces a variety of high energy, deterministic nuclear fusion reactions between relatively large nuclei, "triggered" by low input energies, generally not considered possible in the conventional physics frame. A logical extrapolation of this discovery is that the strong force of the nucleus is in fact an ultra-close range Casimir effect. Fusing ions capturing electron to convert excess protons to neutrons is a common occurrence and a key to the production of stable isotopes without neutrons or radiation.

A system as an anomalous transmutation reaction discovered by Yuguang Zhang is described in this paper. A micro-emission exhaust gas handling device(publication number of patent: WO 2008 083530) due to nuclear transmutation by vortex dynamics, is provided, which is a container only having inlets. A model of sonic black hole with the acoustic version of Hawking radiation by using de Laval nozzle is supposed to explaine the behaviors of micro-emission exhaust for the system.

1. Introduction

"No problem can be solved from the same level of consciousness that created it "—Albert Einstein.

Researchers fail to explain the phenomena related to so called "Cold Fusion" within the framework of main stream physics. The theories of tapping the zero point energy, dynamic Casimir effect and the torsion field including the spin and rotation movement, are suggested to be used for describing the phenomena of "cold fusion"[1,2].

Many scientists have long been aware that our earth is immersed in an extremely dense sea of energy, which permeates every nook and cranny of the universe[3]. Recently it was realized that this huge reservoir could be an available source of usable energy. Science employs a variety of names to describe

this new field: space energy, vacuum energy, dark energy, the quantum vacuum, and Zero Point Energy (ZPE). Until about twenty years ago, scientists did not consider it possible to tap it for practical use. Nikola Tesla, the genius who gave birth to alternating current, said in a talk to electrical engineers in 1891: "Ere many generations pass, our machinery will be driven by a power obtainable at any point in the universe. …Throughout space there is energy." Trying to unravel this mystery has taken many paths, Cold Fusion, bubble fusion, LENR, cavitation and Casimir cavities to name a few.

For Bohm, "an invisible, intrinsic connectedness uniting everything in the universe was merely perceived, but fundamentally real." In his words: " Ultimately, the entire universe (with all its 'particles,' including those constituting human beings, their laboratories, observing instruments, etc.) has to be understood as a single undivided whole, in which analysis in separately and independently existent parts has no fundamental status."

Kovac explains the cold fusion and transmutation processes in term of Gauss' pseudosphere-cantenoid geometry determining the bending of space to form the toroid knots[4]. The tightly wound toroid (centripetally bound and compressed) mass can then either unwind back through its axis(as it turns inside-out) as energy production (heat, electricity, and light), or it can unwind equatorially as a catenoid spiral in secondary mass formation to form various elements.. Thus mass-energy transmutations occurring as in Russell' descriptions of motion to and from wave field cube well boundaries to and from mass spherical center boundary. The creation of mass 5 element is offered as support for the notion that cold fusion, ultra subatomic particles, electricity, and magnetism are each a consequence of special interrelated geometric formation moving in microscopic space

2. Nuclear transmutation in non-equilibrium system

For discuss of nuclear transmutation, the issues of low-energy nuclear synthesis and transmutation of stable and radioactive isotopes in non-equilibrium systems listed as following: such as (1)diffusion processes of hydrogen and deuterium gases in a new type "Solid Fusion Reactor" of two types of nanomaterial ($ZrO2\_Pd35$ and $ZrO2\_Ni30Pd5$) by Arata and Y.C. Zhang; (2) piezonuclear reactions occurring in stable iron nuclides contained in aqueous solutions of iron chloride or nitrate by A. Carpinteri, F. Cardone, G. Lacidogna; and (3)the anomalous characteristics of nuclear transmutation by V. Vysotskii and A. Kornilova observed in biological cells (including numerous Kervran's experiments evidencing the nuclear transmutation of chemical elements in animals and plants) should be mentioned.

Sonoluminescence can be explained in terms of quantum radiation by moving interfaces between media of different polarizability. The long distance quantum radiative phenomenon associated not with atoms but with fast moving surfaces in the collapsing bubble following the dynamical Casimir effect..

3. Vortex dynamics and torsion field

During the period of March to May, 1989, Xingliu Jiang detected nuclear tracks with solid detector of CR-39 by on site of the tip of cathode electrode in a electrolyte cell. A manuscript, "Micropinch in cold nuclear fusion" about the experimental results by Xingliu Jiang, Ning Xu and Lijun Han was sent to Editor of Nature magazine at September 1989, Dr. Philip Ball, Assistant Editor wrote on this manuscript (Registration no: J10535 PB/HH):" The referee finds your results interesting", "The referee clearly feels that your experiments represent an interesting approach to studies of cold fusion". For the referee, he wrote: "I found manuscript J10535 quite interesting and recommend that you publish it " .The tracks of

Fig. 1 - Tracks of nuclear reaction products on the CR-39 detector under the torsion field effect.

highly directional particles (Fig. 1) might be products of nuclear reactions in the electrolyte cell, such as protons and alpha particles including clusters of high density charge of electrons with different size according the experimental results by Shoulders. Such pattern of tracks offers the evident factors for channeling effect of crystalline metal electrodes and particle acceleration by torsion field.

The experimental results of anomalous nuclear reaction reported by Jiang, Borkris, Miley and Patterson plus similar results reported by Mizuno, et al challenge the current atomic model[5,6,7].. The phenomenon seems highly reproducible. It appears that there are situations in which nuclei split open at the stimulus only chemical energies. Ronald J. Kovac reported [3]that elemental transmutation appears to have occurred when a vacuum tube containing only nitrogen(14N) was exposed to an electromagnetic force field. Gas spectrometer analysis revealed that the contents in the tube after electromagnetic shaping included substantial amounts of helium 4He and lithium 5Li.

Recently, Ron Kovac and Toby Grotz of Colorado, repeated Russell's 1927 work, which was verified at the time by Westinghouse Laboratories. Russell found a novel way to change the ratio of hydrogen to oxygen in water vapor inside a sealed quartz tube, or to change the vapor to completely different elements. Their conclusion agrees with Russell: the geometry of motion in space is important in atomic transmutation. Kovac short hands that idea to geometry of space-bending. It is well known "matter" is a wave form energy-pattern in the medium. Quanta turned out to be more like waves than like corpuscles. According to Russell's description of the Wave of Creation: The wave is described as causing "the integration of matter at poles and disintegration at equators. Matter integrates by the contraction of one pair of spirals around the shafts which wind it into spheres by the way of its poles, and disintegrates it by the expansion of the other pair which unwinds it by the way of equators".

A system as an anomalous transmutation reaction discovered by Yuguang Zhang is described in this paper. An micro-emission exhaust gas handling device (publication number of patent: WO 2008 083530) is provided, which is a container only having inlets. At least two stages of exchangers (2) are provided in series in the container from an exhaust gas inlet (1) and a mixing gas chamber (3) is arranged at the communicating location between two stages of exchangers. An exchanging gas chamber (23) in the first stage of the exchanger (2) is provided with an orifice (4) communicating with air and each of the mixing gas chambers (3) from the second to the last stage of exchangers is disposed with a return pipe (4) communicating with the inlet of the first stage of the exchanger.

For the gas handling device, the straight pipes or cylinder channels with the geometry similar to the de Laval nozzle will generate supersonic gas flow with vortexes in the form of turbulence in order to brake the flow of straight line, laminar motion [8]. A model of the sonic black hole with Hawking radiation
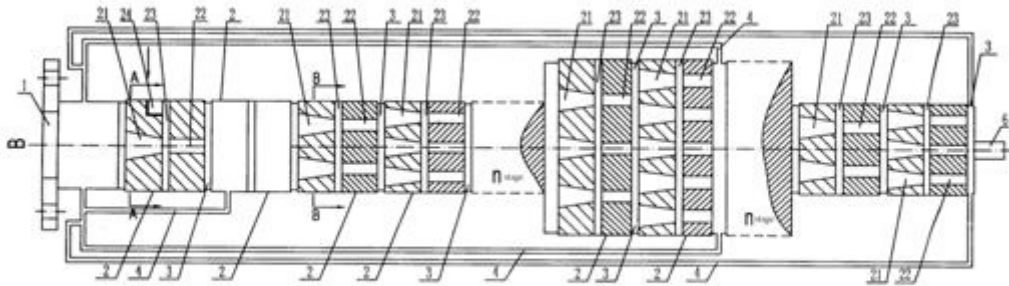
Fig. .2 - A micro-emission exhaust gas handling device

could be used to describe the annihilation of exhaust gas 9,10]. Thus the vortex body and the mass of the medium is affected toward the dissipation and breaking apart. Such dissipation, expansion and slow explosion of many natural elements could be observed in the micro-emission exhaust gas handling device due to dynamic Casimir effect and torsion coherence with zero point energy [1]. The polarization of particle spin and angular moment generate the torsion field. The filamentation of turbulence flow shows the effect of dynamic Casimir force with the zero point electromagnetic fluctuation. The axial acceleration and memorial effect (heat after death) of character for torsion field have been observed in many laboratories.

4. Conclusion

  The vacuum is the matrix that contains all matter and all energy. Our current understanding of science is like a puzzle with a large missing piece-quantum vacuum zero point energy. Various scientists have been discovering anomalies of phenomena attributed to the conversion of the zero point energy.. The combination of ion vortex or vortex rings with abruptly pulsed bucking electromagnetic field or turbulence fluid could result in the direct manifestation of energy and matter transformation. Based on the theories of quantum vacuum zero point energy, torsion field, further study of sonic black hole should be carried out for explanation of anomalies [10].

5. References

[1]   X. L. Jiang, Frontier Science, **4(3),** 15(2010)

[2]   Xingliu Jiang, et al.. Nuclear Physics B. **166**, 290 (2007)

[3]   H. E. Puthoff , Phys. Rev. A, **40**, 4857(1989); **44**, 3385(1991)

[4]   Ronald J. Kovac, J. of New E nergy, **1(1)**, 87.(1996)

[5]   George H. Miley and James A. Patterson, J. of New Energy,   **1(3)**, 5(1996).

[6]   J. O'M Bockris, G. H. Lin and R. Bush, J. of New Energy, **1(2),** 17(1996).

[7]   Mark Porringa.. Annales de la Fondation Louis de Broglie, **3:29**, 1109(2004)

[8]   J.E. Cater, J. Soria, T.T. Lam, J. Fluid Mech. **499**, 327(2004)

[9]   Stefano Giovanazzi, Phys. Rev. Lett. **106,** 011302(2011)

[10] T. A. Jacobson, R. Parentani, Scientific American Reports, **April 2007**, p. 13

A Practical Way to Generate Protons (Deuterons) of Energy Between 500 and 1000 eV.

J. Dufour, X. Dufour and D. Murat
Laboratoire des Sciences Nucléaires - CNAM, 2 rue Conté, 75003 Paris, France

E-mail: 3jdufour@laposte.net

Abstract. *Research tools used in the field of d/d fusion are protons (deuterons) accelerators producing ion beams of energies between 10 keV up to several MeV . Another source of protons (deuterons) are low pressure electrical discharge, yielding ions of energies between 1 to some tens of eV. Based on this second source, a way to generate protons (deuterons) in the range 500 to 1000 eV is described.*

1. Introduction

It was recently proposed [1] to study d/d fusion reactions initiated by bombarding targets loaded with deuterium, with deuterons of energies between 500 and 1000 eV. These levels of energy can easily be achieved by using ion generators of several kW power, that are now available on the market (surface treatment, electronic industry). They can produce ion (proton, deuteron) beams of high intensity (several A) with ion energies in the range 100 to 4000 eV and are thus able to work in the 500 to 1000 eV energy window. Due to budget limitations, such an equipment cannot be envisaged for the time being. The existing laboratory accelerators are limited on the low energy side to some 5 to 10 keV. A device was thus developed, based on the acceleration of ions generated in a low pressure (50 Pa) glow discharge. Ionic current up to 30 μA, with ion energies of some 850 eV are expected.

2. Principle of the device

Glow discharges in hydrogen isotopes at pressures between 10 to 50 Pa, mainly yield H^+ (D^+) ions and atomic hydrogen (deuterium). The principle of the device is described in *Fig 1*. Technical features to control operating conditions (pressures cascades for instance) are given in *Fig 2*.
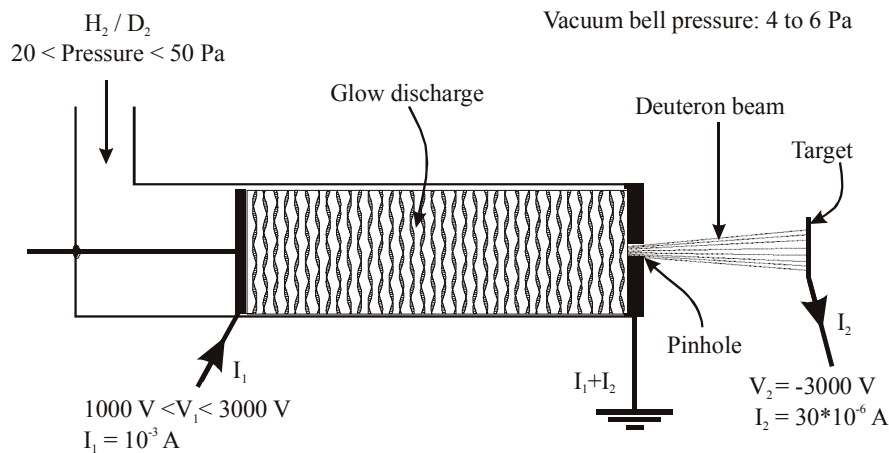
Fig. 1 – Principle of the device of glow discharge

The concentration of molecular deuterium entering the system is some $8*10^{21}$ m^{-3} (at a representative pressure of 30 Pa) and the current I_1 of the main glow discharge is measured to be 10^{-3} A for a voltage V_1 = + 2000V. Part of the deuterons, generated in the glow discharge, go through a pinhole (0.5 mm diameter) in the earthed electrode and are collected on the target. At low voltage of the target, the current I_2 is some $5*10^{-6}$ A, increasing from 30 to $40*10^{-6}$ A when V_2 reaches 3000V. At a pressure of 5 Pa, the mean free path of hydrogen (deuterium) is round 2 mm. For V_2 = 3000 V and a distance between the grounded electrode and the target of 5 mm, the mean energy of the D$^+$ ions impinging the target can be estimated to be some 850 eV (See below more details on the modeling of the discharge)
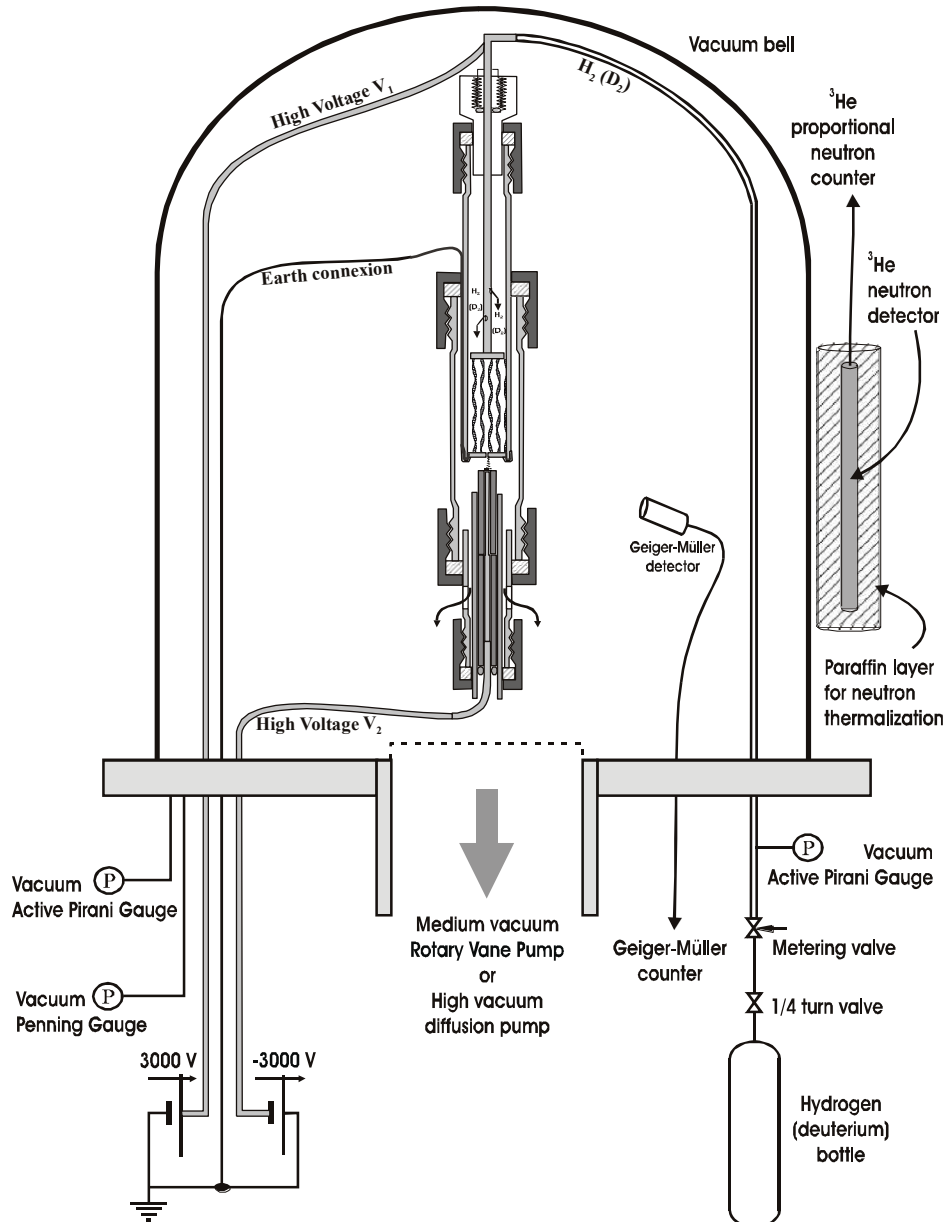
Fig. 2 – Overall experimental set-up

3. Detailed description of the device

3.1 Over all experimental set-up:

The overall experimental set-up is given *Fig 2*.

The reactor is placed in a vacuum bell. Pressures down to 1 Pa can be reached when using the medium rotary pump and down to 10^{-2} Pa when using the combination rotary/diffusion pumps. The pressures before and after the reactor are measured by 2 Pirani gauges, when the rotary pump only is used (1 Pirani before and 1 Penning gauge after the reactor when the combination rotary/diffusion pumps is used). Hydrogen (deuterium) gas is fed into the reactor through a metering valve. The pressure drop through the pinhole of the glow discharge cathode is measured by the pressure gauges. The glow discharge cathode (tantalum) is connected to earth. The glow discharge anode (stainless steel) is connected to a positive high voltage generator (GAMMA High Voltage Research) delivering a regulated current up to 3 mA under a regulated voltage up to 20 kV. The target is connected to a negative high voltage generator (HP 6110 A) delivering a regulated current up to 6 mA under a regulated voltage up to 3 kV. Pressures, currents and voltages are monitored, using an AOIP LS20 monitoring device.
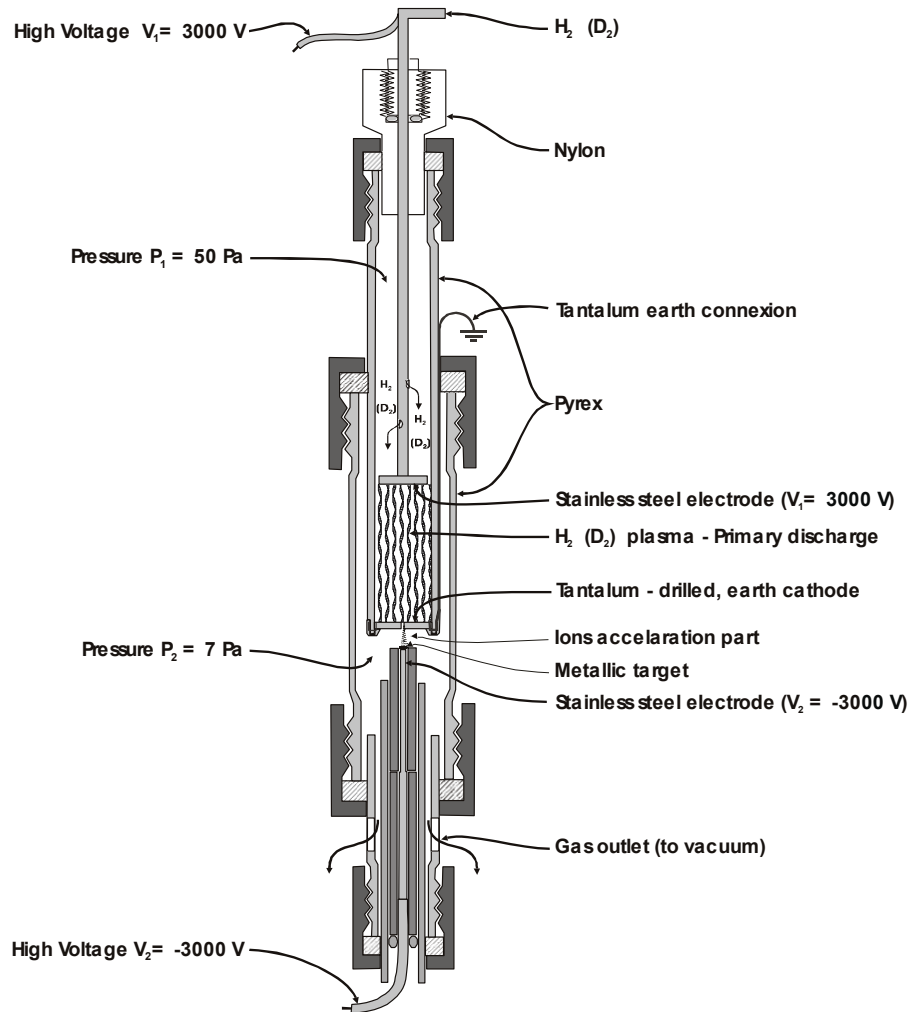
Fig. 3 – Reactor design

274

3.2 Reactor design

The reactor is shown on *Fig 3*.

The glow discharge is struck between the stainless steel anode and the tantalum cathode. A pinhole (surface $S_{Pin\ Hole}$) in the cathode (surface $S_{Cathode}$) allows the hydrogen (deuterium) flowing through the glow discharge at a pressure P_1 of a few tens of Pa, to expand down to a pressure P_2 of a few Pa. A current of protons (deuterons) also flows with the expanded hydrogen (deuterium), through the pinhole and is accelerated, under vacuum, by the high negative voltage of the target. Energies of the ions up to some 850 eV are expected (see below modeling of the discharge).

An helium 3 neutron detector with 2 cm paraffin thermalization covering is placed outside the vacuum bell (see above)

4. Modeling of the process

4.1 The glow discharge

The principles for a global model of a glow discharge can be found in [2]. The particles balance yields the temperature of the electrons T_e and the power balance yields the ions (and electrons) concentrations $n_0 = n_i = n_e$. If l is the length, R the radius of the plasma of the cylindrical discharge (*Fig 4*) and n_g the neutral gas concentration, the particles balance expresses that the charged particles production through ionization (coefficient K_{IZ} $m^3 s^{-1}$) is equal to the charged particles lost by recombination in the gas (axial losses, dimensionnless fraction h_l) and on the surface of the reactor (surface losses, dimensionless fraction

$$K_{IZ} n_g n_0 \pi R^2 l = \left(2\pi R^2 h_l n_0 + 2\pi R l h_R n_0\right) u_B, \text{ with } u_B = \sqrt{\frac{kT_e}{m_i}} \text{ (Bohm velocity of the ions, mass } m_i)$$

From this balance, the following relation is obtained:

$$\frac{K_{IZ}(T_e)}{u_B(T_e)} = \frac{1}{n_g d_{eff}} \tag{1}$$

with $d_{eff} = \frac{1}{2} \frac{Rl}{Rh_l + lh_R}$, (m) linear dimension describing the geometry of the plasma.
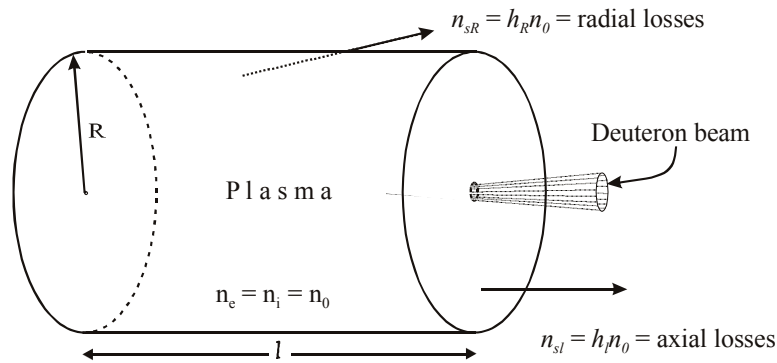
Fig. 4 – The glow discharge

The energy balance can be written $P_{abs} = \left(h_l n_0 2\pi R^2 + h_R n_0 2\pi Rl \right) u_B E_T$ expressing that the total power absorbed P_{abs} is used for electron-ion pair production, E_T being the total energy required per pair (ionization, excitation, ion acceleration…)

From this balance, the following relation is obtained:

$$n_0 = \frac{P_{abs}}{A_{eff} u_B E_T} \qquad (2)$$

with $A_{eff} = 2\pi R (Rh_l + lh_R)$, (m^2) surface dimension describing the geometry of the plasma.

Relations (1) and (2) combined with the relation:

$$A_{eff} d_{eff} = \pi R^2 l \ , \ \left(m^3 \right) \text{ (plasma volume)} \qquad (3)$$

allow the calculation of the parameters of the discharge $\left(n_0 \text{ and } T_e \right)$, using the experimental relation between T_e and $n_g d_{eff}$ given by *Fig 5* which is valid for any discharge. T_e is used as the fitting parameter.

Typical values for the conditions used (P$_1$ = 50 Pa, V$_1$ = 3000 V, I$_1$ = 3 mA) are $n_0 = 2*10^{16}$ m^{-3}, temperature of the electrons T$_e$ = 4,2 eV and energy of the ions leaving the cathode 2 eV.

4.2 The positive ions acceleration zone

A fraction of the positive ions (protons, deuterons) generated in the discharge (in the ratio $S_{Pin\ Hole} / S_{Cathode}$) are expanded, with the neutral atoms, from P_1 to P_2, through the pinhole of the cathode, which they leave with an energy of a few eV (see above). They are accelerated by the target negative voltage. Their mean free path λ is assumed to be the same as atomic hydrogen,

$\lambda_H \ (mm) = \dfrac{100}{P_2 \ (Pa)} 10^{-1}$. For a distance cathode-target of 5 mm and a target voltage of -3000 V, the

energy of the protons (deuterons) impinging on the target will be some 850 eV for P_2 = 7 Pa, assuming that the expansion is complete at a few (2 to 3) mm from the cathode.
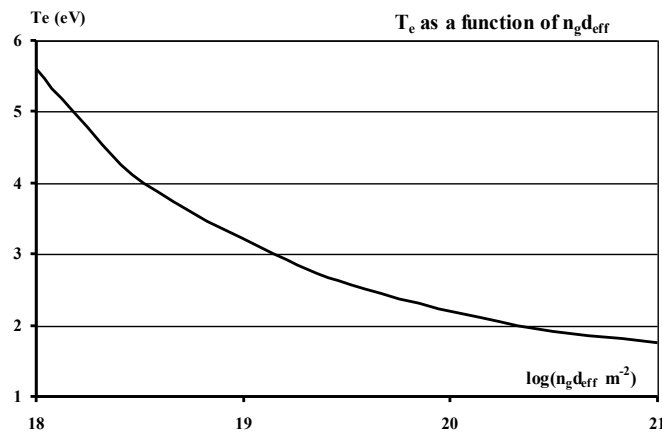
Fig. 5 – T$_e$ as a function of n$_g$d$_{eff}$

5. Monitoring the fusion reaction

To monitor the fusion reaction, the production of neutrons will be measured, using a 65NH45 Helium 3 detector (active detection surface $S = 100$ cm^2). The active part of the detector is surrounded by a cylindrical layer of paraffin, resulting in a paraffin thickness of 2 cm. The spectra are recorded using a CANBERRA 2006 pre-amplifier, an ORTEC 570 amplifier and a CANBERRA AccuSpec NaI multi-channel analyser. The back ground of the laboratory has been measured and found to be equal to 1.5±0.2 10^{-2} cps, corresponding to a background neutron flux $\Phi_{N-back.}$ of some 1.5 10^{-4} cps/cm^2.

Assuming an efficiency of 100% of the detection chain, the neutron activity A_{N-meas} of the target, will be evaluated from the measured neutron flux $\Phi_{N-meas.}$ by $A_{N-meas.} = 4\pi R^2 \left(\Phi_{N-meas.} - \Phi_{N-back.} \right)$, (Bq) , with R being the distance target/detector (taken as 25 cm which is the minimum distance between the cylindrical detector and the target). Thus calculated, Φ_{N-meas} gives a low side value of the neutron activity of the target, that will then be compared to the value $A_{N-mod.}$, computed from the model described in [1].
In order to detect possible γ emission from the target, a Geiger counter has been placed inside the vacuum bell.

6. Conclusion

The proposed device will be used to test various targets (diameter 2 to 4 mm). The choice of these targets (nature of the metal and its physical and chemical characteristics) will be guided by the results already obtained in the field. In a first step, the objective will be to verify the validity of phenomenological model. In a second step, the possibility of gaining a better knowledge of the mechanisms involved could result in a further improvement of the targets.

Finally, in case of success, ion generators, with kW power level and energies of the ions in the range 200 to 4000 eV, that are now available on the market (surface treatment and electronic industries) could be used for an industrial up-scaling.

7. References

[1] J. Dufour. "Evaluation of d/d reaction rates in metallic lattices as a function of the deuteron energy. A phenomenological model of nuclear fusion in solids" *ICCF15 Proceedings. Rome 5-9 October 2009*

[2] Lieberman and Lichtenberg "Principles of Plasma Discharges and Materials processing" *John Wiley and Sons*

Lithium Fluoride X-ray Imaging Film Detectors for Condensed Matter Nuclear Measurements

R.M. Montereali[1], S. Almaviva[1], E. Castagna[2], F. Bonfigli[1], M.A.Vincenti[1]
[1]*ENEA, FISACC, C.R. Frascati, V. E. Fermi, 45,00044 Frascati (RM), Italy*
[2]*Associazione Euratom-ENEA sulla Fusione, C.R. Frascati, V. E. Fermi, 45,00044 Frascati (RM), Italy*

E-mail: rosa.montereali@enea.it

Abstract. A novel thin-film imaging detector for X-rays, based on photoluminescence from aggregate color centers in lithium fluoride, has been proposed and tested. The detector consists in a radiation-sensitive thin film of lithium fluoride thermally evaporated on a glass substrate. The morphological properties of the lithium fluoride thin films, which influence the detector performances, have been investigated.

1. Introduction

Among alkali halides, lithium fluoride (LiF) is particularly interesting because it is practically not hygroscopic, it possesses good physical and optical properties and it can host laser active electronic defects stable at room temperature (RT). Various kinds of radiation can generate stable primary and aggregate defects, known as color centers (CC) [1] in LiF crystals and thin films. Some of these CC are optically active and emit photoluminescence efficiently in the visible spectral range at RT, under optical pumping. The primary CC is the F one, which consists of an anionic vacancy occupied by an electron. Its absorption band is located at around 248 nm and up to now the photoluminescence originating from the F defect in LiF has not been detected unambiguosly. The aggregate centers F_2 and F_3^+ (two electrons bound to two and three anion vacancies, respectively) possess almost overlapping absorption bands, around 450 nm, generally called M band [2]; under optical pumping in this spectral region, at RT they emit broad photoluminescence bands peaked at 678 nm and 541 nm for F_2 and F_3^+ CC, respectively. Due to these properties, LiF is a radiation-sensitive dielectric material well-known in dosimetry [3] and utilized in optoelectronic devices [4-7].

2. Novel lithium fluoride imaging film detectors

In recent years the area of growth, characterization and coloration of LiF thin films has seen a considerable expansion [8]. Polycrystalline LiF films grown by thermal evaporation were proposed for gamma dosimetry [9], as nuclear sensors for neutrons [10,11] and as novel soft X-ray imaging detectors [12] based on F_2 and F_3^+ photoluminescence.
Recently the use of LiF thin films as innovative X-ray imaging detectors based on photoluminescence from optically active CC in LiF thin films [13] has been successfully extended to higher energies, up to 10 keV [14]. Their main peculiarities [12,14], which are intrinsic high spatial resolution on a large field of view, wide dynamic range, easiness of handling and versatility make a very powerful tool to reveal X radiation eventually emitted during low energy nuclear reactions (LENR)experiments.
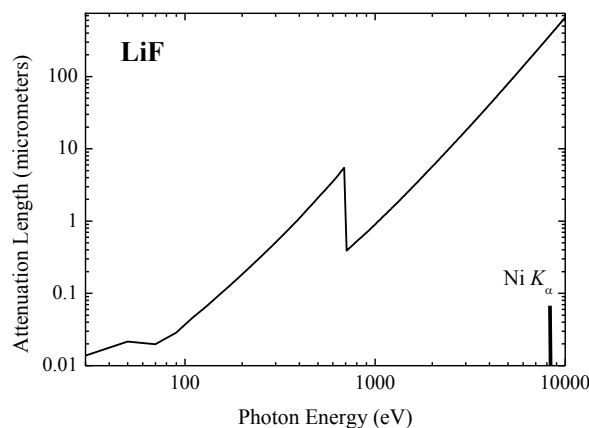
Fig. 1 – Attenuation length of X-rays in lithium fluoride as a function of their energy.

3. Experimental results and discussion

The electro-magnetic radiation interacts with the matter by three processes: photoelectric effect, Compton effect and electron-positron pair creation. Depending on X-rays energy, their penetration in LiF ranges from few tens of nanometers to several hundreds of micrometers; the deposited energy per unit length is constant in a certain material and the radiation intensity along the depth decreases as an exponential function, approximately. Figure 1 shows the attenuation length of X-rays in LiF as a function of their energy, below the Ni K_α edge (8.333 keV). The exposure to X-rays produces the stable formation of CC in LiF in layers of thickness comparable with their attenuation length.

Uniform thickness, good optical quality, polycrystalline LiF films of different thicknesses, from 0.1 to 4 μm, have been grown by thermal evaporation [8] on heated amorphous and crystalline substrates. The substrates were clamped to a rotating plate, controlled at fixed temperatures up to 350 °C during the deposition process. The starting material consists of LiF microcrystalline powder (Merck Suprapur, 99.99% pure), heated at about 800°C in a tantalum crucible, placed below the substrate at a distance of 22 cm, under a typical vacuum pressure below 5 10^{-6} mbar. The evaporation rate, monitored in situ by an INFICON quartz oscillator, was controlled at a fixed value of 1 nm/s during the growth. The total thickness of the deposited films was also directly measured by using a Tencor Alpha-Step 200 profilometer. The morphological analysis was performed by an Assing Perception Device Atomic Force Microscope (AFM) equipped with a Veeco MLCT-AUNM-10 tip operating in contact mode, maximum scan area of (25 x 25) μm^2 and a z-axis range of 5 μm. The estimated relative error for x, y and z axis is ~3%. Measurements are performed with a resolution of 257 x 257 points on xy plane (sample plane).

The structural, morphological and optical properties of the films grown on optically transparent amorphous substrates, like glass and silica, are dependent on the deposition parameters, in particular the substrate temperature, which influences the features of films of different thickness and the stable formation of primary and aggregate color centers [15].

Figure 2 shows the two-dimensional (2D) AFM image (5 x 5) μm^2 of the surface of a LiF thin film deposited by thermal evaporation on a glass substrate kept at 28 °C and of total thickness = 1.9 μm.
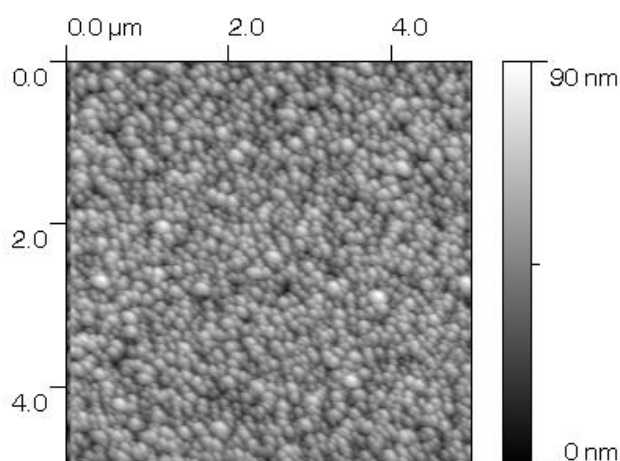
Fig. 2 – 2D AFM image of a LiF film, of thickness 1.9 μm, thermally evaporated on a glass substrate kept at 28 °C.

The images show a quite compact grain structure with regular and uniform grain size distribution; average grain size is about 10 nm and the Root Mean Square (RMS) roughness value compute from the image is 11 nm on the 5x5 μm^2 mapped area, which is comparable with the typical roughness of a thicker LiF film grown on glass microscope slides.

X-rays of energy higher than 2 eV are entirely absorbed by this film, as it can be deduced by the curve of Fig. 1, making it coloured along its full thickness. The CC produced in the LiF film by the X-rays exposition can be made visible by blue light excitation of the photoluminescence of the F_2 and F_3^+ defects, which emit in the red and green spectral regions, respectively.

The exposed LiF film is analyzed by using a Confocal Laser Scanning Microscope (CLSM) Nikon Eclipse C1-80i equipped with a coherent CW Argon laser operating at 458 nm. It allows to integrate, acquire and store the signature of the emitted radiation in a fluorescence image reaching a spatial resolution below 300 nm at the used wavelength. The same optical microscope was used in different optical operation modes, with white and blue light lamp illumination, in order to exclude and/or distinguish artifacts in the registered fluorescence image. The presented morphological investigation confirm the good surface quality of the LiF-film based detector.

3. Conclusions

Novel LiF-film based X-ray detectors were proposed, realized and characterized. These two-dimensional imaging detectors found application in photonics, biology, material science, device investigation and in the characterization of intense X-ray sources, including very short duration ones [16]. They allow great versatility, as they can grown in the form of thin films by well-assessed physical deposition techniques. The stored fluorescence images, based on the stable formation of aggregate electronic defects in the exposed areas, can be directly read without the need of any development procedure, which could introduce some artifacts. A good optical quality and a uniform surface of the deposited LiF film, which is the radiation-sensitive element in the X-ray detector, improve the quality of the images and reduces reading artifacts. Further studies are in progress on the LiF films growth on several substrates and their characterization in order to improve the optical quality and adhesion properties, as well as progress are under way in the full spectral analysis of the stored fluorescence images.

6. References

[1] W.B. Fowler, *Physics of Color Centers* (Academic Press, New York and London, 1968).
[2] J. Nahum, D.A. Wiegand: *Phys. Rev.* **154** 817 (1967).
[3] A.T. Davidson, A.G. Kozakiewicz, J.D. Comins, *J. Appl. Phys.* **82** 3722 (1997).
[4] V.V. Ter-Mikirtychev, T.T. Tsuboi, *Prog. Quant. Electr.* **20** 219 (1996).
[5] R.M. Montereali, A. Mancini, G.C. Righini, S. Pelli, *Opt. Commun.* **153** 223 (1998).
[6] A. Belarouci, F. Menchini, H. Rigneault, B. Jacquier, R.M. Montereali, F. Somma, P. Moretti, *Opt. Commun.* **189** 281 (2001).
[7] K. Kawamura, M. Hirano, T. Kurobori, D. Takamizu, H. Hosono, *Appl. Phys. Lett.* **84** 311 (2004).
[8] R.M. Montereali, *Handbook of Thin Film Materials*, edited by H.S. Nalwa, Vol. 3, Ch.7, Academic Press 2002.
[9] M. Montecchi, S. Baccaro, E. Nichelatti, F. Bonfigli, T. Marolo, R.M. Montereali, *Proceedings of the 7th ICATPP-7 Conference, Villa Olmo, Como, 2001*, edited by M. Barone, E. Borchi, J. Huston, C. Leroy, P.G. Rancoita, P. Riboni, R. Ruchiti, World Scientific, 819 (2002).
[10] F. Cosset, A. Celerier, B. Barelaud, J.C. Vareille, *Thin Solid Films* **303** 191 (1997).
[11] S. Almaviva, M. Marinelli, E. Milani, G. Prestopino, A. Tucciarone, C. Verona-Rinati, M. Angelone, D. Lattanzi, M. Pillon, R.M. Montereali, M.A. Vincenti, *J. Appl. Phys.* **103** 0545011 (2008).
[12] G. Baldacchini, F. Bonfigli, A. Faenov, F. Flora, R.M. Montereali, A. Pace, T. Pikuz, L. Reale, *J. Nanoscience and Nanotechnology* **3** (6) 483 (2003).
[13] ENEA Patent TO2002A000575, G. Baldacchini, F. Bonfigli, A. Faenov, F. Flora, R.M. Montereali, A. Pace, T. Pikuz, L. Reale, (International N°: WO 2004/005906°1).
[14] S. Almaviva, F. Bonfigli, I. Franzini, A. Lai, R.M. Montereali, D. Pelliccia, A. Cedola, S. Lagomarsino, *Appl. Phys. Lett.* **89** 54102 (2006).
[15] G. Baldacchini, M. Cremona, G. d'Auria, S. Martelli, R.M. Montereali, M. Montecchi, E. Burattini, A. Grilli, A. Raco, *Nuclear Instruments and Methods in Physics Research B* **116** 447 (1996).
[16] F. Calegari, S. Stagira, C. D'Andrea, G. Valentini, C. Vozzi C, M. Nisoli, S. De Silvestri, L. Paletto, P. Villoresi, A. Faenov, T. Pikuz, Appl. Phys. Lett. **89** 111122 (2006).

Arguments for dideuterium near monovacancies in PdD

Peter L. Hagelstein[1] **and Irfan U. Chaudhary**[2]
[1]*Research Laboratory of Electronics, MIT*
[2]University of Engineering and Technology, Lahore

E-mail: plh@mit.edu

Abstract. Molecular D_2 does not form in bulk PdD because the electron density sufficiently high so that antibonding orbitals are occupied. The electron density can be lower in the vicinity of a vacancy. We examine the possibility that sigma-bonded dideuterium can occur at the lowered electron density near a monovacancy in PdD.

1. Introduction

Excess heat has been observed in many Fleischmann-Pons experiments over the years, generally supporting the claims made by Fleischmann and Pons in 1989 [1,2]. The many negative results found in the early experiments of 1989 can be attributed in part to a lack of understanding of basic requirements that were clarified later on [3-5]. A remarkable feature of the effect is that a prodigious amount of energy is produced; much greater than can be attributed to chemical reactions (for which physical evidence is absent). The conjecture that the energy is due to a new nuclear process has historically been met with much skepticism, due to the absence of commensurate energetic particles which would be expected if nuclear reactions were responsible [6]. In a nuclear reaction, the energy produced is expressed as energetic particles as a consequence of local energy and momentum conservation. Excess energy produced in the Fleischmann-Pons experiment without commensurate energetic particles challenges long established ideas about how nuclei react, suggesting that there is a new kind of physical process in which nuclei interact in some new way in which the energy is expressed through other degrees of freedom.

We have described in earlier publications a new mechanism which is capable of coherent energy exchange between two-level systems and an oscillator under conditions where the transition energy of the two-level system is a great many times the characteristic energy of the oscillator [7,8]. This mechanism seems to be capable of converting an MeV-level nuclear energy quantum into a very large number of meV-level phonons under conditions relevant to the Fleischmann-Pons experiment. We have proposed a two-step reaction mechanism that involves first the transfer of excitation from the hindered D_2/^{4}He system to unhindered two-level systems which then convert the nuclear energy quantum to phonons using this new energy conversion mechanism. Under conditions where the excitation transfer step is the "bottleneck" which determines the overall rate for the two-step reaction, the reaction rate can be estimated from the associated excitation transfer matrix element. We have recently computed the nuclear part of this matrix element using a brute force numerical calculation, and we find that it is sufficiently large to account for the rate of excess heat production if the screening energy [9] is about 150 eV.

For the process consistent with our model to occur, molecular D_2 must be present in the lattice. In this respect, our model differs from other models which are currently more popular [10,11]. In our view, many practical aspects of the Fleischmann-Pons experiment and related experiments can be understood in terms of maximizing molecular D_2 inside the lattice. In this proceedings paper, we will focus on the issue of D_2 in PdD, which will focus our attention on issues related to the local electron density and vacancies.

2. Preferred electron density

Our arguments in this paper are based on the notion (from embedded atom theory [12-14]) that there exists a preferred electron density that deuterium or dideuterium wants to see, that is similar in molecular or solid state environments. If so, then we might use PdH as a reference for deuterium in Pd, and PdH_2 as

a reference for dideuterium in Pd.

In the case of PdH, we make use of the results of Balasubramanian et al [15] who give an atomic separation of 1.53 Angstroms. For PdH$_2$, we use the results of Balasubramanian et al [16], who give an a separation between the Pd atom and the center of the H$_2$ molecule to be 1.67 Angstroms. In this case, the two hydrogen atoms bond as a molecule with a separation of 0.81 Angstroms. To estimate the Pd electron density at 1.67 Angstroms for PdH$_2$, we performed a Dirac-Fock calculation for atomic Pd in the ground state (4d)^{10} configuration (which was found by Balasubramanian et al to be the dominant Pd configuration), and found the Pd electron density to be 0.0332 electrons/Angstrom^3 (see Figure 1). A similar computation for the Pd (4d)$^{9.35}$(5s)$^{0.65}$ configuration leads to an electron density at 1.53 Angstroms of 0.0686 electrons/Angstrom^3.
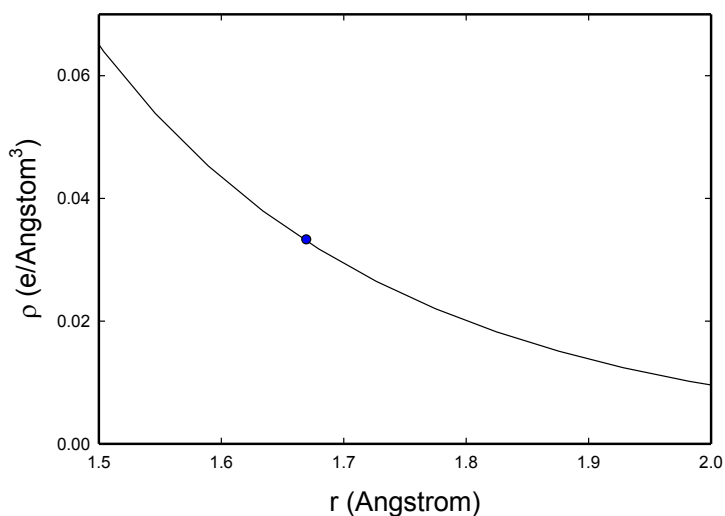
Fig. 1. – Electron density from a Dirac-Fock calculation of Pd (4d)^{10} configuration in the vicinity of 1.67 Angstroms relevant to the PdH$_2$ molecule.
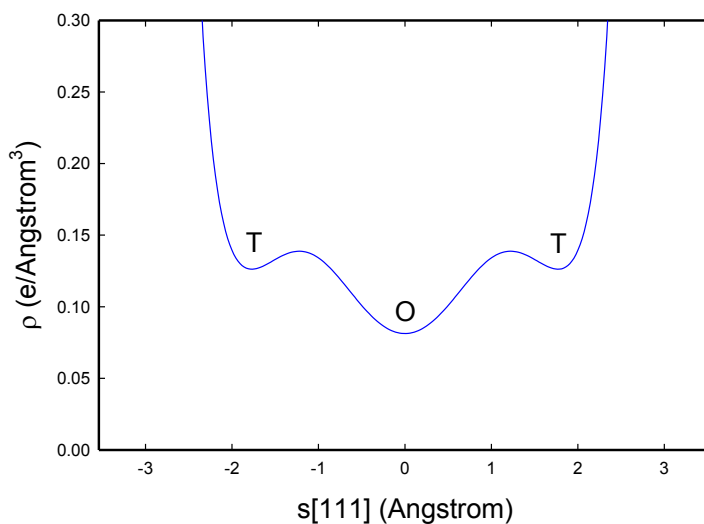
Fig. 2. – Model electron density due to Pd in the vicinity of an octahedral site in PdH.

3. Pd electron density in PdH

If we consider the electron density due to only the Pd atoms in PdH from a simple superposition of the atomic orbitals, we obtain the result for a scan centered at an octahedral site along the [111] direction shown in Figure 2. We see that the electron density is lowest at the octahedral site in this model, with a density of 0.081 electrons/Angstrom^3. The electron density in this model is significantly higher at the tetrahedral sites, indicating that one would expect hydrogen in PdH to occupy the octahedral sites since the Pd electron density at these sites is closer to the Pd electron density in molecular PdH.

A computation of H_2 in electron gas at an electron density of 9.3×10^{-3} electrons/a_0^3 was published by Christensen et al [17].   This electron density corresponds to 0.0628 electrons/Angstrom^3, and is reasonably close to the octahedral site electron density in PdH from above (0.081 electrons/Angstrom^3). The equilibrium distance between the two hydrogen atoms in this case is about 1.9 a_0, which is 1.005 Angstroms. This perhaps provides the closest connection to the discussion above. The electron density once again is higher than in the case of σ-bonded PdH_2, and the H_2 molecule responds by increasing its separation because of the occupation of antibonding states.

4. Electron density near a monovacancy in PdH

We next consider the electron density due Pd atoms near a monovacancy in PdH. In Figure 3 we show the Pd electron density from a simple superposition of Pd atomic orbitals, where the vacancy is indicated at -3.54 Angstroms, and where the along the [111] direction the electron density is equal to the preferred electron density of molecular H_2.
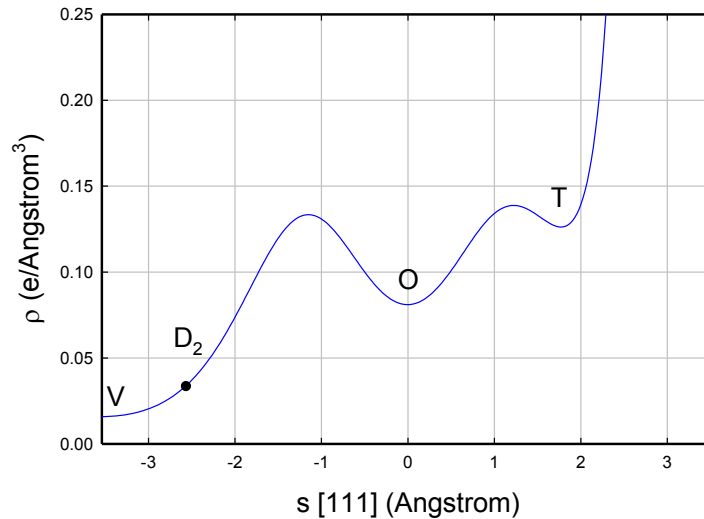
Fig. 3. – Model electron density due to Pd near a monovacancy in PdH.

We note that this model gives an electron density at the octahedral site location near the vacancy to be very close to the optimum for single H as judged by the PdH molecule. The calculation of Velikova et al [18] is consistent with a displacement of 0.26 Angstroms for single H occupation from the octahedral site location.

5. Statistical mechanics

To estimate the probability that a D_2 molecule is present in a monovacancy, we require a statistical model. Binding energies for single hydrogen atoms in octahedral sites have been estimated by several authors, including Nordlander et al [14] and Velikova et al [18]. The binding energies of Velikova et al are relative to hydrogen in solution at low concentration, which suggests that we need consistent models for deuterium in the bulk and trapped in vacancies. We begin with the bulk model, where the chemical potential can be related to the loading above the beta phase boundary through

$$\mu(x) - E_D(0) \ = \ k_B T \ln \frac{x}{1-x} + \Delta E + (x - 0.60) \frac{d\mu}{dx} \tag{1}$$

Here $E_D(0)$ is the deuterium binding energy in dilute PdD_x; the variable x is the D/Pd ratio; and ΔE is the binding energy at D/Pd = 0.60 minus the binding energy at D/Pd=0. We have used ΔE = -135 meV [19], and

$$\frac{d\mu}{dx} \ = \ 514 \ \frac{meV}{D} \tag{2}$$

This is consistent with the measurements of Chun and Ra [20].
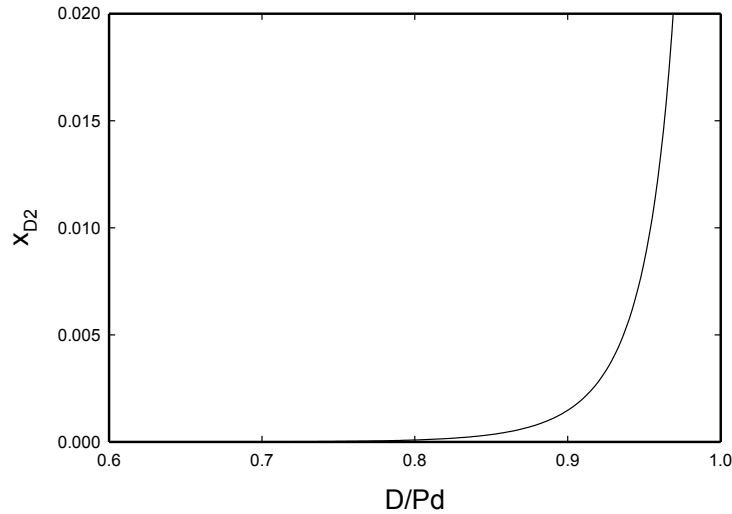
Fig. 4. – Model calclation of occupation of D_2 near monovacancies.

For the occupation of the octahedral sites in the vicinity of a vacancy, we can use a model based on

$$p_m \ = \ \frac{g_m e^{-(E_m - \mu m)/k_B T}}{\sum_n g_n e^{-(E_n - \mu n)/k_B T}} \tag{3}$$

For the degeneracy g_m, we have included the spin and statistical factors; for the energies E_m, we have used the results of Velikova et al [18]. From the computations in [18], we know that a dideuterium molecule is unstable in the presence of unoccupied octahedral sites in the vicinity of a monovacancy. So we have added the possibility of D_2 occupation only when there are 7 deuterons in the vicinity of the monovacancy. This is consistent with the computations of Liu et al for hydrogen in W [21]. In the

calculation of Velikova et al, the energy of the D_2 molecule is about 1 eV above deuterium atom occupation of the octahedral sites. Unfortunately, we do not as yet have a good number for the D_2 energy relative to bulk deuterium for $5D+D_2$ occupation around a monovacancy. In the computation shown in Figure 4, we have assumed that the additional D has to go up by 200 meV from $E_D(0)$ to make a D_2 molecule.

The amount of D_2 in this model increases with loading above a threshold near 0.85. We recall that the excess heat increases with loading above a threshold in much the same way. This is consistent with models that we have put forth which start with D_2 in the lattice as a prerequisite for the reactions which result in excess power and ^{4}He.

6. Conclusions

Excess heat in the Fleischmann-Pons experiment has been seen in a large number of experiments. At present there is no consensus among those in the field as to what physical mechanism is responsible. Our attention over the past decade has been focused on new reaction mechanisms which are driven by D_2 to ^{4}He transitions, with the energy converted into phonon excitation. For this reaction mechanism to work, we require D_2 to be present in the lattice, which is not an easy thing to happen if the lattice is PdD. Molecular D_2 cannot form in bulk PdD because the electron density is too high. According to the arguments here, D_2 can form near vacancies, and we have focused on the occurrence of D_2 near a monovacancy. Since the electron density due to Pd is reduced near the site of a missing Pd atom, the electron density in our simple models drops to levels at which D_2 normally binds to Pd.

We have been of the opinion for many years now that important aspects of the Fleischmann-Pons experiment can be understood simply if we are trying to maximize D_2 occupation. Since D_2 doesn't form in bulk PdD, and since there are very few vacancies initially in Pd, the cathodes start out with essentially no ability to host molecular D_2. So, according to the discussion above, we need to create vacancies. Vacancies are stabilized when Pd is highly loaded with deuterium [22-23]. Previously we estimated that a D/Pd loading of about 0.95 was required in order for the vacancies to become favored thermodynamically. However, since the diffusion coefficient for vacancies is so small near room temperature, vacancies have great difficulty diffusing in from nearby surfaces. Instead, it seems more probable that inadvertent codeposition of Pd on highly loaded Pd is responsible. This is consistent with observations of impurities below the outer surface of cathodes, and it is consistent with the very long time that cathodes need to remain loaded prior to observations of excess power. Codeposition has been verified as being able to produce superabundant vacancies [24]. The short onset time of excess power in the Szpak experiment is consistent with this point of view. Vacancies in this scenario would be created near the outer surface, so that only the near-surface region would be active. This is consistent with the observation of produce ^{4}He in the gas phase, which could not diffuse if created in the interior.

Once vacancies have been produced, then they need to be filled with molecular D_2. According to the model described above, this requires high loading above D/Pd of about 0.85. The correlation between loading and excess power has been observed in experiments [3], and the results are consistent if one assumes that the level of excess power production is correlated with D_2 occupancy. It remains to compute the D_2 binding energy in a monovacancy with 7 deuterium atoms present.

7. References

[1]   M. Fleischmann, S. Pons, M. Hawkins, *J. Electroanalytical Chem.* **261** 301 (1989); errata **263** 187 (1990).
[2]   M. Fleischmann, S. Pons, M.W. Anderson, L.J. Li, and M. Hawkins, *J. Electroanalytical Chem.* **287** 293 (1990).
[3]   M.C.H. McKubre, S. Crouch-Baker, A.M. Riley, S.I. Smedley, *Proceedings of ICCF3*, Nagoya, 1992, Nagoya, edited by H Ikegami, page 5 (Universal Academy Press, Tokyo, 1993).

[4] M.C.H. McKubre, S. Crouch-Baker, R.C. Rocha-Filho, S.I. Smedley, F.L. Tanzella, T.O. Passell, J. Santucci, *J Electroanal. Chem.* **368** 55 (1994).

[5] M.C.H. McKubre and F.L. Tanzella, Proceedings of ICCF12, Yokohama, edited by A Takahashi, K.-I. Ota, and Y Iwamura, page 392 (World Scientific, Singapore, 2005).

[6] J.R. Huizenga, Cold fusion, the fiasco of the century, (University of Rochester Press, Rochester NY, 1992).

[7] P.L. Hagelstein and I.U. Chaudhary, *Proceedings of ICCF14,* Washington, DC (in press).

[8] P.L. Hagelstein and I.U. Chaudhary, Low-energy nuclear reactions sourcebook, edited by J. Marwan and S. Krivit (Oxford University Press, 2008).

[9] F. Raiola, L. Gang, C. Bonomo, G. Gyurky, M. Aliotta, H.W.Becker, R. Bonetti, C. Broggini, P. Corvisiero, A. D'Onofrio, Z. Fulop, G. Gervino, L. Gialanella, M. Junker, P. Prati, V. Roca, C. Rolfs, M. Romano, E. Somorjai, F. Streider, F. Terrasi, G. Fiorentini, K. Langanke, and J. Winter, *Eur. Phys. J A* **19** 283 (2004).

[10] A. Takahashi, *J. Cond. Mat. Nucl. Sci.* **2** 33 (2009).

[11] Y.E. Kim, *Naturwissenschaften* **96** 803 (2009).

[12] N. Esbjerg and J.K. Norskov, *Phys. Rev. Lett.* **45** 807 (1980).

[13] M. Manninen, J.K. Norskov, and C. Umrigar, *J Phys. F: Metal Physics* **12** L7 (1982).

[14] P. Nordlander, J.K. Norskov, F. Besenbacher, S.M. Myers, *Phys. Rev. B* **40** 1990 (1989).

[15] K. Balasubramanian, P.Y. Feng, and M.Z. Liao, *J. Chem. Phys.* **87** 3981 (1987).

[16] K. Balasubramanian, P.Y. Feng, and M.Z. Liao, *J. Chem. Phys.* **88** 6955 (1988).

[17] O.B. Christensen, P.D. Ditlevsen, K.W. Jacobsen, P. Stolze, O.H. Nielsen, and J.K. Norskov, *Phys. Rev. B* **40** 1993 (1989).

[18] O.Yu. Velikova, D.I. Bazhanov, S.I. Simak, and I.A. Abrikosov, *Phys. Rev. B* **80** 024101 (2009).

[19] T. Kuji, W.A. Oates, B.S. Bowerman, and T.B. Flanagan, *J. Phys. F: Met. Phys.* **13** 1785 (1983).

[20] J. H. Chun and K. H. Ra, *J. Electrochem. Soc.* **145** 3794 (1998).

[21] Y.-L. Liu, Y. Zhang, H.-B. Zhou, G.-H. Lu, F. Liu, and G.-N. Luo, *Phys. Rev. B* **79** 172103 (2009).

[22] Y. Fukai, *J. Alloys and Compounds* **231** 35 (1995).

[23] Y. Fukai and H. Sugimoto, *J. Phys. Cond. Mat.* **19** 436201 (2007).

[24] Y. Fukai, M. Mizutani, S. Yokota, M. Kanazawa, Y. Miura, T. Watanabe, J. Alloys and Compounds **356-357** 270 (2003).

Bose-Einstein Condensation Nuclear Fusion: Theoretical Predictions and Experimental Tests

Yeong E. Kim

Purdue Nuclear and Many-Body Theory (PNMBT) Group, Department of Physics, Purdue University, West Lafayette, IN 47906, U.S.A.

e-mail: yekim@physics.purdue.edu

Abstract. It is shown that theory of Bose-Einstein condensation nuclear fusion (BECNF) [1] is capable of explaining many diverse experimental results of deuteron induced nuclear reactions in metals, observed in electrolysis and gas loading experiments. The theory is based on a single conventional physical concept of Bose-Einstein condensation of deuterons in metal and provides a consistent theoretical description of the experimental results. The theory also has predictive powers as expected for a quantitatively predictive physical theory. It is shown that the fusion energy transfer can be accomplished by the stopping power of metal without invoking hypothesis of fusion energy transfer to metal lattice vibrations. It is also shown that observed anomalous tritium production can be explained by incorporating a sub-threshold resonance reaction mechanism into the BECNF theory. The basic concept and important features of the BECNF theory is presented, and theoretical explanations of the experimental observations are described. Key experimental tests of theoretical predictions are proposed and discussed.

1. Introduction

Recently, it has been shown that the BECNF theory [1] can provide a consistent conventional theoretical explanation for anomalous results of deuteron induced nuclear reactions in metal at ultra low-energies [2-5]. Two decades ago, Fleischmann and Pons reported excess heat generation in electrolysis experiment using the negatively polarized Pd/D – D_2O system [2]. Since then, many others have reported experimental observations of excess heat generation and anomalous nuclear reactions occurring in metal at ultra low energies from electrolysis experiments [3] and gas-loading experiments [3-5]. These anomalous reaction rates cannot be explained using the conventional theory of nuclear reactions in free space, which predicts extremely low nuclear reaction rates at ultra low-energies ($\leq$ 10 eV) due to the Gamow factor arising from the Coulomb repulsion between two charged nuclei undergoing nuclear-reaction process.

The theory is capable of not only explaining most of the experimental observations, but also provides theoretical predictions which can be tested experimentally for the confirmation of the theory. A detailed description of the theoretical explanation, based on the theory of Bose-Einstein condensation nuclear fusion is presented along with suggested experimental tests of predictions of the theory and a discussion of the scalability of the fusion rates based on the theory.

2. Anomalous experimental results

The conventional deuterium fusion in free space proceeds via the following nuclear reactions:

{1} D + D → p (3.02 MeV) + T (1.01 MeV);
{2} D + D → n (2.45 MeV) + ^{3}He (0.82 MeV); and

{3} $D + D \rightarrow {}^4He + \gamma$ (23.8 MeV).
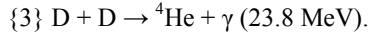
The cross-sections (or reaction rates) for reactions {1} and {2} have been measured by beam experiments at intermediate energies ($\geq$10 keV). The cross-sections for reaction {1} – {3} are expected to be extremely small at low energies ($\leq$ 10 eV) due to the Gamow factor arising from Coulomb barrier between two deuterons. The measured cross-sections have branching ratios: $(\sigma\{1\}, \sigma\{2\}, \sigma\{3\}) \approx (1, 1, 10^{-6})$.

From many experimental measurements by Fleischmann and Pons [2], and many others [3-5] over 20 years since then, the following experimental results have emerged. At ambient temperatures or low energies ($\leq$ 10 eV), deuterium fusion in metal proceeds via the following reactions:

{4} $D(m) + D(m) \rightarrow p(m) + T(m) + 4.03$ MeV (m);
{5} $D(m) + D(m) \rightarrow n(m) + {}^3He(m) + 3.27$ MeV (m); and
{6} $D(m) + D(m) \rightarrow {}^4He(m) + 23.85$ MeV (m),

where m represents a host metal lattice or metal particle. Reaction rate R for {6} is dominant over reaction rates for {4} and {5}, i.e., R{6} >> R{4} and R{6} >> R{5}.

Experimental observations reported from electrolysis and gas-loading experiments are summarized below (not complete):

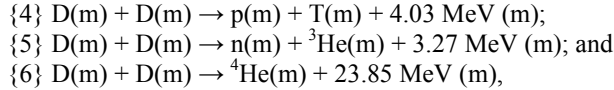[1] The Coulomb barrier between two deuterons are suppressed
[2] Excess heat production (the amount of excess heat indicates its nuclear origin)
[3] ${}^4He$ production commensurate with excess heat production, no 23.85 MeV γ ray
[4] More tritium is produced than neutron R{4} >> R{5}
[5] Production of nuclear ashes with anomalous rates: R{4} << R {6} and R {5} << R{6}
[6] Production of hot spots and micro-scale craters on metal surface
[7] Detection of radiations
[8] "Heat-after-death"
[9] Requirement of deuteron mobility (D/Pd > ~0.9, electric current, pressure gradient, etc.)
[10] Requirement of deuterium purity (H/D << 1)

All of the above experimental observations are explained in terms of theory of Bose-Einstein condensation nuclear fusion (BECNF) in the previous publication [1] and this paper. In this paper, additional theoretical explanations are provided for the **observations [1]** through **[4]** in sections 5 and 6. Theoretical explanations of other observations such as "Heat-after-death" [6] have been described in [1].

3. Bose-Einstein condensation (BEC) of deuterons in metals

Development of Bose-Einstein condensate theory of deuteron fusion in metal is based upon a single hypothesis that deuterons in metal are mobile and hence are capable of forming Bose-Einstein condensates.

Experimental proof of proton (deuteron) mobility in metals was first demonstrated by Coehn in his hydrogen electro-migration experiment [7,8]. The significance of Coehn's experimental results [7] is emphasized by Bartolomeo et al. [9]. A theoretical explanation of Coehn's results [7] is given by Isenberg [10]. The Coehn's experimental fact is not well known in review articles and textbooks. There are other experimental evidences [11-15] that heating and/or applying an electric field in a metal causes hydrogen or deuteron in a metal to become mobile, thus leading to a higher density for quasi-free mobile deuterons in a metal.

BEC condensate fraction $F(T) = N_{BE}/N$ of deuterons in a metal satisfying BEC condition can be estimated as a function of the temperature and using either Bose-Einstein or Maxwell-Boltzmann distribution function. N is the total number of deuterons and N_{BE} is the number of deuterons satisfying the BEC requirement $\lambda_c > d$ where λ_c is the de Broglie wavelength and d is the average distance between two deuterons. For d = 2.5 Å, we obtain F (T=300° K) $\approx$ 0.084 (8.4 %), F (T = 77.3° K) $\approx$ 0.44 (44%), and F(T = 20.3° K) $\approx$ 0.94 (94%). At T = 300° K, F = 0.084 (8.4%) is not large enough to form BEC since motions of deuterons are limited to several lattice sites and the probability of their encounters are very small. On the other hand, at liquid nitrogen (77.3° K) and liquid hydrogen (20.3° K) temperatures, probability of forming BEC of deuterons is expected to be $\Omega \approx 1$. This suggests that experiments at these low temperatures can provide tests for enhancement of the reaction rate R_t, Eq. (4) described below, as predicted by BECNF theory.

4. Bose-Einstein condensation theory of deuteron fusion in metal

N-body Schroedinger equation for the system is given by

$$H\Psi = E\Psi \tag{1}$$

with the Hamiltonian H for the system given by

$$H = \frac{\hbar^2}{2m}\sum_{i=1}^{N}\Delta_i + \frac{1}{2}m\omega^2\sum_{i=1}^{N}r_i^2 + \sum_{i<j}\frac{e^2}{|\mathbf{r}_i - \mathbf{r}_j|} \tag{2}$$

where m is the rest mass of the nucleus. Only two-body interactions (Coulomb and nuclear forces) are considered since we expect that three-body interactions are expected to be much weaker than the two-body interactions.

The approximate ground-state solution of Eq. (1) with H given by Eq. (2) is obtained using the equivalent linear two-body method [16,17]. The use of an alternative method based on the mean-field theory for bosons yields the same result (see Appendix in [18]). Based on the optical theorem formulation of low energy nuclear reactions [19], the ground-state solution is used to derive the approximate theoretical formula for the deuteron-deuteron fusion rate in an ion trap (micro/nano-scale metal grain or particle). The detailed derivations are given elsewhere [18,20].

Our final theoretical formula for the nuclear fusion rate R_{trap} for a single trap containing N deuterons is given by [1]

$$R_{trap} = 4(3/4\pi)^{3/2}\Omega A\frac{N^2}{D_{trap}^3} \propto \Omega\frac{N^2}{D_{trap}^3} \tag{3}$$

where N is the average number of Bose nuclei in a trap/cluster, D_{trap} is the average diameter of the trap, A= $2Sr_B/(\pi\hbar)$, $r_B=\hbar^2/(2\mu e^2)$, and S is the S-factor for the nuclear fusion reaction between two deuterons. For D(d,p)T and D(d,n)^{3}He reactions, we have S ≈ 55 keV-barn. We expect also S ≈ 55 keV-barn or larger for reaction {6}. A = S × (1.4×10^{-18}) cm^3/s with S in units of keV-barn. A = 0.77 × 10^{-16} cm^3/s for S = 55 keV-barn. Only one unknown parameter is the probability of the BEC ground state occupation, Ω.

The total fusion rate R_t is given by

$$R_t = N_{trap}R_{trap} = \frac{N_D}{N}R_{trap} \propto \Omega\frac{N}{D_{trap}^3} \tag{4}$$

where N_D is the total number of deuterons and $N_{trap} = N_D/N$ is the total number of traps.

Eq. (4) shows that the total fusion rates, R_t, are very large if $\Omega \approx 1$.

Eqs. (3) and (4) provide an important result that nuclear fusion rates R_{trap} and R_t do not depend on the Gamow factor in contrast to the conventional theory for nuclear fusion in free space. This could provide explanations for overcoming the Coulomb barrier and for the claimed anomalous effects for low-energy nuclear reactions in metals. This is consistent with the conjecture noted by Dirac [21] and used by Bogolubov [22] that boson creation and annihilation operators can be treated simply as numbers when the ground state occupation number is large. This implies that for large N each charged boson behaves as an independent particle in a common average background potential and the Coulomb interaction between two charged bosons is suppressed. This provides an explanation for the **observation [1]**.

5. Theoretical explanation of anomalous ^{4}He production (**the observations [2]** and **[3]**)

For a single trap (or metal particle) containing N deuterons, the deuteron-deuteron fusion can proceed with the following two reaction channels:

$\{6\}$ $\psi_{\text{BEC}}\{(N-2)\,D's+(D+D)\} \rightarrow \psi *\{^{4}He+(N-2)\,D's\}$ $(Q = 23.85\,\text{MeV})$, $\qquad\qquad$ (5)

and

$\{7\}$ $\psi_{\text{BEC}}\{(N-2)\,D's+(D+D)\} \rightarrow \psi *\{^{4}He^{*}+(N-2)\,D's\}$ $(Q = 3.64\,\text{MeV})$ $\qquad\qquad$ (6)

where ψ_{BEC} is the Bose-Einstein condensate ground state (a coherent quantum state) with N deuterons and $\psi*$ are final excited continuum states. ^{4}He in Eq. (5) represents the ground state with spin-parity, 0^{+}, while ^{4}He* in Eq. (6) represents the 0^{+} excited state at 20.21 MeV above the ^{4}He ground state [23]. Excess energy (Q value) is absorbed by the BEC state and shared by (N-2) deuterons and reaction products in the final state. It is important to note that reactions $\{6\}$ and $\{7\}$, described by Eqs. (5) and (6), cannot occur in free-space due to the momentum conservation.

For micro/nano-scale metal particles, the above consideration shows that excess energies (Q) lead to a micro/nano-scale fire-work type explosion, creating a crater/cavity and a hot spot with fire-work like star tracks. The size of a crater/cavity will depend on number of neighboring Pd nanoparticles participating in BEC fusion almost simultaneously. Hot spots and craters have been observed in experiments reported by Srinivasan et al. [24] and others.

We now consider the total momentum conservation for reaction $\{6\}$ with the reaction channel Eq. (5). The initial total momentum of the initial BEC state with N deuterons (denoted as D^{N}) is given by $\vec{P}_{D^{N}} \approx 0$. Because of the total momentum conservation, the final total momenta for reaction $\{6\}$ is given by

$\{6\}$ $\vec{P}_{D^{N-2}\,^{4}He} \approx 0,\ \langle T_{D} \rangle \approx \langle T_{^{4}He} \rangle \approx Q\{6\}\,/\,N$

where T represents the kinetic energy.

For the reaction $\{6\}$ with Eq. (5), the average kinetic energy for each deuteron is T = Q$\{6\}$/N = 23.85 MeV/N. For the case of 5 nm Pd trap, the number of deuterons in the trap is N = $\sim$ 4450, and T $\approx$ 5.36 keV. With this deuteron kinetic energy of $\sim$ 5.36 keV, a question arises whether the hot-fusion reactions $\{1\}$ and $\{2\}$ can occur as the secondary reactions to the primary reaction $\{6\}$. Since the secondary reactions $\{1\}$ and $\{2\}$ have not been observed, there have been speculations such as a hypothesis that the fusion energy of 23.85 MeV is transferred to lattice vibrations thus producing heat in metal. In the following, a more convincing alternative explanation is described to show that transfer of the fusion energy of 23.85 MeV to the metal can be accomplished by the energy loss of energetic (5.36 keV) deuteron due to the stopping power of the metal.

Experimental values of the conventional hot-fusion cross section σ(E) for reaction $\{1\}$ or $\{2\}$ have been conventionally parameterized as [25]

$$\sigma(E) = \frac{S(E)}{E}\exp\left[-\left(E_{G}\,/\,E\right)^{1/2}\right],$$ $\qquad\qquad$ (7)

where E_{G} is the "Gamow energy" given by $E_{G} = \left(2\pi\alpha Z_{D}Z_{D}\right)^{2} Mc^{2}\,/\,2$ or $E_{G}^{1/2} \approx 31.39(\text{keV})^{1/2}$ for the reduced mass $M \approx M_{D}/2$ for reactions $\{1\}$ or $\{2\}$. The S factor, S(E), is extracted from experimentally measured values [26] of the cross section σ(E) for E $\geq$ 4 keV and is nearly constant [27]; S(E) $\approx$ 52.9 keV - b, for reactions $\{1\}$ or $\{2\}$. The probability P(E_{i}) for a deuteron to undergo the conventional hot-fusion reaction $\{1\}$ or $\{2\}$ while slowing down in the deuterated palladium metal can be written as [28]

$$P(E_{i}) = 1 - \exp\left[\int dx n_{D}\sigma\left(E_{DD}\right)\right] \approx \int dx n_{D}\sigma\left(E_{DD}\right)$$
$$= n_{D}\int_{0}^{E_{i}} dE_{D}\frac{1}{\left|dE_{D}\,/\,dx\right|}\sigma\left(E_{DD}\right).$$ $\qquad\qquad$ (8)

The stopping power [29] for deuterium in PdD for $E_{D} \leq$ 20 keV is given by [28]

$$\frac{dE_{D}}{dx} = 3.1\times10^{5}\sqrt{E_{D}}\ \text{keV}\,/\,\text{cm},$$ $\qquad\qquad$ (9)

for $n_{Pd} = 6.767 \times 10^{22}$ cm^{-3} and $n_D = n_{Pd}$. If we use Eq. (9) and the conventional extrapolation formula for $\sigma(E)$ given by Eq. (7), the integration in Eq. (8) can be performed analytically to yield the following expression for Eq. (8)[27]:

$$P(E_i) = 1.04 \times 10^{-6} \exp\left(-44.40 / \sqrt{E_i}\right), \tag{10}$$

where E_i is in keV (LAB), for reactions {1} or {2} assuming equal branching ratios (50% each).

For the case of 5 nm diameter Pd particle containing ~ 4450 deuterons, $E_i = 5.36$ keV, and Eq. (10) yields P (5.36 keV) ≈ 0.49 x 10^{-14} per deuteron. Therefore, the total fusion probability for 4450 deuterons is P_{total} ≈ 2.2 x 10^{-11}, yielding a branching ratio of R{1}/R{6} ≈ R{2}/R{6} ≈ 10^{-11}. Tritium and neutron production from primary reactions R{1} and R{2} are shown to be both negligible due to a selection rule [1].. Even for the case of E_i ≈ 20 keV with a 3.2 nm Pd particle containing ~ 1200 deuterons, P (20 keV) ≈ 0.5 x 10^{-10}, and the total fusion probability is P_{total}(20 keV) ≈ 0.6 x 10^{-7}. Therefore, the fusion energy of 23.85 MeV from {6} is transferred to the metal by the stopping power of the metal without appreciable production of T and n from secondary reactions {1} and {2}.

6. Theoretical explanation of anomalous tritium production (the observation [4])

There have been many reports of anomalous tritium and neutron production in deuterated metal from electrolysis experiments [30-34] and gas/plasma loading experiments [24, 35-40]. The reported branching ratio of R(T)/R(n) ranges from 10^8 to 10^9 in contrast to the conventional free-space reactions branching ratio of R{1}/R{2} ≈ 1. In this section, we present a theoretical explanation of this anomalous tritium production based on the BECNF theory, using a new energy level scale which sets E = 0 for (D + D) state, and E = − 23.85MeV for the ^{4}He ground state. Q-value remains same since $Q = E_i − E_f$.

The reaction {7}, described by Eq. (6), can proceed via a sub-threshold resonance reaction [41,42]. The S-factor for the sub-threshold resonance reaction can be extracted from the cross-section given by Breit-Wigner expression [41,42], and given by

$$S(E) = \frac{\pi^2 \hbar^4}{4\mu^2 R_n^2} \frac{1}{K_1^2(x)} w\theta_o^2 \frac{\Gamma_2}{\left(E - E_R\right)^2 + (\Gamma/2)^2}, \tag{11}$$

where μ is the reduced mass in units of atomic mass unit (931.494 MeV), R_n is the nuclear radius, and w is the statistical factor. $K_1(x)$ is the modified Bessel function of order unity with argument $x = (8Z_1 Z_2 e^2 R_n \mu/\hbar^2)^{1/2}$. Γ_2 is a partial decay width and Γ is the total decay width to the final states. If E is measured from the threshold energy E = 0 of (D + D) state, we have E_R = (20.21 MeV − 23.85 MeV) = − 3.64 MeV. Eq. (11) shows that the S(E) factor has a finite value at E = 0 and drops off rapidly with increasing energy E. θ_i^2 is the reduced width of a nuclear state, representing the probability of finding the excited state in the configuration i, and the sum of θ_i^2 over i is normalized to 1. The dimensionless number θ_i^2 is generally determined experimentally and contains the nuclear structure information.

For the entrance channel, D + D → ^{4}He*(0$^+$, 20.21 MeV), there are two possible decay channels:

{7a} ^{4}He*(0$^+$, 20.21 MeV) → T (0.1 MeV) + p (0.3 MeV)

{7b} ^{4}He*(0$^+$, 20.21 MeV) → ^{4}He (0$^+$, 0.0 MeV ground state)
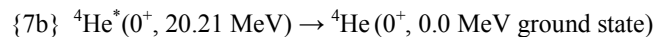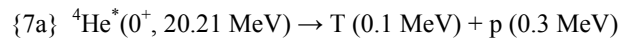
Once S(E) factors are calculated from Eq. (11), it can be used in Eqs. (3) and (4) to obtain the total reaction rate. In the following, S(E) factors are estimated for the decay channels, {7a} and {7b}, using Eq. (11).

For the decay channel {7a}, $\Gamma_2 = \Gamma_a = 0.5$ MeV [23]. When this value of Γ_2 is combining with other appropriate inputs in Eq. (11), the extracted S-factor for the decay channel {7a} is S{7a} ≈ 1.4 x 10^2 θ_0^2 keV − b for E ≈ 0. In reference [1], it was shown that R{5} << R{6} due to a selection rule. Since (^{3}He + n) state at 20.58 MeV

is higher than $^4He^*$ state at 20.21 MeV, and Γ_2 ($^3He + n$) = 0 MeV [23], this value of S{7a} may provide an explanation of the reported branching ratio of R(T)/R(n) $\approx 10^8 \sim 10^9$ [24, 30-40].

From section 5, we have theoretical prediction that R{2}/R{6} or (i) R(n)/R(^4He) $\approx 10^{-11}$. From this section, we have the above theoretical prediction of R{7a}/R{6} $\approx 2.6 \; \theta_0^2$ or (ii) R(T)/R(^4He) $\approx 2.6 \; \theta_0^2$. Combining (i) and (ii), we have R(T)/R(n) $\approx 2.6 \times 10^{11} \; \theta_0^2$. If $\theta_0^2 \approx 10^{-4}$, we have R(T)/R(n) $\approx 10^7$ which is nearly consistent with reported values of $10^8 \sim 10^9$. If we assume S{ 6} $\approx$ 55 keV-b (this could be much larger), we expect the branching ratio R{7a}/R{6}= R(T)/R(^4He) $\approx 2.6 \; \theta_0^2 \approx 2.6 \times 10^{-4}$ if $\theta_0^2 \approx 10^{-4}$. Experimental measurements of R(T)/R(^4He) are needed to determine θ_0^2. If S{6} (=S(^4He)) is determined to be larger from future experiments, R(T)/R(^4He) is reduced accordingly.

For the decay channel {7b} ($0^+ \rightarrow 0^+$ transition), γ-ray transition is forbidden. However, the transition can proceed via the internal e^+e^- pair conversion. The transition rate for the internal electron pair conversion is given by

$$\omega = \frac{1}{135\pi}\left(\frac{e^2}{\hbar c}\right)^2 \frac{\gamma^5}{\hbar^5 c^4} R_N^4, \quad R_N^2 = |< \psi_{exc}, \sum_i r_i^2 \psi_{norm} >|. \tag{12}$$

where γ is the transition energy. Eq. (12) was derived by Oppenheimer and Schwinger [43] in 1939 for their theoretical investigation of $0^+ \rightarrow 0^+$ transition in ^{16}O. The rate for the internal electron conversion is much smaller by many order-of-magnitude.

For our case of $0^+ \rightarrow 0^+$ transition {7b}, we obtain $\omega \approx 0.79 \times 10^{13}$/sec, and $\Gamma_b = \hbar\omega \approx 0.52 \times 10^{-2}$ eV using appropriate inputs in Eq. (12). Using $\Gamma_2 = \Gamma_b = 0.52 \times 10^{-2}$ eV in Eq. (11), the extracted S-factor for decay channel {7b} is obtained as S{7b} $\approx 1.5 \times 10^{-6} \; \theta_0^2$ keV - b for E $\approx$ 0, which in turn yields a branching ratio, R{7b}/R{7a} = S{7b}/S{7a} $\approx 10^{-8}$. Experiments are needed for testing this predicted branching ratio.

7. Proposed experimental tests of theoretical predictions

7.1 Experimental test for metal particle size

The recent report of deuteron gas-loading experiment by Arata and Zhang [4] show positive results of observing excess heat and ^4He production using ~ 5 nm Pd particles imbedded in ZrO_2 and purified deuterium. The recent experimental results by Kitamura et al. [5] using ~ 10 nm Pd particles have confirmed the results of Arata Zhang [4], and also is consistent with one of theoretical predictions of the BECNF theory [1]. The theoretical prediction is that the reaction rate for smaller Palladium particles is expected to be greater than the reaction rate for larger Palladium particles, R(smaller Pd) > R(larger Pd). Their Fig. 3(a) and Fig. 3(c) confirm the above prediction. Their data in Fig. 3(c) are also consistent with the requirement of deuteron mobility in metal (the **observation [9]**).

7.2 Experimental test for anomalous tritium production

For experimental tests of the sub-threshold resonance reaction described in section 6, it is desirable to carry out high-sensitivity detection of weak signals (i) of Bremsstrahlung radiations from energetic electrons going through metal and (ii) of 0.51 MeV γ-rays from e^+e^- annihilation, as well as (iii) ^4He production during tritium production experiments to test the predicted branching ratio R{7b}/R{7a}$\approx 10^{-8}$, and also to determine the branching ratio R{7a}/R{6} (= R(T)/R(^4He)) which in turn can provide information on θ_0^2 for S{7a} and also S(E) for {6}.

7.3 Experimental test for fusion–rate enhancement at low temperatures

As discussed in section 3, the BEC fraction and the probability Ω of the BEC ground-state occupation will increase at lower temperatures. This increase of Ω will enhance the total fusion rate R_t, Eq. (4). This prediction can

be tested by carrying out experiments at low temperatures. For an example, thermal cycling experiment [24] should be repeated with micro/nano-scale titanium particles.

7.4 Experimental test for fusion-rate enhancement at high pressures

High pressures will shorten the average distance between two deuterons in metal, thus enhancing the BEC fraction and hence Ω. This enhances the total fusion rates R_t, Eq. (4). This prediction can be tested by carrying out experiments at high pressures.

7.5 Experimental tests of Bose-Einstein condensation of deuterons in metal

BECNF theory is based on one single physical hypothesis that mobile deuterons in a metal/grain/particle form Bose-Einstein condensate. Therefore, it is important to explore experimental tests of this basic hypothesis.

One of the advantages of carrying out experiments for observing the BEC of deuterons in micro/nano-scale metal particles is that the modern nano-fabrication techniques allow us to fabricate them in multitude with a great precision in one-dimension, two-dimension, and three-dimension. This capability will allow us to produce the BEC of deuterons in metal (i) in a double-well potential trapping two Bose-Einstein condensates for studying the Josephson effect [44], and also (ii) in lower-dimensional traps to study the BEC in one-dimension and two-dimension.

8. Summary and conclusions

Based on a single physical concept of Bose-Einstein condensation of deuterons in metal, theory of Bose-Einstein condensation nuclear fusion (BECNF) is developed to explain deuteron-induced nuclear reactions observed in metal. It is shown that the BECNF theory is capable of explaining qualitatively or quantitatively almost all of ten experimental observations (listed in section 2) reported from electrolysis and gas-loading experiments.

It is shown that the fusion energy transfer to metal can be accomplished by the stopping power of metal without invoking hypothesis of fusion energy transfer to metal lattice vibrations. It is also shown that observed anomalous tritium production can be explained by incorporating a sub-threshold resonance reaction mechanism into the BECNF theory

The BECNF theory has also predictive powers as expected for a quantitatively predictive physical theory. Experimental tests of theoretical predictions are proposed and discussed, including tests of the basic hypothesis of Bose-Einstein condensation of deuterons in metal. Experimental tests are needed not only to test theoretical predictions, but also to improve and/or refine the theory, which are needed for designing reproducible experiments and for scaling up BECNF processes for potential practical applications.

9. References

[1] Y. E. Kim, "Theory of Bose-Einstein Condensation Mechanism for Deuteron-Induced Nuclear Reactions in Micro/Nano-Scale Metal Grains and Particles", Naturwissenschaften **96**, 803 (2009) and references therein.
[2] M. Fleischman and S. Pons, "Elecytrichemically Induced Nuclear Fusion of Deuterium", J. Electroanal. Chem. **261**, 301 (1989); Errata, J. Electroanal. Chem. **263**, 187 (1989).
[3] P.L. Hagelstein, et al., "New Physical Effects in Metal Deuterides", Proceedings of ICCF-11, Marseille, France, *Condensed Matter Nuclear Science,* pp. 23-59, World Scientific Publishing Co., Singapore (2006) and references therein.
[4] Y. Arata and Y.C. Zhang, J. High Temp. Soc **34** (2), 85 (2008).
[5] A. Kitamura, et al., Phys. Lett. A**373**, 3109 (2009), and references therein.
[6] S. Pons and M. Fleischmann, "Heat After Death", Transactions of Fusion Technology **26**, 8(Dec.1994).

[7]   A. Coehn, "Proof of the existence of protons in metals (with discussion)", Z. Electrochem. **35,** 676-680 (1929).

[8]   A. Coehn and W. Specht, "Ueber die Beteiligung von Protonen an der Elektrizitaetsleitung in Metallen (Role of protons in electric conductivity of metals)", Z. Phys. **83**, 1-31 (1930).

[9]   C. Bartolomeo, et al., "Alfred Coehn and After: The α, β, γ of the Palladium-Hydrogen System", Transactions of Fusion Technology **26,** 23 (Dec. 1994).

[10] I. Isenberg, "The ionization of hydrogen in metals", Phys. Rev. **79**, 736 (1950).

[11] B. Duhm, "Diffusion of hydrogen in palladium", Z. Phys. **94**, 435-456 (1935).

[12] Q.M. Barer, *Diffusion in and through Solids,* Cambridge University Press, New York, NY (1941).

[13] J.F. Macheche, J.-C. Rat, and A. Herold, "Study of hydrogen-metal systems: Potential induced by the diffusion of hydrogen in palladium", J. Chim. Phys. Phys. Chim. Biol. **73**, 983-987 (1976).

[14] F.A. Lewis, "Palladium-Hydrogen System 2, Platinum Met. Rev. **26**, 20-27, 70-78, 121-128 (1982).

[15] Y. Fukai, *The Metal-Hydrogen System.* Second Edition, Springer Berlin Heidelberg New York (2005).

[16] Y.E. Kim and A.L.Zubarev, "Ground state of charged bosons confined in a harmonic trap," Physical Review A **64**, 013603-1 (2001).

[17] Y.E. Kim and A.L.Zubarev, "Equivalent linear two-body method for Bose-Einstein condensates in time-dependent harmonic traps", Physical Review A **66**, 053602-1 (2002).

[18] Y.E. Kim and A.L. Zubarev, "Ultra low-energy nuclear fusion of Bose nuclei in nano-scale ion traps", Italian Physical Society Proceedings **70**, 375 (2000).

[19] Y.E. Kim. Y.J. Kim, A.L. Zubarev and J.H. Yoon, "Optical Theorem Formulation of Low-Energy Nuclear Reactions", Physical Review C **55**, 801 (1997).

[20] Y.E. Kim and A.L.Zubarev, "Nuclear Fusion for Bose Nuclei Confined in Ion Traps", Fusion Technology **37**, 151(2000).

[21] P.A.M. Dirac, *The Principles of Quantum Mechanics.* second edition, Clarendon Press, Oxford Chapter XI, Section 62 (1935).

[22] N. Bogolubov, "On the Theory of Superfluidity", Journal of Physics 11:23-29 (1966).

[23] D.R. Tilley, H.R. Weller, and G.M. Hale, "Energy level of light nuclei A=4", Nuclear Physics **A541**, 1 (1992).

[24] M. Srinivasan et al., "Observation of tritium in gas/plasma loaded titanium samples", AIP Conference Proceedings **228**, 514 (1990).

[25] W.A. Fowler, G.R. Caughlan, and B.A. Zimmermann, "Thermonuclear Reactions Rates," Annu. Rev. Astron. Astrophys., 5, 525 (1967); see also "Thermonuclear Reaction Rates II," Annu. Rev. Astron. Astrophys., 13, 69 (1975).

[26] A. von Engel and C.C. Goodyear, "Fusion Cross-Section Measurements with Deuterons of Low Energies," Proc. R. Soc. A, **264**, 445 (1961).

[27] A. Krauss, H.W. Becker, H.P. Trautvetter, and C. Rolfs, "Low Energy Fusion Cross-Sections of D + D and D + ^{3}He Reactions," Nucl. Phys., **465**, 150 (1987).

[28] Y.E. Kim, "Surface Reaction Mechanism for Deuterium-Deuterium Fusion with a Gas/Solid-State Fusion Device", Fusion Technology **19,** 558-566 (1990); AIP Conference Proceedings **228**, 807 (1990).

[29] H.H. Anderson and J.F. Ziegler, *Hydrogen Stopping Powers and Ranges in All Elements,* Pergamon Press, New York (1977).

[30] E. Storm and C. Talcott, "Electrolytic Tritium Production", Fusion Technology **17**, 680 (1990).

[31] K. Cedzynska, S.C. Barrowes, H.E. Bergeson, L.C. Knight, and F.W. Will, "Tritium Analysis in Palladium With an Open System Analytical Procedure", Fusion Technology **20,** 108 (1991).

[32] F.G. Will, K. Cedzynska, D.C. Linton, "Reproducible Tritium Generation in Electrochemical-Cells Employing Palladium Cathodes with High Deuterium loading", Journal of Electroanalytical Chemistry **360**, 161 (1993).

[33] F.G. Will, K. Cedzynska, and D.C. Linton, "Tritium Generation in Palladium Cathodes with High Deuterium Loading", Transactions of Fusion Technology **26,** 209 (Dec. 1994).

[34] J.O'M. Bockris, et al., "Tritium and Helium Production in Palladium Electrodes and the Fugacity of Deuterium Therein", Proceedings of the Third International Conference on Cold Fusion., October 21-25 Nagoya Japan., Ed. H. Ikegami, Universal Academy Press Tokyo Japan., 23 (1993).

[35] A. DeNinno, et al., "Emission of Neutrons as a Consequence of Titanium-Deuterium Interaction", II Nuovo Cimento, **101A** 841 (1989).

[36] T.N. Claytor, et al., "Tritium and Neutron Measurements from a Solid-State Cell", LA-UR-89-3946, October 1989, Presented at the NSF-EPRI workshop.

[37] T.N. Claytor, D.G. Tuggle, H.O. Menlove, P.A. Seeger, W.R. Doty and R.K. Rohwer, "Tritium and Neutron Measurements from Deuterated Pd-Si", AIP Conference Proceedings **228** (1990).

[38] T.N. Claytor, D.G. Tuggle, and S.F. Taylor, "Evolution of Tritium from Deuterided Palladium Subject to High Electrical Currents", Proceedings of the Third International Conference on Cold Fusion., October 21-25 Nagoya Japan., Universal Academy Press Tokyo Japan., 217 (1993).

[39] T.N. Claytor, D.G. Tuggle, and S.F. Taylor, "Tritium Evolution from Various Morphologies of Deuterided Palladium", Proceedings of the Fourth International Conferences on Cold Fusion, December 6-9, 1993, Maui, Hawaii, Ed. T.O. Passel, EPRI-TR-104188-V1 Project 3170, Vol 1 7-2 (1994).

[40] T.N. Claytor et al., "Tritium Production from Palladium Alloys", Proceedings of ICCF-7, 88 (1998).

[41] C.E. Rolfs and W.S. Rodney, *Cauldrons in the Cosmos: Nuclear Astrophysics*, University of Chicago Press (1988), chapter 4.

[42] J.M. Blatt and V.F. Weisskopf, *Theoretical Nuclear Physics*, John Wiley and Sons, Inc., (1952), 8th Printing (1962).

[43] J.R. Oppenheimer and J.S. Schwinger, Phys. Rev. **56**, 1066 (1939).

[44] B.D. Josephson, "Possible New Effects in Superconductive Tunneling", Phys.Lett. **1**, 251 (1962).

Anomalous Heat Generation in Charging of Pd Powders with High Density Hydrogen Isotopes, (II) Discussions on Experimental Results and Underlying Physics

A.Takahashi[1*], A. Kitamura[2], T. Nohmi[2], Y. Sasaki[2], Y. Miyoshi[2], A. Taniike[2], R. Seto[1], and Y. Fujita[1]

[1]*Technova Inc.*
[2]*Kobe University*

E-mail: akito@sutv.zaq.ne.jp

Abstract: By our D(H)-gas charging experiments using Pd/PdO/ZrO$_2$ powders, we obtained: 1) D-gas charge in the 1st phase (zero pressure interval) gave 20~90 % more excess heat than those for H-gas charge. 2) In the 2nd phase of pressure rise (finally up to 1MPa), significant excess heat (about 2 kJ/g-Pd) for D-gas charge was observed, while near zero level excess heat for H-gas charge was observed. We discuss the underlying surface and nano-particle physics in views of the enhanced surface adsorption potential by fractal sub-nano-scale trapping points on nano-Pd grain, the diffusion to inner shallower Bloch potential of regular Pd lattice, and the drastic mesoscopic and isotopic effect of surface and lattice rearrangement of nano-Pd particle by full D(H)-absorption to make deeper D(H) trapping potentials (about 2eV for D).

1. Introduction

The aim, experimental apparatus, experimental procedure and observed results of deuterium (and protium) gas charging experiments with various nano-fabricated Pd powders are written in our paper by Sasaki to this meeting[1]. The observed results for Pd/PdO/ZrO$_2$ nano-composite samples (about 10 nm diameter Pd particles dispersed in about 7 micron size ZrO$_2$ flakes) provided us a confirmation-trial[8] of Arata and Zhang experiment[2] and a very interesting performance of deuterium (D) and protium (H) absorption and exothermic energy generation.

The results by nano-Pd/ZrO$_2$ samples are very interesting since specific surface effects in adsorption and following absorption into inner "lattice" sites look taking place to result in anomalously large stoichiometry values (x>1) of PdDx and deep trapping potential (or released energy). Compared with the results of 100nm Pd particle-powders, 10nm Pd particles dispersed in ZrO$_2$ are regarded to have shown the drastic mesoscopic effects with isotopic difference.

2. Trend of Heat-Power Evolution

The evolutions of heat and gas-pressure can be discussed for two different phases, the 1st phase and the second phase as we show typical data in 'Fig.1'.

The 1st phase is defined as the time-interval where reaction chamber (cell) keeps nominal "zero" gas-pressure. This means almost all D(H)-gas charged was absorbed by nano-Pd powders. Heat-power evolution curve in the 1st phase may be regarded mostly by chemical reaction energy during the D(H)-gas absorption into nano-Pd powders, in the ponit of view of conventional chemistry. However, we may have a component of "nuclear" process that we discuss later. For determining a 1st phase interval for heat-power evolution, we need to take a time-delay (about 15 minutes or three times of calorimetry time constant 5 minutes) into account[1], while the evolution of pressure has quick response.

Trend of heat-power evolution in the second phase is very isotope dependent, as typical data is shown in 'Fig.2'.
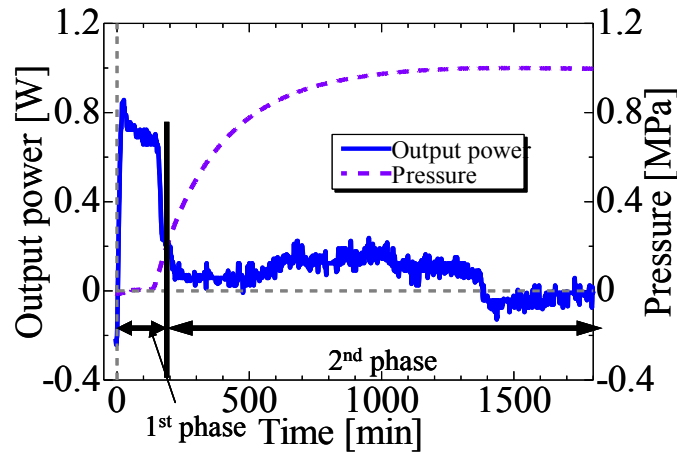
Fig. 1. - Typical heat -power evolution data with Pd/ZrO$_2$ nano-composite sample with D-gas charge (D-PZ1#1 run)
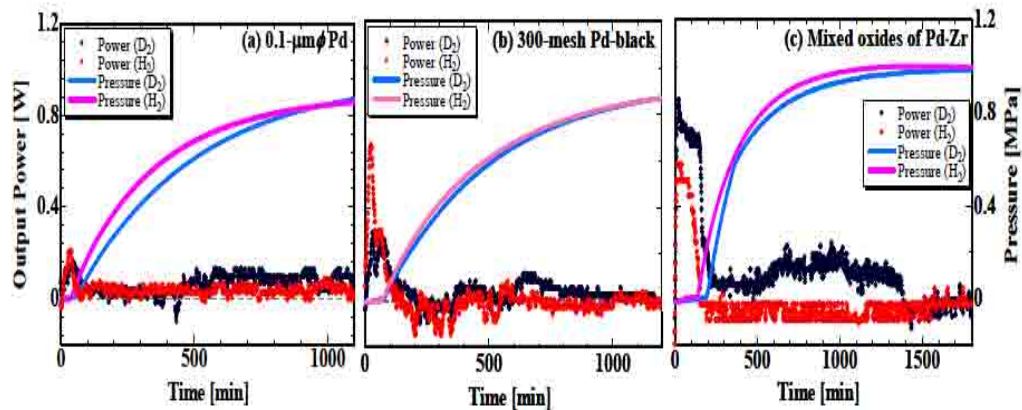
Fig. 2. - Typical "excess heat-power" evolution by D-charge for (c) Pd/ZrO$_2$ sample, net Pd weight = 3g (D-PZ1#1run), together with heat-power level by H-gas charge (H-PZ2#1 run), compared with (a) data by 100nm Pd powder, net Pd weight = 5g, and (b) data by Pd-black, net Pd weight = 3.2g (D) and 3.6g(H)

The H-gas charge has given "zero" power level (sometimes negative integrated values according to a possible zero-level drift of calorimetry or due to possible de-oxidation of PdO by D(H) charge). Obviously, the D-gas charge to the Pd/PdO/ZrO$_2$ nano-composite sample gave much more heat-power than that of the H-gas charge, for (c), which effect looks anomalously large compared to those by (a) and (b) and suggests a mesoscopic effect of Pd nano-particles on heat evolution, as discussed below.

3. Results and Discussions for 1st Phase Data

We summarized the integrated data of D(H)/Pd ratios, Heat per one-gram-Pd, Energy per D(H) atom absorption (E$_{1st}$) and gas-flow rates, and results are given in Table-1 of Reference-1 (see also Ref.8). First we discuss the data for 100nm Pd-particle powders (D-PP and H-PP runs in Table1 of Ref-1). Loading ratios, D(H)/Pd, are 0.43 and 0.44 respectively for deuterium (D) and protium (H) gas charging. Specific energies per absorbed D (or H) atom E$_{1st}$ (or ΔH_s) values are 0.24eV/atom-D and 0.20eV/atom-H. When D(H) is absorbed in metal lattice, surface adsorption works on D(H) molecule (or atom) first and D(H)-atoms diffuse into inner lattice sites (O-sites of Pd, usually) gradually. 'Figure 3' illustrates typical form of surface trapping potential and inner periodical (Bloch) trapping potentials.
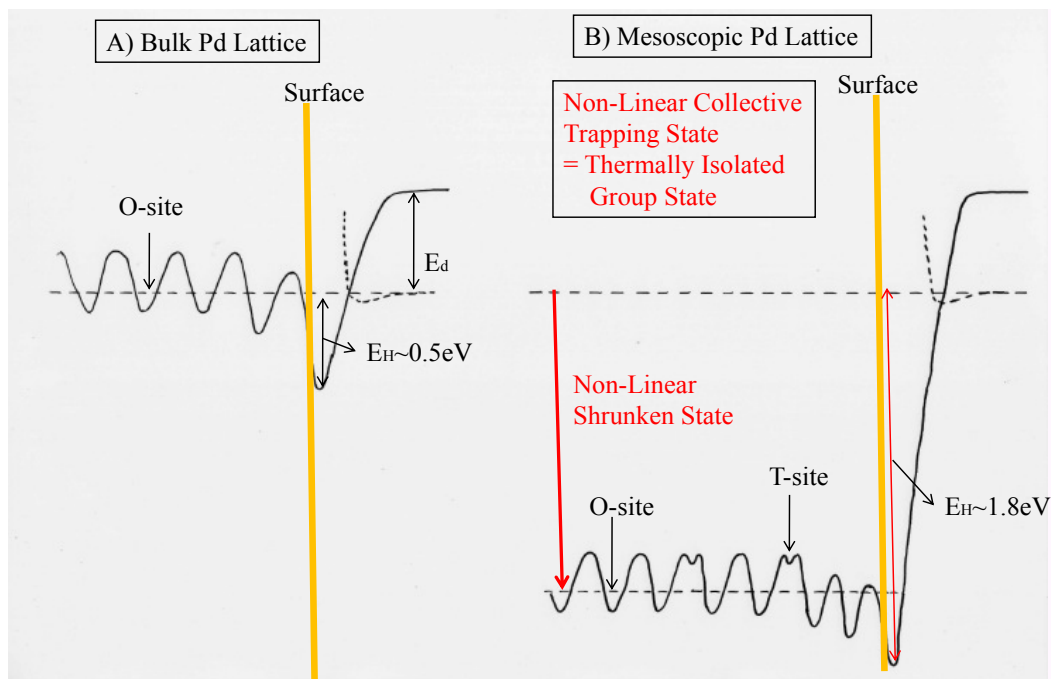
Fig. 3. - Image of D(H) trapping potentials at surface adsorption (depth E_H) and lattice absorption (depth E_{hydr}); trapped D(H) atom diffuses gradually into inner Bloch trapping potentials through the QM tunneling. After full loading (x=1 for PdDx), rearrangement of Pd lattice may happen to make shallower potentials for bulk Pd (left figure), while nano-Pd grain in ZrO_2 flake will have a specific mesoscopic potential (right figure) which reflects a non-linear combination of a deep collectively formed mesoscopic trapping potential (well-shape) and periodical Bloch potential of "local" PdDx lattice.

For known values in text book[3], E_H is about 0.5eV and E_{hydr} is 0.23eV. The difference, E_H-E_{hydr} , is close to the energy released per D(H)-atom absorption in lattice and is about 0.25eV for balk Pd lattice. Observed E_{1st} (ΔH_s) values for 100nm Pd particle powder are near to this value of bulk Pd metal. This means that 100nm Pd particle works as bulk-metal for D(H) absorption. We will see E_{1st} values for Pd-black and Pd/PdO/ZrO_2 nano-composite samples will have given much larger energies (deeper trapping potentials) to show the drastic mesoscopic effects. For the definition of mesoscopic size, we consider a Pd grain having 2,000 to 20,000 of total number of atoms.

Next, we look integrated data for Pd-black samples (D-PB and H-PB runs) in Table-1 of Ref.1. E_{1st} values in averages of runs are 0.70±0.15eV/atom-D and 0.69±0.10eV/atom-H. These values are significantly higher than the bulk value about 0.25eV. For the virgin runs (#1 runs), significantly high loading as PdD$_{0.88}$ or PdH$_{0.79}$ were observed. However, for runs with used samples (#2, #3, #4 runs), loading ratios were as small as 0.23 in average. Nevertheless the specific E_{1st} values were observed as same as the virgin (#1) runs. This fact means that microscopic active adsorption sites on surface of used Pd-black are working in the same way as the virgin Pd-black sample, although effective area of active surface decreased to 1/3 or less.

Now we discuss the integrated data in the 1st phases for Pd/PdO/ZrO_2 samples (D-PZ and H-PZ runs in Table1 of Ref.1). We observed heat-power levels were strongly dependent on the D(H) gas-flow rate. The larger gas-flow rate has trend to give the larger excess heat level in the 1st phase, but the 1st phase ends earlier than the case of smaller flow rate. This is understood as the faster gas-flow meets faster saturation of D(H) absorption in powders. Therefore, to compare specific values of E_{1st} (released energy per D(H)-atom), D(H)/Pd (loading ratio) and heat (in kJ) per g-Pd is more appropriate to understand the underlying physics.

Our first surprise is that all measured loading ratios, D(H)/Pd values for the 1st phases are greater than 1.0, namely overloading (x=1.1 in average for PdD(H)x stoichiometry) in usual sense, even though the background gas pressure were nearly zero (near vacuum). This must be said as the drastic mesoscopic effect of D(H) absorption by the Pd nano-composite samples. For the known bulk Pd-metal, D(H) atoms are trapped in Bloch potentials (see Fig.3) at O-sites for x<1.0. The observed anomalous data of x>1.0 should show that the additional trappings at T-sites or surface happened by the mesoscopic effect (about 5,000 Pd atoms existing in a 5nm diameter particle).

The data for specific released energy E_{1st} values are also anomalously large and isotope (D or H)-dependent. These are 2.2-2.5eV/atom-D and 1.3-2.1eV/atom-H. Deuterium gives larger E_{1st} values. These released energy values are 5-10 times of the conventional value 0.25eV for bulk Pd metal. These values are however dependent on gas-flow rate, and we need further investigation so far. As PZ samples gave drastic mesoscopic effects, compared to the 100nm Pd powder we need further study by changing nano-Pd particle size.

In 'Fig.4' degassing data of Pd/ZrO$_2$ sample is shown compared with that of Pd-black, under baking procedures. Note that the vertical scale of pressure is logarithmic. Clearly, Pd/ZrO$_2$ sample can very highly retain D(H) atoms even after the evacuation. The desorption process of nano-Pd grain is speculated to be very unusual. The D(H) retention of Pd/ZrO$_2$ sample seems about 100-fold greater than that of Pd-black. This degassing results, showing peak at about 200ºC, also suggest that the D(H) trapping potential of Pd/ZrO$_2$ nano-composite sample is much deeper than that of bulk Pd lattice.

4. Excess Heat for the Second Phase

As summarized in Table-1 of Ref-1, we observed positive excess heat in the 2nd phase of D-PZ series runs for virgin (#1 run) samples (we tried three pairs of samples for simultaneous runs with D-gas by A1 (A2 for D-PZ5) and H-gas by A2 (A1 for H-PZ6) cells). For the D-PZ5 run, D-gas cylinder dried out in the 2nd phase and gas-pressure decreased (we had leakage), so that excess heat phenomenon was not observed. For earlier two PZ runs, we observed clear excess heat, only for D-gas charging, 2.27 and 2.07kJ/g-Pd in the time interval of 1,600 minutes, respectively.

Now, we discuss about a possible chemical energy release by oxidation[8] of charged D(H)-gas, as samples contained PdO and ZrO$_2$ components. Already 'Fig.4' shows clearly D(H)-gas was mostly absorbed by Pd-grains in PZ samples, since Pd-black gave the same pattern of degassing. We have to consider a reduction of PdO$_x$ states followed by production of xD$_2$O (xH$_2$O) and PdD$_y$ (PdH$_y$) states. The reaction energies Q_D and Q_H are evaluated to be $(162.6 \times x + 70.0 \times y)$ kJ and $(156.6 \times x + 58.0 \times y)$ kJ, respectively. For assumed values of $x = 1 \sim 0$ and $y = 0 \sim 1$, Q_D and Q_H are 0.84 ~ 0.73 eV/D and 0.81 ~ 0.60eV/H, respectively. These are too small to account for both the observed E_{1st} energies and the isotope effects. Consequently, the main component of heat for a 1st phase cannot be due to the formation of water (D$_2$O or H$_2$O) by the D(H)-gas charging to PdO nano-particles. A role of PdO surface layer of Pd-nano-partilce for making sub-nano-holes on surface under D(H)-chrage will be discussed in our future paper.

There might be an yet-unknown atomic/electronic process governing the phenomenon in the present mesoscopic system, or the concept of "atom clusters" might apply. However, it seems rather difficult to assume that such a large isotope effect is only in the electronic process of adsorption and/or hydride formation. Some nuclear process as suggested by the 4D/TSC model by Takahashi [4-7] could be a candidate mechanism responsible for the phenomenon.

A speculation for the underlying physics of the atomic & molecular-level cluster formation by Coulombic interaction of deuterons and electrons in metal-hydride and the strong nuclear interaction of multi-body deuteron interaction is illustrated in 'Fig.5', viewing the aspect from a few body system to more complicated multi-body systems, namely, cluster, mesoscopic and bulk lattice systems. The 4D/TSC theory predicts a very rapid (in 1.4 fs) condensation[5-7] of 4D-cluster keeping the tetrahedral symmetric configuration with time-dependent TSC trapping potential for a Coulombic interaction between four deuteron QM-waves and four electron QM-waves[4-7].

A speculated deep potential trapping deuterons (or protons) into "local" Pd lattice inside the mesoscopic nano-particle grain is considered to be a combination of a collective deep well potential (resembling shape to the nuclear Woods-Saxon potential) and a "finite" Bloch potential of bulk Pd metal lattice. However the finite Bloch potential (locally periodical) is formed at the bottom of the collective deep well (See also 'Fig.3'). Particles (d or p) trapped in this "mesoscopic potential" will make a non-linear oscillation which magnifies the mobility (kinetic energy of trapped state) of deuterons (or protons) and enhances the cluster (especially 4D/TSC) formation probability under a collective dynamics. Possible formation of sub-nano-holes on surface of Pd-particle may arrange places for TSC formation.

The formation of collective deep well potential and more mobile particle motion inside it will enhance the speed of D(H) adsorption on surface and absorption into grain. The observed high retention of D(H) by Pd/ZrO$_2$ powder in vacuum will be also explained by such a mesoscopic potential. Nuclear strong interaction for simultaneous 3 and 4 deuterons in very condensed 4D/TSC is modeled[4-7] based on the pion-exchange model (Hideki Yukawa) and potential (Hamada-Johnston). The pion exchange force for many body interaction has been scaled by the unit of PEF.
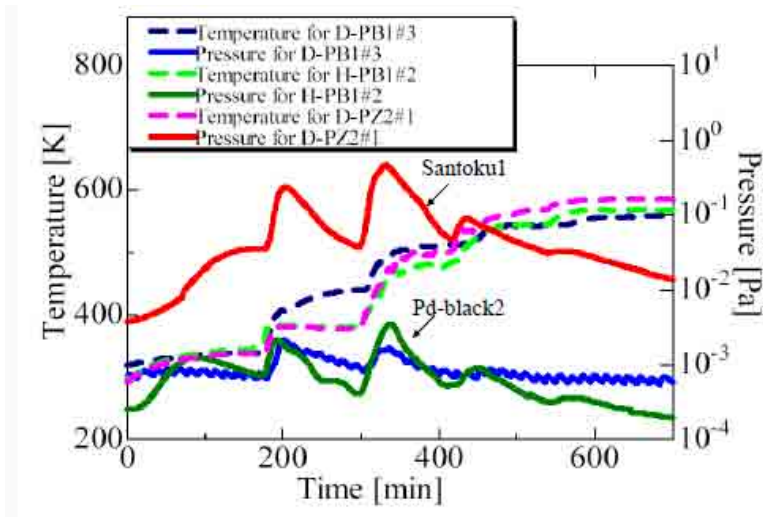
Fig. 4. - De-gassing data for Pd/ZrO$_2$(Santoku)-sample compared with that for Pd-black; Santoku-sample retains 100 times D(H)-atoms, presumably by its very deep trapping potentials of the mesoscopic effect of dispersed Pd-nano particles
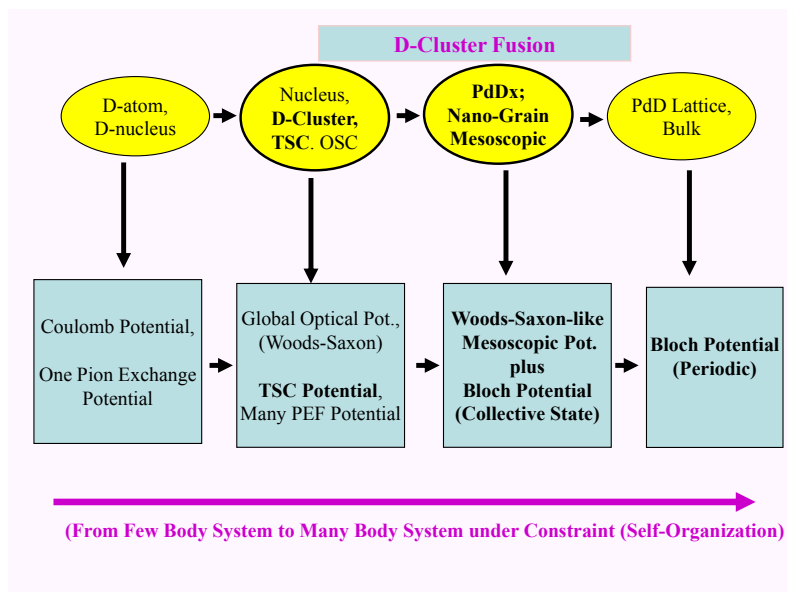
Fig. 5. - Speculation of potential change from a few body interaction to cluster, mesoscopic grain and bulk lattice of metal-deuterium (-protium) system, both for Coulombic and strong nuclear interaction. The proposed condensed cluster fusion is speculated to take place for the cluster, mesoscopic grain systems and near-surface of bulk metal as Pd.

5. Concluding Remarks

For Pd/PdO/ZrO$_2$ powders (Santoku-samples), we obtained results 1) through 4):

1) The D-gas charge in the 1st phase (zero pressure) gave 20-90% excess heat than the H-gas charge.
2) In the 2nd phase, significant excess heat (about 2 kJ/g-Pd) for the D-gas charge, while zero level for the H-gas charge, was observed.
3) No increase of neutron counts was seen, neither increase of gamma-rays over natural backgrounds.
4) D(H)/Pd ratios in the end of 1st phase was x>1.0, namely over-loading (x=1.1 in average). Flow rate dependence of x-values should be investigated further. Nano-Pd dispersed sample (Santoku, Pd/ZrO$_2$) retained 100 times more D(H) atoms after evacuation, than the Pd-black case.

We discussed that there may be a strong mesoscopic effect by Pd-nano-particle, namely surface and lattice rearrangement probably makes deep D(H) trapping potentials (1.0-2.5eV) by a nonlinearly coupled vibration states, of trapped D(H)-particles, between a deep collective trapping well potential and a periodical Bloch potential.

References

[1]   Y. Sasaki, A. Kitamura, Y. Miyoshi, T. Nohmi, A. Taniike, A. Takahashi, R. Seto, and Y. Fujita: Anomalous Heat Generation in Charging of Pd Powders with High Density Hydrogen Isotopes, (I) Results of absorption experiments using Pd powders, this meeting.

[2]   Y. Arata and Y. Zhang: The special report on research project for creation of new energy, *J. High Temperature Society*, No. 1. 2008.

[3]   Y. Fukai, K. Tanaka, Y. Uchida, Hydrogen and Metal (in Japanese), Uchida-Roukakuho Pub., Tokyo, ISBN=4-7536-5608-X (2002)

[4]   A. Takahashi, Cold Fusion 2008- Mechanism of Condensed Cluster Fusion (in Japanese), Kogakusha, ISBN=978-4-7775-1361-1 (2008)

[5]   A. Takahashi, N. Yabuuchi: Study on 4D/TSC condensation motion by non-linear Langevin equation, *LENR Source-Book 1,* **2008,** pp**.** 57-83

[6]   A. Takahashi: Basics of deuteron cluster dynamics by Langevin equation, *LENR Source-Book 2*, American Chemical Society, Oxford University Press, **2009**, in press

[7]   A. Takahashi: Dynamic mechanism of TSC condensation motion, *J. Condensed Matter Nuclear Science,* 2 **(2009**) 33-44

[8]   A. Kitamura, T. Nohmi, Y. Sasaki, A. Taniike, A. Takahashi, R.Seto, Y. Fujita: Anomalous effect in charging of Pd powders with high density hydrogen isotopes, *Physics Letters A*, 373 (2009) 3109-3112

Neutron Spectra in CMNS - Model Predictions and Past Data –

A. Takahashi[1]
[1]*Technova Inc.*

E-mail: akito@sutv.zaq.ne.jp

Abstract: According to the recent SPAWAR claim on ^{12}C(n,n')3α detection due to 14 MeV neutrons by D-T reaction in a D_2O/Pd co-deposition cell, we reminds our old discussion on observed neutron spectra from CMNS/CF cells in the past. Structure or shape of neutron spectra should give important (decisive) evidences on underlying physical mechanisms on possible deuteron-related nuclear fusions in PdDx systems. This paper discusses plausible neutron spectra as consequences of major theoretical model predictions.

1. Introduction

According to the recent SPAWAR claim on ^{12}C(n,n')3α detection due to 14 MeV neutrons by D-T reaction in D_2O/Pd co-deposition cell, we reminds our old discussion on observed neutron spectra from CMNS/CF cells in the past. Structure or shape of neutron spectra should give important (decisive) evidences on underlying physical mechanisms on possible deuteron-related nuclear fusions in PdDx systems. This paper discusses plausible neutron spectra as consequences of major theoretical model predictions.

2. The SPAWAR Claim

Mosier-Boss et al. have observed triplet tracks in CR39 detectors used in their co-deposition Pd/D_2O electrolysis type CMNS/CF experiments[1]. They claimed the triplet tracks should be due to forward-peaked emission of three alpha-particles from ^{12}C(n,n')3α reactions by D+T fusion reactions as byproducts of D+D reactions in the co-deposition experiments. The ^{12}C(n,n')3α reaction has however threshold at 7.8MeV of incident neutron energy[7]. The author conceives that the explanation by secondary d + t reactions after d + d fusions is not plausible, because the yield of d + t reactions by one 1MeV triton slowing down in PdDx matter is very small on the order of 10^{-5}, d + d → p(3.015MeV) + t (1.005MeV)+ 4.02MeV for the conventionally known DD fusion. Estimation using available neutron cross sections (JEDL3 for instance)[7], one ^{12}C(n, n')3α event needs about 100 fluence of 14MeV neutrons getting into the used CR39 track detector by SPAWAR. This should correspond to 10^7 neutrons of 2.45MeV by the d + d reactions. If we had 10^7 neutrons emitted from CF cells, we could detect very easily significant counting events and their recoil-proton-tracks of 2.45MeV neutrons. These can easily be detected, but has never been observed with so high 2.45 MeV neutron yield, by CR39 dtectors. The author concerns that the conclusion of secondary D+T fusion by SPAWAR for triplet tracks is not plausible.

3. Model Prediction Case-1

 [Case-1]: Some theoretical models[8-11] conceiving the d + d to ^{4}He + lattice energy (23.8MeV) processes have been thought as possible explanation for the CMNS/CF phenomena since 1989, in spite of very negative view from the nuclear physics point of view[12].

If the "Dream" of the **"d+d to ^{4}He + lattice energy (23.8MeV)"** [8-12] were taking place, the doping tritons make "d + t to ^{5}He + lattice energy" reactions, in the same path and we shall have neutron emission by,

- ^{5}He → n(0.716MeV) + ^{4}He(0.179MeV)

14 MeV neutrons are not major products in consequence of this theoretical model, but **low energy neutrons (0.716 MeV)** should be detected with the tritium doping of micro-Curie/cc-DTO; doping in experimental CMNS/CF cells. These "low" energy neutrons could not be detected by a CR39 detector because recoil-proton energies are too small to cause enough large ionization tracks. We shall use special neutron spectroscopy systems to detect and identify the 0.716 MeV neutrons.

4. Model Prediction Case-2

[Case-2]: Our **4D/TSC fusion model**[13-15] predicts 23.8MeV/^{4}He energy deposit in PdDx lattice as main product by the major channel 4D → ^{4}He + ^{4}He + 47.6MeV reactions. Minor branch products of triton and higher energy neutrons from 4D fusion are predicted as a product of symmetric fragmentation of ^{8}Be* via excited state of ^{4}He*(Ex=20.21 MeV: first excited state) as shown in 'Fig.1'.
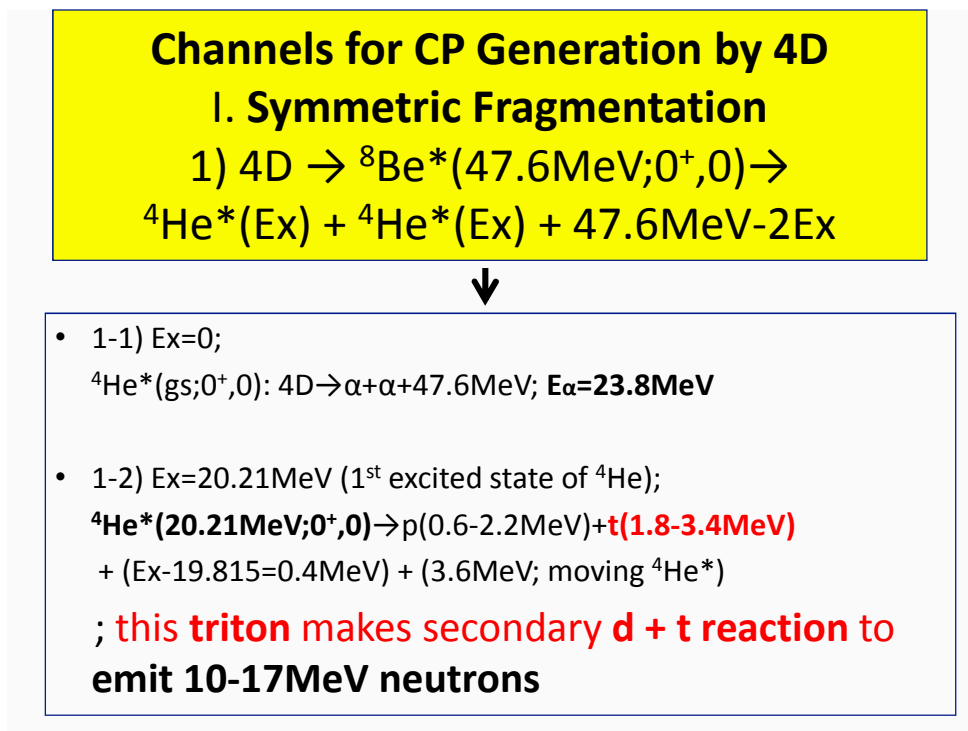
Fig.1 - Generation of triton by a symmetric fragmentation of ^{8}Be* by 4D fusion and its secondary t + d reaction to emit high energy neutrons in a 10 – 17 MeV region which may correspond to the SPARWAR result.

Secondary t + d reactions, during the slowing down of thus produced tritons in PdDx matter, produce a 10-17MeV high energy component as observed by SPAWAR[1]. In the symmetric fragmentation, higher excited states such as Ex=21.01MeV(0$^-$,0), 21.84MeV(2$^-$,0), 22.33MeV(2$^-$,1), 23.04MeV(1$^-$,1), from which neutrons can be emitted, are forbidden by odd parity (spin-parity conservation – selection rule).

If we make a doping of tritium (on the level of micro Curie) in the process, (3D+T)/TSC makes ^{9}Be*(43.01MeV) intermediate compound state to break up as,

- ^{9}Be*(43.01MeV) → ^{4}He(22.53MeV) + ^{5}He(18.01MeV)
- ^{5}He → n + ^{4}He + 0.895MeV (for ^{5}He at rest)
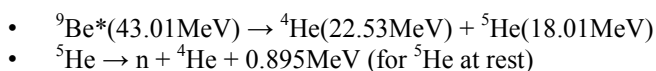
Neutron energy appears in 0.41 to 6.79 MeV (emitted from the break-up of moving ^{5}He of 18.01MeV kinetic energy, as calculated by kinematics). We may predict the broad higher energy spectrum in 0.4 to 7MeV region as major component (minor component in much higher energy region) by the tritium doping into on-going CMNS/CF cell experiments. This is the consequence of TSC model[13-15]. Obviously we can verify which theoretical model, Case-1 or Case-2 matches the observed phenomena of neutron emission in CMNS/CF experiments.
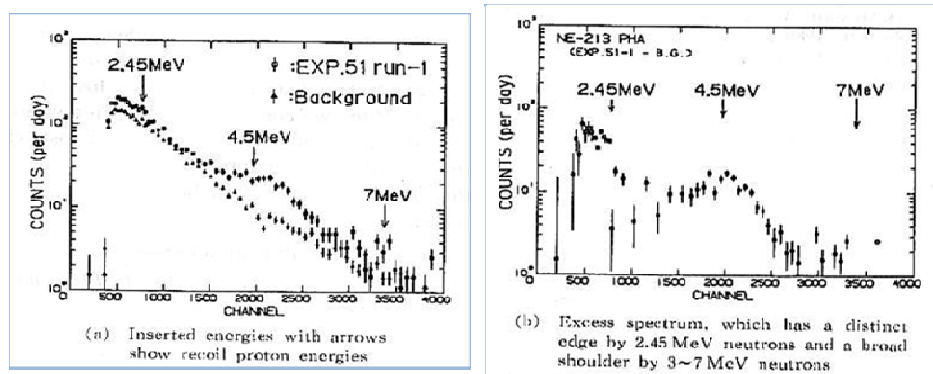
Two components: 2.45MeV peak and 3-7 MeV Higher Energy Group

Fig. 2 - Two component neutron spectra observed by the past Pd/D$_2$O electrolysis experiments, copied from published paper[2)]

5. Our Past Data of Neutron Emission and Discussions

We refer now our past measurements[2-6] of neutron spectra from CF-electrolysis experiments to be discussed under the above predictions. A typical result of measured neutron spectra from Pd/D$_2$O electrolysis cell[2] is copied in 'Fig.2'.

Fast neutron spectroscopy was done by measuring recoil-proton pulse height distribution of NE213 liquid scintillator with an n-gamma pulse shape separation technique[4)]. The background spectrum has "near-exponentially decreasing" recoil-proton pulse height distribution which was of spallation neutrons of cosmic-ray-origin showing similar spectrum as the fission-neutrons having a near Maxwellian distribution with a nuclear temperature 1.4MeV. High energy protons by cosmic rays induce spallation reactions with nuclei in the matter surrounding the detector. The near Maxwellian spectrum has therefore a high energy tail in En>10MeV. The excess neutrons observed has two components in its energy spectrum: one is of 2.45 MeV neutrons, very probably by the D+D fusion reactions. The other broad component in the 3-7 MeV region (and we might expect higher energy- more than 7 MeV- tail to observe if statistics of experiment is improved) is unidentified origin (See Fig.2). In our past papers[2,3,16], we speculated that the higher energy component could be the product of the secondary high energy d + d reactions after the primary d + d+ d three body fusion in PdDx-lattice; D+D+D → d(15.9MeV) + ^{4}He(7.9MeV) ; In the slowing down process of 15.9MeV deuterons, d + d reactions in PdDx produce higher energy component of neutrons seen in the 3-10MeV region.

Now, we have to reconsider this explanation by referring our other past results shown in 'Fig.3'. In our reconsideration, the higher energy neutron component might have been the 0.4-7MeV neutron emission by the (3D+T)/TSC 4-body fusion reaction in PdDx lattice dynamics (Case-2), because we had seen the significant accumulation of tritium atoms in the electrolyte (curve c) in Fig.2: This was already a kind of T-doped experiment which happened by chance. However, 4D fusions may emit much higher energy neutrons in the 10-17 MeV region, from minor out-going channels emitting tritons, as predicted in this paper. These high energy neurons are considered to have caused the triplet tracks in CR39 detectors used in the SPAWAR experiments.
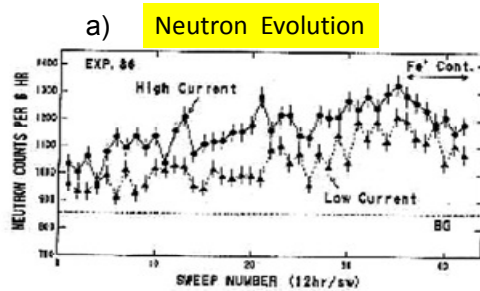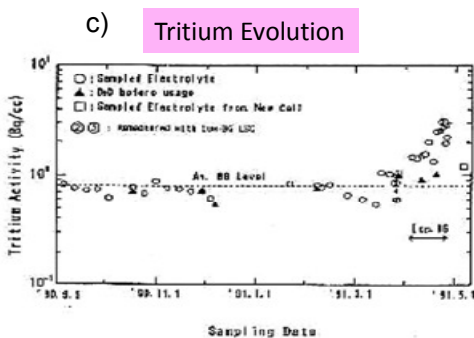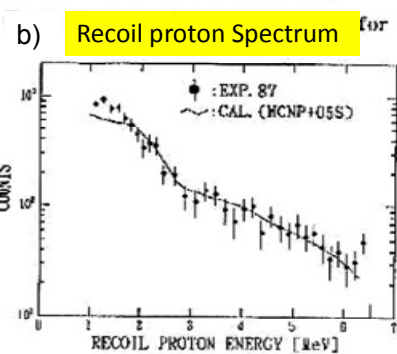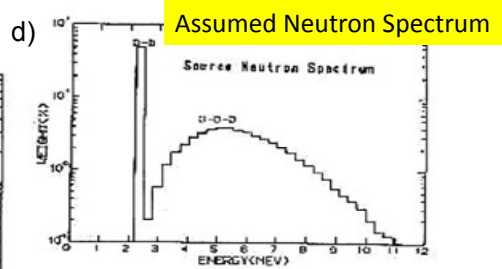
Fig. 3 - Our past data, copied from published prints[3,16], of neutron emission and evolution of tritium concentration in Pd/D₂O pulsed electrolysis experiments; a) evolution of excess neutron counts, b) recoil-proton pulse height spectra for excess neutrons, c) evolution of tritium concentration measured by LSC with sample electrolyte and d) assumed two component neutron spectrum for folding calculation of model.

6. References

[1] P. Mosier-Boss, S. Szpak, F. Gordon, L. Forsley: *Naturwissenschaften*, 96(2009)135-142
[2] A. Takahashi, T.Takeuchi, T. Iida, M. Watanabe: *J. Nuclear Science and Technology*, 27 (1990)663-666
[3] A. Takahashi, T. Takeuchi, T. Iida, M. Watanabe: *AIP Conf. Proc.* 228 (1990)323-340
[4] A. Takahashi, T. Iida, F. Maekawa, H. Sugimoto, S. Yoshida: *Fusion Technology*, 19(1991)380-390
[5] A. Takahashi, T. Iida, T. Takeuchi, A. Mega: *Int. J. Appl. Electromagnetics in Materials*, 3(1992)221-230
[6] A. Takahashi, H. Fukuoka, K. Yasuda, M. Taniguchi: *Int. J. Soc. Material Eng. For Resources*, 6(1998)4-13
[7] K. Kondo, I. Murata, K..Ochiai, N. Kubota, H. Miyamaru, C. Konno, T. Nishitani: *J. Nucl. Sci. Technol.*, 45(2008)103-115
[8] G. Preparata: *Trans. Fusion Technology*, 26(1994)397-407
[9] P. Hagelstein: *Condensed Matter Nuclear Science*, ICCF12, World Scientific, pp.441-453 (2006)
[10] S. Chubb: *ibid.*, pp.646-664
[11] M. Swartz: *Fusion Technology*, 31(1997)228-236
[12] A. Takahashi, N. Yabuuchi: *Condensed Matter Nuclear Science*, ICCF13, Moscow, ISBN=978-5-93271-428-7, pp.569-578 (2008)
[13] A. Takahashi, N. Yabuuchi: *LENR Source Book* Vol.1, American Chemical Soc., ACS Symp. Series 998, pp.57-83 (2008)
[14] A. Takahashi: "Basics of Deuteron Cluster Dynamics by Langevin Equation", *LENR Source Book* Vol.2, American Chemical Society, to be appeared in 2009
[15] A. Takahashi, "Cold Fusion 2008- Mechanism of Condensed Cluster Fusion", (in Japanese), Kogakusha, Tokyo, ISBN=978-4-7775-1361-1 (2008)
[16] A. Takahashi, T. Iida, T. Takeuchi, A. Mega, S. Yoshida, M. Watanabe: *The Science of Cold Fusion* (ed.; T. Bressani, E.D. Giudice, G. Preparata), Proc. ACCF2, Italian Physical Soc., pp.93-97 (1991)

SuperWaves™ as the Natural Origin of Excess Heat

Irving I. Dardik, M.D.

Abstract. Energetics Technologies has had excellent reproducibility of its own experimental results on cold fusion; significantly, its work has been replicated at independent laboratories, at SRI and ENEA. We believe that one of the most important reasons for these results is the use t of complex fractally nested current excitation From this perspective, these results in replicating the production of excess heat are a further confirmation that natural phenomena, including the electrochemical processes for producing excess of heat, can be correctly described by these fractal dynamics. . In this paper I describe basic concepts of the *SuperWaves*™ theory, which is an original general approach to model and understand natural phenomena.

1. Introduction

According to our current understanding of Cold Fusion, we are faced with a paradox. On one hand, we get positive results for excess heat. But on the other hand, there is no theory to back it. The following is a short overview of *SuperWave™ Reality*, which clarifies this issue on two fronts: it is a new understanding of nature, and therefore a new approach of how to go about understanding nature in the first place. The production of excess heat becomes not an anomaly but something expected and natural. This is because *SuperWaves*™ reveals something new: an underlying truth about the details in science and in nature. It does not negate the findings of science but places them firmly in a new context. It is not an alternate view, but a way to imbed what we already know into an entirely new framework. It is the ultimate underlying reality of nature. And, it is exceedingly simple.

I derived this new understanding from life. Life is the most complex thing that we know of, and it offers vastly different insights from what is considered to be simple, *i.e.* the reductionist, scientific approach to understanding physical reality. I had dealt with the problems of disease and death as a vascular surgeon, and dealt with life, human performance, and health as founding Chairman of the United States Olympic Sports Medicine Council. While working in these capacities, I discovered an entirely new approach for understanding the dynamics of biological systems in terms of their *rhythms*.

First, we must understand that all motion and all processes in a living organism are rhythmic. Everything moves in waves: from the circadian rhythms of day and night to the behavioral cycles of exercise and recovery or anxiety and relaxation, to organ cycles such as the heart beating or the lungs breathing, to the cell cycle, to molecular oscillations and the metabolism. Everything in the human body is oscillatory. This simple, extraordinary discovery is that the heart beat itself cycles simultaneously within the exercise-recovery cycles of the entire organism --waves waving within waves. Thus, our familiar view of the heart rate, graphed as linear motion in an electrocardiogram, misrepresents nature. In nature, the heartbeat follows no line, but rather accelerates up and down, speeding/intensifying then slowing/relaxing, in synchrony with the whole body as it makes a larger cycle of exercise and recovery. That which we separate conceptually into two scales is inextricably joined in nature. The heart and blood vessels pulsate in cyclic patterns of waves of contraction and relaxation, which simultaneously nest as an inherent continuum within the exercise and recovery cycles of the organism as a whole. No boundaries separate the different modes of function – they merge into each other. I call this the HeartWave.

2. Fractal properties of natural phenomena

The concept of HeartWave incorporates many features of "fractal" dynamics. "Fractal" objects, in nature, are the same on different observation scales; in particular, properly fractal objects are the same if the scale changes are the same in all directions; intermediate fractal or "self-affine" objects are the same if the scale changes are different in each directions.

Fractal structure in the human body may be easily recognized by observing, for instance, the lungs and the circulatory system. A fractal motion shows similar patterns on different time scales, just as in the

case of the heartbeat. The heart beat is a complex motion, made of an extended set of oscillations, whose amplitudes vary continuously over the full frequency scale. The measurement of such a kind of motion with a standard instrument inevitably fails to give a complete description of it, due to the limitations of scale and sensitivity of the instrument. The right approach to measure / describe such a "complex" (*i.e.* fractal) motion, is to extract from the single measurements, each on a limited scale, the scale-invariant relationship embedded in them.

There are three major characteristics of the HeartWave, all properties of the inherent continuity of the cross-scalar relationships of waves waving:

> 1. Frequency and amplitude are a continuum across scales. The standard approach of treating waves using orthogonal dimensions including amplitude and frequency, allowing linear deconvolution via Fourier transforms, are practical means of working with waves that nonetheless fail to capture important ways in which waves interact. A shift of frequency in one scale simultaneously influences amplitude on the next scale, and vice versa, as an inherent continuum across all scales. Waves waving necessitates that these waves are ultimately not linear on any scale*;* waves waving are responsible for what science has been calling the ubiquity of non-linearity in nature

> 2. Since waves waving within waves occurs simultaneously across scales, we have what science calls non-locality or action-at-a-distance. The continuity of nested waves simultaneously affects each other across scales, top-down and bottom-up as they move forward, and change in time. They exhibit action-at-a-distance, at the same time that they change causally. I call this "simulcausality".

> 3. This unremitting pattern of nested waves is an unbroken fractal phenomenon of order. The sharper the slope of the carrier wave, the faster the inner waves accelerate, which simultaneously increases frequency and amplitude of the inner waves, and thereby increases their density as they climb the carrier wave. Therefore, within the peak of the carrier wave is the highest density and motion, of inner waves – what we call attraction. Conversely, towards the trough, the waves slow down, flatten, and disperse – what we call repulsion. All of this arises from the cross-scale continuum of the fractal order of nature.

This powerfully constructive order of the HeartWave is present down through all levels of physiology, chemistry, and molecular biology, and in particular, what we call energy metabolism. The same three points outlined above: (1) frequency-amplitude as a continuum; (2) simulcausality; (3) the inherent fractal order of waves waving. The fractal order of the HeartWave explains why Brownian motion in a living organism exhibits highly elevated degree of order in its many levels of cybernetic feed-forward and feed-back loops [1]. This motion becomes enfolded and constrained within all the rhythms of the organism as a whole.

With the increased wave density and motion in the peak of exercise, the chemistry and metabolism exhibit an increase of heat. In contrast, there is a cool down in the troughs of recovery. Where there is motion, there is heat, therefore it can be understood that waves waving is the origin of temperature differences throughout nature.

In summation, the HeartWave encompasses the whole organism, the organs, cells, the molecular biology, and the metabolism. They all exhibit the same pattern of motion as waves waving within waves. If we take this down another level of scientific investigation, we reach the world of the atom and quantum physics. It is here that I concluded that all nature is, in reality, an inherent continuum of waves waving. This is in sharp contrast to our current thinking. The HeartWave, when followed down through all scales of nested oscillatory motion, tells us by logical extrapolation that the particle recognized by science as a wave packet (or wavicle) is not boundaried independently in space but is nested as an inherent continuum within a carrier wave.

Recently fractal waves have been involved in approaching and solving quantum mechanics problems. It has been demonstrated that fractal waves are fractal solution of the Shrodinger equation for a wide class of quantum problems, including the infinite potential well, harmonic oscillator, linear potential and free particle [1]. Fractal mathematics was also applied to other complex fields of physics, as, for instance, in investigating the fractal structure of the universe [2] and the fractal structure of surfaces. Fractal concepts apply also in chemistry, as for instance to the structure and chemistry of porous solids and to the growth of polymers and colloids. Fractal science is in progress and is extending across an increasing number of disciplines.

We extend such a concept to fractal modulated electric currents applied to electrochemical and glow discharge cells, since the signal can be traced back to a self similar shape. The signal is composed by several nested waves (SuperWaves™ see Fig.1) characterized by the same amplitude frequency ratio (the fractal dimension in this picture).
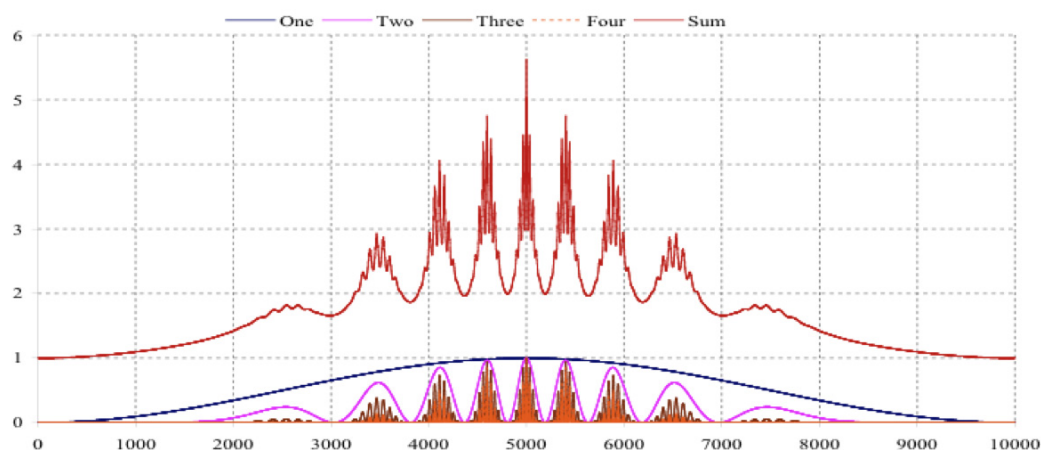
Fig. 1. - Showing nature and synthesis of fractally nested SuperWaves™.

The organization of fractal waves (*SuperWaves™*) in our electrochemical, glow discharge (and other) experiments were intended to bring this principle to bear by stimulating cyclic processes across scales. Peaking of *SuperWaves™* is the natural origin of what is termed excess heat. Clear evidence of the SW effect in controlling the excess of power production during electrochemical loading of palladium with deuterium is described in the appendix.

Acknowledgments

3. Appendix

An example of one of the ways that *SuperWaves™* can contribute to enhancing LENR excess heat effects can be demonstrated from the advantage of pulsatile (rather than dc) current or pressure driven loading of hydrogen (and its isotopes) into metals that has been demonstrated to be a necessary condition for the occurrence of the effect.

The dissolution of hydrogen isotopes into a metal lattice is not only a problem of thermodynamic equilibrium between the hydrogen inside the lattice and the hydrogen in the external phase (gas or liquid) it is also a problem of dis-equilibrium produced by mass transfer. Both aspects of the phenomenon are correlated since the equilibrium concentration of the solute is achieved when the chemical potentials of the hydrogen in both phases are equal.

The chemical potential of the hydrogen in solid solution in a metal lattice is strongly influenced by all field force, like the stress field, modifying the free energy of the system [3]. Hydrogen isotopes dissolved into a metal (*i.e.* palladium) occupy interstitial positions causing lattice expansion. This process generates a stress field when remarkable concentration differences (strong gradients or coexistence of different phases) are created.

Therefore the loading process can be inhibited by an opposing stress gradient, particularly adjacent to the external surface. When a stress field is created is the hydrogen chemical potential into the metal lattice, increased by the product between the molar volume of the hydrogen in the lattice and the trace of the stress tensor.

$$\mu_s = \mu * + V_s \sigma_h \qquad [1]$$

Also the flux equation modify :

$$J = -D(\nabla C - \frac{C\overline{V}}{RT}\nabla\sigma) \qquad [2]$$

Compared with Fick's law there is an additional term involving the stress gradient. Equation [2] shows that a zero flux condition may occur even if the concentration gradient has a non zero value (if the two terms into the brackets have the same value). A mass transfer equation has been obtained to describe the evolution of the hydrogen concentration profile during the loading of H into Pd [3]:

$$\frac{\partial \overline{c}}{\partial \tau} = \frac{\partial^2 \overline{c}}{\partial \overline{x}^2} - (1-\eta)b\frac{\overline{V}E}{RT}\left(\frac{\partial c}{\partial x}\right)^2 - (1-\eta)b\frac{\overline{V}E}{RT}\overline{c}\frac{\partial^2 \overline{c}}{\partial \overline{x}^2} \qquad [3]$$

Appropriate metallurgical treatments may help in reducing the concentration gradients (*i.e.* the stress) in loading palladium with deuterium. In addition a proper loading dynamics can contribute to have a better loading.

We may explain this with an example. Figure A1 shows the H concentration profile evolution when the effective pressure is changing between two pressure levels arbitrarily labeled Hi and Low. When the pressure is high (Hi) a strong concentration gradient is created close to the surface of the sample to be loaded. A reduction of the pressure followed by a further increasing, destroys the gradient close the surface and move the region of high loading further into the sample, while relaxing the surface condition. If we again repeat the same operation using a new period that is comparable with the diffusion time required to move the hydrogen from the surface to the inside position were the gradient exists we may destroy the gradient again moving it into further inside, and so on.

The problem is that the real systems we are working with are made up of polycrystalline materials with distributed grain size. This requires many periods and amplitudes to make effective the process above described across the whole domain. A fractal wave (SW) can perform this task and provide a strong enhancement to both the loading and flux, both conditions that are known or believed to be important preconditions for LENR excess heat in the Fleischmann-Pons Effect. The experimental evidence of the effect of Super Waves on Deuterium loading is shown in Figure A2

Pressure Hi   Pressure Low   Pressure Hi
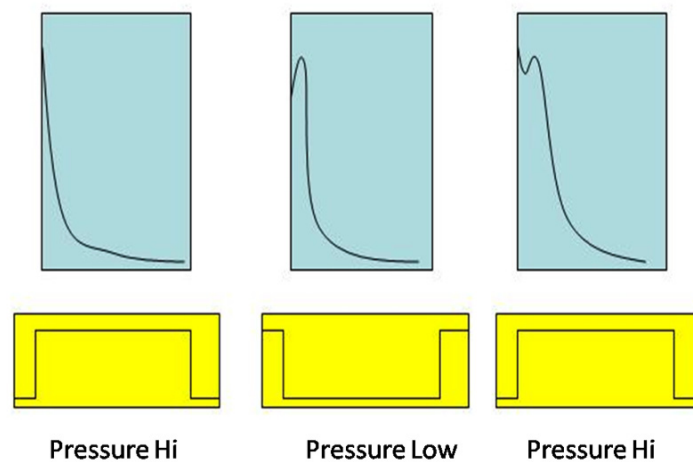
Fig. A1 - Concentration profile evolution under high-low pressure cycling

Loading of Palladium Foil 50 microns, in 0.1M LiOD
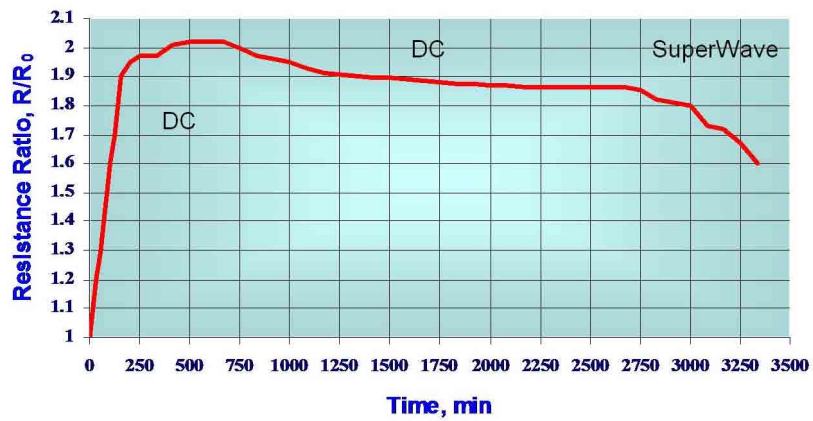
Fig. A2 - Experimental evidence of the SuperWave effect on loading.

4. References

[1] M. Haw, "*From Steam Engines to Life?"*, American Scientist, **95**, p. 472, (2007).
[1] D. Wojcik, I.B. Birula, K. Zyczkowski, Phys. Rev. Lett. **85**, N. 24 (2000) 5023.
[2] Pieronero, L. "*The Fractal Structure of the Universe: Correlations of Galaxies and Clusters*".
Physics A (144): 257., (1987).
[3] A. De Ninno, V. Violante, A. La Barbera, Phys. Rev. B. **56**, N.5 (1997) 2417.

Theoretical Model Of The Probability of Fusion Between Deuterons within Deformed Crystalline Lattices with Micro-Cracks at Room Temperature

F. Frisone

*Department of Physics, University of Catania, Via Santa Sofia, 64 95123
Catania (Italy), Phone +39-095-3785227, Fax +39-095-3785231*

E-mail: frisone@ct.infn.it

Abstract. In this paper, we wish to demonstrate that the deformation of the crystalline lattice, at room temperature, can influence the process of fusion of the deuterons introduced into the lattice by deuterium loading. In fact, calculating the probability of deuteron-plasmon fusion within a micro-crack, showed, together with the enhancement of the tunnelling effect, an increase of at least 1-3 orders of magnitude compared to the probability of fusion on the surface of the lattice. These phenomena open the way to the theoretical hypothesis that a kind of chain reaction, catalysed by the micro-cracks produced in the structure as a result of deuterium loading, can favour the process.

1. Introduction

As a result of the numerical calculation performed for different metals, varying the temperature, the total energy and the concentration of impurities, it was possible to conclude that the probability of fusion was in effect substantially enhanced by increasing these parameters. In this paper, we wish to confirm the hypothesis regarding micro-cracks, by means of quantitative theoretical estimates of the coefficient of structural deformation of the perturbed[2] crystalline lattice independent of time, obtained for different temperature values in the range 100-300 K. In particular, we calculated the probability of fusion within a micro-crack, comparing it with that calculated on the surface, to evidence a possible enhancing effect.

Further, we also wish to observe, theoretically, any influence on the phenomenon produced by variation in temperature, which could favour the fusion of the deuterium nuclei as a consequence of the deformations and micro-cracks produced in the lattice. In fact these may be able to concentrate in their vicinity a relevant fraction of the deuterons present in the metal.

The phenomenon hypothesised above could possess characteristics analogous to the formation of the Cottrell atmosphere in metals[2], known for some time in solid state physics, which essentially consists of a redistribution of the impurities present in the metal around a dislocation of the ions making up the lattice.

In these cases, the interaction between the dislocation and the impurities present can significantly modify the electrical properties of the material; further, some particular reactions can occur, incorporating the impurities in the nucleus of the dislocations, as a result of the different arrangement of the atoms with respect to that of the unperturbed lattice. This type of process has been extensively studied in the literature for the case of crystalline semiconductors at high temperature[2] and for metals[2]. In the latter, for example, it is found that the concentration of interstitial impurities around a linear dislocation, with a point component, depends on the temperature according to a law of the type:

$$c = c_0 \exp\left[\frac{\beta}{bkT}\right] \tag{1}$$

where c_0 is the concentration of impurities in the zone with zero internal pressure, $b^3 \simeq v_i$ the volume of the ions constituting the lattice, while β is proportional to the difference

v_d - v_i between the volume of the atoms of the impurities and that of the lattice ions.

Our conjecture is that in a metal, such as Pd, a similar phenomena could occur between the atoms of deuterium penetrating the lattice as a result of deuterium loading and the micro-cracks produced by variations in temperature.

In this case, the parameter β of the previous expression would be *negative*, determining an increase in the concentration of deuterons in the vicinity of the micro-crack, which would then catalyse the phenomenon of fusion.

The procedures, such as deuterium loading within lattices[3].

In effect, it is found that with the appearance of micro-cracks, in agreement with the "chain reaction" hypothesis proposed in reference[1], there is an increase in the rate of deuteron fusion within the lattice, obtained by evaluating the number of events per minute with a numerical simulation programme which employs the "WKB" method for the approximate solution of the wave equation. This calculation, which takes account of all the physical parameters, provides theoretical information, which we consider interesting, for "impure" metals at room temperature and for average deuteron energies.

2. Three-dimensional model of spherical symmetry

The numerical calculation, performed for three typical metals (Pd, Ti and Pt) on varying the temperature and total energy, in turn dependent within certain limits on the temperature, made it possible to conclude that the probability of fusion is in effect enhanced by increasing *P, T* and *E*.

The following table refers to the probability of fusion calculated on the surface of Palladium[1]). It shows the trend of the probability of deuteron fusion in impure Pd (*J* = 0.75%) on varying *T* and *E* (Tab.1 in reference[1]). Palladium, which has CFC symmetry, shows higher values for the probability of fusion than Pt and Ti, for temperatures between 36.7 K and 63.7 K and energies between 140 eV and 240 eV.

T ≈	36.7 K	45.7 K	54.7 K	63.7 K
E ≈	P ≈	P ≈	P ≈	P ≈
140	10^{-60}	10^{-55}	10^{-59}	10^{-54}
160	10^{-52}	10^{-47}	10^{-50}	10^{-44}
180	10^{-45}	10^{-43}	10^{-42}	10^{-40}
200	10^{-42}	10^{-41}	10^{-39}	10^{-38}
220	10^{-40}	10^{-39}	10^{-37}	10^{-36}
240	10^{-37}	10^{-35}	10^{-35}	10^{-33}

An important effect on the reaction, due to the metal lattice, is represented by electronic screening. This effect, already studied by Rabinowitz et al.[4], can be taken into account using a model in which the negative charge is distributed around the nucleon in a thin shell and can be schematised supposing the electric charge to be uniformly distributed with a thin spherical shell, with a radius R ≥ r_1 equal to the effective range of the interaction between the nucleons, describable in terms of a "shifted[4]" Coulomb potential.

$$V = \left(kq^2\right)\left[1/r - 1/R\right] \qquad\qquad r_1 \leq r \leq R \qquad\qquad (2)$$

where q is the charge of the deuton, r_1 is the nuclear radius, $k = 1/4\pi\varepsilon_0$. Then $V = 0$ for $r > R$. The solution for the semi-classic tunnelling factor Λ is[4]:

$$\Lambda = D \exp\left[-2\gamma(r_2)\right] \tag{3}$$

$$\gamma(r_2) = (\pi/2\hbar)\left[\left(2q^2/4\pi\varepsilon_0\right)\mu r_2\right]^{1/2} \tag{4}$$

In equations (3) and (4), D is a numerical constant of the order of unity, μ the effective reduced mass of the deuton, r_2 the classic point of inversion, and $\hbar$ is the reduced Planck constant. To take account of the effect of the impurities present in the metal, we modify the constant D in (3) substituting the product $J\eta$, where J is the concentration of impurities and η a numerical constant, $\eta \cong 1$.

The function γ is proportional to the electrical charge of the nucleons and to the square root of the product μr_2, where μ is the reduced mass of the mass centre system for an interaction of two bodies, and r_2 is the classic point of inversion.

Of the three metals considered, Palladium seems to be the most effective in catalysing fusion, as a result of its structural characteristics: This can be understood from a qualitative point of view, observing that the curve of interaction potential, within the metal, has a trend which requires a lower quantity of total energy.

The numerical calculation d-d in this case can be expressed as follows[1]:

$$V(r) = k_0 \frac{q^2}{r} \cdot M_d \left(V(r)_M - \frac{JkTR}{r} \right) \tag{5}$$

where $V(r)_M$ is the Morse potential, $k_0 = 1/4\pi\varepsilon_0$, q is the charge of the deuton and therefore q^2/r is a potential, M_d the reduced mass of the deuterium nuclei, T the absolute temperature at which the metal is experimentally placed, J the concentration of impurities in the crystalline lattice and R is the nuclear radius.

3. Deformation in cubic lattices

In this section we wish to establish whether, and within what limits, the rate of fusion within a micro-crack in a generic cubic lattice subjected to deuterium loading can be conditioned or influenced, as well as by extensive lattice defects and by the other characteristics and thermodynamic conditions, also by any "deformations" produced in the crystalline lattice by variations in the temperature.

If this effectively occurs, it is not difficult to hypothesise that the energy produced by the micro-explosions within the micro-cracks present, could favour the creation of new fractures, which in turn would, by the same mechanism, capture other deuterons, and so on.

On the other hand, the formation of micro-cracks in Palladium electrodes produced by the energy released during long periods of electrolysis[5] has already been observed experimentally for some time, but has until now been considered only a consequence of nuclear fusion. In fact, Heui Kyeong An, et al.[6] an energy peak within micro-cracks during electrolysis.

Our hypothesis is that deuterons are injected into the micro-crack with force during loading and are therefore more likely to emit energy in micro-explosions, which in turn produce further micro-cracks. In this way the phenomenon observed could favour the process, enhancing the probability of fusion of the deutons absorbed by the metal lattice.

We wish to study the internal perturbations which can take place in the lattice following D_2 loading and the consequent modifications in the properties of the metal. The loading does not, in fact, simply provide an increase in the percentage of deuterium present, with a resulting disequilibrium of the "d" band; rather this type of procedure also determines, according to our hypothesis, lattice deformations followed by dislocations which cause micro-cracks in the structure.

It can happen then that the interaction between the impurities present and the dislocations produced in the metal during deformation, significantly modify the electrical properties of the material. Some particular reactions can then take place which incorporate the impurities in the nucleus of the dislocations[7], as a result of the different arrangement of the atoms with respect to that of the unperturbed lattice. An adequate theoretical description of the loading can therefore be obtained, in our opinion, only by treating it as a

perturbation independent of time.

We must also consider the fact that, under conditions far from those of saturation, the rate of fusion, within the metal depends on the number of deuterium nuclei absorbed in unit time, which could also depend on the deformation of the lattice. It is necessary therefore to study both phenomena.

It is known that in the presence of interaction between deuterium nuclei and collective plasmonic excitation in the metal, the number of fusions λ_f in a gas consisting of λ deuterons with density ρ is given by[11]:

$$\lambda_f = \lambda \cdot \frac{4\pi \rho \hbar}{\mu_d} \cdot \langle \frac{1}{p} \rangle \tag{6}$$

where μ_d is the reduced mass of the deuterium nuclei, p is their impulse, and where the parentheses $\langle\ \rangle$ represent the thermal mean.

For simplicity we can now consider a cubic lattice structure subjected to deformations and calculate the probability of fusion within a micro-crack, Γ, on varying the temperature.

Indicating the volume of a single cell by $d\Omega$, the deformation of the entire lattice is given by:

$$\Psi \cong \left\{ \iiint_\Omega \eta \left(J \frac{\rho L^2 \nu b^2}{\alpha 2 hR} \chi \exp\left(-\frac{U_0}{kT}\right) \xi_{(r)} \right) d\Omega \right\} \tag{7}$$

where J is the concentration of impurities and η is a parameter which depends on the lattice and electronic structure of the metal under consideration.

In this study we have concentrated on the cubic structure of the lattice, in the specific case of Palladium, because it has an easily observable geometry and we have indicated by ρ the density of the mobile dislocation[8] within the lattice at non constant lattice temperature, so that the thermodynamic stress of the deuterium nuclei per unit volume must be taken into consideration.

Further, demonstrate this, approximate calculations were made in which the lattice[7,8,9] deformation and the micro-crack depth were taken into account.

Taking the centre of mass system as that of reference, the probability of fusion in a zone of the metal in which there is no micro-crack (e.g. on the surface) can be written[1] as:

$$\left|P\right|^2_{int} = \exp\left(-2\int_0^\alpha K(r)_{int}\, dr \right) \tag{8} \tag{12}$$

α is 0.15Å, $K(r)_{int}$ is given by:

$$K(r)_{int} = \sqrt{2\mu\left[E - V(r)\right]/\hbar^2} \tag{9} \tag{13}$$

E is the total initial energy, principally thermal in nature; μ is reduced mass of the deuteron; $\hbar$ is Plank's constant.

Equations (8) and (9) refer to the process of fusion within the crystalline lattice.

The Coulomb potential $V(r)$, containing the temperature contribution, is given by the expression (5) :

The symbols adopted here are the same as those used in (5). In (14), the Morse potential $V(r)_M$ is given by:

$$V(r)_M = (J/\zeta)\{\exp\left(-2\varphi(r-r_0)\right) - 2\exp\left(-\varphi(r-r_0)\right)\} \tag{10} \tag{15}$$

Here, J indicates the concentration of impurities present in the metal, while the parameters φ and r_0 depend on the dynamic conditions of the system.

ζ is a parameter depending on the structural characteristics of the lattice, the number of "d" band electrons

and the type of lattice symmetry, and variable between 0.015 and 0.025.

If we divide (8) by (6) and multiply by (7), it follows that:

$$\Gamma \approx \frac{\exp\left(-2\int_0^\alpha K(r)_{int}\,dr\right)}{\lambda \cdot \dfrac{4\pi\rho\hbar}{\mu_d}\cdot\langle\frac{1}{p}\rangle}\cdot\Psi \qquad\qquad (11)\qquad(16)$$

Expression (11) represents the probability of deuteron fusion within a micro-crack: it is directly proportional to the number of deuterons absorbed by the metal until the target is saturated, thereafter the probability of fusion will be inversely proportional to the number of nuclei absorbed by the metal. In the context of the approximations made, the probability of fusion calculated in this way is equal to the edge deformation coefficient per unit of total deformation of the whole lattice.

From (11), with K$(r)_{int}$ calculated adopting the Morse potential, a numerical simulation programme employing the "WKB" method was used to determine the probability of fusion, normalised to the number of events per minute.

The results of Tab.1 can be compared with those of Tab.2, where the potential (5) was substituted by a "shell" potential of the (2) type, modified as followed:

$$V = \left(kq^2\right)\left((1/r)-\frac{KT}{J\varepsilon R}\right)\cdot \quad r_1 \leq r \leq R \qquad\qquad (12)$$

where KT is the mean kinetic energy of the gas, ε is the vibrational energy which is typically of the order of some eV for the quantum states under consideration and q is the charge of a deuton.

Table 1. – For "impure" metals ($J \approx 0.75\%$), adopting the Morse potential, the probability of fusion Γ was calculated for Pd within a micro-crack, in the presence of D$_2$ loading, normalised to number of events per minute, for different values of temperature (100 ÷ 300 K) and energy (150 ÷ 250 eV). It can be seen that the probability generally increases with T and E, and is systematically greater by some orders of magnitude than the probability of fusion **P** on the surface.

Palladium $J \approx 0.75\%$ T-range ≈ 100 - 300 K $\alpha \approx 34$ Å $\lambda_f = 1.38\cdot10^{-3}$ eV/min M$_{pd}$/µg

T ≈	100 K		140 K		180 K		220 K		260 K		300 K	
E ≈	Γ ≈	P ≈	Γ ≈	P ≈	Γ ≈	P ≈	Γ ≈	P ≈	Γ ≈	P ≈	Γ ≈	P ≈
150	10^{-75}	10^{-77}	10^{-66}	10^{-69}	10^{-67}	10^{-68}	10^{-63}	10^{-64}	10^{-64}	10^{-66}	10^{-60}	10^{-68}
160	10^{-73}	10^{-75}	10^{-65}	10^{-68}	10^{-64}	10^{-67}	10^{-61}	10^{-63}	10^{-63}	10^{-65}	10^{-58}	10^{-65}
170	10^{-70}	10^{-73}	10^{-63}	10^{-65}	10^{-62}	10^{-65}	10^{-59}	10^{-62}	10^{-60}	10^{-64}	10^{-56}	10^{-62}
180	10^{-69}	10^{-72}	10^{-58}	10^{-62}	10^{-60}	10^{-64}	10^{-57}	10^{-61}	10^{-58}	10^{-63}	10^{-55}	10^{-60}
190	10^{-67}	10^{-71}	10^{-56}	10^{-60}	10^{-59}	10^{-63}	10^{-55}	10^{-60}	10^{-56}	10^{-62}	10^{-50}	10^{-58}
200	10^{-65}	10^{-70}	10^{-55}	10^{-59}	10^{-57}	10^{-62}	10^{-54}	10^{-59}	10^{-53}	10^{-61}	10^{-47}	10^{-54}
210	10^{-64}	10^{-69}	10^{-54}	10^{-58}	10^{-56}	10^{-61}	10^{-53}	10^{-57}	10^{-52}	10^{-60}	10^{-44}	10^{-51}
220	10^{-62}	10^{-67}	10^{-52}	10^{-57}	10^{-54}	10^{-60}	10^{-52}	10^{-56}	10^{-51}	10^{-59}	10^{-40}	10^{-47}
230	10^{-60}	10^{-66}	10^{-51}	10^{-56}	10^{-53}	10^{-59}	10^{-50}	10^{-55}	10^{-50}	10^{-58}	10^{-32}	10^{-40}
240	10^{-59}	10^{-65}	10^{-50}	10^{-55}	10^{-52}	10^{-58}	10^{-49}	10^{-54}	10^{-49}	10^{-57}	10^{-27}	10^{-34}
250	10^{-58}	10^{-63}	10^{-49}	10^{-53}	10^{-51}	10^{-56}	10^{-48}	10^{-51}	10^{-48}	10^{-53}	10^{-21}	10^{-25}

Table 2..- For "pure" metals ($J \approx 0.25\%$), adopting the "shell" potential, the probability of fusion Γ was calculated for Pd within a micro-crack, in the presence of D_2 loading, normalised to number of events per second, under the same dynamic conditions as Tab.1. Also here Γ is systematically higher by some orders of magnitude compared to the probability of fusion P on the surface, but the values are systematically lower that those of the previous case.

Palladium $J \approx 0.25\%$ T-range $\approx 100-300$ K $\alpha \approx .34$ Å $\lambda_f = 1.38 \cdot 10^{-3}$ eV/min M_{pd}/µg

T ≈	100 K		140 K		180 K		220 K		260 K		300 K	
E ≈	Γ ≈	P ≈	Γ ≈	P ≈	Γ ≈	P ≈	Γ ≈	P ≈	Γ ≈	P ≈	Γ ≈	P ≈
150	10^{-75}	10^{-81}	10^{-76}	10^{-85}	10^{-73}	10^{-78}	10^{-69}	10^{-75}	10^{-66}	10^{-76}	10^{-65}	10^{-71}
160	10^{-74}	10^{-79}	10^{-78}	10^{-83}	10^{-70}	10^{-77}	10^{-68}	10^{-74}	10^{-65}	10^{-75}	10^{-63}	10^{-70}
170	10^{-73}	10^{-76}	10^{-76}	10^{-81}	10^{-69}	10^{-76}	10^{-67}	10^{-73}	10^{-63}	10^{-74}	10^{-59}	10^{-66}
180	10^{-71}	10^{-75}	10^{-75}	10^{-80}	10^{-68}	10^{-75}	10^{-65}	10^{-72}	10^{-62}	10^{-73}	10^{-55}	10^{-65}
190	10^{-69}	10^{-73}	10^{-73}	10^{-78}	10^{-67}	10^{-74}	10^{-64}	10^{-70}	10^{-60}	10^{-72}	10^{-53}	10^{-64}
200	10^{-67}	10^{-72}	10^{-72}	10^{-75}	10^{-65}	10^{-73}	10^{-62}	10^{-69}	10^{-58}	10^{-71}	10^{-49}	10^{-62}
210	10^{-65}	10^{-70}	10^{-67}	10^{-74}	10^{-64}	10^{-72}	10^{-60}	10^{-68}	10^{-56}	10^{-68}	10^{-46}	10^{-59}
220	10^{-64}	10^{-67}	10^{-68}	10^{-73}	10^{-63}	10^{-70}	10^{-59}	10^{-67}	10^{-54}	10^{-67}	10^{-43}	10^{-55}
230	10^{-63}	10^{-65}	10^{-66}	10^{-71}	10^{-61}	10^{-69}	10^{-57}	10^{-66}	10^{-52}	10^{-65}	10^{-41}	10^{-52}
240	10^{-61}	10^{-63}	10^{-64}	10^{-70}	10^{-60}	10^{-68}	10^{-55}	10^{-64}	10^{-51}	10^{-61}	10^{-38}	10^{-50}
250	10^{-60}	10^{-61}	10^{-63}	10^{-68}	10^{-58}	10^{-64}	10^{-54}	10^{-62}	10^{-49}	10^{-56}	10^{-35}	10^{-47}

To confirm qualitatively the effect of enhancing the probability of fusion, the trend of the potential curve was obtained on varying the temperature[12] in the range 100 - 300 K, in the case of Palladium. It can be seen that both the height and the thickness of the potential barrier are less in the impure metal ($J \approx 0.75\%$). Fig.1 shows an example of the potential curves obtained.
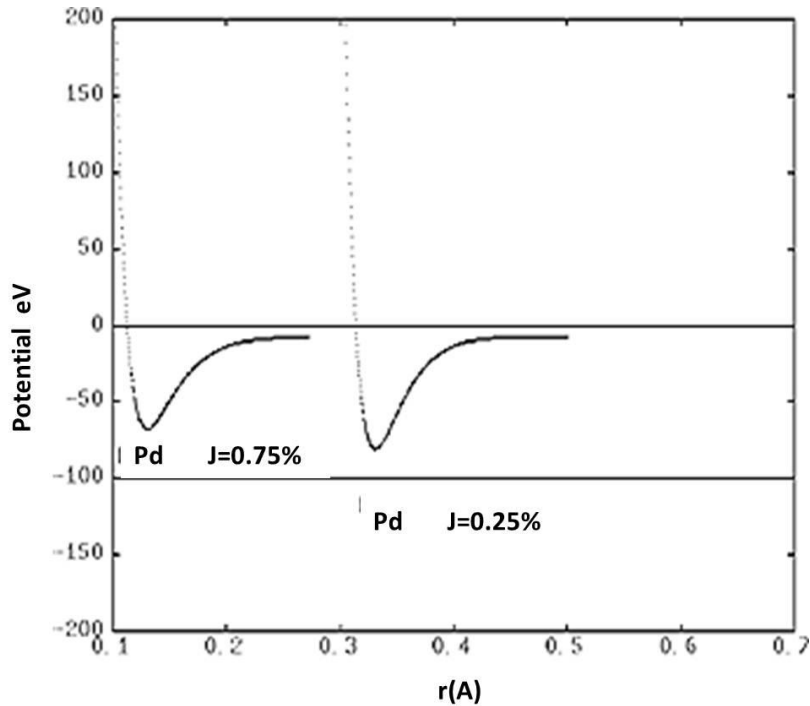

Fig.1. - Comparison between the potentials (14) and (17), in the presence of D_2 for $J \approx 0.75\%$ and $J \approx 0.25\%$, respectively, at temperature T = 290 K. In the first case, both the height and the thickness of the potential barrier are reduced.

4. Conclusions

The present study was to demonstrate if and how the deformation of the crystalline lattice and the formation of a micro-crack could influence the process of fusion at room temperature. More precisely, we calculated numerically the probability of fusion within a micro-crack, comparing it with that calculated on the surface to evidence a possible enhancement effect. The factors which most catalyse the fusion reactions remain however, in the three-dimensional case, the percentage of impurities *J*, the deformation of the lattice and the consequent formation of micro-cracks, as can be seen by comparing Tab.1 and 2. Further, tunnelling in the presence of deuterium loading was analysed, observing that, from the *theoretical* point of view, the phenomenon can be treated as an internal perturbation of the lattice. As shown in Fig. 1, it was found that in the presence of loading, the tunnelling appears enhanced due to the reduction[1], in both height and thickness, of the barrier "K". The loading seems therefore to be an important factor conditioning the phenomenon of fusion. One of these mechanisms essentially "consists" of a kind of chain reaction between deuterons and plasmons, catalysed by the deformations and micro-cracks which arise in the structure as a result of variations in the thermodynamic conditions and other causes, such as deuterium loading.

This was hypothesised in the present paper and constitutes one of the principal motives of its inspiration. It is however possible to confirm that the initial results obtained so far validate the hypothesis presented here.

5. References

[1]   F. Frisone: *Can variations in temperature influence deuteron interaction within crystalline lattices?*, Nuovo Cimento D, **18**, (1996) p.1279.

[2]   K. Sumino: *In Point and extended defects in semiconductors*, Nato Asi ser. B, Vol. **202** (Plenum Publ. Corp.) (1988), pp. 77-83. J. Price Hirt and J. Lothe, *Theory of dislocation* (McGraw Hill) (1968), p.463, eqs. (14-46)

[3]   F. Frisone: *Deuteron interaction within a micro-crack in a lattice at room temperature accepted for publication,* june 13,2000; Fusion Tecnology Vol. 39 mar. 2001.

[4]   M. Rabinowitz: *High temperature Superconductivity and cold fusion*, Mod. Phys. Lett. B, **4**, (1990) p.233.

[5]   M. Fleishmann and S. Pons: *Electrochemically Induced Nuclear Fusion of Deuterium*, J. Electroanal. Chem*, **261**, (1989) pp.301-316, and erratum, Vol. **263**, (1989) pp.187.

[6]   Heui Kyeong An. et al.: *Analysis of Deformed Palladium Cathodes Resulting From Heavy Water Electrolysis*, Fusion Technology Vol. **27** (1995) pp. 408-415.

[7]   J. Price Hirt and J. Lothe: *Theory of dislocation*, McGraw Hill, Z. Phys., (1960) pp.156:457.

[8]   F. R. N. Nabarro: Proc. Roy. Soc. **A 209**, (1952) p.219, Adv. Physisc p. 1,271.

[9]   J. Friedel : *Dislocations*, Chapter **V**, (1960) pp.116 – 458.

[10]   M. Yu. Gutkin and I. A. Ovid'Ko: *Disclinations, Amorphization and Micro-crack Generation at Grain Boundary Junctions in Polycrystalline solids*, Philosophical Magazine **A**, Vol. **70**, N° 4, (1994) pp. 561-575.

[11]   M. Baldo, R. Pucci, Plasmons Enhance Fusion, Conf. Proceed. Vol.24 undersatnding Cold Fusion Phenomena, Eds. R.A. Ricci, E. Sindoni and F. De Marco. SIF, Bologna (1989) p. 283.

Usefulness of Quasi-Particle Ion Band States in Modeling LENR Processes

T.A. Chubb
Greenwich Corporation

Abstract. The density of atoms with 3 or more electrons is determined by Pauli exclusion. Conduction electrons in a metal and reactant deuterium atoms are in Bloch function form, in which corresponding positions in a lattice are equivalent. 2-dimensional symmetry D-atoms are thin, flat, and have reduced Coulomb repulsion between pairs. Fusion takes place inside an interface between an ionic crystal and an epitaxy metal layer. 2-dimensional and 3-dimensional systems are different. Both are real, benefit from shock stimulation, and are Bloch systems; but they require different environments.

1. Introduction

Low Energy Nuclear Reaction (LENR) processes are new types of catalyzed reactions. They depend on causing potential reactants to assume non-classical geometric configurations. Nature does this sort of thing when it creates a metal. But we are now so familiar with a metal's non-classical geometry that we accept it as a routine part of the Quantum Mechanics of solids and liquids. When electrons become part of the electron medium of a metal that carries electricity, we call them quasiparticles. Their charge is "coherently partitioned". They have adopted a many-centers[1] geometry modeled by Felix Bloch. Bloch function physics explains how a solid with a density greater than that of insulators like salt can be a good conductor of electricity.

LENR processes are those in which a laboratory chemical process can cause some sort of nuclear reaction to occur.

LENR processes that produce measurable heat or measurable quantities of transmutation products are of primary interest. There are secondary LENR processes that can occur when an overvoltage main stream process produces a 2-dimensional symmetry product and the process is disturbed or interrupted. The result can be rare side-effects like those that cause MeV nuclear particles to be produced. These strange quantum processes when reproducible have important diagnostic value.

There is no single road to identifiable LENR products

This paper considers 3 classes of process:

Production of heat in electrochemical systems
Production of heat in gas loading systems
Production of MeV particles resulting from overvoltage electrolysis LENR

We first consider the physics by which heat is produced in gas loading systems.

2. Quasiparticle Physics

Quantum Mechanics textbooks typically start off with solving problems like the behavior of an electron in a harmonic potential well, an electron in an inverse square potential (hydrogen atom), or a particle-in-a-box. In these problems there is an identifiable center-of-mass. Bloch asked the question, what happens when the electron is in lattice electric field that extends in 3 directions in space and repeats and repeats forever? In this problem there is no identifiable center-of-mass. Such electrons are called quasiparticles. Corresponding positions in each unit cell of the lattice are equivalent. The charge in each unit cell is its partition fraction. This idealized picture is clearly unphysical and has no boundaries, but the solutions to

Bloch's lattice potential proved effective in describing the observed behavior of electrons in a real metal to within a few layers of the metal's surface. Most of a metal's electrons are not involved in conducting electricity and are permanently part of the metal's atom lattice. Only the quasiparticle electrons carry the electric current. LENR physics is quasiparticle physics applied to deuterons, and in some cases to other ions like protons and Li^+ ions.

Reaction rate modeling of deuteron quasiparticle systems can be studied using time-dependent Schrodinger wave equations, or it can be studied using stationary state wave equations plus time dependent perturbation theory to connect "initial" and "final "states. When one is using stationary state wave equations, one has the option of representing them in terms of a sum over Wannier functions. Wannier functions portray quasiparticles as a sum of random snapshots of collapsed many-centers wave functions. I think it is easier to understand the physics if one avoids the Wannier function approach. I also adopt the view that a complete fusion reaction may occur in successive steps in which the final state of step 1 is the initial state of step 2. In this picture, a sequence of metastable states plays a major role in LENR fusion events. Each transition delivers heat to the adjoining metal lattice.

3. 2-Dimensional Symmetry Reactions

We start our study by focusing on 2-dimensional symmetry LENR. 2-dimensional DD-fusion reactions are examined because they are the easiest to picture. They are called DD reactions rather than dd reactions, because the deuterons are always neutralized by an electron. D designates a D atom. A D atom is a D^+ ion plus its accompanying electron. Neutralization occurs because it is required by equilibrium chemistry, which insists on minimizing system Gibbs free energy. By an electron I mean a quantum of electron charge. In our initial simplified picture we ignore a requirement for imposing coordinate exchange symmetry on an entangled 2-body system, but recognize that the electron is a fermion with spin 1/2. We also recognize that the K-shell of an atom is an entangled spin-zero electron pair.

4. Permeation Transport

It is important to recognize that conduction by quasiparticles is not the only form of D transport. In permeation studies, D quasiparticle conduction competes with D-atom diffusion. D diffusion is driven by the local negative gradient of the interstitial D concentration. D quasiparticle conduction is driven by a difference in D concentration at entry and exit boundaries of a discrete finite volume of ordered lattice.

5. Gas Loading Reactions with ZrO_2 + NanoPd Catalyst

Arata and Zhang (A-Z) made major progress toward production of DD fusion heat when they first used ZrO_2 + NanoPd Catalyst.[2] In switching from Pd black they introduced a highly stable ionic solid into their composite catalyst. ZrO_2 has a large negative Gibbs free energy, which means its crystalline structure is not easily influenced by adjacent layers of metal. The metal is a much more malleable lattice component.

A-Z made a second major step when they switched from using electrolysis to gas loading as their means of adding deuterium to the nanoPd employed.[3] Iwamura had previously made a similar discovery when he discovered that measurable heat could be produced by diffusion of deuterium through a plate with embedded CaO.[4] CaO also has a highly negative Gibbs free energy. These developments suggested that the interface between stable oxides and Pd metal is a likely site for deuteron quasiparticle transport and DD fusion reactions.

6. Essential Role of Pauli Exclusion

Pauli exclusion as applied as an axiom in Quantum Mechanics includes two features. The primary feature is that there is a limit to the number of electrons that can occupy a cell in quantum phase space. Quantum phase space is a 6-dimensional theory space in which occupyable cells are designated by position

coordinates x,y,z and momentum coordinates p_x, p_y, p_z. Adding a spin phase space dimension doubles the density of a solid. Pauli exclusion as applied to electrons largely determines the density of atoms having atomic number greater than helium. The electrons largely determine the density of condensed matter because condensed matter is nothing more than an assembly of contacting atoms. In contrast, protons, neutrons, and nuclei play almost no role in determining the density of atoms and solids. This is an enormously important aspect of quantum physics. It also applies to white dwarf stars,[5] and is confirmed by their difference from neutrons stars. White dwarf stars are supported by a completely degenerate electron phase-space lattice. Neutron stars are dwarfs that have lost their electron-based structure by inverse beta decay. White dwarfs have the mass of the sun in a volume equal to that of the earth. Neutron stars have the mass of the sun in a volume whose diameter is that of Washington, DC.

7. Interface between Perfect Crystal Surface and Epitaxy Metal Layer

ZrO_2 crystals appear to be able to provide flat faces on which there are areas with perfect lattice order. Imperfect Pd metal seems able to configure itself so as to form an epitaxy fit to this layer.[6] When a diffusing D encounters the interface volume containing an area of lattice with perfect order, it switches to quasiparticle form. The D atom suddenly becomes a superthin flat atom, as shown in Fig. (1).

If the perfect area exceeds 1000, or maybe 10,000 contacting lattice atoms, additional important physics occurs. The superthin flat atoms have at thickness of 0.001 or maybe 0.0001 times the thickness of a normal metal layer. It then becomes possible for two flat atoms to occupy the same volume of space. Their joint occupancy is no longer prevented by Coulomb repulsion. The required area of perfect lattice order for hosting double flat atoms has been calculated based on a requirement for system energy minimization..

The double flat D atom is a form of flat ^{4}He. Successive momentum transfers deliver released nuclear energy to quasiparticle electrons in the adjoining bulk Pd metal lattice.

Flat ^{4}He extends to a boundary of the perfect order region. At the boundary the flat ^{4}He converts to spherical atom form. This conversion to spherical form completes the primary fusion process.

8. Reduction of Coulomb Repulsion

Fig. 2 shows pictorially why the large area occupied by a super-thin geometry of individual D quasiparticles reduces the Coulomb repulsion between two parallel D atoms. The partition fraction local charge associated with the area next to one of the ionic crystal atoms is repulsed by the same segment area of local charge in its neighbor. Adding up all these neighbor-neighbor repulsions leads to a segment-segment repulsion of $1/N_{cell}$, where a segment area roughly that of a normal spherical D atom cross section. See Eq. (1). The means that the larger the area of perfect order on the ZrO_2 face, the lower the energy of the fusion product ^{4}He. It also means that system energy is lowered if the flat atom can move so as to expand its area.

$$
\text{For a pair of flat atoms at small separation distance } d, \text{ the Coulomb force } \mathbf{F}_{Coul} \text{ is:}
$$

$$
\mathbf{F}_{Coul} = \sum_1^{N_{cell}} \left(\frac{e}{N_{cell}} \right)^2 \left(\frac{1}{d} \right)^2
$$

$$
\text{As } N_{cell} \rightarrow , \quad \mathbf{F}_{Coul} \rightarrow 0 \qquad \text{Eq. (1)}
$$

The same process that allows flat D atoms to form ^{4}He allows flat ^{4}He atoms to form flat ^{8}Be and flat ^{12}C. These entities are seen as the players in Mossier-Boss's CR39 studies.[7]

Spherical Atom Change into Flat Atom

●

Spherical Atom

_____

Flat Atom

_____

Same volume
1000 times thinner

edge view   side view
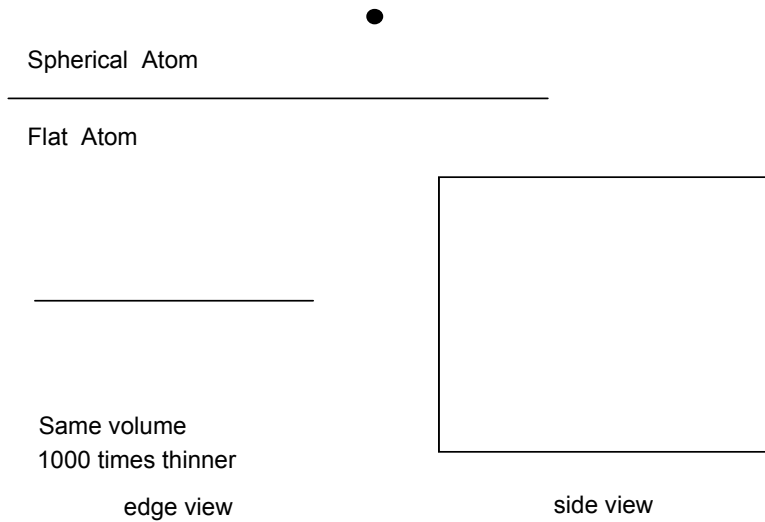
Fig. 1 - A normal spherical atom changes into a flat atom. Its volume is preserved but it becomes much thinner. If the area covers a 1000 atom array, the atom's thickness is reduced by a factor of 1000.

Flat Atom Has Lower Coulomb Repulsion

Flat Atoms

Back Plate

Front Plate

Thick Spot
Back Plate

Thick Spot
Front Plate

As plates approach each other, spot on bottom plate
repels only adjacent spot on back plate

Sum over all spots makes atom-atom repulsion
proportional to 1/number of spots
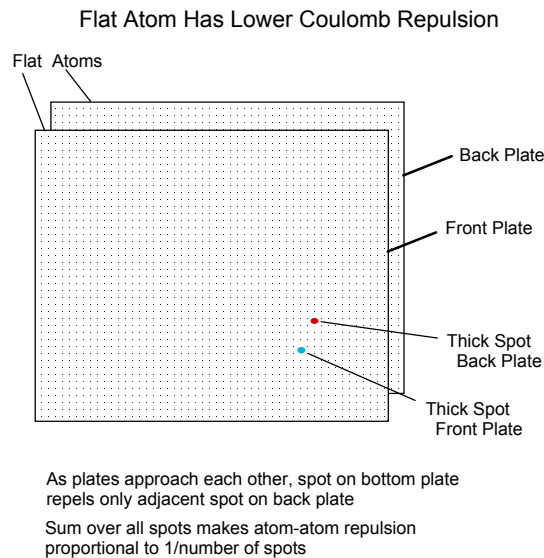
Fig. 2 - Flat deuterium atoms have an array of relatively thick spots. When two flat D approach each other and are separated by nuclear scale distance, a thick spot on the one is repelled only by the corresponding thick spot on the other. Summing over the repulsion potentials shows that the atom-atom repulsion is reduced by the number of thick spots in the array, designated N_{cell}. Each atoms is said to be coherently partitioned into N_{cell} equivalent spots. See Eq,(1).

Apparently similar flat atoms are produced from flat Li atoms fusing with flat D and H atoms in Oriani's CR39 studies.[8] In some of the Oriani experiments the stable ionic crystal involved could be NiO, but in Mossier-Boss's case it may be that the crystalline plastic container used to house the electrolysis cell could be the ordering crystal. In both cases the crystal that imposes lattice order may be an ionic crystal formed by oxidation of an impurity in the electrolyte employed, or on the containment vessel.

9. Interruption of Fusion Cascade

Mossier-Boss and Oriani have observed MeV-energy particle tracks that start and end inside CR39 plastic detectors. The source of these tracks is believed to be the breakup of a metastable ^{8}Be or ^{12}C flat nucleus accompanying its transition to normal atom form. The flat nuclei are stable when residing in their birthing interface. When a flat atom is released from its birthing interface, it can temporarily adopt an independent existence. When electrolytic loading is employed, flat are nuclei probably rare side products of overvoltage electrolysis. Also, it may be that on some occasions the energy transfer cascade that leads to a flat ^{8}Be and ^{12}C atom can be interrupted prior to its transition to its ground state. It is predicted, but not certain, that no CR39 double or triple tracks will be observed in gas loading experiments because of nearly reversible chemistry.

10. 3-Dimensional Symmetry Fusion

The discovery of cold fusion by Fleischmann and Pons appears to be the result of the fusion of 3-dimensional symmetry D quasiparticles in electrolytically loaded PdD$_x$ where x > 0.85. 2-dimensional and 3-dimensional systems are different. Both are real, benefit from shock stimulation, and are Bloch systems; but they require different environments.

To explain 3-dimensional cold fusion it is helpful to examine the behavior of atoms in optical lattices.[9] An optical lattice is an array of potential wells separated by barriers created by interfering laser beams. Bose atoms show different behavior when the barriers between potential wells are high than when they are low. When high, the atoms behave as "particles"; when low, they behave as quasiparticles. When high, but not too high, the center of each potential well is occupied by a "particle", while the periphery is occupied by the partition-fraction of a shared quasiparticle. In PdD$_x$ with x near 1, the periphery of the octahedral sites of Pd metal plus the centers of the 2 tetrahedral sites constitute a communication network of shallow potential wells. This network can become occupied by D quasiparticles in the same manner that the interface volume in a 2-dimensional fusion system becomes occupied. Therefore, paired 3-dimensional quasiparticles are subject to the same reduction in Coulomb repulsion between overlapping partners as occurs with 2-dimensional quasiparticles.[10]

11. A Historic Experiment

Oriani and Fisher have described an experiment in which they constructed an electrolysis cell in which they placed paired CR39 detector detectors facing each other in the gas space above the cell's mixed H$_2$ and O$_2$ offgas. They observed a shower of MeV particles from a source that moved during the during detector exposure interval. They wrote, "It is clear from Fig. 3 that the shower of charged particles that created the tracks originated somewhere in the region above the lower left corner of the chip. One can also infer that the source of the particles was not stationary during the duration of the burst because of the absence of circular symmetry in the density distribution. .... The intersection of these surfaces occurs approximately 2 mm from the chip surface (Fig. 5B). ..... ¶ ..... . This suggests that a fairly compact source of energetic particles moved away from the chip surface as it rose ....we estimate that the burst produced about 250,000 charged particles ..... ¶ ..... . One might expect that a shower of particles near one chip would have affected the other; indeed this is the case ...."

Based on this description I concluded that Oriani-Fisher showers were caused by clusters of very thin "flake" atoms.[11] It seems to me that for an entity to be suspended in a slowly rising gas stream such as produced by electrolysis requires that the entity be incomparably less dense that any previously known macroscopic material. The flat ^{8}Be atoms described in this paper would seem to fit this requirement

12. Don't Be Too Pure

It is probably desirable that the hydrogen gas that is used to chemically reduce ZrO$_2$ + nanoPd catalyst during its preparation should not be too pure. The creation of an epitaxy layer on an ionic crystal requires

an assembly of Pd fragments, as described by Barcaro et al.[6]. Having both interstitial H and D atoms within the Pd metal should be helpful.

13. References

[1] T.A. Chubb, "Many-Centers Nuclei", *Infinite Energy*, **Vol. 13, Issue 74**, 44 (2007).

[2] Y. Arata and Y-C Zhang, "Formation of condensed metallic deuterium lattice and nuclear fusion", *Proc. Japan Acad.* **78B**, 57 (2002).

[3] Y. Arata and Y-C Zhang, "Development of 'DS-Reactor' as the practical reactor of 'cold fusion' based on 'DS-cell' with 'DS cathode'", *Proc. ICCF12*, pp. 44-54 (2006).

[4] Y. Iwamura, T. Itoh, N. Gotoh, M. Sakano, I. Toyoda, and H. Sakano, "Detection of anomalous elements, x-ray and excess heat induced by continuous diffusion of deuterium through multi-layer cathode (Pd/CaO/Pd)", *Proc. ICCF7*, 167-171, (1998).

[5] S. Chandrasekhar, An Introduction to the Study of Stellar Structure, (University of Chicago Press, Chicago IL, 1939) pp. 412- 486.

[6] G. Barcaro, A. Fortunelli, G. Rossi, F. Nina, and R. Ferrando, "Epitaxy, Truncations, and Overhangs in Palladium Nanoclusters Adsorbed on MgO(001)", *Phys. Rev. Lett.* **98**, 156101 (2007).

[7] L. Forsley, P. Mossier-Boss, "Quantitative Spatial Analysis of Pd/D Co-Deposition Iduced Particle Tracks" *Proc. ICCF14*, In Press.

[8] R.A. Oriani, "Reproducible Evidence for the Generation of a Nuclear Reaction During Electrolysis", *Proc. ICCF14*, In Press.

[9] D. Jaksch, C. Bruder, J. I. Cirac, C. W. Gardiner, and P. Zoller, "Cold Bosonic Atoms in Optical Lattices", *Phys. Rev. Lett.* **81**, 3108 (1998).

[10] M. McKubre, F. Tanzella, P. L. Hagelstein, K. Mullican, and M. Trevithick, "The Need for Triggering in Cold Fusion Reactions", *Proc. ICCF 10*, pp. 199-212. (2006). See pp. 202-203.

[11] R.A. Oriani and J.C. Fisher, "Energetic Charged Particles Produced in the Gas Phase by Electrolysis", *Proc. ICCF 10*, 567 (2006).

[12] T.A. Chubb, "III. Bloch Nuclides, Iwamura Transmutations, and Oriani Showers", *Proc. ICCF10*, 685 (2004).

Evaluation of d/d Reaction Rates in Metallic Lattices as a Function of the Deuteron Energy. A Phenomenological Model of Nuclear Fusion in Solids

J. Dufour and X. Dufour

CNAM - Laboratoire des Sciences Nucléaires, 2 rue Conté, 75003 Paris - France

E-mail: 3jdufour@laposte.net

Abstract. Recently, unexplained enhancements of d/d reaction rates in solids were observed. This enhancement is lower than a factor of 10 at low energies of the deuteron (a few keV) and as high as a factor of 10^{18} for extremely low energies (0,025 eV). Based on the calculation of d/d reaction rates in a lattice, a phenomenological model is proposed to infer the enhancement that can be expected for deuterons of energies in between these two extremes. A potentially interesting zone (between 500 and 2000 eV) has been identified.

1. Introduction

Recently, experiments on d/d reactions were run, in 2 zones of the reacting deuteron energy: the zone of low energy (3 to 20 keV) [1] and the zone of extremely low deuteron energy (eV level, SPAWAR heavy water electrolysis experiments [2]). In [1], the cross sections of the d/d reactions were measured using a high energy proton (deuteron) generator. In [2], track-etching detectors (CR 39 chips) were used to record tracks of high energy charged particles. The number of tracks recorded gives an estimation of the reaction rates (assuming these tracks come from d/d fusion products). In [1] and [2] an enhancement is observed compared to the calculated reaction probabilities. The enhancement factor is 2 to 10 in [1] and many orders of magnitude (10^{18}) in [2]. This was in both cases attributed to the screening effect of the electrons of the metallic lattice where the reactions take place.

In [3], the contribution to the d/d reaction rate enhancement, of an attractive Yukawa type of potential, acting between nucleons, was evaluated. Its effect was shown to be of the same order of magnitude as the screening of the lattice electrons for deuteron energies of a few keV [1]. Nevertheless, the combined effect of this potential and of the screening of the lattice electrons (150 to 300 V) was shown not to be sufficient to explain the whole enhancement [1,3]. Under SPAWAR electrolysis experimental conditions, the effect of the Yukawa potential was found to be negligible compared to the screening effect of the lattice electrons, which in turn fails by a many orders of magnitude to explain the enhancement observed [3].

A coupling between the deuterons in the target with the incident deuteron beam was thus suggested [3] to explain the enhancement observed, by fusion reactions taking place between the deuterons already trapped in the target. The consequences of this hypothesis on d/d reaction rates are examined, for energies of the incident deuteron beam varying from 2 to some 100 000 eV.

2. Evaluation of d/d reaction rates as a function of the reacting deuteron energy

Using the model developed in [3], the reaction rates and the power production resulting from the interaction of a 1 W beam of deuterons with a metallic target (palladium) loaded with deuterium (1 mmole, loading ratio 0.7), was evaluated as a function of the incident deuteron energy. For a thick target, the reaction rate r is: $r(cm^{-3}s^{-1}) = \sigma(cm^2)\varphi(cm^{-2}s^{-1})N_0(cm^{-3})$, with $\sigma\,(cm^2)$ being the reaction cross-section, $\varphi\,(cm^{-2}s^{-1})$ the deuteron flux and $N_0\,(cm^{-3})$ the deuteron concentration in the target. From [3], the reaction cross section is: $\sigma = \sigma_{geom.}P(E_d)$ with $\sigma_{geom.}$ being the geometrical cross section of the target deuteron ($\approx 0.5\,barn$) and $P(E_d)$ the probability for the deuteron of energy E_d, to tunnel through the potential barrier of the target deuterons, calculated from [3]. The probability $P_{S+Y}(E_d)$ of tunneling through the screened Coulomb potential under the influence of the Yukawa potential is $P_{S+Y}(E_d) = F_{S+Y}P_B(E_d)$, the probability of tunneling through

the bare Coulomb potential being $P_B(E_d)$ (corresponding to a rate r_B) and F_{S+Y} being the enhancement factor due to the screening of the electrons and the action of the Yukawa potential. Hence, $r_{S+Y} = F_{S+Y} r_B$. The deuterons concentration n_0 (cm^{-3}) outside the target, corresponding to a deuteron flux (mass m and energy E_d (J)), depositing 1W on the target is:

$$n_0 = \frac{1}{100 E_d} \sqrt{\frac{m}{2 E_d}} \ , (cm^{-3}) \ \text{ corresponding to a flux: } \varphi = \frac{1}{E_d} \ (cm^{-2} s^{-1})$$

For 1 mmole of deuterium (d) loaded in a palladium target with loading ratio 0.7:

$$N_0 = 4.74 * 10^{22} \ (cm^{-3}, \text{ palladium thickness:} 127 \mu m)$$

For an incident deuteron flux of 1 Wcm^{-2} and for 1 mmole of deuterium in the target, the power produced from the fusion reactions is (after correction for the target thickness):

$$W_{S+Y} = r_{S+Y} \frac{Q}{2} \ 1.6 \ 10^{-13} * 0.0127 = 7.39 \ r_{s+y} \ 10^{-15} \ \left(J.s^{-1}.cm^{-2}.mmole^{-1} \right)$$

Q= 1+ 3+ 0.83+ 2.44= 7.27 MeV is the total energy of the two main d/d fusion channels.

3. Effect of electron screening and Yukawa potential on reaction rates and energy production

The reaction rates r and the power produced W, were evaluated, for the incident deuteron energy varying from 2 to 100 000 eV. Calculations were run in two situations: bare Coulomb potential (r_B and W_B) and screened (screening energy 150 V) Coulomb and Yukawa potential (r_{S+Y} and W_{S+Y}). Results are summarized in *Fig. 1* and *Fig. 2*
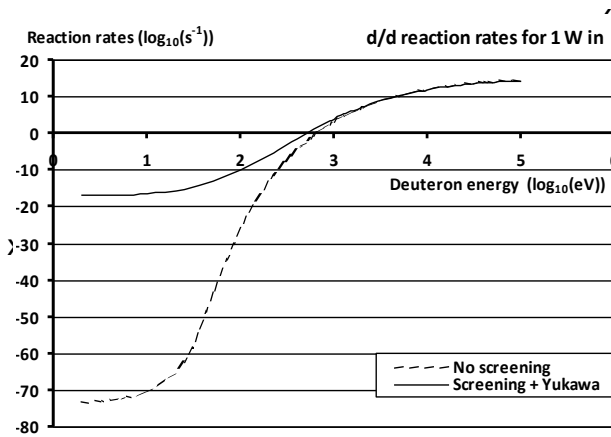
Fig. 1 – d/d reaction rates for 1W in.   Fig. 2 – Power out for 1W in.
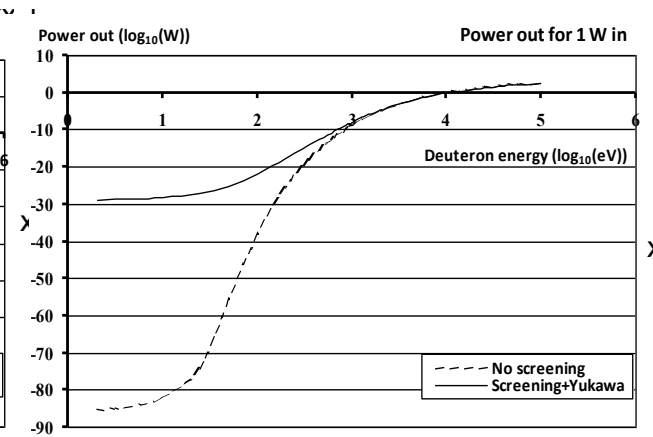
It can be seen from *Fig. 1*, that for deuteron of energy 0,025 eV, the reaction rates r without screening, are extremely low ($1.32*10^{-74}$ reactions per second), corresponding to a very small amount of produced power W ($1.9*10^{-88}$ W). Taking into account the screening effect of the electrons acting on the combined repulsive Coulomb potential and the attractive Yukawa one, considerably increases the reaction rates r_{S+Y} ($7*10^{-18}$ reactions per second) and the power production W_{S+Y} (some $1.1*10^{-31}$ W). At these extremely low energies, the contribution of the Yukawa potential and of the energy of the deuteron (up to 2 to 3 eV), are negligible compared to the screening of the electrons. Anyhow, the reaction rates are still very much lower than what is observed in SPAWAR experiments (which can be estimated to be round 10^{-1} reactions per second ($\approx 7*10^4$ in 1 week), assuming that the charged particles observed in SPAWAR experiments are the signature of d/d reactions. At energies of the deuteron round 2 to 3 keV, the effects of the screening of the electrons and of the Yukawa potential are of the same order of magnitude, but their combined effects do not account for the totality of the enhancement factor observed at these energies. In [3] it was thus proposed that the incoming deuteron could

couple with the deuterons already present in the lattice, inducing additional fusion reactions between them. A phenomenological model based on these ideas is proposed.

4. The resonant coupling phenomenological model

4.1 The concepts that back the phenomenological model

A plasma is a globally neutral collection of free charged particles, with the same concentrations: 10^{20} m^{-3} (T$\approx$ 10 keV) in nuclear fusion and 10^{29} m^{-3} (T$\approx$ 3 keV) in dense astrophysical plasmas. In both cases, nuclear fusion reactions occur at a high rate, only because the high thermal energy of the hydrogen isotopes ions allows significant tunneling through their Coulomb potential barrier.

In order to measure the d/d nuclear fusion reactions rates, use is made of a deuteron gun that projects deuterons on a target loaded with deuterium, under vacuum and with a controlled energy. Recently it has been experimentally observed [1], that at low energy (3 to 20 keV) of the impinging deuteron, the reaction cross sections are increased by a factor that can reach 2 to 10 compared to what is expected from the Gamow factor at these low energies. This was attributed [1], to the screening effect of the electrons of the target. The corresponding potential was experimentally found to be as high as 500 V. It is only 150 V when evaluated from the Thomas Fermi approximation (low temperature of the deuterons) and some 300 V when considering the Debye-Hückel one (high temperature > tens of keV of the deuterons). Similar screening effect is invoked when considering the calculation of alpha disintegration constants from the tunneling of the alpha particle through the Coulomb barrier of the daughter nucleus of the decaying atom [1,4].

A screened potential naturally arises for the conduction electrons in a metal. The screening acts on the pseudo potential that the electrons of the conduction band experience from the cations in the lattice. In first approximation, this unscreened pseudo-potential is taken equal to zero for distances lower than a distance in the order of the Bohr radius and equal to the Coulomb one for distances higher. This is a semi-empirical way to simplify, in a representative way, the wave functions of the electrons in the conduction band of the metal, which mostly ignore the cations of the metal, (hence the empty lattice name of the method) [5].

The interactions of charged particles with a metallic lattice, are understood in two extreme situations:

- Extremely low energy charged particle: metallic hydrides can be viewed as the typical interaction. They have a metallic character (electrical conduction). The protons (deuterons) in the lattice are very mobile: their diffusion coefficients are very high and they move under the influence of an electrical field. In that respect, metallic hydrides can be viewed as a plasma of protons (deuterons) and electrons embedded in the lattice of the host metal. But contrary to electrons, protons (deuterons) in a lattice experience the screened full Coulomb potential of the lattice ions and not the screened pseudo-potential, resulting in potential wells at tetrahedral or octahedral sites, where the hydrogen isotopes find a stable equilibrium position. So they are not completely free to move, but the potential wells have a depth E_A (activation energy of the diffusion process) in the order of a few tenths of eV. They are thus easy to activate (acquiring an energy higher than E_A) and can thus move more or less freely.

- High energy charged particle. This is typically the interactions of an alpha particle (a few MeV energy) impinging a metallic lattice (in that case the interaction would be similar with a non metallic lattice) the alpha looses most of its energy through inelastic collisions with the electrons of the lattice (ionization, resulting in the range of the alpha measured by nuclear physicists) and rarely with the nuclei of the lattice.

- A situation much less explored, is that of a metallic lattice loaded with deuterium, submitted to a flux of deuterons of energy between say a few eV to 15 000 eV. In that case, the impinging deuteron will mainly exchange energy with the loaded deuterons, through very efficient elastic collisions (same mass). A non equilibrium situation is created where the hotter part of the deuterons partition could activate the main deuteron population, inducing movements of the deuterons in the lattice beyond the diffusion rates observed at thermodynamic equilibrium and yielding an increase of the fusion reaction rates (note that hot spots, even macroscopic, have been observed in certain experiments). Moreover, the possible focusing action of the periodic potential of the embedding metallic lattice ("conduction band" of the activated deuterons) could result in increasing the apparent geometric cross sections determining the fusion reactions rates.

4.2 Proposed phenomenological model

So far, no model exists describing this hypothetical mechanism. It is reasonable to think that it is more and more efficient as the de Broglie wavelength of the impinging deuteron increases with the decrease of its energy E_d (2 eV = 15 000 fm, 10 000 eV = 200 fm). It is thus proposed to describe this interaction by a phenomenological model: a resonant coupling enhancement factor F_C, which adds its effects to the already observed enhancements

due to the electron screening (and to the Yukawa potential for low energies used in [1]). The reaction rates are given by $r_{S+Y+C} = F_C F_{S+Y} r_B = F_C r_{S+Y}$. In this concept, F_C is a function of the energy of the impinging activating deuteron. The Fermi energy E_f of the metal is likely to play a role in this mechanism. The maximum of F_C is thus hypothesized to occur at this energy. The deuteron plasma activation mechanism is rather clear in the case of deuteron gun experiments. It requires some additional hypothesis in the case of electrolysis and more generally of extremely low energy experiments. Modifications of surface and bulk conditions (cracks) of the cathode during electrolysis, conditions of preparation of the cathode (metallurgy and pretreatment, size and morphology of the small metal particles when supported on a porous dielectric material etc…) forced diffusion of deuterons through the embedding metal, could provide explanations for the formation of a hot population of deuterons of energy E_d of a few eV.
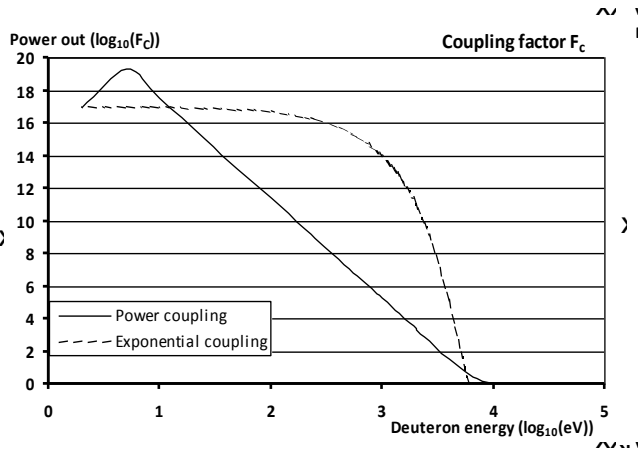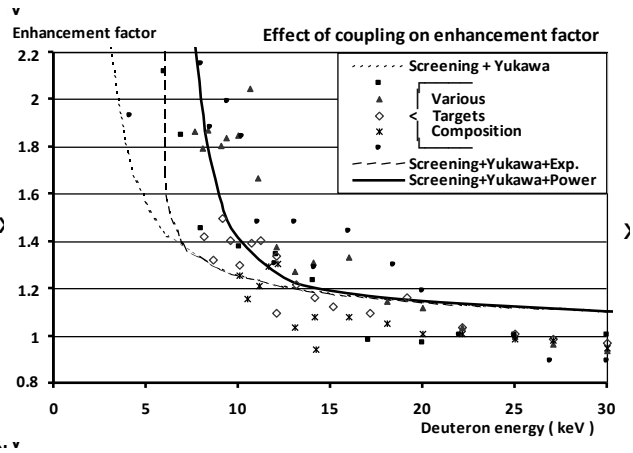

Fig. 3 – Coupling factor F_C. Fig. 4 – Effect of coupling on enhancement factor.

The coupling invoked in [3] could thus be a general phenomenon, extending form extremely low energies (a few eV) to low energies (a few keV) of the deuteron. To define the coefficients of the resonance coupling curve, use is made of the experimental results given by [1] and [2]. In the case of [1], an additional enhancement factor (F_C) of 6 is required for E_d = 5500 eV (see *Fig. 4*). From the experimental results of [2], a reaction rate of 10^{-1} s^{-1} can be inferred. In that case, the energy of the activating deuterons is supposed to be 2 eV. The corresponding calculated (screened) reaction rate $r_{S+Y} = F_{S+Y} r_B$ is $1.3*10^{-17}$ [2], requiring for F_C a value $F_C (2) = 8.14*10^{16}$, giving $r_{S+Y+C} = F_{S+Y+C} r_B = 0.1\ s^{-1}$. Two coupling laws have been examined: a power law and an exponential one.

4.3 Determination of the coupling factor F_C as a function of E_d

4.3.1 Power coupling: in that case, $F_C = 1 + \lambda \left(E_d / E_f \right)^{\pm n}$, + for $E_d \leq E_f$ and - for $E_d > E_f$

λ ($2.24*10^{19}$) is determined by the condition $F_c (2) = 8{,}14*10^{16}$ and n (6.13) by the condition $F_c (5500) = 6$.

4.3.2 Exponential coupling: in that case: $F_C = 1 + \lambda' \exp\left(-n' \left(|E_d - E_f|/E_f \right) \right)$

λ' ($8.31*10^{16}$) is determined by the condition $F_C (2) = 8.14*10^{16}$ and n' (0.034) by the condition $F_C (5500) = 6$. The two laws are shown on *Fig. 3*

5. Effect of the coupling on reaction rates r_{S+Y+C} and power production W_{S+Y+C}

Fig. 5 and *6* give the result of the calculation of r_{S+Y+C} and W_{S+Y+C}, for both coupling laws.

The parameters of both laws have been computed to fit the experimental data at extremely low (2 eV) and low (5500 *eV*) energy of the deuteron. As can be seen in *Fig. 4* the fitting is not very good, for the exponential law at low energy of the deuteron (5500 eV). The power fitting is better (*Fig. 4*). This could be a consequence of the non thermodynamic equilibrium of the populations of deuterons in the lattice. The objective of the phenomenological model is to infer the behavior of the deuterons in the lattice for all energies E_d, from the 2 extreme and experimentally known situations (E_d = 2 eV and 5500 eV). *Fig. 5* shows that the reaction rates

r_{S+Y+C} are significantly increased by the power coupling when compared to the "Screened + Yukawa" reaction rates r_{S+Y}. Values as high as 10^5 to 10^{10} s^{-1} are predicted, for E_d between 500 and 1000 eV, whereas in this zone, r_{S+Y} vary from 1 to 10^5 s^{-1}. It is thought that this energy window could be used in a research program, to optimize the target characteristics. From results presented in [1] it can be seen that the enhancement factor varies very much with the target used. These variations are of much bigger amplitudes than the standard deviations presented in [1]. They can be attributed to the exact characteristics of the target used, hence opening the possibility for optimization. This optimization could be done, by using as an optimizing criterion the neutron emission of the studied targets. This emission is predicted to be significantly higher than the background against which the optimization would done, the calculated r_{S+Y} emission rate. This optimization could result in a very significant increase of the enhancement factor.

Fig. 6 shows that the reaction rates r_{S+Y+C} are considerably increased by the exponential coupling. From *Fig. 3*, it can be seen that this type of coupling is not representative for energies E_d of the deuteron higher than some 3 keV. It cannot be excluded that with the decrease of the energy, the exponential coupling becomes more and more representative (less departure from thermodynamic equilibrium) and that the true coupling is in between power and exponential for lower values of E_d.
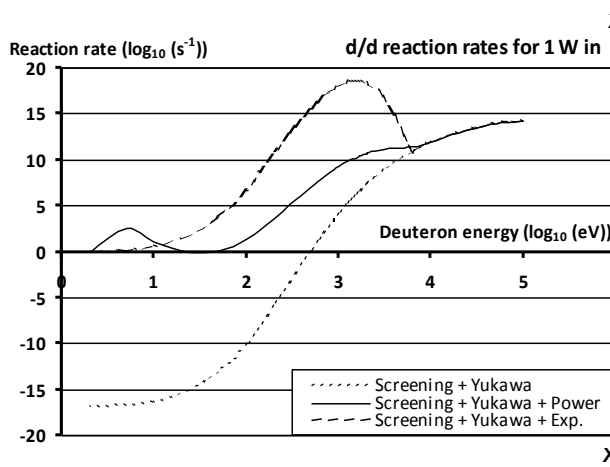
Fig. 5 – d/d reaction rates for 1 W in.   Fig. 6 – Power out for 1 W in.
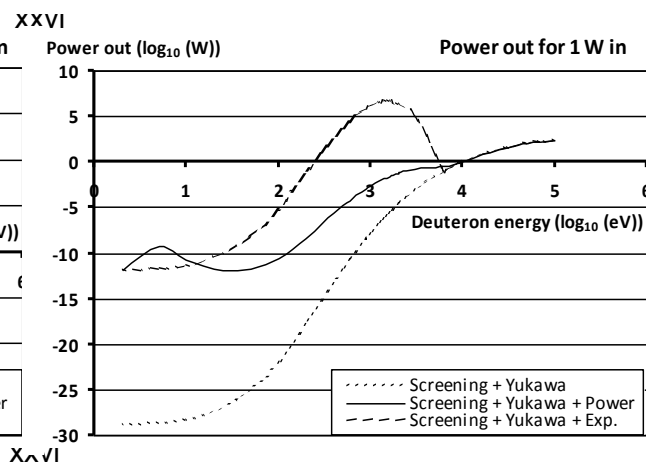
6. Conclusion

Because of the development of surface treatment and electronic industries, ion generators of several kW power are now available on the market. They can produce ion (proton, deuteron) beams of high intensity (several A), with ion energies in the range 100 to 4000 eV and are thus able to work in the 500 to 1000 eV energy window. Technological devices can be imagined, to generate energy by bombarding appropriate targets with such ion beams.

It is thought that much of the work done in the field (on the cathodes physico-chemical characteristics), could be used to test the possibility of this hypothetical coupling. Such materials could be good candidates as targets for this last approach. A prototype has been built in the lab, using a two steps glow discharge to generate the ions and able to produce currents up to some tens of μA [6]. The energy of the ions is in the order of hundreds eV and the hydrogen (deuterium) pressure at the level of the target is 3 to 4 Pa. A neutron detector (helium 3) monitors the fusion reactions that are expected. Experiments will be run to define precisely the requirements for a lab scale ion generator based on a μwave discharge. Finally, more insight could also be gained on what happens in the extremely low energy region (<2 eV).

7. References

[1] A. Huke, K. Czerski, P. Heide, G. Ruprecht N. Targosz and W.Zebrowski, "Enhancement of deuterons fusion reactions in metals and experimental implications". *Physical Review C*, 78:015803, 2008.

[2] P.A Mossier Boss, S.Szpak, F.E Gordon, and L.P.G Forsley. "Use of CR-39 in Pd/D co-deposition experiments". *Eur. Phys. J.appli. Phys.* **40**, 293-303 (2007)

[3] J. Dufour. "Possible existence of an attractive Yukawa type of potential and consequences on the understanding of alpha disintegration constants and d/d reactions at low energy of the deuteron". Journ. of Condensed Matter Nuclear Science **1** (2007) 47-61

[4] Victor A. Erma, "Electrons effects on barrier penetration" *Physical Review* (**105**) p.1784 (1956)

[5] W. Shockley, "The Empty Lattice test of the Cellular Method in Solids" *Physical Review* (**52**) p.866 (1937)

[6] J. Dufour, X. Dufour and D. Murat, "Practical ways to generate protons (deuteron) of energy between 500 and 1000 eV". "*ICCF 15 proceedings*". *Rome 5-9 October 2009*

Role of cluster formation in the LENR process

E. Storms, B. Scanlan
KivaLabs, Santa Fe, NM and Greenwich, CT

E-mail: storms2@ix.netcom.com

Abstract. Presence and absence of expected radiation, occurrence of nuclear reactions having only one apparent product, and transmutation reactions involving addition of more than one deuteron all indicate involvement of large clusters of deuterons in the LENR process. These clusters are proposed to hide their Coulomb barrier and to react with isolated deuterons to produce fusion and to react with larger nuclei to produce transmutation. Members of the cluster not directly involved in the nuclear reaction might be scattered by the released energy, thereby allowing momentum to be conserved and the resulting energy to produce particles having energy too small to be easily detected or to cause easily detectable secondary reactions. Justification of this model is discussed. This proposed model is consistent with most observations, but raises additional questions about the nature of such super-clusters and other ways the energy may be communicated directly to the lattice that will be addressed in future papers.

1. Introduction

Many attempts have been published in an attempt to explain how fusion and transmutation are possible at or near ambient conditions in solid materials. A successful theory must show how the Coulomb barrier is lowered and how the resulting energy is dissipated into the environment. This dissipation process can be imagined to take two forms: emission of energetic radiation or dissipation of energy directly into the environment. If radiation carries the energy, the amount detected should be consistent with the amount of heat produced. Some radiation has been detected but not enough to account for the energy being generated as heat. Consequently, either several processes dissipate the energy or most emitted radiation is absorbed before it reaches the detector. In addition, the energy of emitted particles must be too low to produce secondary reactions that should be easy to detect. This paper will explore one possible mechanism for production of energetic particles fitting these requirements.

The cold fusion process can release a large amount of energy from very energetic nuclear reactions. This aspect of the phenomenon has been demonstrated by too many studies, as reviewed by Storms,[1] to cite here and needs to be accepted as an important characteristic of cold fusion. Conventional nuclear reactions release energy either promptly as radiation, consisting of energetic particles and/or gamma emission, or slowly as radioactive decay. The only known example of direct coupling of nuclear energy to an atomic lattice is the Mossbauer Effect. However, the energy involved in this process is much smaller than that produced by the nuclear reactions associated with cold fusion, which makes this mechanism hard to relate to the cold fusion process. If radiation has sufficient energy, secondary reactions will be detected, which can reveal more information about the process. Absence of such secondary radiation limits the possible energy of the primary energetic particle. Nevertheless, a variety of particle and X-ray energies are reported, which demonstrate that not all energy is being directly deposited in the lattice. In addition, a model must explain the observed complex collection of emission energies and types of detected radiation.

Most models focus on the periodic structure that exists in solid PdD as being the location of the nuclear active environment (NAE). In contrast, this proposal draws attention to the surface of nanoparticles where large clusters of deuterium are thought to form. These clusters are proposed to be involved in the initiation of the fusion and transmutation reactions as well as allowing at least some energy to be released into the environment as energetic particles without producing easily detectable radiation. Logic requires the clusters to contain many more deuterons than has been considered in the past, so called super-clusters.

Although the cluster concept is not new, the full extent of their involvement, their proposed large size, and the location of their formation have not been published before. This paper shows the logical connection between this concept and observed behavior.

2. Discussion

Table 1 summarizes some of the possible fusion reactions. In each case, two products are formed and observed to result when high energy is applied. Two products allow momentum to be conserved while depositing the energy into the environment. If only one product is observed, a different type of reaction must be proposed to achieve the same result.

Table 1. Reactions resulting from fusion involving deuterons.

$$d + d = {}^3He(0.82\ MeV) + n(2.45\ MeV)$$
$$d + d = p(3.02\ MeV) + t(1.01\ MeV)$$
$$d + d = {}^4He + gamma\ (23.5\ MeV)$$
$$d + t\ = n(14.01\ MeV) + {}^4He(3.5\ MeV)$$
$$d + p = {}^3He + gamma\ (5.5\ MeV)$$
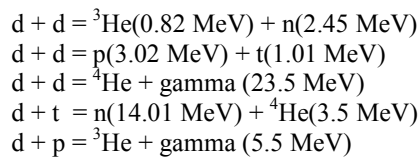
For example, many studies have shown that helium results when extra heat is produced.[1] Because the expected gamma of 23.5 MeV is absent, the reaction cannot occur as written in Table 1. A more complex process must take place. Takahashi[2, 3] proposed that four deuterons came together as a cluster to form two helium nuclei each of which carry away 23.8 MeV and the necessary momentum. Such a reaction conflicts with the absence of signif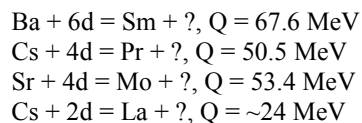icant neutron radiation resulting from the well-known (α, n) reaction, mainly involving lithium, that such high-energy alpha will initiate. Consequently, a small cluster, the members of which completely fuse, is not consistent with observation, even if a plausible process, such as formation of a Bose-Einstein Condensate [4], could create the cluster. While many models have been proposed to avoid some of these issues, each has limitations that encourage a new approach.

Creation of isotopes and elements not present in the initial environment by addition of deuterons to the nucleus of certain elements has been frequently reported.[1] While some elements or isotopes might have been present as contamination, this argument has not been applied successfully to all the observed reactions. Two studies stand out in showing the role of clusters in such transmutation reactions. For the first, Iwamura et al. [5-9] in a series of papers claimed to detect the reactions shown in Table 2. Clusters containing as many as 6 deuterons are required to enter the nucleus as a unit. However, a problem remains to explain how the significant energy released by the process is communicated to the environment. Clearly, something must be emitted that is not detected, as indicated by the question mark.

Table 2. Observed transmutation reactions reported by Iwamura et al.

$$Ba + 6d = Sm + ?,\ Q = 67.6\ MeV$$
$$Cs + 4d = Pr + ?,\ Q = 50.5\ MeV$$
$$Sr + 4d = Mo + ?,\ Q = 53.4\ MeV$$
$$Cs + 2d = La + ?,\ Q = \sim24\ MeV$$

The second study involves the work of Miley et al.[10, 11]. His results, based on use of SIMS, AES, EDX and NAA for analysis, is summarized in Fig. 1[2]. The work is based on the use of thin films of nickel and/or palladium with a small amount of platinum as an impurity from the anode and perhaps a little sulfur as an impurity from the electrolyte, which contained Li_2SO_4 in H_2O. Elemental analysis was made before and after electrolytic action. The general pattern shows the following: regions of atoms having high concentration are found from about mass 106 (Pd) to mass 130; from mass 195 (Pt) to mass 210; and from about mass 25 (S?) to mass 32. The region around nickel (58) shows elements on both the high mass and

---

[1] This work has been previously evaluated1. Storms, E.K., *The science of low energy nuclear reaction*. 2007, Singapore: World Scientific. 312. and is too extensive to cite here.
[2] Although of poor quality, this is the only representation of the summary that is available.

the low mass sides. The question is, "What process can explain these general observations"? Transmutation requires a target nucleus to which something is added. The possible addition of neutrons, protons or deuterons to Pd is explored next.

Figure 2 shows the position of the stable isotopes near palladium with respect to their atomic number and atomic weight. If neutrons are added to palladium, the resulting isotopes would follow a horizontal line on the figure and eventually produce beta emitters. These have half-lives that decrease from minutes to milliseconds as more neutrons are added. To produce the observed elements near the upper limit of the Miley data, a series of decays from parent to daughter would have to take place over a significant length of time as each isotope decayed to another radioactive isotope with gradually increasing atomic number. In addition, the radioactivity is not detected even though this would be an easy measurement. Therefore, transmutation does not result from neutron addition from any source. If protons were added to palladium, the resulting isotopes would follow a line parallel to the one shown on the figure for protons.
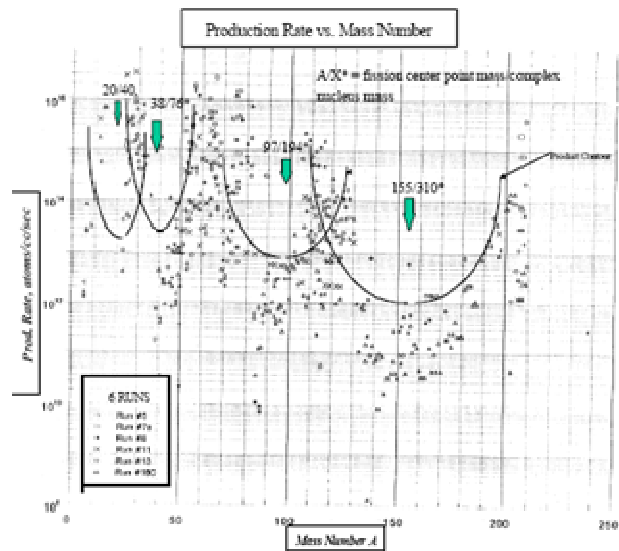
Fig. 1 - Log rate of production vs mass number of elements produced in thin films by electrolysis in $H_2O + Li_2SO_4$.
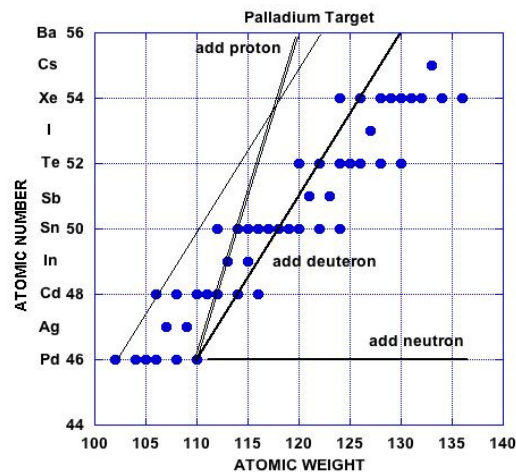
Fig. 2 - Stable elements as a function of atomic weight and atomic number near palladium.

Radioactive isotopes are produced above mass 114, which is not high enough to explain the full range of reported data. Only addition of deuterons results in the full range of observed stable isotopes. This same process can be applied to nickel, platinum and sulfur to give the same conclusion in spite of normal water being in the electrolyte. Apparently, deuterons, regardless of their concentration, produce active clusters

and most transmutation. In the case of elements having a mass lower than nickel, these cannot result from a reaction with deuterons or any other particle. These elements might result from fission of nuclei after addition of deuterons to palladium, as has been suggested by several authors. Because the resulting nuclei are at and near iron, additional energy can be released by formation of these very stable nuclei. Consequently, a certain fraction of nuclei resulting from addition of deuterons to Pd split into two parts during the transmutation process and may account for the frequent reported presence of iron on the palladium cathode of electrolytic cells. These two studies, as well as many others, suggest a role for clusters containing at least 8 deuterons in the transmutation process. Where are these clusters formed?

The only universal feature found in all successful cold fusion experiments are nanoparticles. These form slowly on the surface of electrolytic cathodes, they form as a result of gas discharge, and they are known to be active when certain such materials are exposed to deuterium gas.[12, 13] Consequently, a feature associated with such a structure can be assumed to initiate all of the observed cold fusion reactions.

The difficulty in producing cold fusion indicates a special condition is required before the nuclear reaction can occur, presumably after nanoparticles are formed. This special condition is hard to create, occurs only in small and variable amounts, and presently is produced largely by accidental conditions within the apparatus. Where is this special condition located?

McKubre et al. used the following equation to describe excess power (EP) obtained from wire cathodes in a Fleischmann-Pons cell. [14, 15]

$$EP = M*(x-x_o)^2*(i-i_o)*\delta x/\delta t, \text{ where } x_o = \text{critical average D/Pd of the bulk cathode, } i_o = \text{critical average I/cm}^2$$

We can expand this equation by adding the equation:

$$M = n * [nae], \text{ where } [nae] \text{ is the amount of NAE having 'n' efficiency.}$$

Consequently, the heat producing reaction favors locations where the deuterium concentration is greatest. This location exists at the surface of the cathode in an electrolytic cell and on the surface of nanoparticles.[16-18] The deuterium concentration becomes especially great on the surface of a cathode as the bulk composition approaches unity and on the surface of nanoparticles as they become smaller. This analysis reveals the bulk composition is only important because it affects the surface composition where the nuclear reactions actually occur.

3. Conclusion

The goal of this paper is to show a logical connection between selected observations and a proposed mechanism involving energetic particle emission and super-clusters without describing exactly how the mechanism works. In addition, the proposed mechanism is not likely to be the only one operating. The nature of the proposed super-cluster and its manner of formation will be subjects of future papers.

A mechanism must dispose of energy resulting from a nuclear reaction in a manner consistent with observation and known laws of nature. The same mechanism is expected to operate regardless of the energy source, whether it is fusion or transmutation. The absence of detectable gamma radiation when helium is produced means the energy is either being directly absorbed by the lattice[19-21] or particles are being emitted by an unconventional process and these are absorbed before most can reach a detector. The fact that some particles do reach a detector[22-24] puts greater emphasis on the role of energetic particles and the need to find the unusual mechanism for their creation. Indeed, the nature of these particles and the mechanism of their formation is the unique challenge facing any theory of cold fusion. One solution to this challenge involves clusters, but in a way that has not been suggested before.

Clusters of deuterons are clearly involved in transmutation reactions. Apparently, a variety of new elements are made based on the number of deuterons in an active clusters and availability of suitable targets. Various rules must determine how many d can enter at the same time to avoid producing radioactive products, which are rarely found. We next assume the same mechanism is operating to cause fusion between deuterons.

The fusion rate will depend on the number of active clusters and the concentration of deuteron targets. Consequently, the fusion rate will be more sensitive to the deuterium concentration than is transmutation. Because clusters are made from deuterium and form where the deuterium concentration is

greatest, fusion as expected to occur close to where clusters form. Transmutation, on the other hand, is expected to occur at a distance from the site of cluster formation, as has been observed.

For any nuclear reaction to occur, the clusters must hide their nuclear charge. Fusion would require less reduction in charge than does transmutation, hence would involve smaller[3] hence more numerous clusters. However, the charge-hiding process requires a critical number of deuterons to be in a cluster before it becomes active. Even though small clusters are more numerous, they are not able to initiate a nuclear reaction until a critical number of deuterons are combined. This charge-reduction process is an essential feature of this model, but will not be addressed here.

Once a cluster reacts to produce a nuclear reaction, energy is dissipated. While this process might involve direct coupling of some energy to the atomic lattice, this paper focuses only on a method for particle production. If the cluster contains more deuterons than actually enter the nucleus during transmutation or are involved in the fusion reaction, these extra deuterons are proposed to dissipate the energy as energetic deuterons. However, the energy of these particles must be low enough not to produce secondary reactions, such as fusion with other deuterons the emitted deuterons might encounter. Consequently, the majority of clusters involved in the fusion reaction would need to contain nearly 50 deuterons and even more when transmutation occurs if all energy is dissipated this way. However, active clusters would not all have the same size, resulting in a spectrum of sizes. The complex variety of observed particle energies would result from clusters of various sizes being involved in a nuclear reaction. For example, Karabut et al.[25] detected a spectrum of individual peaks corresponding to energies from about 1 MeV to 18.5 MeV that they identified as alpha emission. This emission occurred immediately after glow discharge in D_2. This observation is similar to the radiation spectrum of individual peaks reported by Storms and Scanlan[26] during glow discharge that they attributed to deuterons. This behavior can be explained by energy being shared between a different number of deuterons. Smaller, less abundant clusters would produce a few very energetic emissions that could produce secondary radiation. This rare energetic primary radiation might be detected occasionally as periodic but low intensity secondary neutron emission. Meanwhile, most deuterons would have energy too low to be easily detected and too low to produce secondary reactions. While the large cluster size required by this logic seems implausible, the proposed process should be explored, perhaps in relationship to other dissipation processes.

These clusters of deuterons are proposed to form by an exothermic reaction requiring a catalyst or template. Once formed, an active cluster is small enough, thanks to its unusual structure, to diffuse through the PdD lattice and react with targets of opportunity. This catalyst is rare so that cold fusion occurs infrequently only when and near where this catalyst is present. This rarity results because the catalyst is proposed to be a complex combination of certain atoms that seldom combine in the require formation. Several different combinations of several different elements are probably active, all in the form of nanoparticles. Consequently, the NAE is located on the surface of nanoparticles that are formed on a surface or present after having been placed in the apparatus fully formed. Naturally, not all such particles will be active. As a result, the amount of power produced by a cell will be highly variable, as is observed. The challenge is to identity the nature of the active nanoparticle and to make these in large amounts. Only then can the effect be made reproducible and a source of significant power.

Depending on their size, these clusters react with deuterons where the deuterium concentration is highest to produce d-d fusion and with other atoms to generate transmutation products at a lesser rate. The environment in which this occurs is very inhomogeneous and complex, resulting in a wide variation in reaction rates including no detectable rate. The process can be detected by measuring short-range particle emission, low-energy X-rays, He^4, and extra heat. Tritium may be produced by clusters having a critical number of deuterons, hence is a rare product.

The proposed model is still very incomplete and ignores many observations. Nevertheless, the logic suggests a new way to look at the problem that might be helpful in the development of more complete models. While many questions remain, the approach has many ways it can be tested and suggests how the cold fusion effect might be increased.

---

[3] Smaller means fewer deuterons. The actual dimension is proposed to become smaller as the number of deuterons increases in a cluster as a result of an increased number of bonding states.

4. References

[1]. Storms, E.K., *The science of low energy nuclear reaction*. 2007, Singapore: World Scientific. 312.

[2]. Takahashi, A., *Some considerations of multibody fusion in metal-deuterides*. Trans. Fusion Technol., 1994. **26**(4T): p. 451.

[3]. Takahashi, A. *Tetrahedral and octahedral resonance fusion under transient condensation of deuterons at lattice focal points*. in *ICCF9, Ninth International Conference on Cold Fusion*. 2002. Beijing, China: Tsinghua University: Tsinghua Univ., China.

[4]. Kim, Y.E. and A.L. Zubarev. *Ultra low-energy nuclear fusion of Bose nuclei in nano-scale ion traps*. in *8th International Conference on Cold Fusion*. 2000. Lerici (La Spezia), Italy: Italian Physical Society, Bologna, Italy.

[5]. Iwamura, Y., et al., *Detection of anomalous elements, X-ray and excess heat induced by continuous diffusion of deuterium through multi-layer cathode (Pd/CaO/Pd)*. Infinite Energy, 1998. **4**(20): p. 56.

[6]. Iwamura, Y., et al. *Correlation between behavior of deuterium in palladium and occurance of nuclear reactions observed by simultaneous measurement of excess heat and nuclear products*. in *Sixth International Conference on Cold Fusion,Progress in New Hydrogen Energy*. 1996. Lake Toya, Hokkaido, Japan: Lake Toya, Hokkaido, Japan.

[7]. Iwamura, Y., et al., *Detection of anomalous elements, X-ray, and excess heat in a D_2-Pd system and its interpretation by the electron-induced nuclear reaction model*. Fusion Technol., 1998. **33**: p. 476.

[8]. Iwamura, Y., et al. *Observation of nuclear transmutation reactions induced by D_2 gas permeation through Pd complexes*. in *ICCF-11, International Conference on Condensed Matter Nuclear Science*. 2004. Marseilles, France: World Scientific.

[9]. Iwamura, Y., et al. *Observation of surface distribution of products by X-ray fluorescence spectrometry during D_2 gas permeation through Pd cathodes*. in *Condensed Matter Nuclear Science, ICCF-12*. 2005. Yokohama, Japan: World Scientific.

[10]. Miley, G.H. and J.A. Patterson, *Nuclear transmutations in thin-film nickel coatings undergoing electrolysis*. J. New Energy, 1996. **1**(3): p. 5.

[11]. Miley, G. *Characteristics of reaction product patterns in thin metallic films experiments*. in *Asti Workshop on Anomalies in Hydrogen/Deuterium Loaded Metals*. 1997. Villa Riccardi, Rocca d'Arazzo, Italy: Italian Phys. Soc.

[12]. Arata, Y. and Y.C. Zhang, *Formation of condensed metallic deuterium lattice and nuclear fusion*. Proc. Jpn. Acad., Ser. B, 2002. **78**(Ser. B): p. 57.

[13]. Arata, Y. and Y.C. Zhang, *Anomalous production of gaseous ^{4}He at the inside of 'DS cathode' during D_2O-electrolysis*. Proc. Jpn. Acad., Ser. B, 1999. **75**(10): p. 281.

[14]. McKubre, M.C.H., et al. *Concerning reproducibility of excess power production*. in *5th International Conference on Cold Fusion*. 1995. Monte-Carlo, Monaco: IMRA Europe, Sophia Antipolis Cedex, France.

[15]. McKubre, M.C., et al., *Replication of condensed matter heat production*, in *ACS Symposium Series 998, Low-Energy Nuclear Reactions Sourcebook*, J. Marwan and S.B. Krivit, Editors. 2008, American Chemical Society: Washington, DC. p. 219.

[16]. Dus, R. and E. Nowicka, *Segregation of deuterium and hydrogen on surfaces of palladium deuteride and hydride at low temperatures*. Langmuir, 2000. **16**(2): p. 584.

[17]. Kuji, T., et al., *Hydrogen absorption of nanocrystalline palladium*. J. Alloys and Compounds, 2002. **330-332**: p. 718-722.

[18]. Marwan, J., *Study of the nanostructured paladium hydride system*, in *ACS Symposium Series 998, Low-Energy Nuclear Reactions Sourcebook*, J. Marwan and S.B. Krivit, Editors. 2008, American Chemical Society: Washington, DC. p. 353.

[19]. Hagelstein, P.L. *Phonon-exchange models: Some new results*. in *11th International Conference on Cold Fusion*. 2004. Marseilles, France: World Scientific Co.

[20]. Chubb, S.R. *Roles of approximate symmetry and finite size in the quantum electrodynamics of d+d=^{4}He in condensed matter nuclear science*. in *8th International Workshop on Anomalies in Hydrogen/Deuterium Loaded Metals*. 2007. Catania, Sicily, Italy: The International Society for Condensed Matter Science.

[21]. Chubb, T.A. *The dd cold fusion-transmutation connection*. in *Tenth International Conference on Cold Fusion*. 2003. Cambridge, MA: World Scientific Publishing Co.

[22]. Szpak, S., P.A. Mosier-Boss, and F. Gordon, *Further evidence of nuclear reactions in the Pd/D lattice: emission of charged particles*. Naturwiss., 2009.

[23]. Mosier-Boss, P.A., et al., *Characterization of tracks in CR-39 detectors obtained as a result of Pd/D Co-deposition*. Eur. Phys. J. Appl. Phys., 2009. **46**: p. 30901.

[24]. Lipson, A.G., A.S. Roussetski, and G. Miley, *Energetic alpha and proton emissions on the electrolysis of thin-Pd films*. Trans. Am. Nucl. Soc., 2003. **88**: p. 638.

[25]. Karabut, A.B., Y.R. Kucherov, and I.B. Savvatimova, *Nuclear product ratio for glow discharge in deuterium*. Phys. Lett. A, 1992. **170**: p. 265.

[26]. Storms, E.K. and B. Scanlan. Radiation produced by glow discharge in a deuterium containing gas (Part 2). in *American Physical Society*. 2008. New Orleans

Tunneling beneath the ^{4}He* fragmentation energy

A. Meulenberg[a] and K. P. Sinha[b]

[a] *HiPi Consulting, Frederick, MD, USA*
[b] *Department of Physics, IISc, Bangalore 560012, India*

E-mail: mules333@gmail.com

Abstract. The repulsive Coulomb barrier between deuterium nuclei is reduced in length and height by a catalytic mechanism involving optical phonons and electric fields in a lattice. If the mechanism induces the formation of D$^-$ D$^+$ pairs, the tightly-bound and energetic electron pair (in the D$^-$ ion) becomes a binding force between the nuclei. The lattice constraints and **slow** collision processes, force the ions into a near 1-D configuration that deepens the electron ground-state potential well. This permits the electron pair to remain closely bound to one deuteron and to do work in bringing the D$^-$ D$^+$ pair together. These tightly-bound electrons may remain as a pair, attached to a single deuteron, during the fusion process. In reducing the Coulomb repulsion of the nuclear protons, these electrons bring down the total energy of the fusing D$^-$ D$^+$ pair and raise the fragmentation energy level. This process accounts for the observations in CMNS of excess heat (in both p-p and d-d reactions) and for the differing observations (or their absence) of tritium, ^{3}He, neutrons, and ^{4}He in the d-d reaction. Thus, all major observed CMNS processes are explained.

1. Introduction

At ICCF-14, we presented the means whereby the repulsive Coulomb barrier between hydrogen (deuterium) nuclei is reduced in length, perhaps by orders of magnitude [1]. This mechanism, involving optical phonons and electric fields (internally or externally generated) in a lattice that induce the formation of D$^-$ D$^+$ pairs, increases the tunneling probability by more than 100 orders of magnitude [2]. It has additional major consequences described below.

In brief: the lattice constraints and collision processes force the interstitial deuterium ions into a temporary, but cyclic, nearly one-dimensional (1-D) configuration that greatly deepens the D-D and electron ground-state potential well. The proposed tightly-bound and energetic-electron pair (a local-charged Boson - the lochon) results in sub-lattice D$^-$ D$^+$ pairs and becomes more than strong screening; it becomes a binding force between the nuclei [3]. Thus, the Coulomb-barrier height is reduced as well as its length. With this greatly enhanced barrier-penetration probability, the energy level of nuclei with reasonable tunneling probability drops from the multi-100 keV range down into the eV range.

In this earlier version of our model (only concerned with the barrier-penetration problem), normal tunneling is into resonant states above the fragmentation levels [4]. Thus, even if the Coulomb barrier is overcome by the tightly-bound electron pair and fusion is possible, the major observations of LENR (e.g. more heat than neutrons) are not accounted for. This requirement of tunneling into states above fragmentation is dictated by the mass deficit [5] between the two colliding D atoms and the resultant ^{4}He atom (2D - ^{4}He = Q = 23.8 MeV). Therefore, even with zero incident energy, a deuteron pair will have too much energy to tunnel beneath the fragmentation levels at 20.6 and 19.8 MeV above the ^{4}He ground state. Nevertheless, the model was successful in providing a mechanism to overcome a major argument against LENR. The present work shows how its extension also explains most of the experimental results observed in the field.

2. Extended Lochon Model

In a more detailed study of the model, new and unexpected effects are found. Just as slow-motion photography can reveal unsuspected processes, low-energy collisions (i. e., eV compared to MeV) have

provided some surprises. It is the non-equilibrium conditions of a "slow" D^- D+ collision in a linear sub-lattice that provides an answer to the "nuclear ash" problem of CMNS. The deuteron motion is slow; but, the bound-electron motion is not. This distinction allows us to separate the actions and use the Born-Oppenheimer approximation [6] (common in quantum chemistry) to solve for the electron quasi-steady-state parameters, step-by-step, as the D^- D^+ pair approach each other over the PdD lattice barrier separating them.

As the nuclear potential well deepens while a D_2 molecule is being confined to 2 dimensions, so does the electron potential well. A deepening of the electron potential wells does not necessarily mean that the electrons go deeper into the well; they must lose total energy to do that (although they gain kinetic energy as they move into the well, they lose it again on the way back out). However, being in a ground state ($l = 0$), they cannot directly radiate photons or induce phonon excitation. Nevertheless, in a critical concept provided online by Tom Barnard, a mechanism is provided whereby they may dissipate energy as the separation of the electron and D^- D^+ pairs is reduced. Since work is done by the electrons during this motion (they transfer energy to the deuterons), they fall deeper into the deuteron's Coulomb potential well. Being deeper in the well means that neither of the paired electrons is likely to transfer to the potential well of the other deuteron during this process. **This is a critical assumption of the model.**[i] Since this electron pairing is a possible state, quantum mechanics can calculate the probability of a 2-electron deuterium sub-lattice state relative to that of zero or single-electron occupancy. However, the probability depends on the energy of the electron pair and the local Fermi levels, and those depend on the recent history of the D^- D^+ pair.

Collisions in nuclear physics experiments are so fast that, except for the electrons directly involved, equilibrium electron-energy levels do not have time to change before the event is over. On the other hand, during the critical portion of the D^- D^+ interaction in a lattice, the "slow" motion of the converging deuterons allows the electrons to orbit hundreds of time during each increment of deuteron closing and therefore allows the electrons to experience and respond to the changing fields - and to do work. As the electrons move deeper into the D^- Coulomb potential well, the cancellation of electric fields (electron and proton) reduces the total field energy (potential energy) and therefore (initially very slightly) the mass of the particles. Since energy is conserved, part of this loss in field energy goes into the increased kinetic energy of the electrons (T_e), part into the increased kinetic energy of the deuterons (T_d), and part into increasing the e-e and d-d electric field strengths as the like-charge particles move closer together. (Just as the electrons do work in bringing the deuterons together, the deuterons and electrons have work done on them to move them closer together.) The net result of this 4-body interaction is that the paired, tightly-bound, energetic, electrons (e*) remain at nearly constant total energy (more KE and deeper in Coulomb well), the D^+ gains some total energy, and the D^- loses total energy.

As the colliding deuterons move still closer together (and climb the barrier between the deuteron sites), the screening from the lattice electrons and the residual barrier between the deuterons becomes smaller. The D^- D^+ Coulomb potential grows and the collapse of the D^- D^+ pair is accelerated. However, the energy expended in overcoming the lattice barrier keeps the D^- D^+ pair moving slowly until the pair gets very close (~1 picometer). As the pair gets even closer together, the D^- D^+ potential dominates the lattice barrier and the closing velocity increases.

The electron's kinetic-energy increase and its movement deeper into the Coulomb well about the deuteron causes the electron orbit to "shrink." Its deBroglie wavelength decreases with increased velocity and, as it spirals in, its field energy is further "cancelled" and concentrated by that of the proton (within the deuteron). With an increase in energy from the $T_e = 10$ eV range of the electron in the "free" deuterium atoms to a 1 keV of a bound electron as it approaches the deuteron, the deBroglie wavelength is reduced by an order of magnitude. As the energy of this "shrinking-orbit" electron, e*, increases to the 100 keV range, its wavelength drops by 10x again and approaches that of an electron's Compton wavelength. However, by this time, the electron field (and therefore the electron center of "mass") has shifted to within 10s of Fermi of the nucleus. The e* may no longer be a separate entity. The e*-proton pair has become a relativistic rotating dipole field (quadrapole field, if two bound electrons are present). The cancelled charge-field energy has been transformed to electromagnetic and relativistic-mass energy.

---

[i] The existence of D^- D^+ pairs in a lattice is accepted physics ([2] and references therein). Their existence in a PdD lattice must still be verified.

3. Nuclear Interactions

The reduced Coulomb repulsion between the protons (resulting from the shrunken e* or lochon orbits) increases the total nuclear attraction between them relative to that of normal ^{4}He. Thus, the nucleons spend more time closer together and therefore more time in the nuclear-potential well. This increases the effective "depth" of the well and decreases the energy of the excited states of the ^{2}He* or ^{4}He* structures formed. There are other reasons why the nucleus might shrink even further. Both the closer binding of the nucleons and the deeper potential well reduces the probability of fragmentation.

Examining the traditional D-D to ^{4}He* transition (Fig. 1), we see the broad transition region > 23.8 MeV above the ^{4}He ground state. This is the energy difference that corresponds to the mass difference between the deuterium pair and ^{4}He. Even with tunneling from zero kinetic energy states (i.e., $E_k = 0$), the excess mass of the deuterium atoms would put the deuterons into this high level. This excited ^{4}He* state is above the fragmentation levels at $\sim$ 20.6 and $\sim$ 19.8 MeV. While fragments from both levels have been observed in LENR experiments, the radiation levels are not nearly high enough to explain the excess heat observed. Furthermore, the levels of ^{4}He measured have been orders of magnitude higher than would be expected and, in some cases, have been high enough to account for the observed heat. How does this happen? Conventional physics sees the overcoming of the Coulomb barrier at low temperatures/energies, the distortion of the normal fragmentation ratio (p:n = 50:50 from E > 22 MeV), the high levels of ^{4}He, and, more recently, transmutation of elements as reasons for considering the Cold Fusion results as impossible.

Since the observed data is not possible within the known framework of nuclear physics, something else must be going on. We have shown how the Coulomb barrier problem is solved and laid a foundation for the D-D nuclear interaction with the help of tightly-bound, high-kinetic-energy electrons. Now we put the parts together.
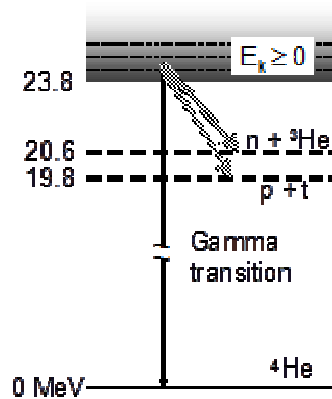

Fig. 1 - Energy levels and decay branches associated with conventional D-D to ^{4}He* fusion reactions.

4. Reduced Energy ^{4}He*

With the ability of deuterons to tunnel from an appropriate PdD lattice site through the nuclear Coulomb barrier of an adjacent **reduced-energy** ($E_t = T + V$) nucleus of a D$^-$ ion, the possibility of a low-energy excited compound nuclei becomes real. If, with the lochon, the excited (but neutralized) helium-4 nucleus does not have sufficient energy to fragment, and gamma decay is highly forbidden, how does it shed the excess energy to get to its ground state? It is proposed that this condition and the subsequent decay process is the basis for the experimental observations of CMNS.

To see how this "new" process can occur, we must take a closer look at Fig. 1. There are no energy levels below the ^{3}H + p (or t+p) fragmentation level. In a d-d interaction, if fusion were to take place, it would be resonance tunneling into one of the many levels above the region at 23.8 MeV. Decay from these excited states would almost always give nearly equal probabilities of fragmenting into the p or n channels. If a state existed below ~20 (or 19) MeV, then n (and p)-channel fragmentation would become unlikely. Unsuccessful attempts have been made specifically to find such an excited state. We propose a non-fragmentation mechanism that does not rely on a new state below 19.8 MeV. It shifts some of the existing states down below that level and it demonstrates how the fragmentation levels are shifted up in energy.

The key to the mechanism is the lochon, which during the collision process attains significant energy (keV to MeV range); but, remaining in an $l = 0$ ground state, it does not radiate. If it survives the final tunneling process of the d^+ through the thin, residual, D^- Coulomb barrier, it may have attained multiple MeV energies from the work done at the expense of the D^- Coulomb potential energy. Thus, it is very-tightly and closely bound and both the lochon and the D^- nucleus have lost electric-field mass. Since the lochon mass and orbital radius is now so small, even in a circular orbit, the orbital angular momentum is less that $\hbar/2$. Therefore, there is little possibility of photonic radiation.

5. The new ^{4}He*

Once the D^+ is inside the D^- nuclear-Coulomb barrier, the situation is different from that of the normal d-d scattering problem. The nuclear potential is greatly different, because the Coulomb barrier between the protons is much reduced. Thus, they can be much closer together. Since most of the normal nucleon wavefunction is outside the d-d nuclear well, the depth of the nuclear potential well with which the nucleons are bound is increased by both the loss of Coulomb repulsion and the gain in nucleon time spent in the well (increased wavefunction overlap). As a consequence, the effective depth of the nuclear well is increased; the excited nuclear-state energies become lower; and the energy required to break apart (fragment) the excited nucleus is higher.

If the new ^{4}He* energy, is too low to fragment and it has an e* or two spending much of their time inside the nuclear region, it cannot form a stable nuclear state (even if one existed in the normal ^{4}He* nucleus). The continual and extreme proximity of the highly-excited deuterons to these electrons (in the femtometer range) allows resonance transfer of energy between them, via near-field EM coupling, at a frequency associated with, or below that of, soft x-rays. Thus, the nuclear energy is able to be transferred to the shrunken-orbital electron(s) and from there it is radiatively transferred to the lattice, since the e* is also close-coupled (in the nanometer range) to the bound Pd electrons. If the average radiated x-ray energy is in the keV range, it takes little time for most of the nuclear energy to be dissipated. However, as decay progresses, the rate of energy transfer and dissipation decreases, giving more time for the electron(s) to be ejected from the nuclear region (e* => e⁻) with the remaining energy. Since e* is deep in the nuclear Coulomb potential this ejection is not as an energetic electron, but as a gradually slowing (and expanding-orbit) electron being driven out of the well by energy from the proton-generated EM field.

This extended fusion / radiation process lasts:
   a) until the neutral entity (^{2}He* or ^{4}He*) drifts into a neighboring nucleus, resulting in a transmutation process;
   b) until one (or more) of the energetic shrunken electrons combines with a proton (p + e* => n+ν, via the p-e*-p, p-2e*-p, d-e*-d, or d-2e*-d reaction); or,
   c) until diproton fragmentation or the ^{4}He ground state is reached, on ejection of the electron(s).

6. Conclusion

Depending on the actual energy of the excited (compound) nuclei and the number of e* still present (0, 1, or 2) after the nuclear Coulomb barrier has been penetrated, the decay process could include fragmentation, or not. This accounts for the observations in CMNS of excess heat, in both p-p and d-d reactions, and the observations (or absence) of tritium, ^{3}He, neutrons, and ^{4}He in the d-d reaction. The ability of the lochon to alter the nuclear potential well and fragmentation energies permits radiation-free decay to the ^{2}H or the ^{4}He ground state and transmutation. This variation (apparent unpredictability) of results, heretofore the stumbling block to acceptability of LENR, is now perhaps the greatest validation of its existence. Thus, all major observed CMNS processes are explained, but not necessarily the best means of, or materials for, producing them. That comes next.

Acknowledgments

7. References

[1] K. P. Sinha and A. Meulenberg, *ICCF-14 International Conference on Condensed Matter Nuclear Science*, 2008, Washington, DC. http://www.lenr-canr.org/acrobat/SinhaKPamodelfore.pdf

[2] K.P. Sinha and A. Meulenberg, *Current Science,* 91, 907 (2006), (arXiv:cond-mat/0603213)

[3] K. P. Sinha and A. Meulenberg, *Nat. Acad. of Sc. (India) Letters*, Vol.30, No. 7&8, 2007, (arXiv:0705.0595v1)

[4] A. Takahashi and N. Yabuuchi, *ICCF-14 International Conference on Condensed Matter Nuclear Science*, 2008, Washington, DC. http://www.lenr-canr.org/acrobat/TakahashiAdeuteronst.pdf

[5] http://en.wikipedia.org/wiki/Mass_deficit

[6] M. Born and K. Huang, *"Dynamical Theory of Crystal Lattices,"* Oxford University Press (1956)

Bose-Einstein type D-cluster Electrode Development

G. H. Miley[1], X. Yang[1], H. Hora[2]
[1]Department of Nuclear, Plasma and Radiological Engineering, University of Illinois, Urbana, IL, 61801, USA
[2]Department of Theoretical Physics, Univ. of New South Wales, Sydney, Australia

E-mail: ghmiley@illinois.edu

Abstract. Our recent research has developed a technique for imbedding ultra high density deuterium "clusters" (D cluster) in Palladium (Pd) thin film. Experiments have shown that in Pd these condensed matter state clusters approach metallic conditions, exhibiting super conducting properties. Using Temperature Programmed Desorption TPD system, the local concentration of hydrogen in the dislocation core is found to be [H]/[Pd]~1.8. At near 70 ºK Pd foil with abundant D clusters also show class II superconductivity, indicating the trapped hydrogen condensed into a metallic-like phase. Room temperature cluster formation is found to be adequate for the desired "nuclear reactive" sites. By careful calculation and experimentation, it is found the D cluster has a Bose Einstein Condensation state when a high deuteron diffusion flux is triggered. The resulting momentum transfer initiates reactions. The trigger can be electrochemical, giving LENR reactions. Thus this configuration can provide a small LENR power cell. Currently, we are searching for new methods to improve the volume density of dislocations. These methods mainly involve modifying Pd thin film with multi-layer structure.

1. Introduction

Recent SQUID measurement has shown ultra-dense states of deuterons with many more than 100 deuterons within a crystal defect in a palladium crystal are possible, and a superconductive state of these clusters was demonstrated in these experiments [1, 2]. Similar ultra-dense state of deuterons was seen at surface defects of iron oxide resulted in ion energies of 630 eV through Mass spectrometry measurements [3]. It may well be assumed that both cluster states are of the same nature though the states are concentrated at the surface in the iron oxide case due to the catalytic generation in contrast to the Pd samples with localization in the bulk volume [2]. In both cases their existence was confirmed by the LENR process [4] which likewise should be valid including when an inverted Rydberg state is present. Based on the excess heat measurements, local power densities exceeding a kW/cc are possible, promising very high energy density power units. Since the radiations emitted (protons, alphas, and x-rays) are not very penetrating (do not escape the cell structure) and no long lived radioactive reaction products are observed, LENR power units would be a remarkable ―green" nuclear technology.

2. Earlier work on LENR at University of Illinois

There are a wide variety of fusion nuclear reactions. As illustrated in Figure 1, the original Pons-Fleishmann (P-F) reaction involved DD Fusion. But, instead of the normal reaction where the channel passes through deactivation of the He4 by transferring energy to the lattice which ultimately appears as heat, a number of researchers have reported transmutation reactions that involve interaction between deuterium/hydrogen and atoms in the host lattice, typically heavy metals. This branch is commonly termed Low Energy Nuclear Reactions (LENRs), although recently there has been a move to include DD reactions as LENRs as well. In this review we concentrate on host atom reactions.

D-D Reactions

		hot fusion	% branching "P-F" type
T + p		50	< 0.1
D-D → He-3 + n		50	< 10^{-6}
He-4 + gamma		< 10^{-5}	99+

LENRs

p + metal → products or "fission" product array

Fig. 1 - Comparison LENR reactions and the DD reactions.

Transmutation reactions can be broadly classified according to their products. Some experiments have observed a large array of reaction products with mass numbers ranging across the periodic table. These reactions are traced to multi-body events leading to a heavy compound nucleus, which can both decay, and fission into an array of elements [5]. The other set of experiments lead to one or few distinct isolated products [6]. These reactions may or may not involve multi-bodies but the net result is direct formation of the reaction products as opposed to the disintegration of a compound nucleus. Earlier works on transmutation reactions involved thin films on microspheres, while our recent studies at the U of I have converted it to thin films coated on a flat alumina substrate as illustrated conceptually in Figure 2. In this design, a double-layer Pd/Ni thin film, at 8000 Å and 1000 Å respectively, sputtered on ceramic Al_2O_3 substrate at rate 0.41 Å, was used as a cathode. The electrical current flow is parallel to the thin film surface so that a high current density and high proton flow rate are obtained along with a high deuterium density [7].

The possible heat evolution during electrolysis runs was detected by a high sensitivity open-type calorimeter in a fixed temperature of 28.0 ± 0.05 °C. [8] To check actual performance during Foreground electrolysis runs (with Alumina/Pd-Ni samples), including heat convection, bubbling, electrode's geometry, and positioning, as well as H_2+O_2 recombination, smooth Pt sheets were used as cathodes in Reference runs, since Pt does not produce excess heat in the light water electrolysis [9]. The performance of this runs at various current (50 ~ 600 mA) is defined by the calorimeter "heat recovery" value R = Pth/I(U-U0), where, Pth is the thermal power measured in calorimeter by thermistors; I(U-U0) is Joule heating P*, in which I and U are the electrolysis current and voltage, respectively; U0 is an effective water dissociation potential (WDP) (2.01 V for Pt/Pt pair and 2.06 V for Pd-Ni/Pt pair) [10]. A constant electrolysis current ranging from I = 100 ~ 600 mA (j = 8.5 ~ 50.0 mA/cm2) corresponding to a cell voltage U 3.5 ~ 5.5 V were applied to Alumina/Pd-Ni cathodes Typical kinetics of the heat measurement (Pth vs. elapsed time t) are presented in Fig. 3.
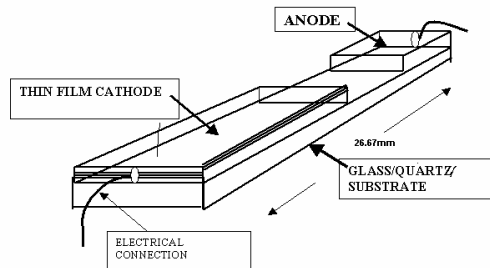

Fig. 2 - Recent Work Uses a Unique Integrated Thin film Plate-Type Electrode.
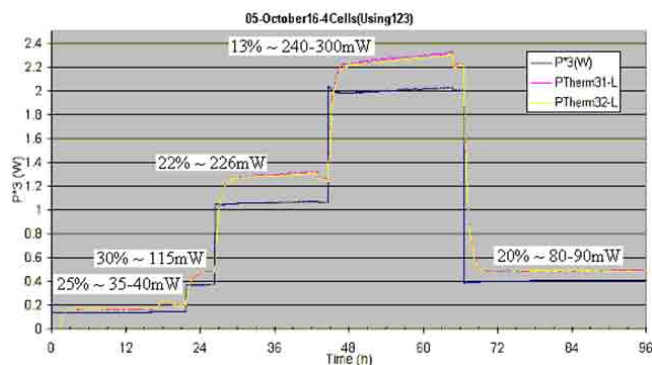
Fig. 3 - Heat measurement for two layers electrode: 8000Å Pd and 1000Å Ni on Alumina. Correlation between Transmutation Products and Excess Heat

As seen, shortly after stating the run, the thermal yield P_{th} exceeds Joule heating P*. The current was run in "jumps" purposely to examine changes as a function of input power. The maximal heat recovery R of 135 % occurs at electrolysis current I=100 mA (j = 8.0 mA/cm2), while the corresponding absolute value of excess heat production is W_{ex} = 60 ± 28 mW. Increasing the current density to 48 mA/cm2 leads to decrease in heat recovery R from 135 to 115 %. In typical cases the excesses heat evolution from the cathode at I = 200 mA continues for ~ 15 days. The decrease in R during a long Foreground run is accompanied by an increase in cell voltage. The last process indicates an increase in the cell inner resistance due to defects and micro-cracks generation in Pd/Ni cathode. The cathode samples survive, i.e. they do not detach the Alumina substrate during these long runs. Thermistor calibration runs repeated immediately after this Foreground run show that calorimeter parameters, (including temperature change vs. input power) did not change during the time of operation with Alumina/Pd-Ni sample (15 days). This gives a proof of stability of the calorimetry system and indicates that our measurements of excess heat production were actually correct.

Although good progress has been made on direct correlating He-4 production and excess heat, supporting the D-D reaction hypothesis, the correlation between the transmutation and excess heat production, as well as the product measurements, still leave open a fairly large error band. Earlier, we have observed a variety of reaction products (isotopes) with masses both higher and lower than that of the host electrode material in thin film electrodes, [11][12][13], suggesting the existence of proton-metal initiated reactions in such LENR cells. Later, we discussed evidence that the production of these reaction products is correlated with the excess heat described above [14]. Such a correlation for LENR reactions would be equivalent, in principle, to the correlation of He-4 with excess heat that is reported for heavy water-Pd experiments where a D-D reaction is postulated.

A characteristic result, shown in Fig. 4, indicates that a variety of reaction products occur with masses lying well below and above that of the base electrode metal (Ni and Pd in Fig. 4, of cf. numbers defined in the references). A striking pattern consistently observed in these measurements is that the high-yield reaction products occur in four mass ranges, roughly A = 20-30, 50-80, 110-130, and 190-210 [12] [13]. The high-yield products (> 10^{13} atoms/cc-sec in Fig. 4) are well above background impurity limits, but some uncertainties due to possible impurities, especially in the electrolyte, still plague measurements of the lower yield products (< 10^{13} atoms/cc-sec in Fig. 4). Interestingly, a recent study by Widom and Larsen claimed that the theoretical transmutation calculations reasonably well match the Miley & Patterson result (see fig. 3 in [15]).

Two other points should be stressed. First, no neutrons have been observed in these experiments despite repeated attempts with sensitive detectors Likewise, no tritium has been observed in electrolyte analysis after runs. [Note: some LENR experiments run other quite different conditions have reported neutrons and tritium production. Thus, depending on the experimental design, there appear to be different braches to the LENR reactions]. Second, as noted in Miley and Patterson [11], long exposure of photographic films to electrodes removed after extensive runs indicate low levels of soft x-ray and/or beta particle emission.

This is consistent with the recent theoretical models where the fission-like process occurring in the transmutations has little excess energy. Thus, unlike uranium fission where the intermediate compound nucleus is highly excited, this energetically "soft" type fission leads to many products that are stable and others only slightly unstable [15] [16]. This process then avoids energetic gamma emission and the production of highly radioactive nuclear waste encountered in uranium fission systems. These remarkable results are basic to this new field of LENR nuclear physics and the unique processes that can be created by causing nuclear reactions in condensed matter. Please note that the "production rates" shown represent a time average over the experiment run-time since it was only possible to take samples at the beginning and end of a run. Likewise, the excess heat reported represents an average over the run, so that a comparison of these two results is consistent. Thus, to test a possible correlation between transmutation products and excess heat, the measured product yields are used along with their respective binding energies to compute a theoretical "excess power", W_{ex}, as shown in Fig. 5a. The computation is straightforward but tedious due to the large number of reaction products produced. Basically, W_{ex} is computed by taking the product of all the isotope yield rates times their binding energies and subtracting the corresponding product for the "fuel". A key point is the determination of the amount of original material that is consumed or "burned up." This calculation is done by first allotting the maximum number of reaction product nucleons to the metal nucleons. Then, any remaining nucleons are attributed to the protons, allowing for a variable proton/metal atom ratio to retain generality. This balance rests on the assumption that the protons plus the electrode metal (e.g. Ni in this case) are the reactants in LENR cells. This follows because protons in the light water electrolyte cannot react with themselves. The 'salt' employed in the electrolyte, e.g. Li_2SO_4, should not be involved in the reaction either, because various workers have used different salts while still obtaining similar reaction products.

Product yield results from three runs (run numbers refer to experiments described in Miley and Patterson (1996) where adequate information was available for this type of evaluation are summarized in Fig. 5b. Although one has a mean measured value that is a factor of two larger than the calculated value, two of the results show quite close agreement. While these results are not definitive, in view of the many uncertainties in both of the calculated values (due to uncertainties in the yield measurements) and in the calorimetry, the agreement obtained strongly suggests a relation between products and excess heat. The situation where heavy water is used instead of light water, as reported in some other LENR studies (see [17]), is less clear but again appears to involve proton-metal reactions. In that case, p-metal reactions could occur simultaneously with D-D reactions. More study is needed to resolve possible reactions involved this important regime.
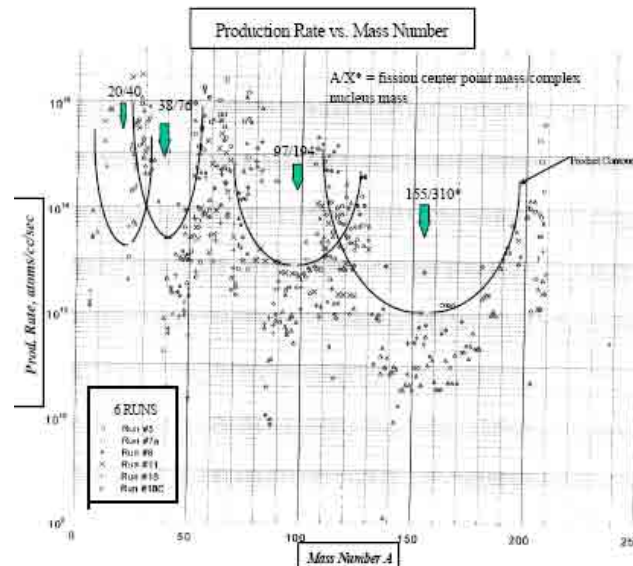

Fig. 4 - Reaction Product Yield vs. Mass Curve.

$$\left[\sum_{RPs} (RP * BE/n) - \sum_{\substack{metal\ atom,\\ p\ burned}} (fuel * BE/n)\right] / run\ time = P_{out}$$

$$\equiv W_{excess}$$

Computation of Excess Power from measured
reaction products and binding energies where:
RP = reaction product yield or atoms of product formed nuclei
BE /n= Binding energy per nucleon for RP or fuel
fuel = metal nuclei + protons reacted (from nucleon balance)
p = proton

(a)

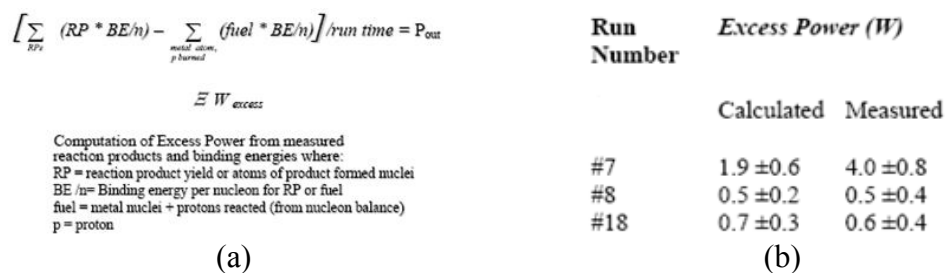| Run Number	Excess Power (W)	
	Calculated	Measured
#7	1.9 ±0.6	4.0 ±0.8
#8	0.5 ±0.2	0.5 ±0.4
#18	0.7 ±0.3	0.6 ±0.4

(b)

Fig. 5 - (a) Computation of excess power from reaction n product measurements. (b) Results from Energy Balance Calculations for Three earlier Thin-Film experiments. All experiments used Li_2SO_4 in H_2O for the electrolyte and thin-film Ni coated cathodes.

Another way of viewing these data is to calculate the energy released (the observed excess heat times the run time) and divide by the number of Ni atoms reacted (based again on the number of nucleons associated with the measured quantities of reaction products observed). Then, for the runs referred in Fig. 5b, an energy release of order of 150 keV/Ni atom reacted is obtained. This value is consistent with nuclear as opposed to chemical processes. It is several orders of magnitude less than the energy released in neutron-induced fission, but is roughly in the range of "soft" fission releases predicted for LENR conditions [16].

These results also bear on an issue that is often raised about the LENR experiments: how can a positive excess power occur since the base metal involved, such as Ni, has a binding energy per nucleon near the peak of the binding energy-mass curve? In the present analysis this can be explained by noting that the "fuel" i.e. the reactants, are a mixture of protons and metal. Then the average binding energy of the reactants (p + metal) is reduced below that of the metal alone. As a result, there is an expanded range of reaction product masses laying around the mass of the base metal that offer a positive energy release, i.e. a positive Q-value for the reaction. Still, the fact that some reaction products lie outside of this range might seem to infer that reactions occur despite a negative Q-value, but then a very large input energy would be needed to drive the reactions. This dilemma is overcome, however, if the reaction occurs through multi-step excitation and/or formation of a compound nucleus which can split up or fission into a variety of reaction products of different masses [11] [16]. The energy balance requirement is that the formation energy of the compound nucleus must be supplied. Subsequently, the break-up energy is, in effect, shared among products.

In order to obtain further proof for nuclear reactions in the thin-film cathodes [18], the detection of nuclear radiation accompanying the electrochemical loading of those cathodes is strongly desirable. Although the studies of long-range alpha emission have been done after the electrochemical loading of Pd with deuterium/hydrogen [19], it was a great interest to expand the experiments on charged particle detection to in-situ measurements during the electrolysis process. Unfortunately, it is hard to apply electronic SSB and X-ray detectors directly to the cathode during electrolysis experiment. Thus, a technique using non-electronic detectors (CR-39 and thermal luminescence detector (TLD)) was employed to allow in-situ measurement of energetic charged particles and X-rays during the electrochemical loading of the flat-plate Pd-thin film cathodes.

In the electrolysis experiments the freshly opened CR-39 detector chips or TLD crystal were attached either to the Pd thin-film cathode (Foreground) or to the substrate side or/and immersed in electrolyte in the cell (Background). The charged particle and x-ray detection were carried out simultaneously with excess heat measurements in open type calorimeter. The electrolysis current and duration during one Foreground run were normally varied in the range of 50-400 mA and 2-30 days, respectively.

Fig. 6 and insets show the Foreground and Background CR-39 reading for both alpha particles and protons. The count rates of protons and alphas after Background subtracting are statistically significant with Background level being close to zero. In the control experiment with CR-39 detector attached to the thin film NiO_x (obtained by annealing of Alumina/Ni(4000A) sample in air atmosphere), where despite of the high voltage applied (U~10.0 V), the electrolysis current in the cell was very low (I~1.0 mA), and no tracks with d < 7.8 μm were detected.
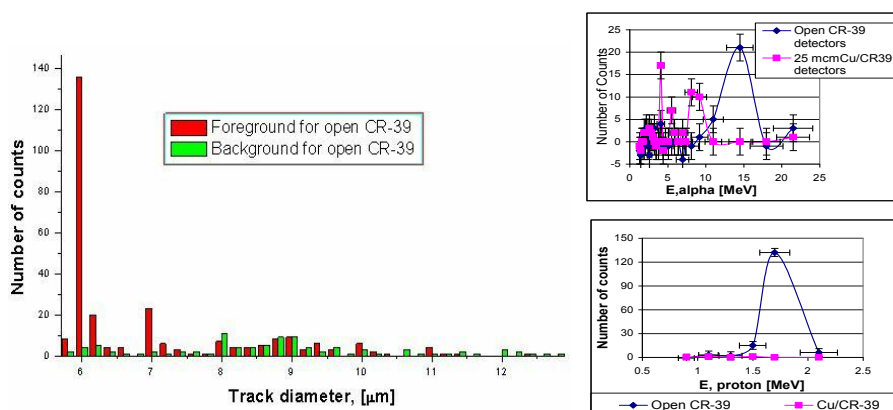
Fig. 6 - Electrochemical loading of Pd thin film cathodes on dielectric substrates unambiguously produced high-energy charged particles: 1.5-1.7 MeV protons and 11-16 MeV alphas. Insets: Alpha-tracks energy distribution and Proton energy distribution after background subtracting.

In contrast to charged particle detection results, the statistical significant level and reproducibility of X-ray emission was not satisfied. Some result (e.g. Pd/Glass sample with LIF TLD) showed consistency between the emitted X-ray fluency and absorbed dose but others (e.g. other cathode with Al_2O_3:C TLD) did not show statistically significant results due to higher initial background level ($\sim$ 10 mrad) of these TLD compared to that for LiF. The X-ray measurement results indicate the absence of massive nuclear reactions caused by nuclear transmutation in Pd [18]. However, these results could not rule out the possibility of a weak X-ray emission as a result of the charged particle generation or Pd thin film fracture or detachment from the dielectric substrate.

In summary, the observation of MeV particle emission, combined with the transmutations and excess heat measurements, provide extremely strong evidence for nuclear reactions occurring in the thin films during electrolysis. There results, combined with recent observations of localized sites ("clusters", discussed next) have lead us to consider the new approach to power producing LENR cells described here.

3. Ultra High Density Deuterium Cluster Electrode Fabrication

The SQUID magnetic measurements described in Lipson *et al*. [1] show "clusters" have characteristics of a type- II superconductor. Cluster regions can have hydrogen densities approaching 10^{24}/cc (See Fig. 7). Dislocation loop cluster type electrodes are fabricated by cyclic loading-deloading, hence being named "Dislocation Loops by Repetitive Loading-Deloading (DLRLD)"electrodes. These DLRLD electrodes are based on studies where high loadings in dislocation loops in treated Pd have exhibited properties associated with a superconducting phase termed a "cluster".

After several loading-unloading cyclings, the Pd/PdO:H_x was annealed at 300 ^{o}C for 2 hr to remove all the weakly bond hydrogen or deuterium. Then, a high-vacuum thermal desorption technique is used to estimate residual hydrogen concentration in the Pd/PdO:H_x samples (Fig. 7C). The samples were heated in a high vacuum (10^{-8} Torr) chamber with a quadruple mass-spectrometer. The hydrogen desorption peak area and the temperature of its maximum were found by analyzing the desorption species and comparing their yields to background data from the Pd/PdO : H_x or Pd/PdO).

By using Garlic-Gibson kinetics model, the activation energy of desorption is found to be approximately 0.65 ± 0.10 eV, which is consistent with the result of Kirchheim for hydrogen trapping at dislocation core sites in cycle Pd. This indicates that the hydrogen is solely bound inside the deepest core sites [approximately one Burgers vector (2.75 Å)], meaning that all residual hydrogen is localized inside the dislocation loops (in the direction of Pd) determined by Burgers vector b [101] = 2.75 Å. Then, the dislocation density calculation give x_{eff} is $\sim$ 1.8, suggesting superstoichiometric hydride formation in the deep dislocation cores.

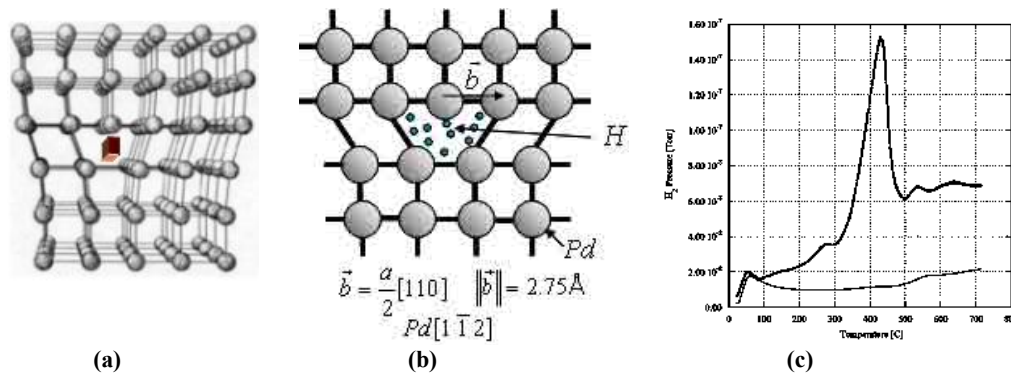|		
(a)	(b)	(c)

Fig. 7 - SQUID magnetic measurements show clusters have characteristics of a type-II superconductor. Cluster regions can have hydrogen densities approaching 10^{24}/cc. (a) 3D scheme of typical edge dislocation core (see orange bar) in the Pd crystal. (b) Cross-section of A. (c) Thermal desorption measurements of Pd/PdO : Hx (thick solid line) and Pd/PdO (thin solid line).

4. Other Ultra-High-Density Deuterium Cluster – Rydberg Matter

Encouraged about the result [1, 2] that SQUID measurements confirmed the localization of more than 100 nuclei of hydrogen in a crystal defect within a palladium crystal, an estimation was given [20] how many such defects may be generated in a crystal. A density of such defects in crystals may well be more than 10^{19} cm^{-3} before the crystal is breaking. This is the experience from the property in silicon crystals where such densities of doped atoms are well known. Similar density of defects with voids has been produced in silicon too by very intense electron bombardment. [21, 22, 23, 24] If these voids are then in an average distance of 10 atoms in the crystals for laser fusion targets based on LiH or similar crystals at room temperature, the targets with a density of fusion fuel of 1000 times solid state density may be possible [b].

A necessary condition, however, is that the clusters in the crystal volume should have the density of 10^{24} cm^{-3}. These densities have been confirmed [3] from clusters which were produced in crystal defects at the surface of iron oxide by catalytic processes of inverted Rydberg states. These densities were proved from the Coulomb repulsion energy of deuterons in such states as time-of-flight measurements showed 630 eV w. This corresponds to a distance of the deuterons of 2.3 pm within the inverted Rydberg clusters. The repulsion process is given, when laser irradiation of 546 nm wave length removes the neutralizing electrons between the deuterons [3].

The mechanism of the electron emission by the laser radiation has been analyzed by inclusion of the correspondence principle of electromagnetic interaction [25]. A virtual quiver motion of the electrons in the quantum state in the inverted Rydberg cluster arrives at a quiver elongation of 2.3 pm at a laser intensity of 1.01×10^{10} W/cm^2. This intensity was just measured as the lowest threshold [3] for the measurement of the 630 eV deuterons.

A further conclusion of this analysis is that the state of the deuterons in these clusters represents an effective Bose-Einstein condensation at room temperature. [26] A further result is for a hydrogen atom, the virtual quiver motion of the electron within the laser field with an elongation of the Bohr radius corresponds to the well known ionization energy of 13.6 eV. This energy has the unique value of $\alpha^2 mc^2/2$ expressed by the fine structure constant α and the rest mass energy of the electrons mc^2 with the electron mass m and the vacuum speed of light c.

5. Conclusion

This paper makes a strong case that condensed matter deuterium cluster formed in dislocation loops are one way to achieve nuclear reactive sites in LENR electrodes. The problem to date has been that the volumetric density of such cites, which is highly reactive, have a low density of sites per unit volume.
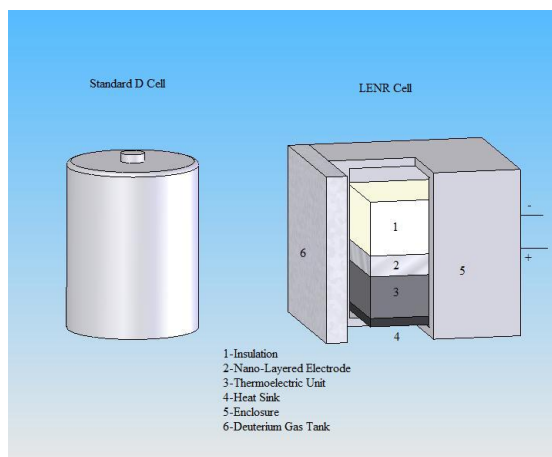
Fig. 8 - Small LENR Battery -- design based on present experimental data base

Possible methods to achieve a high volumetric density of sites (i.e. achieve a massive cluster electrode (MCE) that are under study are briefly outlined. This is thought to offer an orderly ‒roadmap' for moving on to very unique future power cells for both space and commercial use. Such cells would employ nuclear reactions for energy but enjoy no neutron release and a minimal radioactive product buildup. These characteristics are based on the experimental observations cited here where any neutron levels were below detection limits; MeV particles, while observed, had very low emission rates; and the reaction (transmutation) products created are generally close to stable, with only soft x-ray or beta emission being observed.

Based on the excess heat measurements, local power densities exceeding a kW/cc are possible, promising very high energy density power units. Since the radiations emitted (protons, alphas, and x-rays) are not very penetrating (do not escape the cell structure) and no long lived radioactive reaction products are observed, LENR power units would be a remarkable ‒green" nuclear technology. A sketch of a small D-cell equivalent LENR battery is shown in Fig. 8. The cell shown has a deuterium gas ‒fuel" tank attached.

Gas loading is used rather than electrolysis for compactness. Heat flow is directed to the outer casing through a thermoelectric element using an insulation and heat sink design. Modular sections connected in series allow a 1.5 V output at 0.1 A. This type of battery must be used in devices where natural convection air cooling or other heat flow dissipates heat fro the battery casing. The battery run time is determined by the amount of deuterium stored refilling the depleted tank is provided by pump down and gas injection through a filtered line connected to a ‒filling station". The unit shown is designed for 1000 Ahr per gas fill. The main technological step needed before construction of this battery is to finish development of the nano-layered electrode structure described earlier.

6. References

[1] A. Lipson, B.J. Heuser, C. Castanov, G. Miley, B. Lyakov, A. Mittin. Transport and magnetic anomalies below 70 K in a hydrogen cycles Pd foil with a thermally grown oxide, *Phys. Rev. B* 72 (21): 212507-10, 2005

[2] G. H. Miley and X. Yang, (2009), Deuterium Cluster Target for Ultra-High Density Fusion, *Fusion Science and Technology*, 56 (1), 395-400

[3] Shahriar Bardei, Patrick U. Andersson, Leif Holmlid. (2009) High-energy Coulomb explosions in ultra-dense deuterium: Time-of-flight-mass spectrometry with variable energy and flight length, *International Journal of Mass Spectrometry*, 282 (1-2), 70-76.

[4] H. Hora, G.H. Miley. Maruhn-Greiner maximum from uranium fission for confirmation of low energy nuclear reactions LENR via a compound nucleus with double layer magic numbers. *Journal of Fusion Energy*. 26 (2007) 349-354 & 347.

[5] Miley, G. H., Narne, G., Williams, M. J., Patterson, J. A., Nix, J., Cravens, D. and Hora, H., ‒Quantitative Observation of Transmutation Products Occurring in Thin-Film Coated

Microscopheres During Electrolysis," *Progress in New hydrogen*, (1997), pp. 629-644.

[6]   Iwamura, Y., Sakano, M. and Itoh, T., ―Elemental Analysis of Pd Complexes: Effects of D2 Gas Permeation," *Japan Society of App. Physics*, 41(7A), Pt. 1, (2002), pp. 4642-4650.

[7]   Miley, G. H., Hora, H., Batyrbekov, E. G. and Zich, R. L., ―Electrolytic Cell with Multilayer Thin-Film Electrodes," *Trans. Fusion Technol.*, 26, (1994), pp. 313.

[8]   Miley, G. H., Hora, H., Lipson A., Kim S.O., Luo N., Castano C. H., and Woo, T., ―Progress in thin-film electrode research at the University of Illinois," *The 9th International Conference on Condensed Matter Nuclear Science*, (2002).

[9]   Storms, E., ―How to produce the Pons-Fleischmann effect," *Fusion Technol.*, 29, (1996), p. 261.

[10] Glasstone, S., An Introduction to Electrochemistry, [Chapter 13], *Wiley, New York*, (1951).

[11] Miley, G. H. and Patterson, J. A., ―Nuclear Transmutation in Thin-film Coatings Undergoing Electrolysis," *Journal of New Energy*, 1, (1996), pp. pp. 11-15.

[12] Miley, G. H., ―Possible Evidence of Anomalous Energy Effects in H/D-Loaded Solids—Low Energy Nuclear Reactions (LENRs)," *Journal of New Energy*, 2(3-4), (1997a), pp.6-13.

[13] Miley, G. H., ―Caracteristics of Reaction Product Patterns in Thin Metallic Films Experiments," Proceedings Asti Workshop on Anomalous Effects in Hydrogen/Deuterium Loaded in Metals, Asti, Italy, (1997b), pp. 77-87.

[14] Castano, C. H., Lipson, A. G., Kim, S. O. and Miley, G. H., ―Caloremetric Measurements During Pd-Ni Thin Film–Cathodes Electrolysis in Li2SO4/H2O Solution," *in the proceedings of ICCF-9*, Beijing, China 19-24 May, (2002).

[15] Widom,   A.   and   Larsen,   L.,   ―Nuclear   Abundances   in   Metallic   Hydride", http://www.newenergytimes.com/Library/2006WidomA- NuclearAbundancesInMetallicHydride.pdf, (2006).

[16] Takahashi, A., Ohta, M. and Mizuno, T., ―A Model Analysis of Low-Energy Photo-Fission of Pd Isotopes Under Dynamic Condition of PdH(D)x ," *in the proceedings of ICCF-14*, Washington DC, August, (2008).

[17] Miley, G. H., Selvaggi, G., Tate, A., Okuniewski, M., Williams, M. J., Chicea, D., Hora, H., and Kelly, J., ―Advances in Thin-Film Electrode Experiments," in the proceedings of 8th International Conference on Cold Fusion*, ICCF-8*, Villa Marigola, Lerici, Italy, May 21-26, (2000).

[18] Miley, G. H., ―Emerging physics for a breakthrough thin-film electrolytic cell power unit," in the proceeding of Space Technology Application & International Forum (STAIF-99), edited by M. S. *El-Genk, AIP conference proceedings 458*, (1999), p. 1227.

[19] Lipson, A. G., Roussetski, A. S., Miley, G. H. and Castano, C., ―In-Situ Charged Particles and X-ray Detection in Pd Thin Film-Cathodes During Electrolysis in Li2SO4/H2O," *in the proceedings of ICCF-9, Beijing*, China 19-24 May, (2002).

[20] L. Holmlid, H. Hora, G.H. Miley, X. Yang, (2009) Ultrahigh-density deuterium of Rydberg matter clusters for inertial confinement fusion targets. *Laser and Particle Beams* 27 529-532.

[21] H. Hora, Shift of Absorption of Evaporated Silicon Layers by Bombardment with 75 keV, *Naturwissenschaften* 48, 641 (1961)

[22] H. Hora, Change of Silicon by Intensive Bombardment with 50 keV Electrons, *Zeitschrift f. angew. Phys.* 14, 9-12 (1962).

[23] HORA, H. (1983). Stresses in silicon crystals from ion-implanted amorphous regions *Appl. Phys. A* 32, 1–5.

[24] GOLDSMID, H.J., HORA, H. & PAUL, G.L. (1984). Anomalous heat conduction of ion-implanted amorphous layers in silicon crystals using a laser-probe technique. *Phys. Stat. Sol.* (a) 81, K127–K130.

[25] H. Hora and P.H. Handel, New Experiments and theoretical development of the Quantum Modulation of Electrons (Schwarz-Hora effect), Advances in Electronics and Electron Physics, P.W. Hawkes ed. (*Acad. Press, New York, 1987*) Vol. 69, p.55-113., Chapter III.

[26] Yeong E. Kim, Theory of Bose–Einstein condensation mechanism for deuteron-induced nuclear reactions in micro/nano-scale metal grains and particles, *Naturwissenschaften*. 96(7):803-11, 2009A reference.

Quantum Mechanical Study of the Fleischmann-Pons Effect

S.J. Pemberton, J.L. Mace, and D.G. Tasker

Los Alamos National Laboratory, Dynamic and Energetic Materials Division

Abstract. Resonances in deuterium-deuterium fusion were examined by calculating the transmission behavior of a single deuteron through a deuterium atom, or through a system comprising two or three deuterium atoms, using transfer matrix methodology. Many unit-transmission resonance peaks were observed in the results of the calculations, even at incoming deuteron energies of a few electron volts, but resonance peak widths were found to be very narrow at low energies, so that the probabilities of fusion would be small.

1. Introduction

The Fleischmann-Pons Effect (FPE) was swiftly rejected when first published in 1989, yet many researchers have since reported energy gains in similar experiments [1]. The body of evidence suggests that the energy gains are real, even though the heat production powers are small and often difficult to replicate. Fleischmann and Pons suggested that these gains are the result of "cold fusion", or low energy nuclear reactions, where energy is released from a deuterium-deuterium (D-D) fusion. However, the probability of D-D fusion under the conditions of an FPE cell is vanishingly small as currently understood. As stated by Pons, et al., "It is necessary to reconsider the quantum mechanics of electrons and deuterons in such host lattices" [2].

The current work undertook a simple study of resonance bands that may exist for quantum-mechanical deuterium particles to penetrate through the nucleus of a deuterium atom. Solutions to Schrödinger's equation were developed first for a single-atom system, and then for multi-atom systems using the transfer matrix methodology. The effect of energy perturbations on the atom potentials was also examined.

1.1 Time-Independent Schrödinger's Equation in One Dimension

Phenomena of interest were examined using the simplified, one-dimensional and time-independent Schrödinger's equation for quantum mechanics. This equation can be written

$$-\frac{h^2}{2m}\frac{\partial^2}{\partial x^2}\psi(x) = (E - V(x))\cdot\psi(x) \tag{1}$$

where m is the particle mass, E the particle energy, x the spatial variable, and $V(x)$ is the background potential energy of the system encountered by the particle. The general solution of this equation is the wave equation,

$$\psi(x) = Ae^{ikx} + Be^{-ikx} \tag{2}$$

where A and B are wave magnitudes and $k = \frac{\sqrt{2m}}{h}\sqrt{E-V}$ is the wave number of the particle at position x.

1.2 One-Dimensional Transfer Matrices

The above wave solution can be drafted in matrix notation as

$$\psi(x) = \begin{pmatrix} e^{ikx} & e^{-ikx} \end{pmatrix} \cdot \begin{pmatrix} A \\ B \end{pmatrix} \tag{3}$$

From this it can be observed that the wave can be "propagated" to the left or right by a distance a via the straightforward matrix operation

$$\begin{pmatrix} A \\ B \end{pmatrix}_{x=a} = \begin{pmatrix} e^{ikx} & 0 \\ 0 & e^{-ikx} \end{pmatrix} \cdot \begin{pmatrix} A \\ B \end{pmatrix}_{x=0} \equiv \mathbf{P}(V,a) \cdot \begin{pmatrix} A \\ B \end{pmatrix}_{x=0} \tag{4}$$

Likewise, the background potential can be changed discontinuously from V_1 to V_2 via the "discontinuity matrix" at the origin

$$\mathbf{D}(V_1,V_2)_{x=0} = \begin{pmatrix} 1+\dfrac{k_1}{k_2} & 1-\dfrac{k_1}{k_2} \\ 1-\dfrac{k_1}{k_2} & 1+\dfrac{k_1}{k_2} \end{pmatrix} \tag{5}$$

where the subscripts indicate wave numbers at the respective potentials. A similar discontinuity can be applied at $x = a$ using a combination of the above discontinuity matrix and suitable backward and forward propagation matrices,

$$\mathbf{D}(V_1,V_2)_{x=a} = \mathbf{P}(v_2,-a) \cdot \mathbf{D}(v_1,v_2) \cdot \mathbf{P}(v_1,a) \equiv \mathbf{t}_{total} \tag{6}$$

Finally, the transmission through a system comprising multiple discontinuities, all contained within a system transfer matrix $\mathbf{t}_{total}$, can be calculated using the formula

$$T = 1 - \frac{|\mathbf{t}_{total21}|^2}{|\mathbf{t}_{total,11}|^2} \tag{7}$$

where the subscripts indicate particular matrix elements by row and column. [3]

2. Methodology

2.1 Basic Atom
A single deuterium atom was represented by stepped discontinuities in potential energy.

The most basic atom comprised only a hard core potential at 100 MeV and a potential well at -50 MeV. These values were chosen as representative of the energies in a real atom, but were not meant to be precise duplicates of real potentials. As was discovered in developing the results documented below, a choice of different values of these potentials did affect the locations of the resonance bands found, but did not change the overall resonance structure of the systems in question. Plots of the potential energies for this atom are shown in Fig. 1. The radius chosen for the hard core potential was 0.34 femtometers [4], and a radius of 7.24 femtometers was chosen for the Yukawa well; this is the radius at which a simple Yukawa attractive potential would adopt a value of -50 MeV [adapted from equations in reference 5].
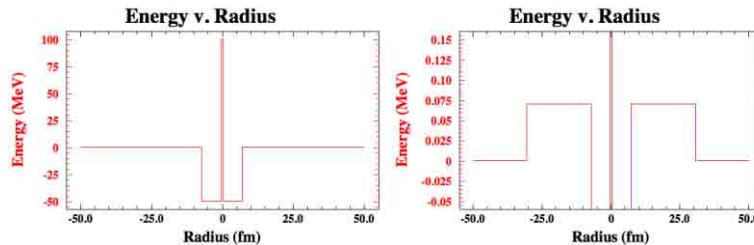

Fig. 1 – Basic atom potentials, including first coulomb potential.

More complicated atoms included additional potentials, which were used to represent the coulomb attraction experienced by a deuteron near a deuterium atom. These included a 70-keV potential from the edge of the Yukawa well to a radius of 30.6 femtometers, to represent the peak energy of a 1s⁻ electron orbital and the radius at which that orbital's energy drops to one-half its peak value. However, differences

352

in the results of those calculations were found to be negligible; for brevity the results have not been included in this paper.

2.2 Systems Studied

Transmission of a deuteron through a single deuterium was studied first, followed by an examination of the additional resonances generated in transmission through two atoms. Finally, results of the two-atom case were compared with those of a system with three atoms.

3. Results

3.1 Single Atom Transmission

Single-atom transmission is perhaps the least interesting case studied, with several resonances below the hard-core energy of 100 MeV, but no unit resonance until well above the hard-core energy. A plot of the result can be seen in Fig. 2.
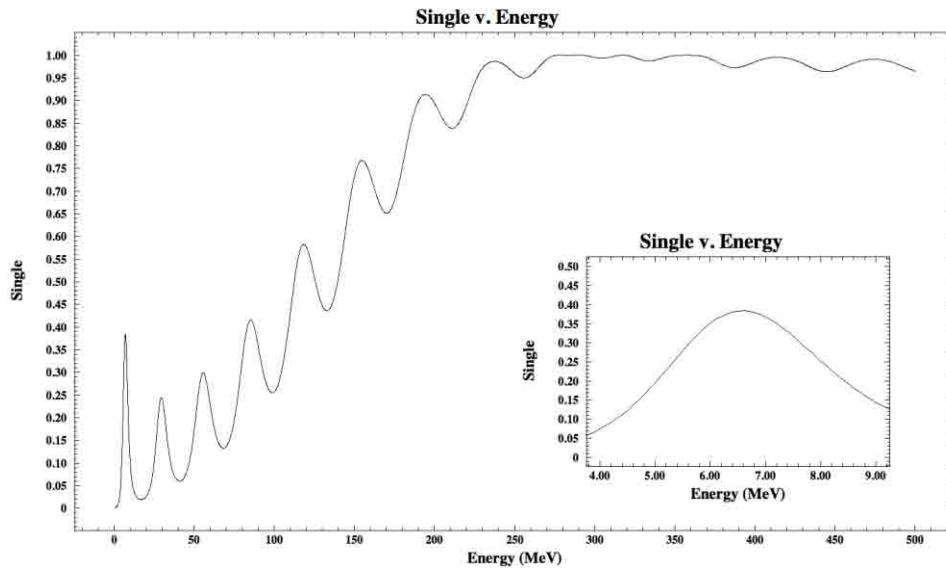

Fig. 2 – Transmission through a single basic atom; the inset shows magnification of the first peak.

3.2 Two- and Three-Atom Transmission

Fig. 3 and Fig. 4 show the transmission through two atoms and three atoms, respectively. Atoms in the system calculated were duplicates of the basic atom above, separated from one another by a distance of one angstrom.

Perturbation of the energy levels in any of the atoms in the multi-atom system had very little effect on the structure of the results, except for changing the particular energies at which resonance bands occur. For brevity, plots have not been included here.
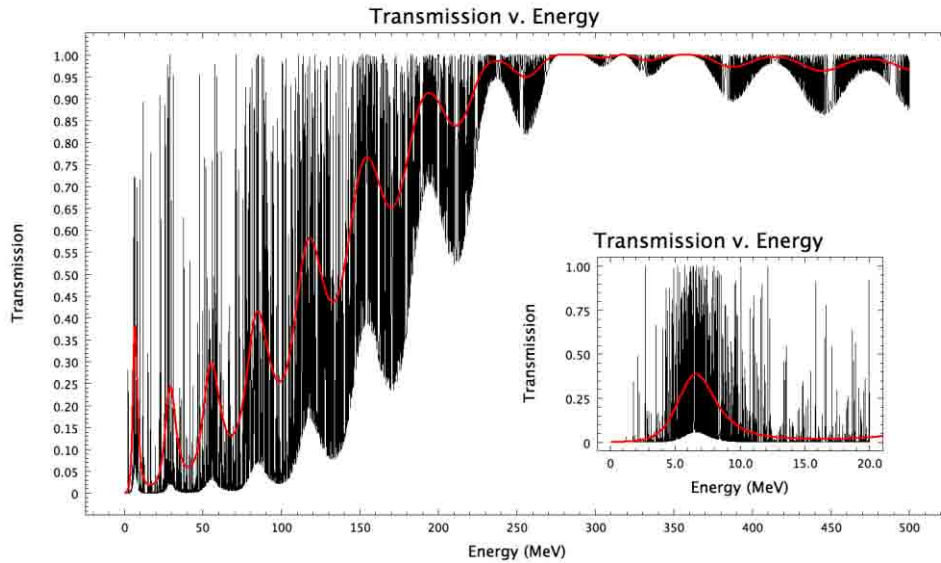
Fig. 3 – Transmission through two atoms separated by 1 angstrom (black curve); the single atom transmission curve from Fig. 2 is shown in red. The inset shows magnification of the first peak in the single-atom spectrum.
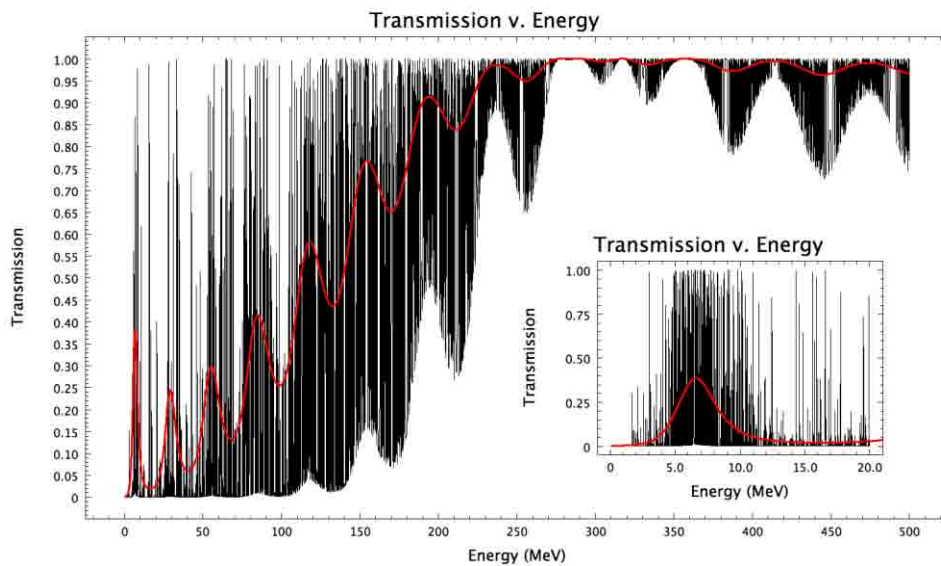

Fig. 4 – Transmission through three atoms separated by 1 angstrom (black curve); the single atom transmission curve from Fig. 2 is shown in red. The inset shows magnification of the first peak in the single-atom spectrum.

Zooming in on various energy regions to examine the resonance bands in greater detail revealed two interesting phenomena. First, the difference between the two-atom case and the three-atom case was noticed to resemble the peak splitting observed in optical spectroscopy or magnetic resonance imaging. A plot of this splitting is shown in Fig. 5.

Second, even at very low energies, the resonance bands that look like spike noise in the coarse plots of Fig. 3 and Fig. 4 were revealed to be *unit* transmission peaks. A plot at low energy with greatly increased resolution can be seen in Fig. 6. The plot illustrates the unit-transmission character of only one peak, but others were examined and found to also be peaks of unit transmission. This character was not obvious in the above figures because the resonance peaks have such narrow energies: a high degree of granularity was required in the transmission calculation to produce transmission values of one.
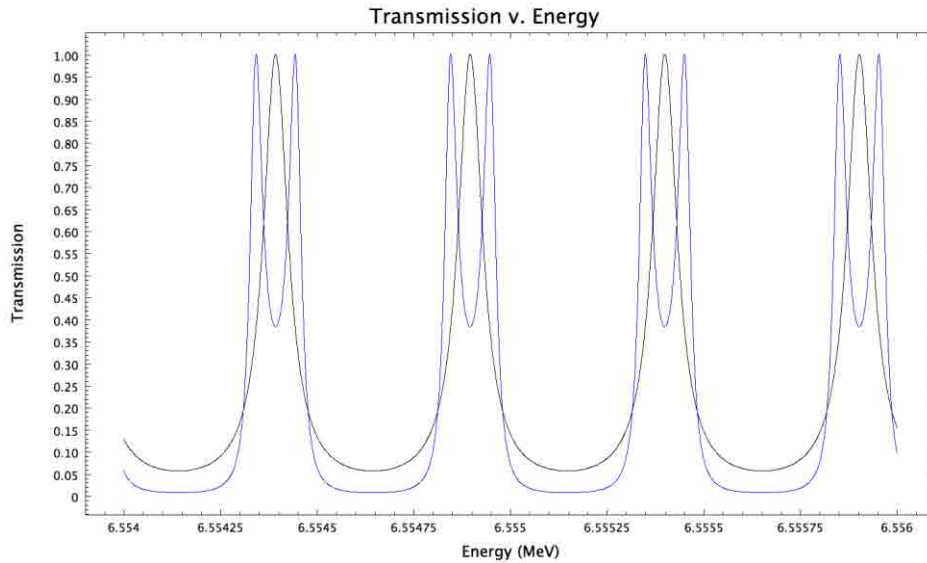
Fig. 5 – Peak splitting observed between two-atom transmission (black curve) and three-atom transmission (blue curve)
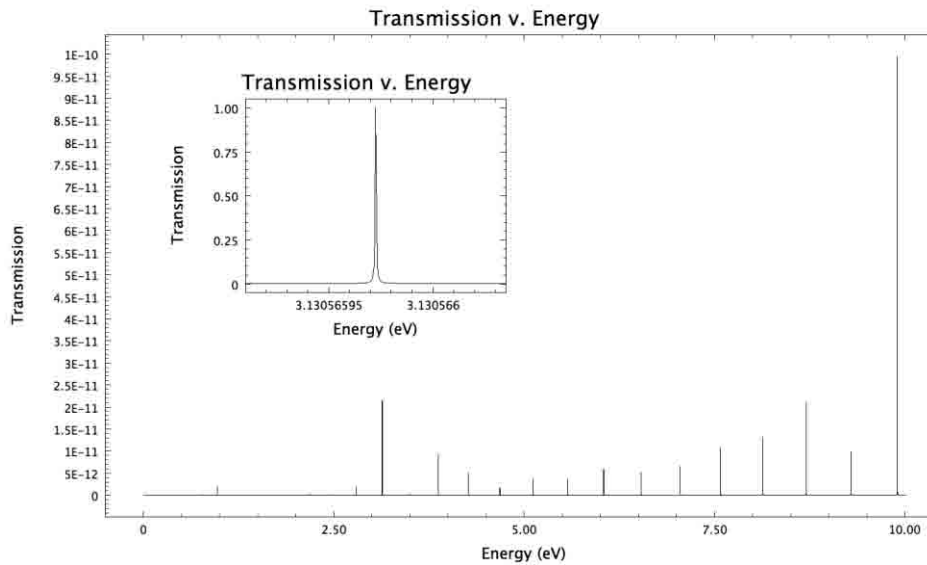
Fig. 6 – Resonance peaks from 0 to 10 eV (outer plot) and the particular peak near 3.1306 eV (inset plot); the ordinate scale on the outer plot is narrow only because the energies in the curve were too coarsely spaced to include larger transmission values – high granularity at each resonance was required in order to observe unit transmission.

4. Conclusions

Transmission has been estimated for a deuteron through one or more deuterium atoms. The estimate was approximate, but the resonance structure observed should represent that of real systems.

A complicated structure of unit-transmission resonance was found for multi-atom systems, even for transmission through a two-atom system.

Large (1%) perturbations in the deuterium-deuterium attractive or repulsive potential energies had very little effect on transmission resonances.

Resonance peaks observed in transmission through two- and three-atom systems are regularly spaced, and a comparison of the two systems illustrated peak splitting reminiscent of optical spectroscopy or magnetic resonance imaging in the chemistry lab.

Resonance peaks at low deuteron energies were extremely narrow.

5. Discussion and Future Work

The narrowness of resonance peaks would imply that transmission is highly improbable when deuteron waves encounter deuterium particles in free space; this is due to the broad, continuous energy distribution of particles in free space. However, deuterium atoms trapped in a lattice structure would behave as "particles in a box", and hence have quantized energy levels. Therefore it is possible that overlaps between the quantized energy levels of trapped deuterium atoms in a palladium lattice, and the narrow resonance peaks for transmission, could lead to an increased probability of transmission, and therefore an increased probability of D-D fusion in the lattice-bound system.

First and foremost, the next segment of this research should relate transmission spectra – such as those included in this paper – with fusion interaction probabilities. For instance, the area under the curve for the 3.1306-eV resonant peak shown in Fig. 6 is only 8.9×10^{-10} eV. However, it is not immediately obvious how this relates to a reaction cross-section.

Future work in this field should include a study of the energy levels deuterium atoms may occupy within a palladium lattice, and some examination of whether those energy levels may overlap with resonance peaks for transmission through real bound-deuterium systems, thereby increasing the fusion probability.

Acknowledgements

References

[1] E. Storms, The Science of Low Energy Nuclear Reaction (World Scientific Publishing Co., Singapore 596224).

[2] M. Fleischmann and S. Pons, "Electrochemically induced nuclear fusion of deuterium," *Journal of Electroanalytical Chemistry*, vol. 261, pp. 301-308, 1989.

[3] J.S. Walker and J. Gathright, "Exploring one-dimensional quantum mechanics with transfer matrices", *Am. J. Physics* **62** (5), May 1994.

[4] Gerald Hale, Los Alamos National Laboratory, personal communication.

[5] H. Frauenfelder and E.M. Henley, Subatomic Physics (Prentice-Hall, Inc., Englewood Cliffs, New Jersey, USA).

Exotic Nuclear Physics: From Cold Fusion To Antikaonic Nuclear Clusters

T. Bressani[1,2]

1. *Dipartimento di Fisica Sperimentale, Università di Torino (Italy)*
2. *Istituto Nazionale di Fisica Nucleare, Sezione di Torino*

E-mail: bressani@to.infn.it

Abstract. A short review of the status of the experimental searches and theoretical speculations on the possible existence of the AntiKaonic Nuclear Clusters is given. There are no scientific relationships with the possible Cold Fusion phenomena, but some similarities and differences in the perception and acceptance by other communities of physicists.

1. Introduction

I am very happy to attend again a Conference on Cold Fusion, ICCF15 and meet old colleagues and friends. As a matter of fact I had the opportunity to hear, nearly exactly twenty years ago (November 1989) the first seminar given in Europe, at CERN, on Cold Fusion by Martin Fleishmann.

I will never forget the enormous interest by the audience, and also the strong, a priori, skepticism. I have always worked in experimental Nuclear Physics, with quite huge detectors in big international Laboratories, but the strong interest in this potentially new class of phenomena convinced me to start with some of my younger collaborators an experimental activity, following a brief theoretical speculation [1]. From 1989 to 1998 I performed several experiments, mainly with the gas-loading technique paying a particular care to the detection of 2.5 MeV neutrons [2,3] and afterwards of ^{4}He [4,5]. The results were in line with those reported by other Groups, i.e. the possible detection of sporadic emissions of particles, with low statistical significance and not reproducible. During these years I attended all ICCF's from 1 to 7. As a matter of fact I organized also, with G. Preparata, ICCF2 at Villa Olmo, on the Como Lake.

My activity on Cold Fusion was stopped in 1999, not for overwhelming difficulties in the funding by public Agencies or private Companies but by the awareness of not having enough personal competence in Condensed Matter Physics, which is to my opinion the key point for understanding Cold Fusion.

However I never denied the reality of the scientific case of Cold Fusion, whereas I was (and I still am) very skeptical about possible applications.

A few years after my return at full time to Nuclear Physics, I faced a scientific problem that presents some similarities with Cold Fusion, but also differences in the acceptance by the other colleagues. This is the reason for which I accepted to give the present talk, scientifically very far from Cold Fusion and not easy to follow for many colleagues not experts of the sector. It is interesting to follow the conclusions.

2. The AntiKaonic Nuclear Clusters

I report here a brief account of a recent Invited Talk that I gave to the big Conference PANIC08 [6]. By AntiKaonic Nuclear Clusters (AKNC) we indicate nuclear states in which a $\overline{\text{K}}$ (K$^-$) is strongly bound to some nucleons.

The first speculation about the possible existence of AKNC's is due to Wycech [7], based on the observation that the driving $\overline{\text{K}}$N interaction in the isospin I=0 channel is strongly attractive near threshold. A large Binding Energy B of about 100 MeV was found, but with a similarly large value of the width Γ.

The theme received a strong boost by the prediction from [8] of the possible existence of narrow discrete AKNC few-body nuclear systems. The $\overline{\text{K}}$-nucleus potential was derived from a phenomenological ($\overline{\text{K}}$N) potential accounting for several observables, with particular emphasis to the rôle of the Λ(1405), assumed to be a bound (K$^-$p) system.

The predicted B for $\overline{K}$-few nucleons systems were quite large (from 50 to more than 100 MeV), but the distinctive feature was the narrowness (Γ of 20-30 MeV). It was due to the circumstance that, due to the high value of B, the main decay channel (K⁻p) (I=0)→Σπ is energetically forbidden, and the decay to Λπ is suppressed by the isospin selection rules.

A very important feature predicted for AKNC was a large density, up to 10 times the normal nuclear density. This possibility is very interesting for explaining the structure and the evolution of the neutron stars.

The K⁻pp bound system was studied in Ref [9] by a coupled-channel Faddeev calculation obtaining a B of (55-70) MeV and a quite large Γ, of the order of 95-100 MeV.

Recently Ref [10] examined the possible existence of AKNC by using energy dependent ($\overline{K}$N) interactions derived with the s-wave coupled-channel amplitudes involving the Λ(1405) and resulting from the chiral SU(3) dynamics, plus p-wave amplitudes dominated by the Σ(1385). It was concluded that AKNC can possibly exist with B from 60 to 100 MeV, but with Γ of similar magnitude. This paper contains a quite complete list of the theoretical papers on the subject.

In 2004 the Collaboration KEK-PS E471, working at the 12 GeV PS at Tsukuba (Japan) published a paper with the triumphant title:"Discovery of a strange tribaryon S° (3115) in ⁴He (stopped K⁻,p) reaction" [11] based on a narrow peak observed in the semi-inclusive proton spectrum. There were some discrepancies between the features of the A=3 AKNC supposedly discovered and the original prediction but anyway this result played the major role at several Conferences and Workshops in the following two years. Unfortunately the same Group, from a further data taking with larger statistics whitdrawn the result as due to an experimental artifact [12].

Thanks to the clever design of the FINUDA spectrometer, installed at one of the two interaction regions of the DAΦNE collider at Laboratori Nazionali di Frascati (Italy) and aiming at a series of studies of Hypernuclear Physics [13], the detector was able to identify in a clean way Λ-hyperons emitted following the interaction of stopped K⁻ with light nuclei (⁶Li, ⁷Li, ¹²C). Fig 1a) shows the invariant mass (I.M.) of a proton and a π⁻ for the events in which these two particles are observed out from the nuclear targets [14]. The peak position agrees well with the known Λ mass and the width of the peak is as narrow as 6 MeV/c². Quite surprisingly the above events in coincidence with a further proton emitted in the interaction of the stopped K⁻ are strongly back-to-back (b.t.b.) correlated. Fig. 1b) shows the angular correlation, acceptance corrected, for the (Λ,p) events.
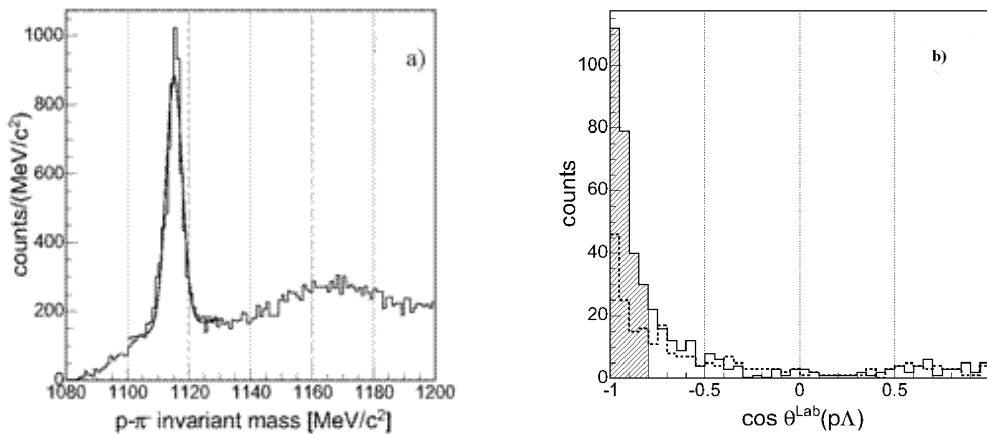

Fig. 1. - a) I. M. distribution of a (p,π−) pair for all the events in which these two particles are observed [4]. b) Opening angle distribution between a Λ and a p: solid line, ⁶Li, ⁷Li and ¹²C targets; dashed line, ²⁷Al and ⁵¹V targets. The shaded area is selected as that of b. to b. events . From [14]

A logical consequence of the observation of the Λ–p b.to.b. correlated events was that of determining their I.M in order to verify whether they could be the result of the decay of an A=2 AKNC. Fig.2 shows the I.M. spectrum for the Λ–p events for the lighter targets. A relatively narrow bump is observed, with B=115±9MeV, Γ=67±15MeV. I notice that, whereas the value of Γ is rather compatible with the prediction of [8], the value of B not; the experimental value is about twice.

Alternative conventional explanations for the above observed bumps were put forward. In [15] the bump in the Λ–p I.M. spectrum was explained as an artifact of the angular cuts applied to the flat spectrum of I.M. of Λ–p events resulting from genuine b.t.b. pairs formed in simple K⁻–(np) interactions in the target nuclei that suffered a Final State Interaction.

Even though such a mechanism cannot be completely excluded, other arguments are contradicting it as discussed in [6].

The consistent theoretical effort and the first results coming from experiments with K⁻ stimulated the search for AKNC also in reactions induced by other projectiles.
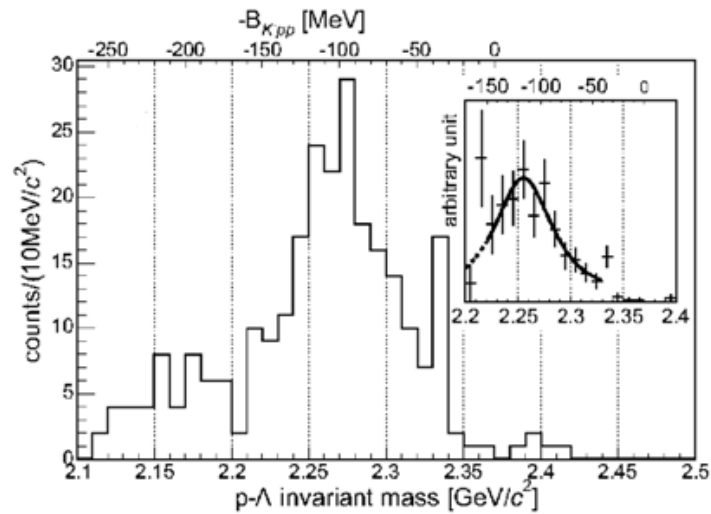
Fig. 2. - I. M. of a Λ and a p in a b. to b. correlation from light targets before the acceptance correction. The inset shows the result after the acceptance correction. From [14].

The best evidence for the possible existence of a narrow A=2 (K⁻pp) AKNC was very recently provided by a reanalysis of the data on annihilations of p at rest on ^{4}He̅ [16,17] collected with the OBELIX spectrometer which operated from 1991 to 1996 at the LEAR complex at CERN. Both the reactions of possible production of the A=2 AKNC and the steps in the data analysis are too complicated or technical to be outlined here. The final result of the I.M. of the Λ-p system, the same studied in FINUDA but produced with a different mechanism is shown by Fig.3). The signal has a statistical significance of 4.9 σ with a B of 151.0±4.4 MeV and a Γ less than 33.9 MeV.
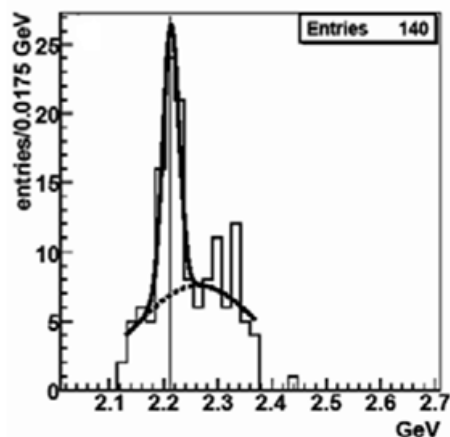
Fig. 3. - I.M. of a Λ and p observed in events produced by the annihilation of p at rest in ^{4}He. From [17].

Finally the data collected by the DISTO Collaboration at the Saturne accelerator in Saclay on the pp→pK⁺Λ reaction at 2.85 GeV were reanalyzed with the aim of finding signatures compatible with the formation of the A=2 AKNC. A strong signal that may be interpreted as due to a state with B= (105±2)MeV and a similar Γ was reported [18]. I notice that the B value agrees within the errors with that reported in [14], but Γ is twice.

Table1. Comparison between the Binding Energies B and Widths Γ of the (K⁻pp) system reported by experiments and Theory.

		B(MeV)	Γ (MeV)	Ref.
$^2_K H$	K⁻ at rest	115±9	67±15	[14]
$^2_K H$	$\bar{p}$ at rest	-151.0±4.4	≤33.9	[17]
$^2_K H$	pp→pK⁺Λ	-105±2	118	[18]
$^2_K H$	Theory	-48	61	[8]

Table 1 summarizes the values of B and Γ reported by the three experiments which investigated with different reactions the possible production of the archetype A=2 AKNC, as well as the theoretical prediction. A remarkable disagreement between the different sets of results is apparent. A similar disagreement exists if one tries to compare by a simple hadronic model the capture rates reported by FINUDA [14] for stopped K⁻ with those reported by OBELIX [16,17] for stopped p. A detailed discussion on this subject as well as a possible explanation based on the hypothesis of a Quark Gluon Plasma formation in p annihilation can be found in [19].

3. Conclusions on the present status of the search for AKNC

From the short review given in Sec.2 the following conclusions can be drawn:
a) the first experiment dedicated to the search of AKNC (KEK-PS E471), which claimed triumphally the discovery of such exotic systems [11] was afterwards obliged to whitdraw the claim, recognizing that it was due to an experimental artifact;
b) three other non-dedicated, general purpose experiments (facilities), namely FINUDA at LNF [14], OBELIX at CERN [16,17] and finally DISTO at Saclay [18] reported the observation of signals that could be interpreted as due to formation of the A=2 AKNC.
However:
  i) the statistical significance is in some cases not very good
  ii) the reported results disagree each other and with the theoretical prediction [8];
c) all theoretical approaches to the problem predict a quite large binding energy B (of the order of 100 or more MeV) of an Antikaon to few nucleons; however all approaches predict a width Γ for such a state of the same order of B. Only the phenomenological approach by (8) suggests a value of Γ of the order of about 30 MeV, then experimentally accessible.
In spite of the above difficulties the problem of the existence of AKNC is one of the hot spots in Hadronic Physics and the debate is very vivid at all the Conferences and Workshops in this sector. It is expected that the final analysis of the data collected by FINUDA with a six times larger statistics as well as the new data that will come from the dedicated experiments E15 and E27 at J-PARC (Japan) and FOPI at GSI (Germany) will clarify the situation in the near future.

Comparison of the AKNC and Cold Fusion cases
In table 2 I report a personal classification of the merits of Cold Fusion (C.F.) and AKNC scientific cases. I will not comment in detail the above classification, but add only a few remarks. The first is the similarity of the two cases with regards to the experimental and theoretical situation. Points a), b) and c) of Sec.3 are reminiscent of similar situations occurring in the C.F. research, in particular at the beginning. The second is the reaction by the community of Nuclear Physicists. After a short transient time, lasting not more than a couple of years, the result was a stopping of the financing by public Agencies in nearly all Countries, a disappearance of papers on C.F. in nearly all the more important Journals in Physics, a disappearance of the C.F. scientific case in all general Conferences of Nuclear Physics. Exactly the opposite occurs for the AKNC's scientific case. In addition, instead of stopping the activity, new dedicated experiments were approved by the Scientific Committees of world leading Laboratories with top priority and adequately financed.
As an old Nuclear Physicist, my concluding wish is that, after recognizing the excellent work carried out in twenty years by a few clever and motivated Groups, Cold Fusion physicists will return again in the community of Nuclear Physics.

Table 2. Personal classification of the merits of C.F. and AKNC scientific cases (*=minimum,*****=maximum)

	CF	AKNC
Applications	*****	*
Impact on media	*****	*
Scientific interest	*****	****
Acceptance by theoreticians	*	****
Acceptance by experimentalists	**	*****
Papers on Physics journals	*	*****
Financement by Public Agencies	*	*****
Positions for young reaserchers	*	***
Interest by students	*****	***

4. References

[1] T. Bressani, E. DelGiudice and G. Preparata, *Nuovo Cim.* **101** 845 (1989)

[2] T. Bressani et al., *Nuovo Cim.* **104** 1413 (1991)

[3] E. Botta et al., *Nuovo Cim.* **105** 1663 (1992)

[4] E. Botta et al., *Proc. 5th Int. Conf. on Cold Fusion (ICCF5), Montecarlo (1995)*, 233

[5] E. Botta et al., *Proc. 6th Int. Conf. on Cold Fusion (ICCF6), Toya, Japan. (1996)*, 29

[6] T. Bressani, *Nucl. Phys. A* **827** 306c (2009)

[7] S. Wycech, *Nucl. Phys. A* **450** 399c (1986)

[8] Y. Akaishi, T. Yamazaki, *Phys. Rev. C* **65** 044005 (2002)

[9] N.V.Shevchenko, A. Gal, J. Mareš, *Phys. Rev. Lett.* **98** 082301 (2007)

[10] W. Weise, R.Hartle, *Nucl. Phys. A* **804** 173 (2008)

[11] T. Suzuki et al., *Phys. Lett. B* **597** 263 (2004)

[12] M. Iwasaki et al., *Nucl. Phys. A* **804** 173 (2008)

[13] A. Zenoni in *Proc. of the International School of Physics "E.Fermi" Course CLVIII (Hadron Physics),(eds. T. Bressani, A. Filippi and U. Wiedner) SIF-IOS Press (2005),* 183

[14] FINUDA Collaboration, M. Agnello et al., *Phys. Rev. Lett.* **94** 212303 (2005)

[15] V.K. Magas, E. Oset, A. Ramos, H. Toki, *Phys. Rev. C* **74** 025206 (2006)

[16] G. Bendiscioli et al., *Nucl. Phys.A* **789** 222 (2007)

[17] G. Bendiscioli et al., *Eur. Phys. Jour. A* **40** 100878 (2009)

[18] T. Yamazaki et al., *Hyperfine Inter.* **193** 181 (2009)

[19] T. Bressani et al., *Hyerfine. Inter.* **193** 201 (2009).

A Possible Mechanism For Cold Fusion

G. Moagăr-Poladian

National Institute for Research and Development in Microtechnology-Bucharest, Str. Erou Iancu Nicolae 126A (32B), Bucharest, ROMANIA; E-mail: gabriel.moagar@imt.ro

> **Abstract.** We describe a mechanism for cold fusion that is able to explain how two hydrogen ions may come close enough so as to fusion as well as many of the different and independent experimental observations made during years of experiments. We present the mechanism, its weak points, the way it explains the respective phenomena and suggest some experiments that may validate further the model described by us.

The initial work of Fleischman and Pons [1] was published more than twenty years ago but the acceptance of the facts by the wide scientific community is still to be obtained. While experiments are beginning to become reproducibilite (see www.lenr-canr.org), it remains the problem that there is no clear explanation on how two positive ions may get so close, at room temperature, so as to fusion. We show how such a mechanism may exist and explain this "exotic" phenomenon. We start from two observations: a) from the literature [2] it results that in Pd hydrogen exists in Pd as a positive ion; b) the ions are moving in a periodic electrostatic potential given by the periodic location of the host lattice ions, being a superposition between the electrostatic screened potential made by the positively charged metal ions. This last aspect suggests an analogy with the case of electrons in solids [3]. Starting from this point and having in mind also the theory of the Kronig-Penney potential [4] that predicts formation of energy bands in case of periodic potentials, we may conclude that the hydrogen ions exists in such energy bands in the solid. Each type of isotopes has its own energy band structure. A model based on energy band structure for the hydrogen ions was proposed earlier by [5], but we follow another route as compared to it, route that allows us to explain the main aspects of the mechanism and why cold fusion may take place at room temperature. The energy bands may be separated by forbidden energy gaps or may superimpose, as in the case of metals. We refer from now on only to the energy band structure corresponding to hydrogen ions. Following the usual route in solid state physics, we describe the kinetics of the hydrogen ion by its energy E and its wavevector k. There is always a relation E = E(k) between these two parameters, relation that is called the dispersion relation. We may deduce from it the ion effective mass m^*:

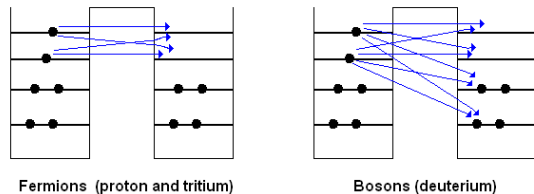$$\frac{1}{m^*} = \left(\frac{\partial E^2}{\partial^2 k} \right) \tag{1}$$

The effective mass (generally, it is a tensor) is applicable especially when considering the particle at one of the energy band edges, namely upper edge or lower edge. At the lower edge the effective mass is positive. At the upper edge the effective mass is negative [3]. An electrically charged particle with negative effective mass behaves in an electric field like a particle of positive effective mass but having an opposite charge [3], which means that a H ion that is excited at the top of an allowed energy band has a negative effective mass and it behaves, in an electric field, as a negative ion with a positive effective mass. This is a very important feature and is the key to our model. A particle may reach the upper part of an energy band only by excitation (thermal or of other nature) and it will stay only a certain interval of time in the respective state because of scattering on different quasi-particles (phonons, lattice ions, impurity ions, etc.). For the sake of simplicity, we consider throughout the work that hydrogen does not form any hydrides or, if it forms, the hydrogen concentration in the material is so high that all the hydride-type bonds are saturated with hydrogen and the remaining hydrogen ions are moving relatively free within the "lattice" formed by the potential wells.

The mechanism we propose is as follows: a hydrogen ion is excited to an upper energy state having negative effective mass. This excited ion will stay a time τ in the excited state. During this period, the excited ion may interact electrostatically with another hydrogen ion that has a positive effective mass. The system of two ions behaves similar to two particles of opposite charges attracting each other. They move in a central potential field, similar to electrons in atoms or two electron and hole in an exciton.

Thus, the combination of the Coulomb potential and the negative effective mass is the mechanism that allows the two H ions to approach each other. It is mandatory to mention the fact that the two ions must be in different allowed energy bands (different Brillouin zones [3]) so as they be able to form a closely orbiting system. If we take into account that heavier ions will get closer than lighter ones, the sequence of fusion probability will be given by T > D > H, where T stands for tritium, D for deuterium and H for proton. For example, deuterium is twice heavier than proton, so that we expect that the orbiting radius for the case of deuterium be approximately half of that corresponding to the proton. In other words, the heavier isotopes are the most probable to fusion by such a mechanism, since the orbiting distance between them will be smaller. Another possibility is that the ions directly collide / coalesce. For the orbiting case, a first temptation is to use the expression of Bohr radius but replacing the electron mass with that of the hydrogen ion. This approach indicates an orbiting radius of few tens of femtometers, small enough so that nuclear fusion takes place with a certain probability. This approach is only generic and useful for showing that, in principle, the two ions may get close enough so as to fusion. The (constant) effective mass formalism is applicable when the interaction potential is of the order of several eV to even few tens of eV. In reality, the overall potential (electrostatic repulsion + lattice) changes as the two ions get close each other. In such a situation, the energy band structure changes as well with the distance between ions and so does also the effective mass. An iterative computation is needed for obtaining a correct estimate of the orbiting distance. Moreover, the host lattice expands as hydrogen is incorporated into it. This means that the band structure (and the effective mass) varies with the content of hydrogen. Such a mathematical computation is complex and, especially, needs a high computational power so as to tackle the problem with sufficient precision. When the two ions get very close to each other, the applicability of the efective mas formalism is not valid anymore. Even if we may still speak about ion mass (positive or negative mass) since the ion is characterized by a certain dynamics inside the periodic crystal, the mathematical use of the respective formalism is questionable. A first approach may be that of considering an effective mass that is energy (and, thus, position) dependent. This approach is based on the observation that the energy band structure is a continuous function everywhere in the lattice, as well as are its first and second derivatives with respect to the coordinates and, respectively, to the wavevector of the ions. It is obvious that the band structure varies dramatically in the region where the two ions interact, but there can still be defined a band structure and a local (energy / position dependent) effective mass. Such an approach may lead to significant computational complexity. Another approach can be that of considering a tight binding model, since the electrostatic interaction at distances useful for fusion process is of the order of tens of keV. Such a start point moel could be that of [6]. However, the aim of this paper is to present the physical mechanism leading to fusion at room temperature and the consequences of it. The elaboration of the mathematical formalism to be used for describing the process is an open matter and does not represent the scope of the paper. However, even with this problem, the model can explain in a unitary manner many experimental results presented in the literature, as will be seen further. This lack of an appropriate mathematical formalism is the weak point of our model. When orbiting, the two ions form a bound system having a discrete energy spectrum, as in the case of excitons in solids [3] and electrons in atoms [4]. Because the interaction energy at such short distances is of the order of tens of keV, we expect that the specific energy spectrum of such a bound system be active in the X-rays region. Emission of X-rays with specific wavelengths was experimentally proven in [7-8]. In [8] the authors claim that the emitted X-ray wavelengths are not specific to any characteristic X-ray spectrum of the known elements. We consider that the X-rays are emitted by the bound system formed by the two orbiting ions, during system de-excitation to a lower energy state, analogue with the case of electrons in excited atoms. Because of the specific, discrete energy levels of the bound system, the emitted X-ray spectrum has wavelengths that are specific for the difference in energy between the levels involved in the de-excitation transition, wavelength that are not encountered in any of the characteristic X-ray spectra of the known elements. An interesting consequence of our model is that illuminating a hydrogen loaded sample with X-rays having wavelengths identical to these experimentally determined ones (that have a specific emission spectrum during reaction) will reduce the reaction rate. This is so because resonant excitation of the bound system will increase the orbiting radius, similar to electrons in atoms (resonant illumination of an atom excites the electron on a state that is further from the nucleus than is the fundamental state). This is a theoretical prediction that, to our knowledge, was not yet reported experimentally. Its experimental verification will check the validity of our model. Let us now consider the ways in which an ion may be excited to the upper energy state of negative effective mass. One way is by excitation at thermal equilibrium, when collisions with different quasi-particles existing in the lattice may give the ion enough energy to reach the top of the energy band. The higher the temperature is the greater is the number of ions with negative effective mass. Another way is to use external factors such as illumination with photons or bombardment

with energetic particles (electrons, ions) [9]. Since we have an energy band structure, only photons with appropriate wavelengths may excite the ions to the energy states of negative effective mass. Such a resonant / selective excitation is observed in [10]. In this case, the energy of excitation may vary from several meV up to several eV. Such a situation is encountered in [10-11]. We mention that in [11] the energy difference between the two incident light beams is claimed to have effect in enhancing the fusion process. It seems that the two beams excite a phonon in the metal, in the THz frequency range, this quasi-particle being responsible for the enhancement. Such a phonon may interact with a hydrogen ion and excites it resonantly at the top of the energy band. We assert that the Born-Oppenheimer approximation [3] is applicable to the hydrogen ion also. We make this assertion because we expect that the mass of the hydrogen ion in the lattice do not differ significantly with respect to hydrogen mass in vacuum. This assumption is based on the analogy with electrons in crystals. Hydrogen has a relatively high mobility in heavy metals that have an atomic mass of at least tens of hydrogen atomic mass. For example, Pd has an atomic mass that is 106 times greater than hydrogen mass [www.webelements.com]. On the other hand, hydrogen diffusion in metals is a slow process, the hydrogen ions being all the time in thermal equilibrium with the lattice / metal ions. Because of these two reasons, hydrogen ions are approximately ten times faster than the lattice ions, so that Born-Oppenheimer approximation may be applied without introducing great errors, of only few percent. As numerical values, we mention that an error of less than 10 % for proton in Pd and of approximately 16 % for tritium in Pd is obtained. These are acceptable errors. The Born-Oppenheimer approximation indicates to us that we may look at the "lattice" formed by the potential wells (for the hydrogen ions) as being frozen, hydrogen ions moving within this lattice. Because such a potential well is formed by the contribution of several atoms that oscillate in an uncorrelated manner, the potential well is also squeezed at the same frequencies as those of atom oscillations. Since the displacements of atoms, at room temperature, are small compared to the interatomic distance within the metal lattice, we may consider that the deformation / squeezing of the potential wells is small compared to the well size.

A very important aspect is that two hydrogen isotopes are fermions (proton and tritium) while deuterium is a boson. This is a very important feature. Consider two adjacent potential wells, one having a higher number of hydrogen ions than the other, as depicted in figure 1. In the left part, we have the case of fermions. In the right part, we have the case of bosons. We simplify and consider discrete energy levels, but the explanation may be extended in a straightforward manner to band structure also.

Fermions (proton and tritium)   Bosons (deuterium)

Figure 1 – Sketch of the way in which fermions, respectively bosons, diffuse.

Let consider fermions first. The fermions from the left quantum well may diffuse / tunnel only on the un-occupied states in the right quantum well because of the Pauli exclusion principle. This means a low number of available states for transfer, as seen from figure 1. In the case of bosons, there is no exclusion principle and they may diffuse / tunnel on any of the states existing in the right-side quantum well since several bosons may share the same energy state. This means a higher probability of transfer from one well to the other than in the case of fermions because of the greater number of available states able to receive an ion. The same arguments are applicable also to the boson ions lying on the lower energy states of the left quantum well from figure 1. Because of that all the bosons participate in the diffusion process and not only those from upper energy levels. Thus, the energy band model may explain why deuterium diffuses easier in metals than the other hydrogen isotopes. Because of the same reason, the boson character makes Pd able to load a very high concentration of deuterium as compared to the case of proton. The normal sequence for the diffusion coefficients would be H > D > T, since the heavier a particle is the lower is its diffusion coefficient. But taking into account the fermion / boson character of each ion and the above arguments, the correct sequence for the diffusion coefficients is D > H > T, as is observed experimentally. Taking into account that the orbiting distance is smaller for heavier isotopes, it results that the most favorable isotope for observing cold fusion is deuterium. This is due to its higher mass (that allow him a smaller orbiting radius than in the case of proton) and to its bosonic character that allow him to diffuse faster and be incorporated in a greater amount than the other isotopes. As regards the true potential in which the ions move, let's consider a direction in the crystal that is along the great diagonal of the lattice cube of Pd. This great diagonal passes through the center of the cube and also through two of the host lattice nuclei. Taking into account that hydrogen interacts electromagnetically with the screened

electrostatic potential of the lattice ions but has also the ability to present strong interaction, it results that the hydrogen ion sees a potential formed by two kinds of quantum wells: electromagnetic and nuclear, as depicted in figure 2. The nuclear quantum well corresponds to the lattice ion. From the quantum mechanics point of view, there is no formal difference between an electromagnetic potential well and a nuclear potential well. Thus, we may consider that for the hydrogen ions there is a coupling between lattice energy levels and host nuclei levels. This is so because solving the Schrödinger equation for this system of quantum wells will results in energy levels / bands that are common to both types of wells, electromagnetic and nuclear. This phenomenon is specific only to the host lattice in its solid state. This fact suggests the possibility that nuclear reaction s in solid state occur in a slightly different manner that in the liquid or gaseous state of the host lattice, cold fusion being only a particular case of that. The situation depicted in figure 5 is idealized, in the sense that we have drawn rectangular walls for the potential wells.
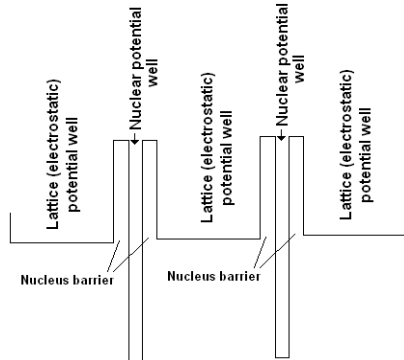

Figure 2 – The true quantum potential for the hydrogen ion in solids.

Let's now consider the behaviour of the system when cold fusion takes place. Suppose that in a certain place in the host metal a fusion process is initiated by using some means. The occurring of the nuclear fusion in that region of the metal produces heat, heat that locally increases the host temperature. Because of the increase in temperature, there will be an increased number of ions excited to higher energy states that are characterized by a negative effective mass. Thus, the number of ions with negative effective mass is increased. This increase in their number has as a result the increase in fusion processes that, at their turn, increase further the local temperature. In this way, a positive feedback appears, in the sense that, once initiated, the fusion process may go further without the need of any external action and can even be self-sustained as described in [12]. Self-sustainability appears in the case when the system generates more energy than it dissipates. There is also a negative feedback, given by several mechanisms such as: a) the lifetime τ in the excited state decreases with increasing temperature because of the increased scattering on lattice specific quasi-particles, thus decreasing the available time for the two ions to approach each other enough for fusioning; b) consumption of reactant particles (at that specific site in the lattice) as a consequence of the fusion process, process that is faster than the supply made by diffusion from outside; c) the deterioration, and even melting, of the host lattice as a result of the collisions of the energetic ions resulted from fusion, deterioration that mitigates the local energy band structure and thus mitigates the mechanism for hydrogen ions approaching; d) hydrogen out-diffusion from the regions where fusion takes place, this process being due to the fact that an increase in local temperature produces an increased diffusion of hydrogen ions from the warmer region to the colder ones, this out-diffusion being able to reduce or even reverse the flux of ions coming from regions with a higher ion concentration; e) heat dissipation rate to the exterior, dissipation that allows the crystal to not overheat excessively (as in the case when is mounted in vacuum) and thus to limit the positive feedback loop. This process of dissipation depends on the metal (through density, specific heat and thermal conductivity) and on the cooling boundary conditions. If non-equilibrium (illumination or particle bombardment) excitation of hydrogen ions is made, a good dissipation of the generated heat to the exterior can make the difference between a successful experiment and an experiment having a more violent, explosive character. These negative feedback mechanisms may dominate at higher reactions rates because of the reasons told above. Thus, we may expect a reaction rate that depends on temperature in a non-linear fashion, having a maximum value at a certain temperature, as described in [13]. This happens because below that temperature, the dominant role is taken by the positive feedback, which tends to increase the temperature. Above the temperature corresponding to the maximum of the reaction rate, the negative feedback becomes dominant, which tends to reduce the reaction rate. Thus, an oscillatory behaviour may be expected for the reaction rate. There is necessary a threshold value of the hydrogen concentration because under this value: a) the fusion processes are rare; b) thermal conduction of the metal carries out the heat sufficiently fast so as the positive feedback be insignificant and no experimental observation of the heating be made; c) let "d" be the mean free path of a negative mass ion during its stay in the excited state. If this mean free path is less than the average distance between ions (equal to $N_0^{-1/3}$ where N_0 is the total ion concentration), then the probability that the excited ion encounter another ion is reduced. As a consequence the reaction rate is reduced correspondingly.

Increasing concentration lowers the average distance between ions and the encounter probability becomes higher, the same happening for the reaction rate. Let denote by "f" the fraction of ions having a negative effective mass and N_0 be as above. "f" depends on temperature and is equal to 0.5 when temperature tends to infinity. It may be computed from the Fermi-Dirac or Bose-Einstein distribution function (depending on the type of isotope) and the density of states specific to the resepctive ions. The concentration of ions with negative effective mass is thus equal to $f*N_0$ while the concentration of ions with positive effective mass is equal to $(1-f)*N_0$. The fusion reaction rate is equal to the product of these two concentrations (there is also the reaction cross-section that multiplies these two concentrations), being equal to $f*(1-f)*N_0^2$. Thus, from our model, it results that the fusion reaction rate is proportional to the square of the hydrogen ions concentration, as is observed experimentally. There is enough experimental evidence that shows that heat emission takes place only after a certain concentration of hydrogen is obtained in the Pd lattice. This can be explained by two main aspects. First, the observation of rise in temperature produced by the nuclear reaction depends on the sensitivity and speed of the devices used for measuring temperature (thermometer, infrared camera) and by the thermal noise of the Pd+calorimeter system. A very sensitive apparatus and a Pd/calorimeter system with very low noise will show a lower threshold concentration. The generated heat flux must be at least comparable to the heat loss flux in order to produce an observable effect (else, the signal is small and extinguishes fast with time). A system with a lower heat dissipation rate will show a lower threshold concentration. Secondly, it must be taken into account the explanation given above when comparing the average distance between hydrogen ions with the mean free path of the negative mass ion. A higher concentration increases the probability of encounter and thus the reaction rate. As regards the generated heat, there is an infrared emission of the metal surface, the spot corresponding to the highest temperature having a position that varies randomly onto the surface [14]. As we have mentioned earlier, a necessary condition for reaction is the thermal excitation of the hydrogen ions on energy states with a negative effective mass. This is a random process. A greater thermal fluctuation at a point may produce a greater reaction rate, with heat emission. The temperature increases at that point and positive feedback is triggered (above a threshold determined by the heat loss rate). This positive feedback consumes some part of the hydrogen at that point, so the spot extinguishes in time. Then, another fluctuation appears at other place, in a random manner (the temperature and concentration fluctuations are random processes) and the process is repeated. A consequence of this explanation is that the bright spot never appears twice at the same place (or at least appears after a long enough time so as the ions concentration be recovered at that place), since the hydrogen ions in that place are consumed during the first spot. We don't have yet data or experimental results to prove this last assertion, it results from the model proposed by us. The excitation of hydrogen ions to upper energy states with a negative effective mass is taking place all the time. Thus, even if the loading process is finished since a certain time interval, these excitations take place and may generate heat by the mechanism proposed by us. This fact explains why is observed the so-called "heat after death" [12], since the excitation processes are independent on the loading means and are occurring all the time during loading and after that. This has as one of the consequences the fact that emission of X-rays with specific wavelengths should be observed even after the external excitation of the Pd loaded sample is switched off, since the start of orbiting of the two hydrogen ions is not necessary to be made directly on the fundamental state of the ions bound system. This may offer an explanation for the experimental data obtained in [15]. These are some of the experimental results that can be explained by our model. Our model does not contradict that one based on the screening effect made by the free electrons of the metal, since screening proves a support for the ions to get closer. As regards the plasma wave model proposed by [16], the plasma wave may be considered as exciting the ions to upper energy states where they acquire a negative effective mass. However, the [16] model cannot explain why X-ray radiation with specific wavelengths is emitted during reaction and why the effect observed by Letts and Cravens is taking place. A similar effect as in [9-10] must be observed by using THz / mm / sub-mm radiation, with a frequency similar to or close to that mentioned in [10]. This is so because of the resonant excitation (direct or phonon mediated) of ions to energy states with a negative effective mass. However, the use of THz / mm / sub-mm radiation should be more favorable to observe enhancement effects than the use of visible or near-infrared lasers, because the skin penetration depth of the THz / mm / sub-mm radiation is larger than the skin depth corresponding to visible or near-infrared light. This feature makes that a greater number of hydrogen ions be excited with THz / mm / sub-mm radiation than with optical light, fact that will increase the amount of generated heat. This assertion is also a theoretical prediction and should be checked experimentally. Another experiment that should be done is that of cyclotronic resonance in deuterium loaded Pd (both at low and at high hydrogen concentration), so as to measure the effective mass of hydrogen in the metal lattice. This measurement should give an experimental indication when

trying to compute the concrete band structure for the hydrogen ions. In conclusion, some experiments that are based on our prediction may be done so as to check our model: a) illuminating a hydrogen loaded sample with X-rays having wavelengths identical to the specific ones emitted during reaction to see if the reaction rate will be reduced; b) illuminating with THz / mm / sub-mm radiation to see if an enhancement effect greater than that reported by Letts and Cravens is obtained; c) X-ray reflection spectra of hydrogen loaded samples, to check if "unusual" absorption lines appear. Caution should be made when exciting the Pd+deuterium system by non-equilibrium means (photons, particle bombardment), since this may end with very energetic, explosive processes, as could be the case reported in [17].

References

[1] M. Fleischman, S. Pons, M. Hawkins – J. Electroanal. Chem., vol. 261, p. 301 (1989), errata vol. 263.
[2] A.H. Verbruggen, R. Griessen, J.H. Rector – Phys. Rev. Lett. vol. 52, no. 18, p. 1625 (1984).
[3] A. S. Davidov – *Teoria Tverdogo Tela (Theory of Solid State)*, Nauka, Moscow (1976).
[4] B. H. Bransden, C. J. Joachain – *Introduction to Quantum Mechanics*, Longman Gr. UK Ltd (1994).
[5] T. A. Chubb, S. R. Chubb – "*The Ion Band State Theory*", in 5th ICCF, (1995).
[6] J. Hermanson, J. C. Phillips – "*Pseudopotential Theory of Exciton and Impurity States*", Phys. Rev. vol. 150 no.2, p. 652, (1966); J. Hermanson – "*Exciton and Impurity States in rare-Gas Solids*", Phys. Rev. vol. 150 no.2, p. 660, (1966); J. Hermanson – "*Kinematic Resonances in Crystalline Xenon*", Phys. Rev. vol. 166, no. 3, p. 893, (1968).
[7] A. B. Karabut, S. A. Kolomeychenko – "Exp. Res. into Charact. of X-ray Emiss. from Solid-State Cathode Medium of High Curr. Glow Disch.", Proc. of 10th ICCF, World Scientific, (2003).
[8] D. Wang, X. Zhang – High Power Laser and Particle Beams vol. 17, no. 9, p. 1335 – 1340, (2005).
[9] A. B. Karabut – "*Exp. Res.& Dev.. of Heat Power Supp. Prot. Based on High-Energy Processes in Solid Medium Interacting with Hydrogen Ions Flux*", Sci. Res. Proj., (2006). http://www.lenr-canr.org .
[10] D. Letts, D. Cravens–"*Laser Stim. of Deut. Pd: Past&Present*", Proc. 10th ICCF, World Scientific (2003).
[11] D. G. Letts, D. Cravens, P. L. Hagelstein – "*Progress on Dual Laser Exp.*", Proc. of 15th ICCF.
[12] S. Pons, M. Fleischman – Transaction on Fusion Technology, vol. 26, p. 87 (1994).
[13] L.C. Case – Proc. 7th ICCF, p. 48 (1998).
[14] S. Szpak, P.A. Mosier-Boss – Tech. rep. 1862, Navy Laboratories, p.7 (February 2002).
[15] A. B. Karabut, E. A. Karabut – "*X-ray Spectra of Excited Long Living 0.6-6.0 keV Energy Levels from the Solid State Cathodes of Electric Disch. Syst.*", Proc. of the 15th ICCF.
[16] I. P. Chernov et al. – "*Plasmon Based Mech. on Nucl. React. in Metal Deuterides*", Proc. 15th ICCF.
[17] X. Zhang, W.-S. Zhang – "On the Explosion in a Deuterium/Palladium Electrolyte System", Proc. of the 3rd ICCF, Universal Academic Press Tokyo, (1992).

The FCC Substructure of the Nucleus and the Magnetic Interaction among Nucleons

N. D. Cook[1], V. Dallacasa[2]
[1]Kansai University, [2]Verona University

E-mail: cook@res.kutc.kansai-u.ac.jp

Abstract. The FCC lattice model of nuclear structure unifies the liquid-phase, gaseous-phase and cluster models within a self-consistent theoretical framework. By discarding the completely fictitious long-range "effective" nuclear force employed by the shell model and yet maintaining the nucleon build-up procedure in the independent-particle model, the FCC model retains the principal strengths of both the liquid-drop and the shell models. In place of the effective nuclear force, we employ the short-range magnetic attraction between suitably aligned nucleons to obtain nuclear binding.

1. Introduction

The strongest objection to "cold fusion" research since 1989 has been the assertion by nuclear theorists that low-energy nuclear reactions (LENR) "violate everything known about nuclear physics." We argue to the contrary that LENR are consistent with quantum mechanics (QM), and "violate" *only* various questionable assumptions of the 30+ models used in nuclear structure theory [1]. In fact, the various nuclear models are known to be mutually-contradictory (a liquid nuclear interior in the liquid-drop model [LDM], a gaseous-phase in the shell model; local cluster formations in the alpha-particle model, no local interactions in the Fermi-gas model; a short-range nuclear force in the LDM, a long-range "effective" force in the shell model; etc.) and clearly indicate that nuclear structure theory itself is unfinished business [2].

2. The FCC Lattice Model

We have previously shown that one model of nuclear structure (the face-centered-cubic [FCC] lattice model) is consistent with both QM (and the shell model description of nucleon states) and the many empirical indications of an extremely high-density LDM-like nuclear interior [2-4] (Fig. 1). Here, we demonstrate that the nuclear force that binds nucleons together into this lattice configuration **cannot** be a fictitious potential-well acting over more than 10 fm (as in the shell model), but, rather, must be a spin- and isospin-dependent, short-range force acting over distances of less than 3.0 fm, as already well-known from nucleon-nucleon experiments. The only known force of sufficient strength to overcome the Coulomb repulsion between two protons is an in-phase magnetic force [5]. That is, at a center-to-center distance of 2.0 fm (which gives the known nuclear core density of 0.17 nucleons/fm^3), the surface-to-surface distance of singlet-paired, same-isospin nucleons (each with an RMS radius of 0.86 fm) is only 0.28 fm, corresponding to an attractive magnetic force of ~3 MeV. Triplet-paired nucleons of opposite-isospin show similar attraction (details of the magnetic interaction in Section 3).

In our previous work [2-4], we simply assumed that a strong, short-range force – similar to that in the LDM – allows for condensation of nuclear matter. A comparison of various lattice configurations of nuclear matter (Z=N) showed the relative stability of an antiferromagnetic FCC lattice with alternating isospin layers (Fig. 1). It is also noteworthy that this same FCC lattice of nucleons has been shown from QM calculations [6] to be the lowest-energy condensate of nuclear matter, possibly present in the crust of neutron stars (although absent in the neutron star "core" consisting of only neutrons or hyperons).

But the most surprising fact about the FCC lattice is that, by placing a tetrahedral alpha particle at the center of the system, it reproduces the entire shell/subshell nucleon build-up procedure that is known from the independent-particle model (IPM) model and empirically well-established. In other words, the **n**-shells and **j**-

subshells that are the essence of the shell model are uniquely reproduced as spherical shells (*n*) and cylindrical subshells (*j*) in the antiferromagnetic FCC lattice with alternating isospin layers. Moreover, using a realistic, short-range nuclear force, the lattice gives binding energies and nuclear radii that are essentially identical to those of the LDM [2-4]. While difficult questions concerning the nature of the nuclear force have remained unanswered in the lattice model – and indeed in all nuclear models! – we have taken the remarkable reproduction of both shell and liquid-drop characteristics within the FCC lattice as *prima facie* evidence that normal nuclei at normal nuclear densities are configured as a lattice. This idea was first voiced by Wigner in 1937 [7], and later developed independently by several others [8, 9].
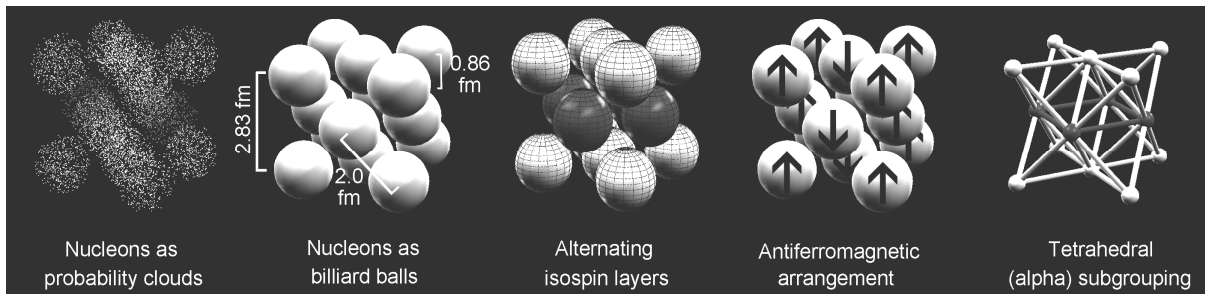

Fig. 1 - The FCC unit structure with dimensions that give the known nuclear density.

3. The Magnetic Interaction among Nucleons in the FCC Lattice

We have previously reported theoretical work on the magnetic interaction among fermions in a lattice [5]. In the traditional Biot-Savart formula, the mutual force between two coils is obtained as the contribution of infinitesimal length elements of currents and ignores any phase relationship between them. In contrast, we have found that the currents of two neighboring coils in a lattice are correlated since there is periodicity. Contrary to the Biot-Savart result in which the potential energy of the two coils is dependent on their separation as $1/y^3$, there is a strongly enhanced contribution which behaves as $1/y$. This energy turns out to depend on the radius R of the coils and increases when this radius decreases.

We have examined the cases in which the coils are on the same plane, as well as on parallel planes along the same axis. If current coils describing the nucleons have radius=0.5 fm, the energy gives the correct order of magnitude for nuclear binding. P-P, N-N and N-P energies for first neighbor bonds give an average value of 2.8 MeV (and this value reproduces the nuclear binding energy curve for all nuclei Z>7).

Figure 2 shows the case of two coils side-by-side. The current elements *dl* have an angle between them in general with no definite relation, varying between $-\pi$ and $+\pi$ and leading to a cancellation of their projections one on the other. In the case in which they are part of coils on a lattice, however, there will be a constant angle between the two, since the current will be periodic along the coils. Therefore the circulation of current in one coil will be repeated periodically in all the coils.
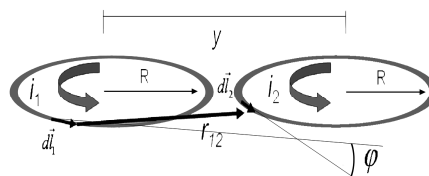

Fig. 2 - The magnetic force between two coils. Unlike the Biot-Savart calculation, the phase relationship between the current elements is taken into consideration.

The magnetic field of the first coil is given by

$$\vec{B}_1 = \frac{\mu_o i_1}{4\pi} \int_{C1} \frac{d\vec{l}_1 \wedge \vec{r}}{r3} \tag{1}$$

The force on the second coil is

$$\vec{F}_{12} = i_2 \int_{C2} d\vec{l}_2 \wedge \vec{B}_1 \tag{2}$$

Therefore, we obtain

$$\vec{F}_{12} = \frac{\mu_o i_1 i_2}{4\pi} \int_{C2} d\vec{l}_2 \wedge \int_{C1} \frac{d\vec{l}_1 \wedge \vec{r}_{12}}{r_{12}^3} \tag{3}$$

This can be expressed as:

$$\vec{F}_{12} = -\frac{\mu_o i_1 i_2}{4\pi} \int_{C2} \int_{C1} \frac{d\vec{l}_2 \cdot d\vec{l}_1}{r_{12}^3} \vec{r}_{12} \tag{4}$$

As an example, consider two coils with the same axis, separated by a distance y. By using cylindrical coordinates, this equation becomes:

$$\vec{F}_{12} = \vec{j} \frac{\mu_o i_1 i_2 R^2}{2} y \int_0^{2\pi} \frac{\cos\varphi}{(y^2 + 2R^2(1-\cos\varphi))^{\frac{3}{2}}} d\varphi \tag{5}$$

where $\varphi = \varphi_1 - \varphi_2$ expressing any phase relation between the two currents and $\vec{j}$ is the unit vector along the y direction. .

A more general expression can be derived for two coils of different radii R_1 and R_2 as follows:

$$\vec{F}_{12} = \vec{j} \frac{\mu_o i_1 i_2 R^2}{2} y \int_0^{2\pi} \frac{\cos\varphi}{(y^2 + R_1^2 + R_2^2 - 2R_1 R_2 \cos\varphi)^{\frac{3}{2}}} d\varphi \tag{6}$$

From the force we can calculate the potential energy, V_{12}.

When no phase relationship exists between the currents, we find that

$$F_{12} = \left(\frac{\mu_o i_1 i_2 yk}{2\sqrt{R_1 R_2}(1-k^2)}\right)\left[(1-k^2)K(k) - (1-k^2/2)E(k)\right] \tag{7}$$

where

$$k = \sqrt{\frac{4R_1 R_2}{(R_1 + R_2)^2 + y^2}} \qquad 0 < k < 1$$

and

$$K(k) = \int_0^{\frac{\pi}{2}} \frac{d\theta}{(1 - k^2 \sin^2 \theta)^{1/2}} \; ; \; E(k) = \int_0^{\frac{\pi}{2}} (1 - k^2 \sin^2 \theta)^{1/2}$$

are elliptic integrals.

V_{12} in this case is composed of terms depending on distance whose leading term is $1/y^n$, where n=3.

$$V_{12} = \frac{\mu_o m_1 m_2}{\pi} \frac{1}{y3} \tag{8}$$

This is the usual Biot-Savart dipole magnetic interaction leading to weak potential energy. However, if a relationship exists between the currents in a lattice we find that

$$V_{12} = \frac{\mu_o m_1 m_2}{\pi} \frac{<\cos \varphi >}{R^2 y3} \tag{9}$$

where for convenience we have introduced the magnetic moment $m = i\pi R^2$. Contrary to the Biot-Savart result in which the potential energy of the two coils is dependent on their separation as y^{-3}, there is a contribution which behaves as $1/y$, strongly enhanced with respect to the Biot-Savart value. This is a much stronger interaction than the usual dipole interaction. Here <...> indicates the average value of the quantity. This energy turns out to depend from the radius R of the coils and increases when this radius decreases.

A definite phase relation is expected to exist for coils in a lattice with $<\cos \varphi >\approx 1$, eventually vanishing at large distances (in the absence of long-range order). We find that the ratio between the in-phase and the out-of-phase of the two expressions is $(y/R)^2$ thus becoming very large for small R.

Similar results can be established for coils on a plane. It follows that the in-phase This energy turns out to depend from the radius R of the coils and increases when this radius decreases.

We have examined the cases in which the coils are on a same plane as well as on parallel planes with the same axis. It follows that V_{12} has quadrupole dependence. When the two coils are side-by-side (with the magnetic moments perpendicular to the vector $\vec{r}$ connecting their centers), the potential energy differs from the case of two coils with the magnetic moments parallel to $\vec{r}$. Also, the phase factor may decrease exponentially with distance, which mimics a "Yukawa" shape of V_{12}.

The force from currents in phase can be reinterpreted as arising from circular motion of charged particles, the current being determined by the motion of the particles. We can use in such a case the Biot-Savart formula for the magnetic field of one coil and the Lorentz force expression to calculate the force on the particle of the second coil. For two circulating particles on parallel planes at distance y on orbits with centers on the y axis we find (for $\varphi = 0$):

$$F_{12} = \frac{\mu_o}{4\pi} q_1 q_2 \frac{v^2}{r^2} \tag{10}$$

where v is the common velocity and q their charge. This can be rewritten in terms of the magnetic moments on the orbits $m = qvR/2$ so that the resultant V_{12} will be coincident with equation (9).
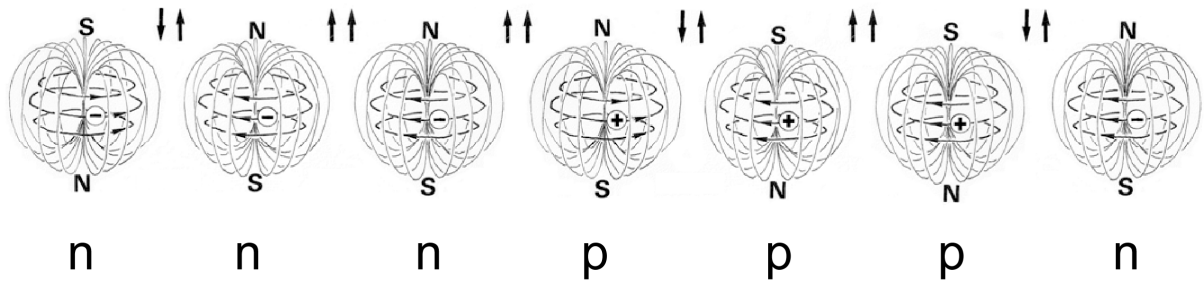
Fig. 3 - The six types of attractive and repulsive magnetic interaction among nearest-neighbor spin up/down protons/neutrons.

Table 1: Numerical estimates of the attractive nucleon interactions at an internucleon distance of 2.0 fm, in comparison with traditional Biot-Savart results (y=2.0 fm; R=0.5 fm; cos φ=1). The average value is 2.82 MeV.

Nucleon pair	V(MeV)	V (MeV)$_{\text{Biot-Savart}}$
P-P (singlet)	3.93	$4.2688 \cdot 10^{-3}$
N-N (singlet)	1.84	$4.2688 \cdot 10^{-3}$
N-P (triplet)	2.69	$4.2688 \cdot 10^{-3}$

4. Discussion

The following properties are found for the in-phase interaction of two particles: The interaction is consistent with a Yukawa form, leading to short-range effects as a result of a dephasing factor with distance and is quadrupole-like, changing according to the angle made by the vector connecting any two coils and the magnetic moments. An interesting feature is the change from attraction/repulsion for first/second neighbors according to the antiferromagnetic arrangement of nucleons in the lattice. The interaction exhibits the right order of magnitude (~1-10 MeV) for nucleons. Higher order terms with increasing distance are much smaller, and are found to produce effects at the normal level of a magnetic force (< 100kev). At large distances the interaction becomes consistent with a generalized OPEP interaction

$$V_{12} = -CS_1 S_2 m_1 m_2 \left\{ 1 + 2 \left[1 + \frac{3}{m_\pi y} + \frac{3}{(m_\pi y)^2} \right] \right\} \frac{e - m_\pi y}{m_\pi y}$$

where S are the spins, m_π the pion mass, y the distance, C a constant. At leading order in 1/y this becomes

$$V_{12} = -3CS_1 S_2 m_1 m_2 \frac{e^{-m_\pi y}}{m_\pi y}$$

In the picture of revolving charges as constituents of the coils, a new feature arises as the time-varying attraction between adjacent coils, when particles are located in the orbit so as to have parallel velocities along the same line. This leads as a consequence to a situation of cancellation of the magnetic attraction and maximization of the Coulomb repulsion between pieces of the nucleus determined by cutting it along suitable planes.

External interactions, like the one produced by particles with a magnetic moment, can also weaken the magnetic interaction through a dephasing of the force, leading to an overall instability of the nucleus. Along particular planes this could again favor the Coulomb repulsion to split the nucleus into (non-symmetrical) parts.

5. Conclusions

We conclude that the so-called "strong" nuclear force that is responsible for the binding of nucleons into stable nuclei may have a classical electromagnetic basis (Figure 4). The effect is essentially the Biot-Savart magnetic force, but what is new in our calculation is the phase-relationship between the currents in neighboring "coils" within the nucleons themselves.
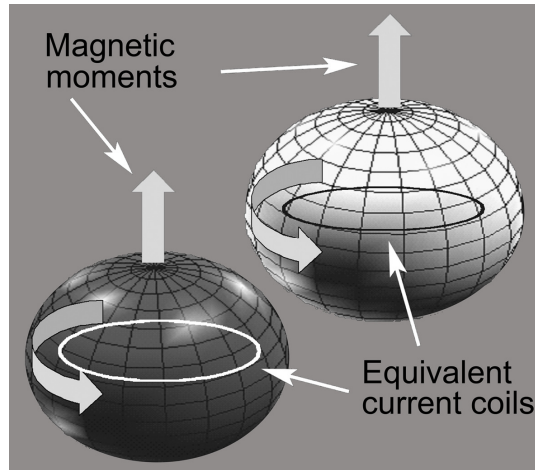

Fig. 4 - The magnetic moments of nucleons viewed as equivalent current coils.

With regard to "cold fusion," the most important implication of our calculations on the magnetic interaction of nucleons in a nuclear lattice is that the magnetic environment may play a role in facilitating or inhibiting low-energy nuclear reactions. Such effects have been reported by Letts in experiments where excess heat production could be turned on or off with 90 degree shifts in magnetic field orientation [10]. Both our theoretical calculations and Letts's experimental results indicate the need for more careful study of classical electromagnetic effects before indulging in quantum mechanical speculations.

6. References

[1] W. Greiner & J.A. Maruhn, *Nuclear Models*, Springer, Berlin (1996).
[2] N.D. Cook, *Models of the Atomic Nucleus*, Springer, Berlin (2006), 2nd Ed. (2010).
[3] N.D. Cook & V. Dallacasa, *Physical Review C,* Vol. 36, 1883 (1987).
[4] V. Dallacasa & N.D. Cook, *Il Nuovo Cimento A,* Vol. 97, 157 (1987).
[5] V. Dallacasa & P. di Sia, *Journal of Nanoscience and Nanotechnology* 9, 3487 (2009).
[6] V. Canuto & S.M. Chitre, *International Astronomical and Astrophysical Union Symposium* 53, 133 (1974).
[7] E. Wigner, *Physical Review* 51, 106 (1937).
[8] K. Lezuo, *Atomkernenergie* 23, 285 (1974).
[9] F. Everling, *Physikalische Verhandlungen* 6, 210 (1988); *Proceedings of an International Workshop PINGST 2000*, 204 (2008).
[10] D. Letts [http://www.lettslab.org See the Chubb Collaboration section.]

Simulation of Palladium Transmutation Products

N. D. Cook[1], V. Dallacasa[2]
[1]*Kansai University,* [2]*Verona University*

E-mail: cook@res.kutc.kansai-u.ac.jp

Abstract. The build-up procedure for the Palladium isotopes is known from the independent-particle model and implies specific 3D structures for these isotopes in the nuclear lattice model [1]. Using those lattice structures, the favorable modes of fission have been simulated and the fission fragments compared with the transmutation products, as reported by Mizuno [2]. It is shown that (i) the changes in relative abundance of the Pd isotopes, and (ii) the main transmutation products in Mizuno-style LENR studies are consistent with the idea that the bulk of the energy released in such experiments is due to the fission of Palladium isotopes.

1. Introduction

The low-energy transmutation of nuclear species was discovered in 1938 and soon put to military and peaceful uses. Despite remarkable experimental and technological advances, nuclear theory has been *unable* to explain the asymmetrical (3:2) masses of the fragments produced by the fission of the actinides. After 7 decades of theorizing, most specialists on fission frankly agree with Moreau & Heyde [3] that "the theoretical description of the fission process is the *oldest problem* in nuclear physics, [but] it appears that a consistent description is still very far away."

A second form of relatively low-energy transmutation of nuclei has been reported in the "cold fusion" literature – specifically, the transmutation of Palladium isotopes (A=102~110) into a variety of small nuclei (A=30~80) subsequent to electrolysis in deuterated solutions. Theoretical controversy continues with regard to the inducing mechanism that leads to the generation of excess heat, but the measured changes in the ratio of Palladium isotopes and the deposition of many small nuclei on the surface of pure Palladium electrodes are strong indication of the fission of the Palladium nuclei. It therefore appears that there are at least two distinct stages in the "cold fusion" reaction: (i) the tunneling of deuterons into the Palladium nucleus, and (ii) the break-up of the Palladium nuclei themselves. The mechanisms of stage (i) remain controversial, but the nuclear transmutation data of stage (ii) have been replicated several times, and have remained essentially unexplained. In computer simulations, we have studied questions concerning the isotopic changes of the Pd electrode themselves [4] and found the Mizuno data [2], in particular, to be self-consistent and indicative of nuclear transmutation. In the present study, we have again made a comparison of simulation results with the experimental data on the Palladium fission products.

2. Simulation of the Fission of Uranium

We have previously reported that a lattice model of nuclear structure [1, 5, 6] – essentially, a "frozen" liquid-drop that is mathematically identical to the standard "independent-particle model" (IPM) – predicts the *asymmetrical* fission fragments produced by the thermal fission of the actinides [5, 7] *without* using any "adjustable parameters" to produce the asymmetry (Figure 1). The basic effect is a consequence of the fact that scission along oblique lattice planes of the somewhat oblate FCC structures for the actinide nuclei requires breaking fewer nearest-neighbor nucleon-nucleon "bonds" than vertical or horizontal slices through the same structures. Because of the large excess of neutrons that give the actinides an oblate shape, the oblique slices through the lattice structures show a 3:2 mass ratio. That result can be verified using the *Nuclear Visualization Software*, available at: http://www.res.kutc.kansai-u.ac.jp/~cook. Similarly, the fission of Palladium (Section 3) can be easily simulated using the same software, and shows that the **symmetrical** fission of the approximately spherical Palladium isotopes is energetically favored.
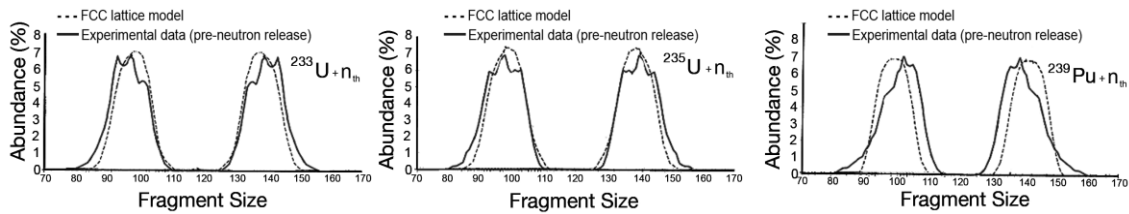
Fig. 1 - The prediction of asymmetrical fragments in the thermal fission of the actinides [5, 7] using a model that employs no parameters to produce the fission phenomena.

3. Simulation of the Fission of Palladium

Here, we apply the *same* lattice technique to the fission of the six stable Palladium isotopes. In a preliminary study, we calculated the total binding energy across each scission plane minus the Coulomb repulsion between the fragments. The lowest energy fission events in each of 6,000 randomizations were then collected (Figure 2). Most fragments were stable or led to rapid β$^-$-decay, with a predominance of ^{24}Cr final products and little ^{23}V, qualitatively similar to the spectrum of deposits on Pd, as reported by Mizuno [2] (Figure 2b, c).

The qualitative agreement between the experimental data and the simulation using the lattice model were encouraging (Figure 2c), but far from definitive. In a recent simulation, we have used a quantitative calculation of the magnetic force between nucleons that is both spin- and isospin-dependent, in order to obtain more precise predictions about the transmutation products. Details of the force are provided in a separate contribution to this Volume [8]. The simulation procedure was similar to that described in [5] and [7], but was done using the magnetic force between nucleons. Specifically, the previous nuclear force was a phenomenological estimate of the mean nearest-neighbor binding among nucleons in the lattice model (i.e., 2.78 MeV). That level of nucleon-nucleon binding among nearest-neighbors has been shown to reproduce the approximate nuclear binding-energy curve of all but the smallest nuclei, but had no dynamical basis. In the present study, we used the spin-, isospin- and distance-dependent magnetic nuclear force described in [8] to calculate the likelihood of scission along various lattice planes. For the purposes of the simulation, it was sufficient to use fixed values for various spin- and isospin-combinations for nearest-neighbors.

The simulation procedure was as follows:

 Each of the six stable isotopes of Palladium was individually constructed in the NVS software following the known (IPM) nucleon build-up sequence. By default, this leads to relatively compact lattice structures, but there are necessarily a large number of alternative surface positions for both protons and neutrons that give similar numbers of total nucleon-nucleon bonds and similar total Coulomb effects for the same Z and N. For simulation of fission fragments, each isotope underwent surface randomization 1000 times and a
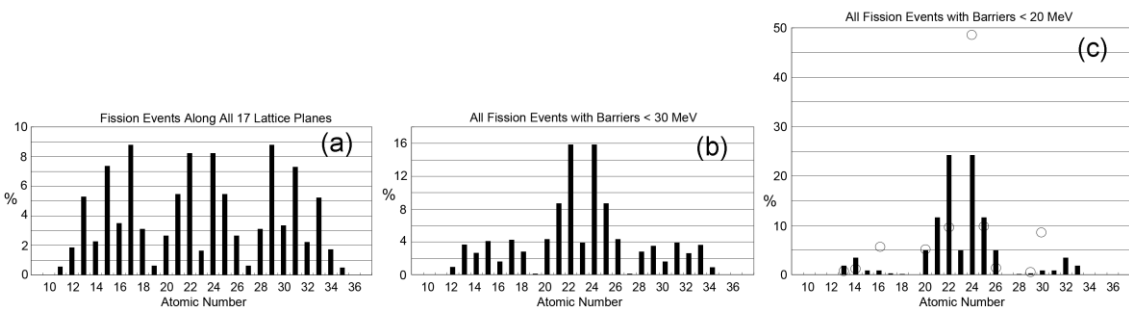

Fig. 2 - Parameter-less lattice model predictions of transmutation products following Pd fission. Circles in (c) indicate the data, as reported by Mizuno [2]. Note that most of the fragments found on the Palladium electrodes are roughly 1/2 the atomic number of Palladium itself (90% between Z=16~30) – strongly

375

indicating that they are indeed fission fragments and ***not*** transmutations built from the repeated addition of neutrons, etc.
small number (arbitrarily set to 9) showing the greatest nuclear binding were retained. These relatively stable structures were then scissioned along 17 lattice planes passing through or near to the center of the lattice. For each isotope undergoing such scission, the lowest energy scission plane was chosen, and the proton and neutron numbers of the fragments were saved for statistical analysis. A total of 46.2% of the Palladium fission products were stable nuclei, 53.8% were unstable. For all unstable fission fragments, the stable end-products were then calculated (without exception a stable isotope was obtained by one or two β^--decay conversions of neutrons into protons). Half-lives ranged from 33 seconds to 5.8 minutes, with a small number leading to exotic decays. Finally, the percentages of such fragments were adjusted in light of the different natural abundance of the six Palladium isotopes (Pd^{102} 1.02%, Pd^{104} 11.14%, Pd^{105} 22.33%, Pd^{106} 27.33%, Pd^{108} 26.46% and Pd^{110} 11.72%).

The results of the simulation in comparison with the Mizuno data [2] are shown in Figure 3(a). The large excess of Chromium isotopes found experimentally was well-reproduced, but other aspects of the results indicate that a wider spectrum of simulated Palladium structures should have been sampled (arbitrarily set to the 9 most stable nuclei – i.e., specifically restricted to the most stable, most compact Palladium structures to avoid the production of the fission products from highly unstable Palladium isotopes). Specifically, fragments with relatively large and small atomic numbers (12, 14, 16, 20, 29 and 30) were not found in the simulation, but would have been obtained if less-compact lattice structures were retained for the simulation of fission (as in Figure 2). By restricting the simulation to the nine most stable lattice structures, the primary fission fragments from each of the Palladium isotopes was Chromium. Relatively strong contributions of Vanadium (Z=23) and Manganese (Z=25) were found in the simulation but not found in the Mizuno data.

Mizuno also reported the abundances of Chromium isotopes before and after the deuterated electrolysis experiments [2, Plate 15]. Specifically, he found that, although the natural abundances of the four principal isotopes (Cr^{50}, Cr^{52}, Cr^{53} and Cr^{54}) are known to be 4.3%, 83.8%, 9.5% and 2.4%, respectively, they were found at abundances of 14.3%, 50.9%, 23.8% and 10.9% in the experimental "ash" following the presumed fission of Palladium. These numbers are of interest primarily because an explanation due to "contamination" with Chromium is extremely unlikely: even if Chromium from the experimental apparatus had somehow appeared on the Palladium electrodes, they should appear at the natural abundances, whereas quite "unnatural" abundances were obtained. In our simulation, the abundances of these isotopes were 0.0%, 7.9%, 76.8% and 15.3%. Clearly, the simulation exaggerated the isotope shifts, but in the right directions for three of the four Chromium isotopes: a significant decrease in Cr^{52} and significant increases in Cr^{53} and Cr^{54} (Figure 3(b)).
The results of computer simulations of all kinds are highly-dependent on the underlying theoretical model and the choice of parameters used. The present simulations are no exception, so that the theoretical results must be considered in full light of the theoretical input. In this regard, it is relevant to note that the FCC

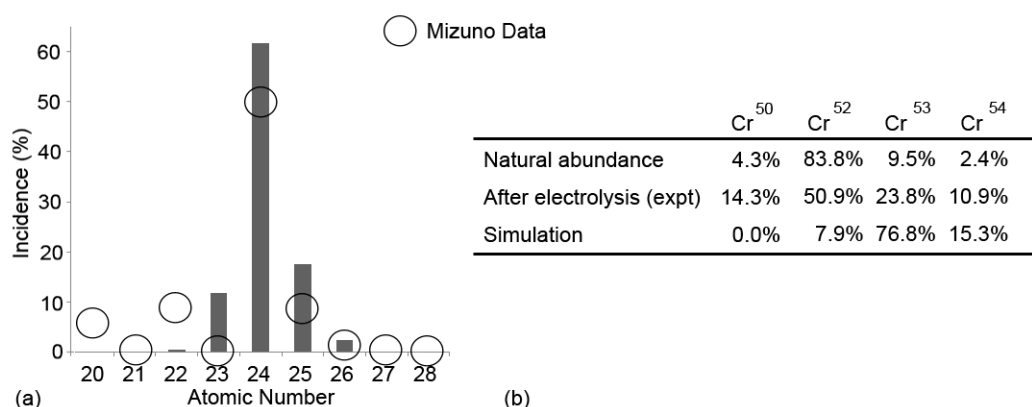|	Cr^{50}	Cr^{52}	Cr^{53}	Cr^{54}
Natural abundance	4.3%	83.8%	9.5%	2.4%
After electrolysis (expt)	14.3%	50.9%	23.8%	10.9%
Simulation	0.0%	7.9%	76.8%	15.3%

(a)   (b)

Fig. 3 - (a) A comparison of simulation results (bar graph) and the data from Mizuno [2], indicated by the open circles. (b) A comparison of the changes in the natural abundances of the four main Chromium isotopes following electrolysis with the simulation results.

lattice model that has been used so simulate the fission of both the actinides (A>230) and Palladium (A~106) was devised, first and foremost, to explain how the long-standing, mutually-contradictory nuclear models in nuclear structure theory can be viewed in a self-consistent manner [1, 4-6]. For that purpose, the lattice model requires both isospin and orthogonal spin layering of nucleons; those are assumptions that must be made to "make the model work" – specifically, to reproduce the known IPM nucleon texture in the lattice. Only much later after the development of the basic model was it realized [7] that scission of the lattice along lattice planes allows for an explanation of the "anomalous" asymmetry of the fission fragments of Uranium. No changes in the model itself and no *post hoc* addition of "asymmetry" parameters were needed to obtain specifically the 3:2 mass asymmetry of the fragments (Figure 1). On the contrary, it is inherent to the lattice build-up procedure that oblique slices through the lattice for oblate structures such as Uranium will produce asymmetrical fragments. In contrast, similar slices through the more spherical (x=y=z) structures of medium-sized nuclei, such as Palladium, lead to nearly symmetrical fragments. In other words, the predictions of both symmetrical and asymmetrical fission for Palladium and Uranium, respectively, are a consequence of the lattice geometry itself – and not a consequence of manipulation of the basic model.

4. Conclusions

Low-energy nuclear reactions continue to pose fundamental questions that conventional nuclear theory cannot answer. With regard to the fission of Uranium and all of the other technologically important actinides, the *asymmetry* of the fission products is regarded as "the perennial puzzle" of nuclear physics [9]. As noted by Vandenbosch and Huizenga [10], "no theoretical model … has been sufficiently free of parameter fitting to be generally accepted." Without a profusion of adjustable parameters, the LDM predicts *symmetrical* fission products and the shell model predicts fragments with "magic" numbers of protons and neutrons. Neither prediction is correct (despite what the textbooks assert), and has led to the development of hybrid models containing parameters that can be adjusted to fit the data. The most comprehensive modern study of asymmetrical fission is that of Möller and colleagues. In a computational *tour de force*, they concluded that "all of the observed fission phenomena [including the asymmetrical fragments] can be understood in terms of nuclear potential-energy surfaces calculated with five appropriately chosen nuclear shape degrees of freedom" in a 2.6-million parameter space. The inconclusive nature of such modeling, however, is apparent from the fact that the "appropriate" *post hoc* selection of parameters must be made in light of the experimental results [11]. Asymmetrical fission is *not predicted*, but rather *reproduced* by cherry-picking model parameters that give the desired results.

In contrast, we have shown that the FCC lattice model does not require any additional parameters to explain the *asymmetry* of Uranium fission fragments. The asymmetry is inherent to the scission of large, oblate nuclei along fission planes with the fewest "bonds" connecting the fragments. Similarly, we find that the *symmetrical* pattern of experimentally-known nuclear "ash" in Mizuno-style cold fusion studies is obtained from the same lattice-scission technique. We therefore conclude that the substructure provided by the nucleon lattice is a necessary addition to conventional nuclear structure theory and allows for an explanation of the masses of the fragments produced by both the thermal fission of Uranium and the nuclear transmutations detected in "cold fusion" experiments.

[1] N.D. Cook & V. Dallacasa, *Physical Review* C 36, 1883 (1987).
[2] T. Mizuno, *Nuclear Transmutation*, Infinite Energy Press, Concord, NH (1998).
[3] J. Moreau & K. Heyde, *The Nuclear Fission Process*, CRC Press, Boca Raton (1991), p. 228.
[4] N.D. Cook, Shizuoka, JCF9 http://dragon.elc.iwate-u.ac.jp/jcf/JCF9/jcf9-abstracts.pdf (2009).
[5] N.D. Cook, *Models of the Atomic Nucleus*, Springer, Berlin (2006), 2nd Edition (2010).
[6] V. Dallacasa & N.D. Cook, *Il Nuovo Cimento* A 97, 157 (1987).
[7] N.D. Cook, *Proceedings of St. Andrews Fission Conference*, World Scientific, Singapore (1999), pp. 217-226.
[8] N.D. Cook & V. Dallacasa, The FCC substructure of the nucleus and the magnetic interaction among nucleons, *Proceedings of ICCF15* (2009).
[9] J.S. Fraser & J.C.D. Milton, *Annual Review of Nuclear Science* 16, 379 (1966).
[10] R. Vandenbosch & J.R. Huizenga, *Nuclear Fission*, Academic, New York (1973), p. 259.
[11] P. Möller et al., *Nature* 409, 785 (2001).

Nuclear and Electronic Structure of Atoms

F. Menegus

Istituto di Biologia e Biotecnologia Agraria, Consiglio Nazionale delle Ricerche,
Via Bassini 15, 20133 Milano, Italy

E-mail: menegus.faustino@gmail.com

Abstract. The plot of Extra Neutron number against the Z number of natural elements reveals a trend that shows the same periodicity observed in the chemical properties of elements. Nuclei appears to direct the electronic structure of atoms.

Different models of the nuclear structure have been proposed. When the electronic structure of atoms was elaborated, the nucleus only provided, with protons, a central positive charge to attract negative electrons [1].

The presence of a precise number of neutrons confers nuclear stability to selected isotopes of natural elements. The aim of the present work is to investigate whether a relationship exists between the number of Extra Neutrons (EN=A-2Z) in the nuclei of stable elements and the electronic structure of atoms.

Fig. 1 shows the number of EN in the nuclei of natural elements, plotted against the Z number. The weighted mean of EN for each element, calculated from [2], is reported. The electronic structure of atoms, the principal and azymutal (letters) quantum numbers, and the atomic volumes [3] are also shown.

The addition of EN to nuclei with the increase of atomic Z number takes place with upsurges and pauses.
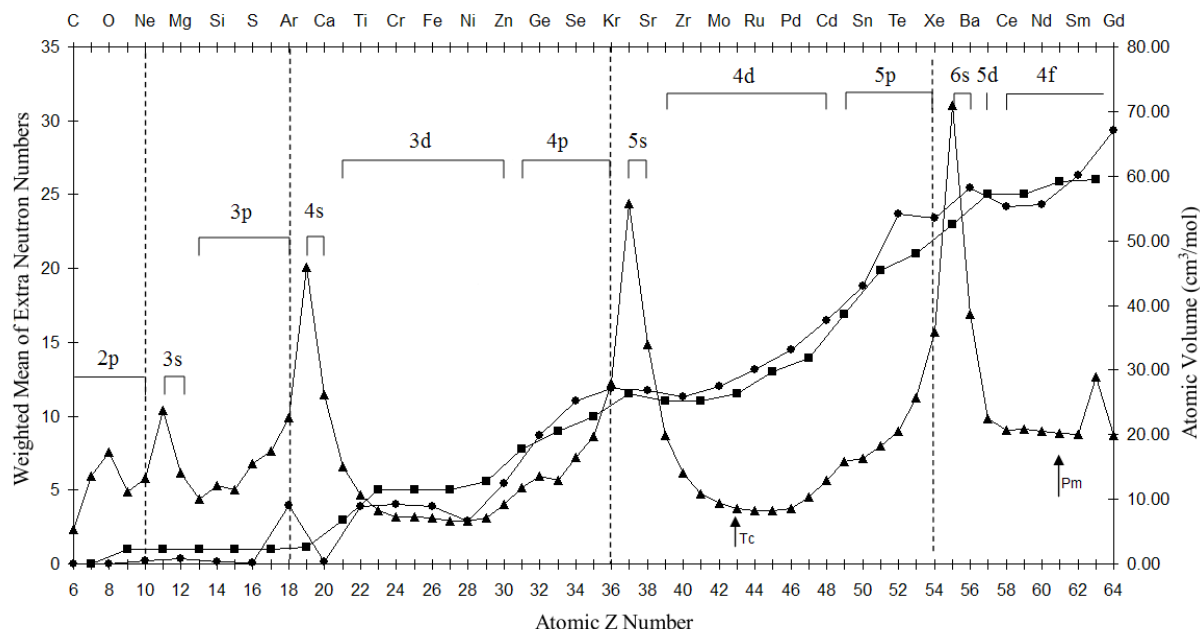

Fig. 1 - The figure shows, as a function of atomic Z number: 1) the weighted means of Extra Neutron (A-2Z) number for the isotopes of natural elements with even ——●—— and odd ——■—— values of Z; 2) The electronic structure of atoms, principal and azymutal (letters) quantum numbers; 3) the atomic volume of atoms ——▲——.

Going from $_5$B to approximately $_{64}$Gd, a sizable central share of the periodic table of elements, it is possible to single out four repetitive events (see also Fig.2) corresponding to the four sequences of electron additions: 2p →3s; 3p →4s; 3d→4p→5s; 4d→5p→6s. The sharp upsurges of EN addition to nuclei culminate at the completion of the six p electrons addition, leading to the electronic structure of the noble gases Ne, Ar, Kr and Xe. Following the noble gases, pauses of EN addition to nuclei, or even reductions in the number of EN, characterize alkaline metals and alkaline earths structures. Pauses extend somehow to 3d and 4d blocks. Hence, the trend of EN addition to nuclei of natural elements parallels the periodicity of the chemical and physical properties of elements, exemplified in Fig.1 by the values of the atomic volume. That is, EN addition to nuclei, a determinant of the stability of nuclear architecture, appears also as a determinant of the electronic structure of atoms.
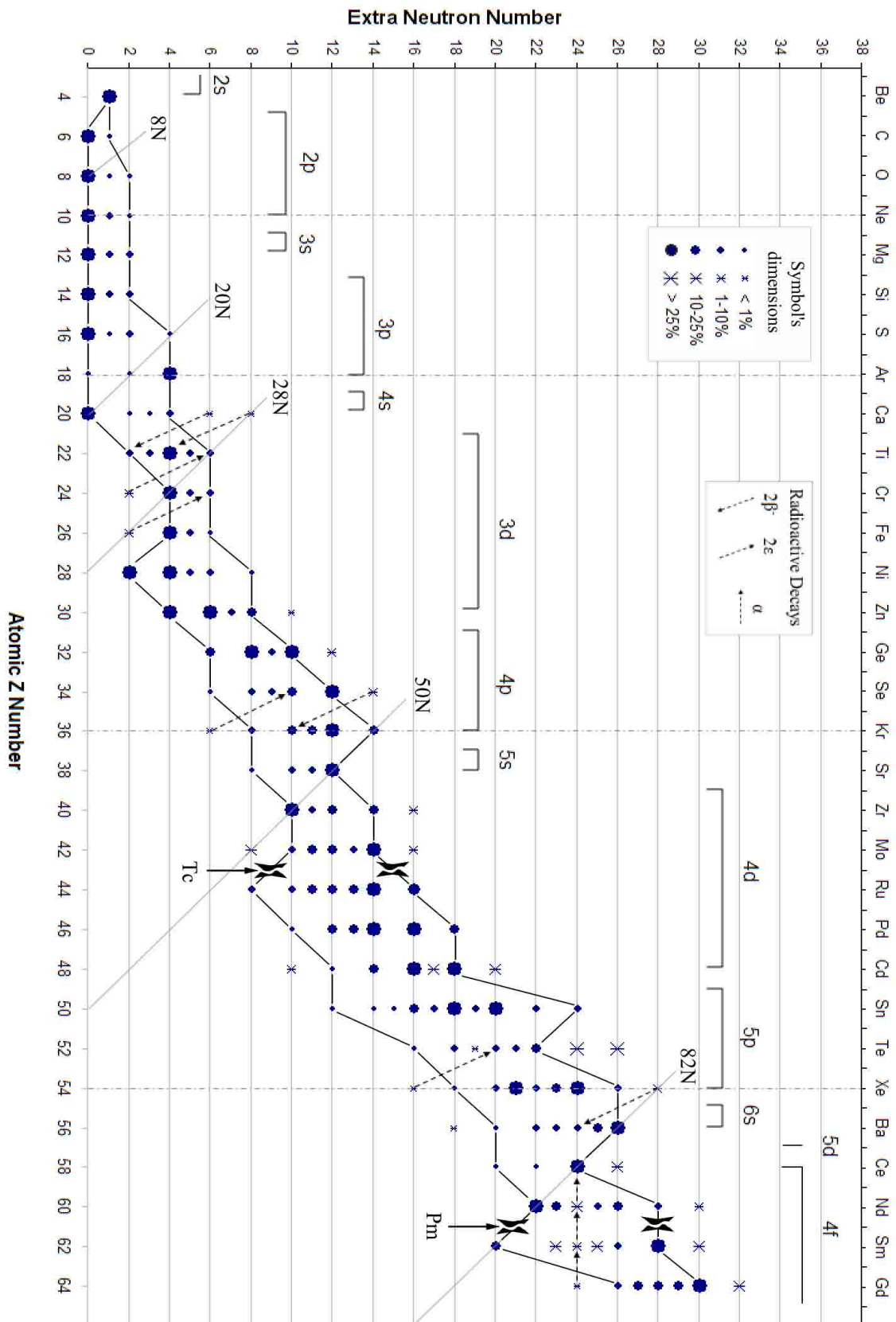
Moreover, the unstable elements Tc and Pm are both located seven places after the noble gases Kr and Xe. This can be read as a further link between the nuclear architecture and the electronic structure of atoms.

Fig. 2 shows the number of EN for the natural isotopes of each element [2] against Z number. Only the Z even elements are considered, a restriction not invalidating the substance of the present work. Lower and upper boundaries of the zone of stability of the isotopes of single elements are shown. Radioactive isotopes, even if extremely long lived, are distinguished from the stable isotopes and, for a few of them, the pathway of decay is shown. All decays lead to elements with stable isotopes inside the area of stability delimited by the two boundaries (Fig. 2). This may suggest that the existing natural radioactive isotopes have been frozen in such a state at the time and in the conditions of their nucleosynthesis, blocking an otherwise faster transformation to stable elements.

The trend of the lower and, in particular, that of the upper boundary of stability in Fig. 2, agrees with the trend of EN addition to nuclei presented in Fig. 1 and with the electronic structure of atoms. However, differences exist between the two boundaries suggesting that the lowest and the highest EN numbers, required for nuclear stability of the isotopes of single elements, may have different physical meanings. Inside the zone of stability all even mass atoms are stable, but several odd mass atoms are unstable (Fig. 2).

Table 1

Extra Neutron Number of Solar System Isotopes of different elements (Fig.2)	Total Trapped Nucleons in Solar System Isotopes of different elements (Fig.2)
0	9.780.897.635
1	5.253.208
2	13.943.984
3	12.118
4	48.644.906
5	1.115.578
6	290.119
7	3.367
8	52.588
9	1.069
10	6.308
11	849
12	7.953
13	91
14	1.665
15	24
16	240
17	55
18	193
19	44

The shell model of nuclear structure stems from the existence of magic numbers of nucleons (Fig. 2) that confer enhanced stability to particular nuclei. Moreover atoms with magic numbers of protons and or neutrons show enhanced natural abundance (n.a.).This is not always true. For example 28, a magic number of neutrons, shows its effect on ^{52}Cr (83.8 % n.a.) but fails to show a clear effect on ^{50}Ti (5.3% n.a.) and on ^{54}Fe (5.8% n.a.). Instead the isotopes of the above elements with the highest abundance are ^{48}Ti (73.72 n.a.) and ^{56}Fe (91.75 % n.a.) in spite of no magic neutron number in their nuclei. The mass of an isotope in Fig. 2 is obtained by the addition of its EN number to twice the value of its atomic number.

Inspection of Fig. 2 reveals that high natural abundance isotopes of different elements populate, in particular, the arrays with 0 and 4 EN.

This observation prompted the investigation of the Total Trapped Nucleons (TTN) in the nuclear species present in the arrays corresponding to single values of the EN number of Fig.2. Table 1 shows that 4 EN, and multiples of 4 EN in the nucleus, lead to enhanced Solar System Abundance (SSA) of the corresponding element's isotopes. Hence multiples of 4 EN appear to be a kind of magic numbers, at least up to 19 EN. This finding is particularly interesting in the case of ^{56}Fe, whose outstanding SSA does not find an explanation in the frame of classical magic numbers. TTN in a singular species was calculated as follows: TTN = SSA of an element, times the isotopic abundance of that species, times its atomic mass. SSA of elements, normalized to 10^6 atoms of Si, was obtained from [4].

One further consideration. Among the different periodic tables of elements [5], the one suggested in 1929 by the French biologist Janet [6], with an eight-period instead of the classical seven-period format, is in best accordance with the periodicity of EN addition to nuclei (Fig. 1 and Fig. 2).

References

[1] G. Herzberg, *Atomic Spectra and Atomic Structure*. (Dover Publications, New York, 1994)
[2] K. Tuli: *Nuclear Wallet Cards.* Sixt Ed. (2000)
[3] C.N. Singman: *J.Chem Ed.* **61** 137 (1984)
[4] K. Lodders: *The Astrophysical Journal*. **591** 1220 (2003)
[5] E.R. Scerri: *The Periodic Table.* (Oxford Univ. Press, 2007)
[6] G. Katz: *The Chemical Educator.* **6** 324 (2001)

Foro romano